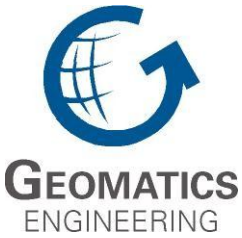

UCGE Reports
Number 20381

Department of Geomatics Engineering

Geopotential of the Geoid-Based North American Vertical Datum

(URL: http://www.geomatics.ucalgary.ca/graduatetheses)

by

TASNUVA TAHIA HAYDEN

July 2013

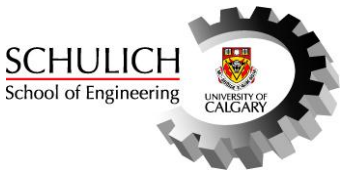

UNIVERSITY OF CALGARY

Geopotential of the Geoid-Based North American Vertical Datum

by

Tasnuva Tahia Hayden

A THESIS

SUBMITTED TO THE FACULTY OF GRADUATE STUDIES

IN PARTIAL FULFILMENT OF THE REQUIREMENTS FOR THE

DEGREE OF MASTER OF SCIENCE

DEPARTMENT OF GEOMATICS ENGINEERING

CALGARY, ALBERTA

JULY, 2013

ABSTRACT

The European Space Agency's dedicated satellite gravity field mission the Gravity Field and Steady-state Ocean Circulation Explorer (GOCE) will at the end of its lifespan achieve 1-2 cm geoid accuracy at a spatial resolution of 100 km. This thesis attempts to answer the question: is a GOCE satellite-only global geopotential model (GGM) sufficient for geodetic applications such as datum unification in North America? The main research objectives that were investigated in order to answer this question include: GOCE GGM evaluation, estimation of height datum offsets for regional vertical datums, and the estimation of the gravity potential for a geoid-based vertical datum. Based on the research objective outcomes, it can be concluded that using only a GOCE satellite-based GGM is not sufficient for geodetic applications such as datum unification in North America. Thus, a GOCE GGM should be rigorously combined with gravity and topography data in a remove-compute-restore geoid modelling scheme.

ACKNOWLEDGEMENTS

I would like to express my sincere thanks to my supervisor, Dr. Michael G. Sideris, for his supervision and support over the past two and a half years. His knowledge and recommendations on a large variety of topics from how to give effective presentations, how to improve my journal papers and thesis, and even how to better my teaching and instructional skills, have been invaluable and much appreciated.

I would also like to thank the very beautiful and intelligent, Dr. Elena Rangelova, whose guidance and friendship has enhanced my time at University of Calgary. Really, this thesis, the journal papers, and even Advanced Physical Geodesy (which has left a scar on my heart) would not have been as successfully completed without her help. Elena, this must be said: you are a strong role model for women wishing to pursue further studies and a career in the sciences.

Next, I would like to thank my dear friend and colleague, Babak Amjadiparvar, for all the stimulating discussions we have had during the preparation of this thesis. Without his help in many matters, I am not sure how this thesis would have ever seen the "light at the end of the tunnel". Truly, he cannot be thanked enough!

Marc Véronneau at the Geodetic Survey Division of Natural Resources Canada is acknowledged for providing me with various datasets, collaborating on journal papers, and for always taking the time to answer my questions. By the same token, the staff at the Canadian Hydrographic Service are thanked for their prompt responses to my questions, as well as Dan Roman from the U.S.A. National Geodetic Survey, and Jianliang Huang from the Geodetic Survey Division of Natural Resources Canada. P. Woodworth and C. Hughes are acknowledged for providing me with ten different global sea surface topography models that have been utilized in this thesis. The late D.G. Wright is acknowledged for the development of the regional Atlantic sea surface topography model utilized in this study. Last but not least, Sinem Ince is acknowledged for providing a gravimetric geoid model of Canada that has been used in this study.

A genuine thank you goes to my graduate committee, which consisted of Dr. J.W. Kim, Dr. Patrick Wu, and Dr. Kyle O'Keefe, for their feedback and constructive comments, which has considerably improved the final version of this thesis.

Finally, I would like to give a big shout out of gratitude to my family and friends for their unconditional love and support. The other graduate students in the gravity and earth observations group are thanked for their friendship. In particular, I would like to thank my office mate, Feng Tang, for providing me with data and helping me to debug C++ code for two course projects, and Jin Baek, for all the pep talks when I really just wanted to call it quits.

This work is a contribution to the ESA STSE – GOCE+ Height System Unification with GOCE project, and was also supported by NSERC, GEOIDE Network Centres of Excellence, Queen Elizabeth II scholarship, and by graduate scholarships and teaching assistantships from the University of Calgary.

TABLE OF CONTENTS

LIST OF TABLES

LIST OF FIGURES

LIST OF SYMBOLS AND ABBREVIATIONS

Symbol	Description
a	semi-major axis of ellipsoid
A_P	attraction of the topography above the geoid at point *P*
$A_{P_0}^C$	attraction of the condensed topography at P_0
$\boldsymbol{a_P^T x}$	bias corrector term
b	semi-minor axis of ellipsoid
const	constant
CD	height of the tidal benchmark above the chart datum
$CD_{2008.0}$	height of the tidal benchmark above the chart datum at epoch 2008.0
$C_P^{(j)}$	geopotential number
$\bar{C}_{nm}$	fully normalized geopotential coefficient of the anomalous potential
C_Q^{normal}	normal geopotential number of a point *Q*
$\frac{dg}{dh}$	gravity gradient
$\frac{d\gamma}{dh}$	normal gravity gradient
dH^*	differential path element along the normal plumb line
$epoch_{CD}$	epoch of the chart datum
g_P	measured gravity at the Earth's surface at a point *P*
$\bar{g}_P^{(j)}$	average value of gravity along the plumb line
$\bar{g}_P^{Prey(j)}$	average gravity along the plumb line obtained using a Prey reduction
G	Newton's gravitational constant
GM	geocentric gravitational constant
$\vec{\boldsymbol{g}}$	gravity vector

h	ellipsoidal height; height above surface of ellipsoid
$h_{2008.0}$	ellipsoidal height in ITRF 2008 epoch 2008.0
h_p	ellipsoidal height at a point *P*
H	orthometric height
$H_P^{dyn(j)}$	dynamic height
$H_P^{Helmert(j)}$	Helmert orthometric height
$H^{(j)}{}_P$	height from point *P* to the vertical datum *j*; also known as orthometric height
$H_P^{norm(j)}$	normal orthometric height
H_Q^*	distance between ellipsoid and telluroid
$H^*_{Q_0^{(j)}}$	distance from point datum origin point to the quasi-geoid
j	local vertical datum in datum zone j
J_2	dynamic form factor
k	local vertical datum in datum zone k
l	planar distance
m	spherical harmonic order
M	mass of the Earth
M^e	mass of reference ellipsoid
n	spherical harmonic degree
n_{max}	maximum degree of spherical harmonic model
N	geoid undulation; also known as geoid height
N_0	zero-degree geoid undulation term
$N^{\Delta g}$	residual geoid signal derived from Stokes integral
N^{GM}	geoid signal derived from a global geopotential model
$N^{GNSS/levelling}$	geoid height obtained from GNSS and levelling data
N^H	geoid signal due to indirect effect of topography
N_P	geoid undulation of point

$N_P^{\Delta g}$	residual geoid height evaluated at point *P* using Stokes integral
N_P^H	indirect effect on the geoid in planar approximation
$N_P^{(j)}$	geoid undulation a point *P* in datum zone *j*
$O^{(j)}$	datum point and in datum zone *j*
$O^{(k)}$	datum point and in datum zone *k*
P	point on the Earth's surface
P_0	point on the geoid
$P^{(j)}{}_0$	datum origin point of a classical levelling based vertical datum
$\bar{P}_{nm}$	fully normalized Legendre function
Q	point on the plumb line where the normal gravity potential equals the actual gravity potential at point *P*
$\bar{Q}$	point on the ellipsoid of the normal plumb line
Q_0	point on the ellipsoid
r	radial distance
r^b	radius of the bounding sphere
r^e	radial distance to the ellipsoid
R	mean Earth radius
R^e	mean radius of the reference ellipsoid
$S(\psi)$	Stokes' kernel function
$SST_{Model,MT}$	sea surface topography obtained from a SST model given in the mean-tide system
SST_{MT}	sea surface topography in mean-tide system
$\bar{S}_{nm}$	fully normalized geopotential coefficient of the anomalous potential
SST_P	sea surface topography at a point *P*
SST_{TF}	sea surface topography in tide-free system
$SST_{TG,TF}$	sea surface topography value obtained using tide gauge records and a geoid model in the tide free system

T	anomalous potential
T_P	anomalous potential at a point P
T_{P_0}	potential of the topographic masses at P_0
$T_{P_0}^C$	potential of the condensed masses at P_0
U	normal gravity potential
U_0	constant normal gravity potential on the ellipsoid
U_{Q_0}	normal potential of a point Q on the ellipsoid
v_P	random error of the geoid height difference at point P
$v_{sea\ level\ rise}$	rate of the sea level rise
V	gravitational potential
V^e	normal gravitational potential generated by the ellipsoid
VLM	vertical land motion velocity
W	gravity potential
W_0	a value of constant gravity potential for an equipotential surface or datum
$W_0^{(j)}$	gravity potential of the local geoid or the local vertical datum in datum zone j
W_P	gravity potential at point P
W_{Pi}	gravity potential of the water surface estimated from a sea surface topography node from a model
W_N	an equipotential surface with a known potential to which sea surface topography values are referenced
W_{P_0}	gravity potential of a point P on the geoid
x	coordinate of data point for the determination of l
x_1	north-south tilt parameter
x_2	west-east tilt parameter
x_P	coordinate of computation point for the determination of l
y	coordinate of data point for the determination of l

y_P	coordinate of computation point for the determination of l
Z_0	height of the local MSL above the chart datum
$Z_{0_{2008.0}}$	height of the local MSL above the chart datum at epoch 2008.0
$Z_{0_{Annual}}$	yearly is averaged water level time series
β	deflection of the vertical
$\bar{\gamma}$	average normal gravity between the corresponding points on the ellipsoid and telluroid
γ_0	normal gravity evaluated at the ellipsoid
γ_{45}	nominal value of normal gravity generally chosen at mid-latitude (e.g., at 45˚ latitude)
γ_a	normal gravity at the equator
γ_b	normal gravity at the pole
γ_i	normal gravity evaluated at the geoid at the point of a node from a sea surface topography model
γ_P	normal gravity computed at the geoid using the latitude of the computational point P
$\bar{\gamma}_Q$	mean value of the normal gravity along the normal plumb line
$\bar{\gamma}_{Q_0^{(J)}}$	average normal gravity along normal plumb line between telluroid and ellipsoid
$\vec{\boldsymbol{\gamma}}$	normal gravity vector
δA_P	indirect effect of the terrain at point P
δg	gravity disturbance
$\delta \Delta g$	indirect effect on gravity
δh	error in height measurement due to the deflection of the vertical
$\delta N^{(j)}$	local vertical datum offset for datum zone j
δN_P	indirect effect of the geoid
δs	scale parameter
δSST	difference between $SST_{TG,TF}$ and $SST_{Model,MT}$
δT	indirect effect on the potential

$\delta W^{(j)}$	potential offset between local vertical datum in zone j and a reference datum
Δf	function that satisfies Laplace equation
Δg	gravity anomaly
Δg^{FA}	free-air gravity anomaly
Δg^{GM}	gravity anomaly determined from a global geopotential model
Δg^{H}	topography reduced gravity anomaly
Δg_P^H	terrain correction in planar approximation
$\Delta g^{(j)}$	biased gravity anomaly derived from terrestrial data
ΔW_0	difference between the potential of the reference datum W_0 and the potential of the normal ellipsoid U_0
ζ_P	height anomaly at P
$\zeta_P^{(j)}$	separation of the local quasi-geoid (coincides with datum origin point) from the ellipsoid
θ	co-latitude
λ	longitude
λ_0	geodetic longitude of centroid of a test network
λ_P	geodetic longitude of point P
π	pi
ρ	crustal density
σ	Earth's surface
$(\sigma_N^2)_n$	degree variances of a GGM
$\sigma_{omission}^{n_{max}}$	omission error of GGM
$\sum_{i=1}^{J} S_P^i \, \delta N^i$	indirect bias term
φ	geodetic latitude
φ_0	geodetic latitude of centroid of a test network
φ_i	latitude of node from a sea surface topography model
φ_P	geodetic latitude of point P

Φ	centrifugal potential
Φ^e	centrifugal potential generated by the ellipsoid
ψ	spherical distance
ω	angular velocity
ω_e	angular velocity of the Earth
Ω	region of integration in Stokes integral for datum offset computations
Ω^0	reference datum
$\Omega^{(j)}$	datum in a particular zone
∇	gradient operator

Abbreviation	**Description**
BVP	Boundary Value Problem
CGVD28	Canadian Geodetic Vertical Datum of 1928
CGVD2013	Canadian Geodetic Vertical Datum of 2013
CHAMP	Challenging Mini-Satellite Payload
CHS	Canadian Hydrographic Service
CML	Canadian Mainland
DEM	Digital Elevation Model
DFO	Department of Fisheries and Oceans Canada
DORIS	Doppler Orbitography and Radiopositioning Integrated by Satellite
ESA	European Space Agency
FFT	Fast Fourier Technique
GBVP	Geodetic Boundary Value Problem
GGM	Global Geopotential Model; Global Gravity Model
GNSS	Global Navigation Satellite Systems
GOCE	Gravity Field and Steady-state Ocean Circulation Explorer
GRACE	Gravity Recovery and Climate Experiment

GSD	Geodetic Survey Division
IERS	International Earth Rotation and Reference Systems Service
LEO	Low Earth Orbit
LSC	Least-Squares Collocation
LVD	Local Vertical Datum
MDT	Mean Dynamic Topography
MSL	Mean Sea Level
MSST	Mean Sea Surface Topography
NOAA	National Oceanic and Atmospheric Administration
NAVD88	North American Vertical Datum of 1988
NFD	Newfoundland
NGS	National Geodetic Survey
NRCan	Natural Resources Canada
RTM	Residual Terrain Model
SEM	Spectral Enhancement Method
SGG	Satellite Gravity Gradiometry
SLR	Satellite Laser Ranging
SST	Sea Surface Topography
SST-hl	Satellite-to-Satellite Tracking between high and low orbiting satellites
SST-ll	Satellite-to-Satellite Tracking between low Earth orbiting satellites
VAN	Vancouver Island
VLBI	Very Long Baseline Interferometry
WHS	World Height System

CHAPTER 1
INTRODUCTION

1.1 Problem Statement

Height observations are among one of the most fundamental measurements for a variety of scientific and engineering applications such as topographic mapping, water system observations, coastal studies, construction projects, among others. With the advent of space-based technologies such as the Global Navigation Satellite Systems (GNSS), Very Long Baseline Interferometry (VLBI), Satellite Laser Ranging (SLR), Doppler Orbitography and Radiopositioning Integrated by Satellite (DORIS), and satellite radar altimetry, heights of any arbitrary point on the Earth's surface or above the Earth's surface can be easily obtained. The heights obtained utilizing space-based techniques refer to a reference ellipsoid, which is an analytically defined geometric surface, and hence these heights, known as ellipsoidal heights, are geometric in nature. The shortcoming of ellipsoidal heights is that one is not able to distinguish the direction of water flow. In other words, heights referenced to the ellipsoid may have water flowing from a lower ellipsoidal height to a higher ellipsoidal height, which intuitively contradicts the notion that water ought to flow from a higher position to a lower one. Heights that can distinguish the direction of water flow are physically meaningful heights and their determination is dependent on the gravity potential of the Earth (i.e., a combination of the gravitational potential due to the Earth's mass or density distribution and the centrifugal potential due to the Earth's rotation) as water will flow from a position of higher gravity potential to a position of lower gravity potential.

Conventionally, heights have been measured with respect to the mean sea level (MSL); therefore, heights are generally referenced to a constant potential or equipotential level surface of the Earth's gravity field that best coincides with the global MSL in a least-squares sense, which is known as the geoid (Gauss 1828; Listing 1873). Over the past two hundred years, height observations have been obtained through spirit levelling and gravity measurements. Spirit levelling yields the relative height between two points in a

levelling network. In order to obtain absolute heights from spirit levelling, a defined zero reference point or a zero reference surface is needed. This zero reference surface to which levelling heights can be referenced is known as a vertical datum. Regional and national vertical datums have traditionally been realized by fixing one or more tide gauge stations as the zero height reference point to which the levelling observations are constrained. This type of vertical datum will be referred to as a classical levelling-based vertical datum throughout this text.

Currently, there exist hundreds of regional and national classical levelling-based vertical datums throughout the world. Since the MSL at a tide gauge varies both spatially and temporally, classical levelling-based vertical datums realized in various parts of the world will refer to different zero level points and surfaces. In order to relate height measurements between different vertical datums, the differences between the zero reference points and surfaces must be known. Thus, the need for a global height system arises when there is an attempt to connect geodetic data from two neighbouring countries or regions that have been using different definitions for the zero point for the vertical datum. Due to its practical importance, vertical datum unification has been one of the main topics of research in the field of geodesy over the past three decades.

Classical levelling-based vertical datums that define their zero point or zero surfaces based on the MSL at a tide gauge do not necessarily coincide with the global geoid due to variations in sea surface topography (SST), which occurs as a result of differences in water salinity, temperature, tides, and waves, among others (Torge 2001). The discrepancy between the reference surface of a classical levelling-based vertical datum and the geoid can reach up to 2 m (Balasubramania 1994). Therefore, the precise determination of the geoid is crucial for the unification of different height systems, as the reference surfaces of various classical levelling-based vertical datums can be compared or determined with respect to a globally consistent and accurate geoid model.

It is expected that the European Space Agency's (ESA) dedicated satellite gravity field mission GOCE (Gravity Field and Steady-state Ocean Circulation Explorer) will

contribute to a cm-level accurate geoid model. The mission objectives include the determination of gravity anomalies with an accuracy of 1 mGal and the geoid with an accuracy of 1-2 cm while achieving a spatial resolution of 100 km (Drinkwater et al. 2003). According to Burša et al. (2009), the geopotential model, which utilizes observations from dedicated satellite gravity missions, is known to limit the accuracy of a world height system (WHS) or a global geoid model that represents the zero height surface of a global vertical datum, as well as the determination of the geoidal geopotential W_0, the connection of local vertical datums to the global geoid-based vertical datum, the computation of geopotential values W, and the computations of heights. Thus, one of the scientific objectives of the GOCE mission is to assist in the unification of existing classical levelling-based vertical datums by providing a globally consistent and unbiased geoid (i.e., one where only satellite-based observations are utilized for the construction of the gravity field or geoid model).

1.2 Thesis Objectives

Within the context of using the latest high-accuracy satellite gravity field mission GOCE for the purpose of vertical datum unification in North America, the main research objectives are:

- GOCE global geopotential model (GGM) evaluation using GNSS and levelling data in order to determine which of the recently released GOCE GGMs have the best agreement with independent terrestrial data, or in other words, which GOCE GGM will have the best performance in North America. This will allow for the selection of the best GGM for the purpose of geoid modelling for applications such as vertical datum unification or the implementation of a geoid-based vertical datum.

- Estimation of local datum shifts from GNSS on benchmark and GNSS on tide gauge data using the best GOCE global geopotential model in North America for the purpose of datum unification. The effect of the following factors on the

determination of local vertical datum shifts or offsets will be examined: GOCE GGM errors, measurement errors in the GNSS and levelling data, the geographic size of the test network, the density and configuration of the GNSS/levelling benchmarks of the test networks, and the spatial tilts found within the test networks.

- Estimation of the gravity potential of the zero-height surface for a North American geoid-based vertical datum using long term tide gauge records and a wide variety of regional and global sea surface topography models.

1.3 Thesis Outline

Chapter 2 provides the background information necessary for understanding the concepts discussed in Chapters 3, 4, and 5. Chapter 3 examines the evaluation of the GOCE global geopotential models in North America while Chapter 4 focuses on the estimation of local vertical datum offsets for North American classical levelling-based vertical datums. Chapter 5 examines the estimation of a W_0 value for the geoid-based vertical datum that could be implemented by government agencies in both Canada and the U.S.A. Finally, Chapter 6 provides the main conclusions with respect to the stated thesis objectives and also provides recommendations for future investigations.

CHAPTER 2
HEIGHTS, VERTICAL DATUMS, AND THE GEOID

2.1 Introduction

The three coordinates used to define points on or near the Earth's surface are: latitude, longitude, and height. The latitude and longitude are more precisely known as geodetic latitude and geodetic longitude as these quantities refer to an oblate ellipsoid of revolution, which is a mathematically-defined surface that is chosen to fit the geoid either globally or regionally. In other words, it can be considered a geometrical approximation of the geoid (i.e., the surface of constant gravity potential that best coincides with the global MSL) that can be determined analytically using four defining parameters: a (the semi-major axis of the ellipsoid), GM (geocentric gravitational constant), J_2 (dynamic form factor), and ω (angular velocity).For globally best fitting ellipsoids, it is usually assumed that the center of the ellipsoid coincides with the Earth's center of mass and that the ellipsoid's minor axis is aligned with the Earth's spin axis. Similarly to the geodetic latitude and longitude of a point P on the Earth's surface, the height of this point may also refer to the ellipsoid. The ellipsoidal height, h_p, is the distance from the ellipsoid to the point P on the Earth's surface, which is measured along the perpendicular to the ellipsoid (see Figure 2.1). The use of ellipsoidal heights is convenient since they are easily related to geocentric coordinates that are obtained using space based techniques such as GNSS.

However, it should be noted that the ellipsoidal surface does not in fact coincide with the MSL. Globally, the difference between the MSL and the globally best fitting ellipsoidal surface ranges between ± 100 meters. Furthermore, although ellipsoidal heights are geometrically meaningful, they cannot be considered physically meaningful heights. In other words, one cannot determine the direction of water flow from ellipsoidal heights, which is crucial for engineering applications such as, e.g., transcontinental pipeline construction. Knowledge of the gravity potential (via gravity observations) is required in order to determine physically meaningful heights. Moreover, for most surveying

applications the height of a point has traditionally referred to the MSL or to a vertical datum that has its origin point tied to the MSL at one or more tide gauges. An example of such is given in Figure 2.1 where the height from point *P* to the vertical datum *j* is denoted by $H^{(j)}_P$.

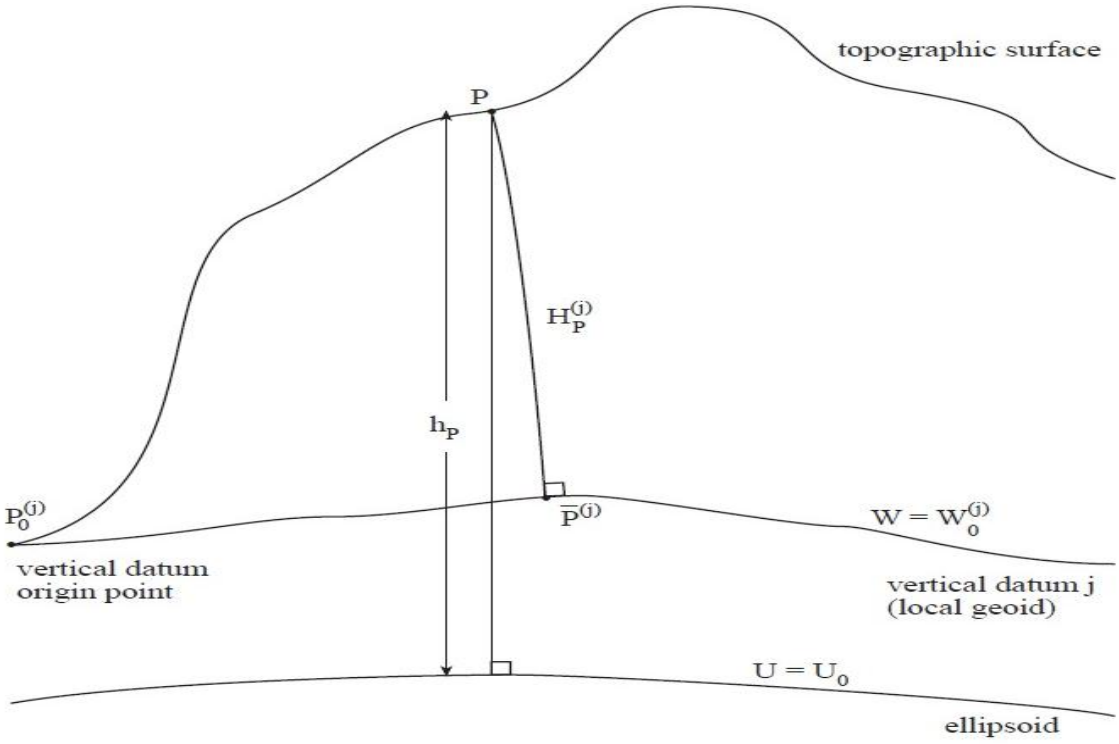

Figure 2.1: Ellipsoidal (h_P) and orthometric ($H^{(j)}_P$) heights (Jekeli 2000).

2.2 Gravity Potential and the Geoid

The gravity potential *W* is the sum of the gravitational potential *V* and centrifugal potential *Φ:*

$$W(r,\theta,\lambda) = V(r,\theta,\lambda) + \Phi(r,\theta), \qquad (2.1)$$

where *(r,θ,λ)* are spherical polar coordinates (radial distance, co-latitude, and longitude, respectively). A surface on which a potential function has a constant value is known as an equipotential surface. The equipotential surface of *W* (i.e., $W(r, \theta, \lambda) = constant = W_0$)

that best agrees with the global MSL at rest is known as the geoid (Gauss 1828; Listing 1873). Today it is understood that the geoid surface will vary with time due to mass deformations and re-distributions within the Earth. The distance between the ellipsoid and the geoid surface is known as the geoid undulation or geoid height. The determination of this quantity will be discussed in Section 2.6. It should be noted that the local geoid in Figure 2.1 is synonymous with the local vertical datum in a specific datum zone, which has traditionally been constrained by the local MSL at one or more tide gauges. Globally, the datum offsets between local vertical datums (LVDs) and a globally consistent geoid model can reach up to 1-2 m (Gerlach and Rummel 2013).

Functions that satisfy the Laplace equation (i.e., $\Delta f = 0$) are called harmonic functions. Harmonic functions are analytic (i.e., continuous with continuous derivatives of any order) and can be expanded into a spherical harmonic series. The gravitational potential (i.e., the geopotential generated by the masses of the Earth including the atmosphere) is a harmonic function, meaning that $\Delta V=0$ outside the masses, or in other words when the density ρ is equal to zero. Thus, the gravitational potential can be expressed most conveniently in terms of spherical harmonic functions (Heiskanen and Moritz 1967; Jekeli 2000):

$$V(r,\theta,\lambda) = \frac{GM}{R}\sum_{n=0}^{\infty}\left(\frac{R}{r}\right)^{n+1}\sum_{m=0}^{n}[\bar{C}_{nm}\cos m\lambda + \bar{S}_{nm}\sin m\lambda]\,\bar{P}_{nm}\cos\theta, \qquad (2.2)$$

where G is the Newton's gravitational constant and M is the Earth's mass (including the atmosphere), R is the mean Earth radius, n is the degree, m is the order, $\bar{C}_{nm}$ and $\bar{S}_{nm}$ are fully normalized spherical harmonic coefficients for degree and order n and m, and $\bar{P}_{nm}$ are fully normalized Legendre functions. Equation (2.2) is the solution to a boundary value problem for the potential and only holds if the point of computation is in free space. The convergence to the true gravitational potential is guaranteed only for points outside a sphere enclosing all masses. In practice Eq. (2.2) will be truncated to a maximum degree n_{max} as it is impossible in practice to expand the series to infinity.

When $m=n=0$, Eq. (2.2) reduces to:

$$V_{00}(r,\theta,\lambda) = \frac{GM}{R}. \quad (2.3)$$

Thus, the zero-degree term is simply the potential of a homogenous sphere and the higher degree terms express the deviations from the potential of such a sphere.

On the other hand, the centrifugal potential is not a harmonic function. The Laplace equation for the centrifugal potential is not zero (i.e., $\Delta\Phi=2\omega^2$). Due to this, the gravity potential W is not a harmonic function either as it is a sum of the gravitational and centrifugal potentials. In spherical coordinates the centrifugal potential can be written as (Jekeli 2000):

$$\Phi(r,\theta) = \frac{1}{2}\omega_e^2 r^2 sin^2\theta, \quad (2.4)$$

where ω_e is the Earth's rotation rate. The gravity potential and its constituent potentials (specifically the gravitational potential) are re-visited in Section 2.6 where geoid modelling is discussed.

2.3 Height Systems

The relationship between the gravity vector and the gravity potential is:

$$\vec{\boldsymbol{g}} = \nabla W, \quad (2.5)$$

where ∇ denotes the gradient operator. The gradient is a vector pointing in the direction of the steepest descent of a function (i.e., perpendicular to its isometric lines). Therefore, in the case of the gravity potential, the gradient of W is the vector perpendicular to the equipotential surfaces. Thus, the relationship between the magnitude of the gravity vector and the gravity potential may be written as:

$$|g| = g = -\frac{dW}{dn}, \tag{2.6}$$

where *dn* is the differential path along the perpendicular. The minus sign indicates that potential decreases with altitude, the path length is positive upwards, and the gravity magnitude is positive. From equation (2.6) it follows that a height, which can be defined as the distance along the plumb line (i.e., the curved line that intersect normally the equipotential surfaces and to which the gravity vector is tangent) from a point *P* on the surface of the Earth to the geoid (W_0), is dependent on the gravity potential and the gravity vector:

$$dH = -\frac{dW}{g} \rightarrow H_P = -\int_{Wo}^{Wp} \frac{dW}{g}, \tag{2.7}$$

where H_p is the height at point *P* with respect to the geoid W_0 and W_p is the gravity potential at point *P*.

There are three types of physical heights: dynamic heights, orthometric heights, and normal heights. Each depends on the difference in gravity potential between the local geoid and the point in question The local geoid can also define a local vertical datum where a single point $P^{(j)}{}_0$, which is assumed to the on the geoid and is accessible, through for example a tide gauge, defines the vertical datum origin point (see Section 2.4).

The difference in the gravity potential between the local geoid and the point *P* is known as the geopotential number:

$$C_P^{(j)} = W_0^{(j)} - W_{P,} \tag{2.8}$$

where $W_0^{(j)}$ is the potential of the local geoid, and W_P is the gravity potential at point *P*. Any point on the Earth's surface has a unique geopotential number. If the geopotential number is appropriately scaled (see Eq. (2.7)) it may be used as the height coordinate of the point in question.

2.3.1 Dynamic Heights

The dynamic height of a point *P* is given by the equation:

$$H_P^{dyn(j)} = \frac{C_P^{(j)}}{\gamma_{45}}, \tag{2.9}$$

where γ_{45} is the nominal value of normal gravity generally chosen at mid-latitude (e.g., at 45˚ latitude). Although dynamic heights are physically meaningful, they have no geometric meaning—it is simply the potential in distance units relative to the geoid, as the same constant scale factor is used for all dynamic heights within a particular datum.

2.3.2 Orthometric Heights

In contrast to dynamic heights, orthometric heights of a point *P* have a very definite geometric interpretation: it is the distance above the local geoid along the plumb line, which is curved due to the fact that equipotential surfaces are not parallel to each other. The orthometric height is given by the following mathematical relationship:

$$H_P^{(j)} = \frac{C_P^{(j)}}{\bar{g}_P^{(j)}}, \tag{2.10}$$

where $\bar{g}_P^{(j)}$ is the average value of gravity along the plumb line:

$$\bar{g}_P^{(j)} = \frac{1}{H_P^{(j)}} \int_{\bar{P}^{(j)}}^{P} g \, dH, \tag{2.11}$$

where *dH* is a differential element along the plumb line and $\bar{P}^{(j)}$ is at the base of the plumb line on the local geoid. The $C_P^{(j)}$ term from Eq. (2.10) can be estimated from measurements using the following relationship:

$$C_P^{(j)} = \int_{\bar{P}^{(j)}}^{P} g \, dH. \tag{2.12}$$

However, the value of $\bar{g}_P^{(j)}$ cannot be evaluated exactly as this requires complete knowledge of the mass density of the Earth's crust. Thus, orthometric heights cannot be exactly determined. The computation of orthometric height therefore depends on a density hypothesis for the crust. For this purpose, a frequently utilized model assumes a constant crustal density and constant topographic height in the region near the point *P*. With this assumption, the average gravity along the plumb line between $\bar{P}^{(j)}$ and *P* can be obtained using a Prey reduction (Heiskanen and Moritz 1967):

$$\bar{g}_P^{Prey(j)} = \frac{1}{2}\left[g_P + \left(g_P - 2\pi G\rho H_P^{(j)} + \frac{d\gamma}{dh} H_P^{(j)} - 2\pi G\rho H_P^{(j)}\right)\right]. \tag{2.13}$$

The Prey reduction models the gravity value inside the crust by removing the attraction of a Bouger plate (i.e., $2\pi G\rho H_P^{(j)}$) of constant density, which is followed by applying a free-air downward continuation using the normal gravity gradient (i.e., $d\gamma/dh$), and lastly the Bouger plate is restored. Using nominal values for the density and the gradient (i.e., 2670 kg/m^3 and -0.0848 mgal/m) Eq. (2.13) simplifies to:

$$\bar{g}_P^{Prey(j)} = g_P + \left(0.0424 \, \frac{mgal}{m}\right) H_P^{(j)}. \tag{2.14}$$

When substituting $\bar{g}_P^{Prey(j)}$ for $\bar{g}_P^{(j)}$ in Eq. (2.10), the orthometric height is known as Helmert orthometric height. It can be determined with the combination of Eq. (2.10) and Eq. (2.13) (Jekeli 2000):

$$H_P^{Helmert(j)} = \frac{C_P^{(j)}}{g_P}\left(1 - \left(0.0424 \, \frac{mgal}{m}\right)\frac{C_P^{(j)}}{g_P^2} + \left(0.00180 \, \frac{mgal^2}{m^2}\right)\left(\frac{C_P^{(j)}}{g_P^2}\right)^2 - \cdots\right), \tag{2.15}$$

where the higher order terms contribute less than 10^{-10}.

Heiskanen and Mortiz (1967) assess that an error in the topographic mass density ρ of approximately 600 kg/m^3 at an elevation of approximately 1000 m will affect the orthometric height by 25 mm, while Strange (1982) estimates this error to be up to 30 mm for elevations greater than 2000m. The topographic density of 600 kg/m^3 represents the largest range in mass-density that should be encountered in practice according to Heiskanen and Mortiz (1967), but the changes in the mass-density may reach up to 1000 kg/m^3.

2.3.3 Normal Heights

In order to avoid making a density hypothesis for the Earth's crust, a geometrically interpretable height may be estimated using an approximation of the gravity field that can be calculated exactly at any given point. The approximation of the gravity field refers to the normal gravity field, where the gravity field is generated by an Earth-fitting ellipsoid that contains the total mass of the Earth, rotates with the Earth around its minor axis, and is itself an equipotential surface of the gravity field it generates. The normal gravitational field generated by the ellipsoid, V^e, can also be expressed by Eq. (2.2), though it will only contain even zonal harmonics (i.e., $m=0$; no dependence on longitude since $cos0\lambda=1$) due to the imposed symmetries of the ellipsoid (Jekeli 2000). Likewise, the normal centrifugal potential can be determined using Eq. (2.4). Thus, the normal gravity potential U can be defined as:

$$U(r,\theta) = V^e(r,\theta) + \Phi^e(r,\theta). \tag{2.16}$$

The normal gravity potential U can be evaluated anywhere in space on and above the ellipsoid using four constants that define the size, shape, mass and rotation of the ellipsoid. U is constant on the ellipsoid (i.e., U_0) and can be calculated using the Pizzetti formula (Heiskanen and Mortiz 1967):

$$U_0 = \frac{GM}{\sqrt{a^2+b^2}}\tan^{-1}\frac{\sqrt{a^2+b^2}}{b} + \frac{1}{3}\omega_e^2 a^2, \tag{2.17}$$

where a and b are respectively the semi-major and semi-minor axis of the ellipsoid.

Similarly to the relationship between gravity and the gravity potential, the normal gravity vector $\vec{\gamma}$ can be derived using

$$\vec{\boldsymbol{\gamma}} = \nabla U, \tag{2.18}$$

where the magnitude of $\vec{\gamma}$ can be calculated exactly anywhere on the ellipsoid using the Somigliana-Pizzetti formula (Heiskanen and Mortiz 1967):

$$\gamma = \frac{a\gamma_a cos^2\varphi + b\gamma_b sin^2\varphi}{\sqrt{a^2 cos^2\varphi + b^2 sin^2\varphi}}, \tag{2.19}$$

where γ_a and γ_b are the normal gravity at the equator and the pole respectively, and are normally given as published values. The normal gravity can also be obtained above the surface of the ellipsoid by the Taylor series expansion of γ, where the final expression up to the 2nd term is given by:

$$\gamma(h) = \gamma\left[1 - \frac{2}{a}\left(1 + \frac{a-b}{a} + \frac{\omega_e^2 a^3}{GM} - 2\left(\frac{a-b}{a}\right) sin^2\varphi\right)h + 3\frac{\gamma_a}{a^2}h^2\right], \tag{2.20}$$

where h is the height above the surface of the ellipsoid and φ is the geodetic latitude.

The normal plumb line through a point P is the line that is perpendicular to equipotential surfaces of the normal gravity field. On this plumb line, there is a point Q where the normal gravity potential equals the actual gravity potential at point P (see Figure 2.2). In other words, U_Q is equivalent to W_P. Thus, the normal geopotential number of Q is defined as (Jekeli 2000):

$$C_Q^{normal} = U_0 - U_Q = U_0 - W_P = C_P^{(j)} + \left(U_0 + W_0^{(j)}\right), \tag{2.21}$$

where W_P has been replaced by the relationship given in Eq. (2.8).

Similarly to Eq. (2.12) from the previous section on orthometric heights, it follows that

$$C_Q^{normal} = \int_{\bar{Q}}^{Q} \gamma dH^*, \tag{2.22}$$

where $\bar{Q}$ is the point on the ellipsoid of the normal plumb line (see Figure 2.2), and dH^* denotes the differential path element along the normal plumb line. By dividing and multiplying the right hand size of Eq. (2.22) by the length of the normal plumb line from the ellipsoid to point Q (i.e., H^*_Q in Figure 2.2) one obtains (Jekeli 2000):

$$H_Q^* = \frac{C_P^{(j)} + \left(U_0 - W_0^{(j)}\right)}{\bar{\gamma}_Q}, \tag{2.23}$$

where

$$\bar{\gamma}_Q = \frac{1}{H_Q^*} \int_{\bar{Q}}^{Q} \gamma dH^* \tag{2.24}$$

is the mean value of the normal gravity along the normal plumb line.

From Figure 2.2, it can be seen that the point Q lies on the telluroid. The telluroid is the surface whose normal potential is equal to the actual gravity potential at the Earth's surface along the ellipsoidal normal. It should be noted that the telluroid is not an equipotential surface. The distance between the telluroid and the Earth's surface is known as the height anomaly at P, ζ_P. The quasi-geoid is the surface defined by the separation ζ_P from the ellipsoid.

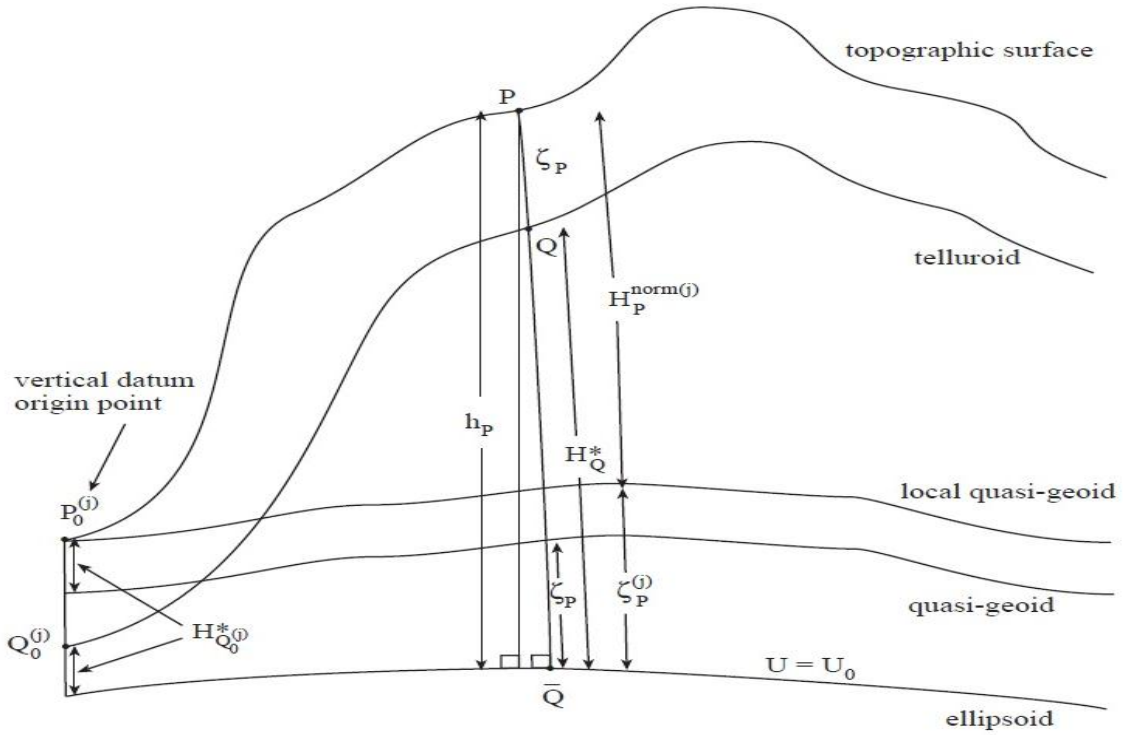

Figure 2.2: Normal heights ($H^{norm(j)}{}_P$), height anomaly (ξ_P), quasi-geoid and local quasi-geoid (Jekeli 2000).

Although the shape of the quasi-geoid is similar to the shape of the geoid, it should be noted that the quasi-geoid is not an equipotential surface for either the normal gravity field or the actual gravity field. The local quasi-geoid shown in Figure 2.2 contains the vertical datum origin point $P^{(j)}{}_0$ and is parallel to the quasi-geoid by the amount $H^*_{Q_0^{(j)}}$, which is defined as (Jekeli 2000):

$$H^*_{Q_0^{(j)}} = \frac{\left(U_0 - W_0^{(j)}\right)}{\bar{\gamma}_{Q_0^{(j)}}}. \tag{2.25}$$

It is shown in Figure 2.2 that $H^*_{Q_0^{(j)}}$ is the distance from the ellipsoid to point $Q_0^{(j)}$ where $U_{Q_0^{(j)}} = W_0^{(j)}$. Another way to view it is as the distance from point $P^{(j)}{}_0$ to the quasi-geoid. The normal height is thus defined as the distance from the local quasi-geoid to the point P (Molodensky et al. 1962, see Figure 2.2):

$$H_P^{norm(j)} = \frac{C_P^{(j)}}{\bar{\gamma}_Q}. \tag{2.26}$$

The average normal gravity $\bar{\gamma}_Q$ can be approximated from the expression (Heiskanen and Mortiz 1967):

$$\bar{\gamma}_Q \approx \gamma \left[1 - \left(1 + \frac{a-b}{a} + \frac{\omega_e^2 a^2 b}{GM} - 2\left(\frac{a-b}{a}\right) sin^2\varphi\right)\frac{H_P^{(j)}}{a} + \left(\frac{H_P^{(j)}}{a}\right)^2\right]. \tag{2.27}$$

Substituting Eq. (2.27) into Eq. (2.26) yields (Jekeli 2000):

$$H_P^{norm(j)} \approx \frac{C_P^{(j)}}{\gamma}\left[1 + \left(1 + \frac{a-b}{a} + \frac{\omega_e^2 a^2 b}{GM} - 2\left(\frac{a-b}{a}\right) sin^2\varphi\right)\frac{C_P^{(j)}}{a\gamma} + \left(\frac{C_P^{(j)}}{a\gamma}\right)^2\right]. \tag{2.28}$$

Lastly, the local height anomaly, which is the separation of the local quasi-geoid from the ellipsoid, can be determined from the following relationship (Jekeli 2000, see Figure 2.2):

$$\zeta_P^{(j)} = \zeta_P + H^*_{Q_0^{(j)}} = \zeta_P + \frac{\left(U_0 - W_0^{(j)}\right)}{\bar{\gamma}_{Q_0^{(j)}}}. \tag{2.29}$$

2.4 Definition and Realization of Classical Levelling Based Vertical Datums

A vertical reference system is defined as a system for elevations that supports physical and geometric heights globally with a relative accuracy better than 10^{-9} (Ihde and Sánchez 2005). A vertical reference frame is a realization of the vertical reference system by a set of physical points or stations with precisely determined geopotential numbers and geocentric coordinates referred to the Conventional Terrestrial Reference System (CVRS Conventions 2007). Hence, the vertical datum has been defined as an equipotential surface with a conventional value of W_0 of Earth's gravity potential. Heights are defined with respect to this surface, or alternatively as a "coordinate surface

to which heights, taken as vertical coordinates, are referred" (Vaníček 1991). According to Vaníček (1991), there are three kinds of vertical datums that are used in geodesy: the geoid, the quasi-geoid, and the reference ellipsoid.

Torge (1980) defines the geoid as a surface of constant gravity potential W_0 having been reduced for the gravitational effects of luni-solar and atmospheric masses, and short periodic variations in the Earth's gravity field that coincides with the MSL after the effect of sea surface topography over the oceans is removed, or more compactly, a level surface where $W=W_0$ that best approximates the MSL at rest. Due to the existence of long term gravity field variations, the geoid is generally referred to a specific time epoch (Heck and Rummel 1989).

Vaníček (1991) presents two practical options for identifying the desired equipotential surface where $W=W_0$. First is the abstract option, where one specifies a constant value of the Earth's gravity potential $W=W_0=const$, which defines the geoid as one specific level surface. The second option is known as the geometrical option, and it requires that the chosen horizontal surface approximates in a specific way the MSL surface.

Traditionally, height systems have been defined by the long-term averages of one or many local reference benchmarks, for example by averaging the sea level observations to obtain MSL constrained to one or several tide gauges, with the assumption that the MSL coincides with the geoid. However, phenomena due to tides, sea surface topography, currents, and storm surges cause the MSL to deviate from an equipotential surface; thus the discrepancy between the MSL and the geoid can reach up to 2 m (Balasubramania 1994). Moreover, the relationship between the observed MSL and land benchmarks is not constant due to changes in sea level and the uplift/subsidence of land, causing datums at different epochs to refer to different reference levels. This effect of defining the vertical datum in relation to a local MSL is responsible for the vertical datum offset between different regional and national datums. Most countries have been using regional vertical datums as local reference systems, and it is estimated that more than one hundred

regional vertical datums have been derived all over the world (Balasubramania 1994; Pan and Sjöberg 1998).

Thus, the realization of a vertical datum has generally been accomplished by locating a point of zero height, which is generally located by obtaining the averaged long term MSL at a tide gauge station, which is linked to a reference benchmark either a short distance away from the tide gauge or located directly on the tide gauge. This benchmark is assigned as the starting point of the levelling network and defines the zero height value of the vertical datum (Vaníček 1991). Orthometric, dynamic, and normal heights can then be determined by adding gravity dependent corrections to the leveled height increments (Rummel and Teunissen 1988). This is what will be referred to as a "classical levelling based vertical datum". Five main approaches for defining a regional vertical datum are described below (Vaníček 1991; Ihde 2007; CVRS Conventions 2007):

1) The geoid surface is defined by the MSL measurements obtained from the tide gauge network on the coasts of the country. The datum is fixed to zero at these stations. Due to the discrepancy between the MSLs at the selected tide gauge stations and the geoid, distorted heights will result from this approach. It is assumed that the tide gauge records do not include any errors or that the error level is acceptable when fixing the datum to zero at the defined tide gauge network.

2) The vertical datum is defined by performing a free-network adjustment where only one tide gauge or point is held fixed. The heights from the adjustment are shifted so that the mean height of all tide gauges equals zero. This approach is similar to (1) with the exception that the MSL observations made at other tide gauges are not included, and thus the MSL is defined from the records of a single tide gauge only.

3) The mean sea surface topography (MSST) values at tide gauge stations are estimated from satellite altimetry and hydrostatic models. Satellite altimetry

measures sea surface heights (SSHs), which is the height of the water surface given with respect to a reference ellipsoid. One can obtain the MSST or the mean dynamic topography (MDT) using a geoid model and altimetry derived SSH values, as the SSH values are generally averaged over time. SST, MSST and MDT are used synonymously in this thesis and refer the height of the mean sea surface above the geoid. The network is adjusted by forcing MSL-MSST to zero for all tide gauge stations. With this method of realizing a regional vertical datum, most of the drawbacks for method (1) and (2) are eliminated, though it should be noted that satellite altimetry has poor performance in coastal regions where tide gauges are located due to contamination of the altimetry footprint by land. Moreover, in shallow regions, global ocean circulation models derived from altimetry and hydrostatic models may have up to a decimeter level uncertainty (Shum et al. 1997).

4) The vertical datum is defined in the same way as in method (3) with the exception that the reference tide gauges are allowed to float in the adjustment by error estimates. In this approach all MSL and SST information at the reference tide gauges can be incorporated.

5) Lastly, the vertical datum is defined as in method (4) with the exception that orthometric heights are estimated from satellite-based ellipsoidal heights and gravimetric geoid heights. As the satellite-derived heights are referenced to a global reference ellipsoid, the regional datum is linked to a global vertical reference surface. This approach may be used to realize an international world height system or a global vertical datum (Colombo 1980; Balasubramania 1994).

The link between the traditional levelling based vertical datum and the geoid is realized by GNSS positioning at the benchmarks of the vertical control network. Theoretically it is expected that $h_P - H^{(j)}_P - N_P = 0$, where h_P is the ellipsoidal height, $H^{(j)}_P$ is the orthometric height, and N_P is the geoid undulation. However, in practice it does not equal zero due to various inconsistencies of the geoid and ellipsoidal heights, systematic errors in the

levelling network, limitations in the measurement accuracy of the vertical component by GNSS, biases present in gravity anomalies, long wavelength geoid errors, and geodynamic phenomena (Rangelova 2007; Kotsakis and Sideris 1999).

2.5 Classical Levelling Based Vertical Datums in North America

There are three commonly used classical levelling based vertical datums in North America: the Canadian Geodetic Vertical Datum of 1928 (CGVD28), the North American Vertical Datum of 1988 (NAVD88), and the Nov07 vertical datum. It should be noted that Nov07 is not an official vertical datum. The main characteristics of these three vertical datums are summarized in Figure 2.3.

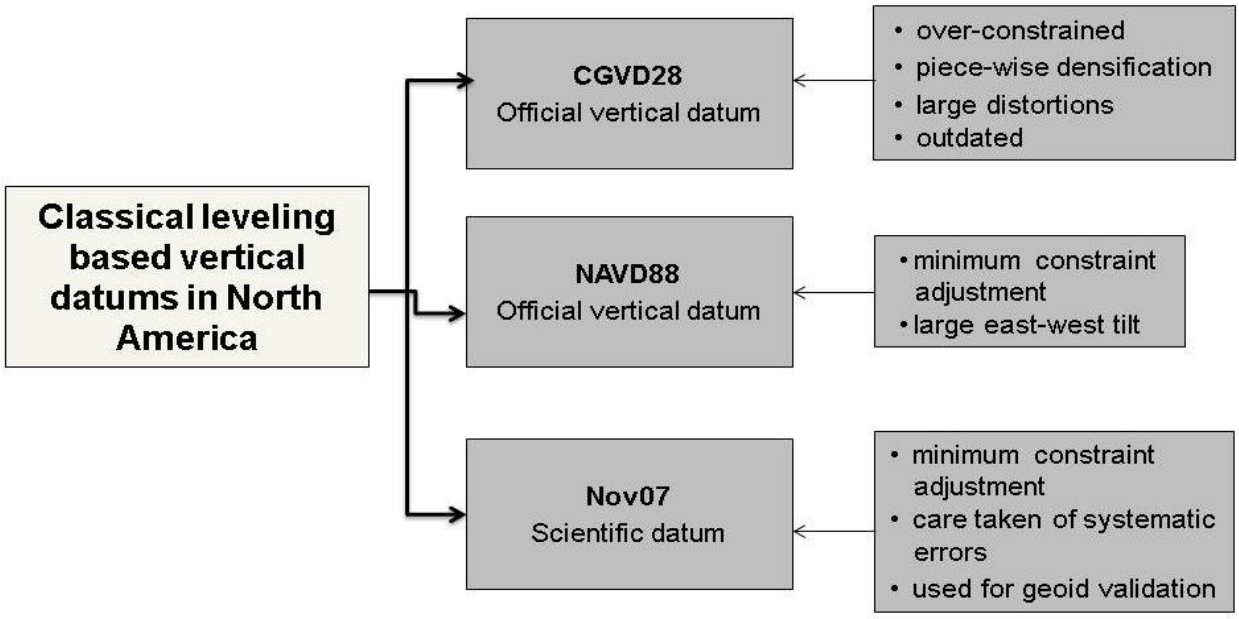

Figure 2.3: Classical levelling based vertical datums in North America.

2.5.1 CGVD28

The Canadian Geodetic Vertical Datum of 1928 (CGVD28) is the official vertical datum of Canada. It is based on an adjustment of levelling measurements prior to 1928 with constraints to the mean sea level at six tide gauges: Vancouver (BC), Prince-Rupert (BC),

Point-au-Père (QC), Halifax (NS), Yarmouth (NS), and New York City and is accessible through approximately 80,000 benchmarks mostly distributed in southern Canada (Véronneau 2006). All levelling measurements consisting of re-observations or extensions since the original adjustment have been processed according to the same procedure and constrained to the 1928 original adjustment. The CGVD28 heights are said to be "normal-orthometric heights" given that the heights are evaluated using normal gravity values based on latitude instead of actual gravity measurements. Hence, the heights are neither orthometric nor normal heights and as a result CGVD28 does not coincide with either the geoid or the quasi-geoid (Véronneau 2006). Moreover, the sea surface topography at the tide gauge stations, the rising of the sea level due to melting of glaciers and thermal expansion, earthquakes, frost heave, local instabilities, and the fact that land elevation is changing due to the rebound/subsidence of the Earth's crust (i.e., post-glacial rebound) have not been accounted for in the realization of the CGVD28. Additionally, the levelling data used in CGVD28 are not corrected for systematic errors due to atmospheric refraction, rod calibration, rod temperature, and the effects of solar and lunar tides on the Earth's geopotential surfaces. The CGVD28 datum has a national distortion that ranges from -65 cm in Eastern Canada to 35 cm in Western Canada with respect to an equipotential surface due to various correction omissions, approximations, and the fact that the vertical control network was established over time in a piece-wise manner (Véronneau and Héroux 2006). Currently, the network is characterized by a rapid rate of degradation due to destruction and loss of physical markers and limited maintenance as Canada is planning to implement a geoid-based GNSS-accessible vertical datum by 2013 (Véronneau et al. 2006).

2.5.2 NAVD88

The North American Vertical Datum of 1988 (NAVD88) was the result of a joint effort in the 1970s and 1980s by the governmental agencies of U.S.A., Canada, and Mexico to unify the vertical control networks on the continent. It is currently the official vertical datum in the U.S.A. The NAVD88 was established by the minimum-constraint adjustment of geodetic levelling observations in Canada, U.S.A., and Mexico, holding

fixed the height of the primary tidal benchmark at Rimouski, Quebec, Canada. Due to the demonstrated spatial (and to a lesser extent temporal) variations in the sea surface topography, additional tidal benchmark elevations were not utilized. NAVD88 heights are Helmert orthometric heights. The NAVD88 datum contains a large east-west tilt of 1.5 m from the Atlantic to Pacific coasts, possibly due to the accumulation of systematic errors in the levelling network, and as a result was never officially adopted in Canada (Véronneau and Héroux 2006).

2.5.3 Nov07

The Nov07 vertical datum is the latest realization of a series of minimum-constraint adjustments of the federal first-order levelling network in Canada. However, it should be noted that Nov07 is not an official vertical datum. It has been realized for the purpose of validating geoid models in North America with the heights of benchmarks given as Helmert orthometric heights. The main network covers the continental main land, and includes independent networks for Newfoundland, Vancouver Island, and various other islands. In addition, there is a series of independent local networks around tide gauges in the northern region of Canada. The former tide gauge in Pointe-au-Père, Quebec (QC), on the lower St. Lawrence River, is the fixed station for the Canadian mainland network. Similarly, each of the other sub-regions, containing their own independent networks, have their adjustments tied to their own respective fixed tide gauge stations. It was found that the best approach to decrease the systematic error for Nov07 was to adjust together only the most recent levelling measurements that allow a continuous network between Vancouver and Halifax. This resulted in a discrepancy between the two coasts of 80 cm, which represents about 20 to 30 cm of systematic error over approximately 6000 km of levelling lines (Véronneau 2012). The remaining 50-60 cm accounts for the separation between the mean water levels on the west and east coasts of Canada (Véronneau 2012). This separation was first reported by Sturges (1967), where it was shown that MSL values at tide gauges on the Pacific coast appeared to be systematically 60-70 cm higher than those of similar latitude on the Atlantic coast, which was later shown to be caused by a combination of ocean density differences and boundary current effects (Sturges 1974).

2.5.4 Problems Presented by Classical Levelling Based Vertical Datums and the Adoption of a Geoid-Based and GNSS-Accessible Vertical Datum

In the discussion of the vertical datums CGVD28, NAVD88, and Nov07 it is evident that classical levelling based vertical datums have many problems. Firstly, maintaining and realizing a vertical datum based on spirit levelling is expensive, time consuming, and laborious. Moreover, it provides limited coverage over a geographic region, and is especially difficult to do in remote areas and mountainous terrain. Other problems relate to maintaining the vertical control network over time, as benchmark become unstable or disappear completely, and there are temporal effects such as post-glacial rebound that also need to be taken into account. Of course, there is the problem of existing systematic levelling errors and distortions found within the vertical control network. Moreover, as the MSL varies both spatially and temporally, regional vertical datums will refer to different reference surfaces. Currently, there are hundreds of classical levelling based vertical datums in the world and as each of these datums refer to their own reference surface defined by a local MSL, there is a need to be able to relate these datum to each other, or in other words, to unify these datums. This is especially important for engineering projects between two neighbouring countries, or even for a country that may have two different datum zones (e.g., island vs. mainland regions).

Due to the various issues presented by classical levelling based vertical datums, the Geodetic Survey Division (GSD) of Natural Resources Canada (NRCan) and the U.S.A. National Geodetic Survey (NGS) have decided to modernize the way vertical datums are realized by implementing a geoid-based and GNSS-accessible vertical datum. Adopting a geoid-based vertical datum means that there will be no more need for expensive and time-consuming spirit levelling in order to establish a vertical control network. The issue of benchmark stability and coverage is also resolved. The geoid is also a fairly stable reference surface that only has to be updated, in the North American context specifically, for temporal effects such as post glacial rebound once every ten years (Rangelova 2007). Moreover, a geoid-based vertical datum is compatible with space-based positioning techniques such as GNSS. This concept is illustrated by Figure 2.4. The geoid surface is

shown with the red line while the ellipsoidal surface is shown in the green line. The ellipsoidal height h_P can be determined from GNSS while the gravimetric geoid model provides the geoid height N_P. The difference between the ellipsoidal height h_P and the geoid undulation N_P will yield the orthometric height $H^{(j)}_P$, which has traditionally been obtained from levelling.

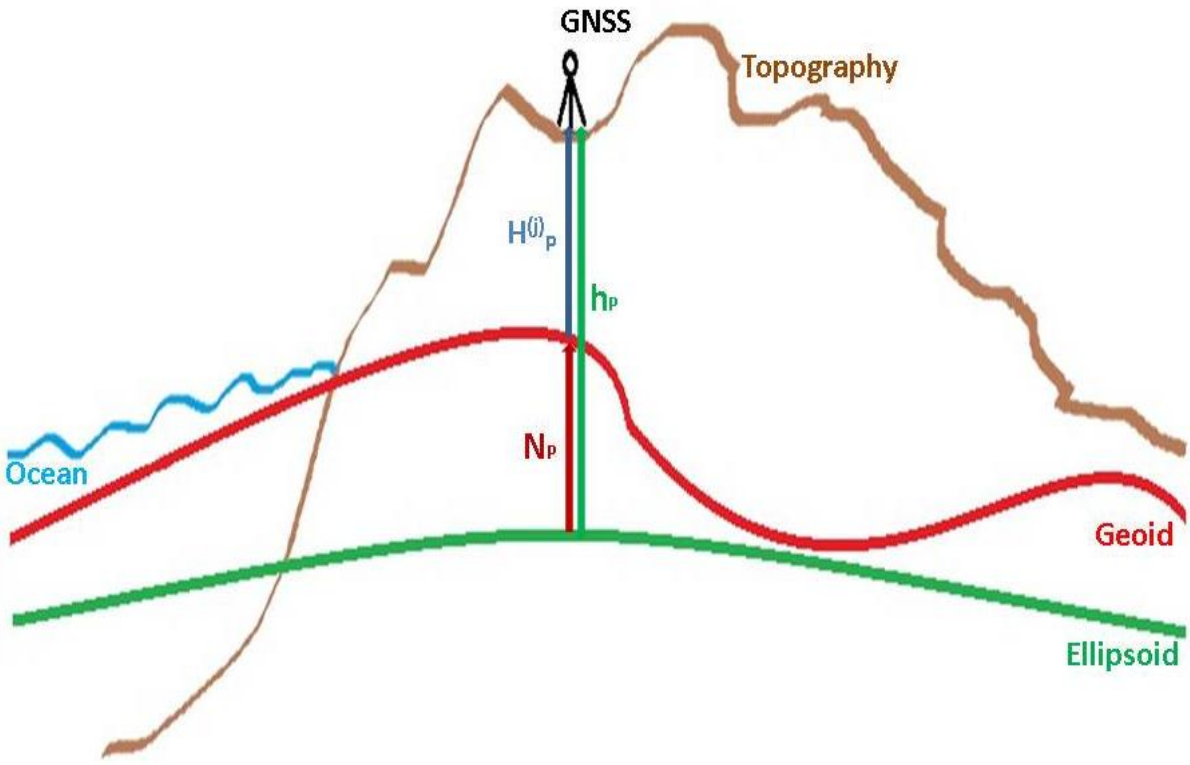

Figure 2.4: Ellipsoidal height *h*, orthometric height *H*, and geoid height *N*.

Figure 2.4 shows the simplified relationship between *h*, *H*, and *N* as *h-H-N=0*. This is because in practice it is assumed that the ellipsoidal normal and the plumb line coincide with each other. In actuality the ellipsoidal normal and the plumb line are offset by an angle β as shown Figure 2.5, which is known as the deflection of the vertical. According to Jekeli (2000), the error that occurs due to the difference between the plumb line and ellipsoidal normal is negligible for topographic heights of the Earth's surface.

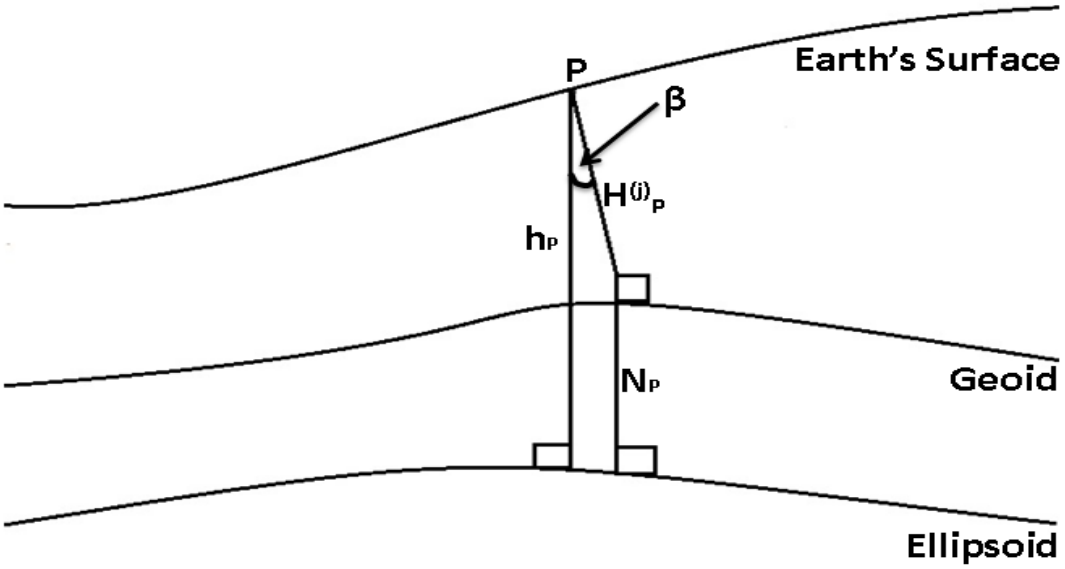

Figure 2.5: Deflection of the vertical β.

For mountainous terrain, β can reach a maximum of 1 arc minute. The effect on the height can be estimated from the height difference, $\delta h \approx h \sin\beta \tan\beta$, which shows that even for the most extreme cases where β is equal to 1 arc minute and h is equal to 4000 meters, the height difference δh is less than 1 mm (Jekeli 2000). As the effect is less than 1 mm, the approximation that the plumb line and the ellipsoidal normal are coincident has no significant effect on results.

Lastly, from the move to implement a geoid based vertical datum, another motivation of datum unification presents itself. The gravity data currently available for North America refer to different vertical datums. Thus, the existing datum offsets between the Canadian and U.S.A. official vertical datums should be computed in order to update the gravity databases for geoid modelling. The estimation of local vertical datum offset for North American vertical datums is the focus of Chapter 4.

2.6 Concepts of Geoid Modelling: The Remove-Compute-Restore Technique

The determination of W is a non-linear problem, which is complicated by the fact that W is not a harmonic function as discussed in Section 2.2. These limitations can be overcome

by linearization and approximation of the shape, size, and gravity field of Earth by those of an equipotential ellipsoid of revolution (i.e., reference ellipsoid) with the same mass and rotational velocity as Earth. The anomalous potential T (i.e., disturbing potential) is defined as the difference between the gravity potential of the Earth and the normal gravity potential of the reference ellipsoid:

$$T = W - U = (V + \Phi) - (V^e + \Phi^e) = V - V^e. \qquad (2.30)$$

From Eq. (2.30) it can be seen that the problem of determining T reduces to determining the difference between the gravitational potentials of the Earth and the ellipsoid. It can be seen that T is a harmonic function (i.e., $\Delta T=0$) as both V and V^e are harmonic. Stokes's theorem states that a harmonic function, such as V or T, can be determined everywhere in free space from values on a boundary surface that encloses all masses.

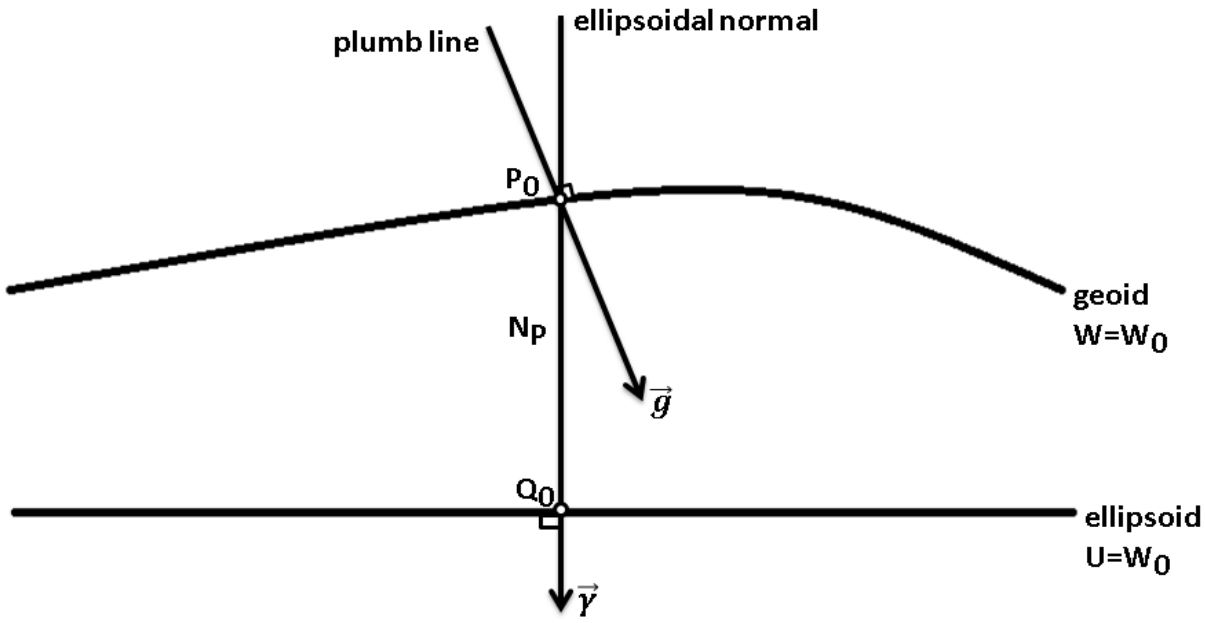

Figure 2.6: Geoid surface W, ellipsoid surface U, gravity vector $\vec{g}$, and geoid undulation N_P (after Heiskanen and Mortiz 1967).

Values that can be measured on the boundary surface are usually gravity measurements, such as gravity disturbances δg and gravity anomalies Δg. The gravity disturbance is the

difference between the gravity the normal gravity at the same point. A gravity anomaly is the difference between the value of gravity at a point P_0 on the geoid and the value of the normal gravity at a point Q_0 on the ellipsoid, which corresponds with the point P_0 on the geoid surface (see Figure 2.6).

The fundamental equation of physical geodesy is an important equation that relates gravity anomalies to the disturbing potential T (Heiskanen and Mortiz 1967):

$$\frac{dT}{dh} - \frac{1}{\gamma}\frac{d\gamma}{dh} + \Delta g = 0. \tag{2.31}$$

Equation (2.31) only holds on the geoid surface and is the boundary condition in Stokes's Boundary Value Problem (BVP). In Stokes's problem the boundary surface is the geoid with potential W, approximated by the ellipsoid with potential U. The surface of the geoid is given by geoid undulations or geoid heights, N, which depends on the disturbing potential through Bruns's equation (Heiskanen and Mortiz 1967):

$$N = \frac{T_P}{\gamma} - \frac{W_{P_0} - U_{Q_0}}{\gamma}, \tag{2.32}$$

and by selecting $W_{P_0} = U_{Q_0} = W_0 = const.$, the equation simplifies to:

$$N = \frac{T_P}{\gamma}. \tag{2.33}$$

Thus, Bruns's formula shows that the surface of the geoid can be determined provided that T is known. Equation (2.31) shows that T can be estimated from gravity observations on the boundary surface. As the boundary surface in Stokes's BVP is the geoid, the gravity measurements need to the reduced to the geoid by terrain reductions, which requires assumptions about the topographic density distribution.

Stokes's BVP is based on the mathematical definition given by the Laplace differential equation:

$$\Delta T = \frac{d^2T}{dx^2} + \frac{d^2T}{dy^2} + \frac{d^2T}{dz^2} = 0, \tag{2.34}$$

with the boundary condition given in spherical approximation (Heiskanen and Mortiz 1967) as:

$$\frac{dT}{dr} + \frac{2}{r}T + \Delta g = 0. \tag{2.35}$$

It should be noted that spherical approximation is used only in equations relating the small quantities of anomalous potential *T*, geoid undulations *N*, gravity anomalies Δg, and deflections of the vertical, among others. The reference is not the sphere but the ellipsoid, thus the normal gravity γ in Δg and δg must be computed precisely for the ellipsoid.

Analytical solutions to the Stokes's BVP can be expressed as spherical harmonic series since *T* is harmonic. Thus, using Bruns's equation the geoid undulation can also be expressed in terms of spherical harmonic series (in a spherical approximation on the geoid):

$$N(\varphi_P, \lambda_P) = R \sum_{n=2}^{\infty} \sum_{m=0}^{n} [\bar{C}_{nm} \cos m\lambda_P + \bar{S}_{nm} \sin m\lambda_P] \bar{P}_{nm} \sin \varphi_P, \tag{2.36}$$

where $\bar{C}_{nm}$ and $\bar{S}_{nm}$ are fully normalized geopotential coefficients of the anomalous potential, $\bar{P}_{nm}$ are the fully normalized Legendre functions (Heiskanen and Moritz 1967), and φ_P, λ_P are the latitude and longitude of the computational point. Similarly, using Eq. (2.35), Δg can also be expressed in terms of spherical harmonic series:

$$\Delta g(\varphi_P, \lambda_P) = \bar{\gamma} \sum_{n=2}^{\infty} (n-1) \sum_{m=0}^{n} [\bar{C}_{nm} \cos m\lambda_P + \bar{S}_{nm} \sin m\lambda_P] \bar{P}_{nm} \sin \varphi_P, \tag{2.37}$$

where $\bar{\gamma}$ is the mean normal gravity.

As well, the analytical solution of Stokes's BVP can be expressed by the Stokes integral (Heiskanen and Moritz 1967):

$$N = \frac{R}{4\pi\gamma} \iint_{\sigma} \Delta g S(\psi) d\sigma, \tag{2.38}$$

where σ denotes the Earth's surface. $S(\psi)$ is the Stokes' kernel function given by (Heiskanen and Moritz 1967):

$$S(\psi) = \frac{1}{\sin(\frac{\psi}{2})} - 6\sin\frac{\psi}{2} + 1 - 5\cos\psi - 3\cos\psi \ln\left(\sin\frac{\psi}{2} + \sin^2\frac{\psi}{2}\right). \tag{2.39}$$

In Eq. (2.39), ψ is the spherical distance between the data point (φ, λ) and the computation point (φ_P, λ_P):

$$\sin^2\frac{\psi}{2} = \sin^2\frac{\varphi_P - \varphi}{2} + \sin^2\frac{\lambda_P - \lambda}{2}\cos\varphi_P\cos\varphi. \tag{2.40}$$

The geoid signal can be decomposed into long, medium, and short wavelength components as shown in Figures 2.7 and 2.8. The long wavelength components of the geoid signal come from the harmonic coefficients of global geopotential models (GGMs; this is also synonymous with global gravity models), which are derived primarily from data collected from dedicated satellite gravity field missions. The medium wavelength components are a result of local gravity anomalies, which can be observed from terrestrial, shipborne, airborne, and even satellite platforms. The short wavelength or high frequency components of the gravity field signal or the geoid signal are mainly a result of the Earth's topography. This information is usually available from digital elevation models (DEMs).

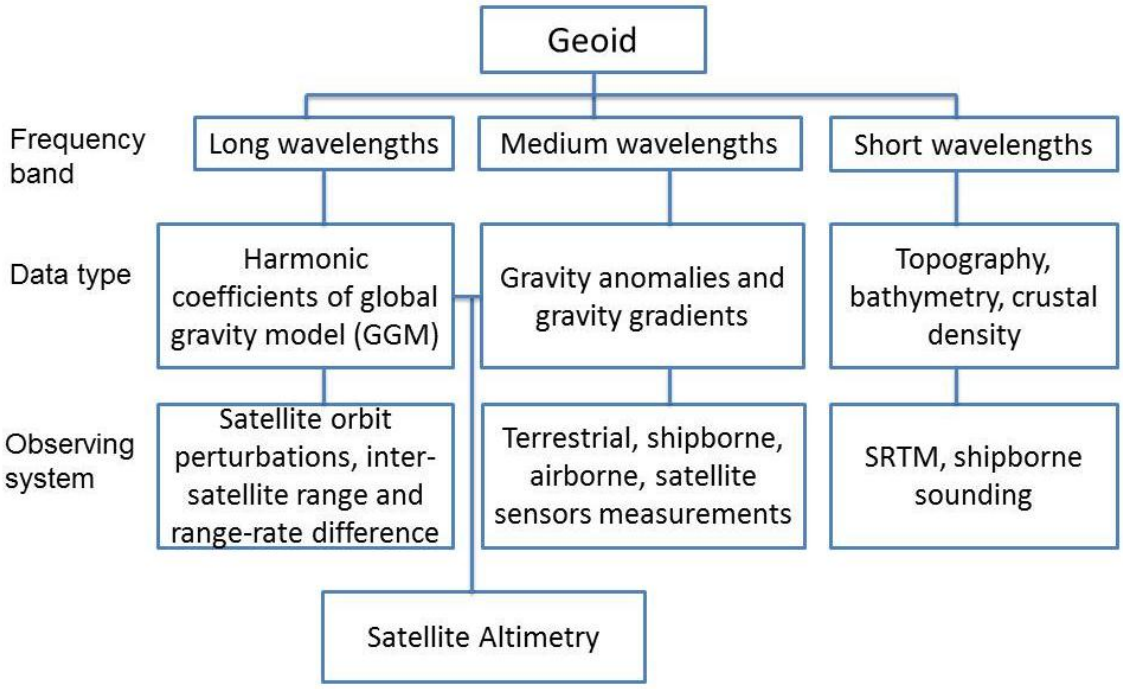

Figure 2.7: Data for geoid computation.

The use of Eq. (2.38) requires gravity anomaly coverage all over the Earth for the computation of a single geoid undulation. Of course this is an impractical requirement, as gravity anomalies do not have global coverage, or even if there is global coverage, the data is not always available for scientific and civilian use. Thus, Eq. (2.38) can only be applied to a limited region. In such a case, the long wavelength contributions of the gravity field will not be present in the results and will have to be computed from the spherical harmonic coefficients of a GGM. Moreover, the integral in Eq. (2.38) is discretized, and is evaluated as a summation using discrete data. Thus, due to the available density of the gravity data, the short wavelength components will be aliased. As a result, the short wavelengths must be evaluated from topographic heights. In other words, the gravity anomalies utilized with Eq. (2.38) have the contributions from the topography and the GGM removed (i.e., short and long wavelength contributions are removed). Thus the 'remove' stage in the remove-compute-restore technique (Molodensky et al. 1962; Mortiz 1966; Vincent and Marsh 1974; Rapp and Rummel 1975) for geoid modelling involves the computation and removal of the GGM and terrain contribution from the free air gravity anomalies while the 'restore' step involves the restoration of the GGM contribution and the terrain contribution to N via the indirect

effect term N^H. This concept is illustrated in Figure 2.8, which shows the contributions of different data to regional geoid determination.

The smooth geoid N^{GM} is the contribution of the spherical harmonic coefficients from a GGM. The slightly more detailed line indicated by $N^{GM}+N^{\Delta g}$ shows the geoid surface with contributions from long and medium wavelength components from GGMs and the use of Stokes's integral with gravity anomalies that have the long and short wavelength contributions of the gravity signal removed (i.e., hence only medium contributions). Lastly, the $N^{GM}+N^{\Delta g}+N^H$ shows the detailed geoid, where short wavelengths due to of the Earth's topography are realized through the indirect effect on the geoid.

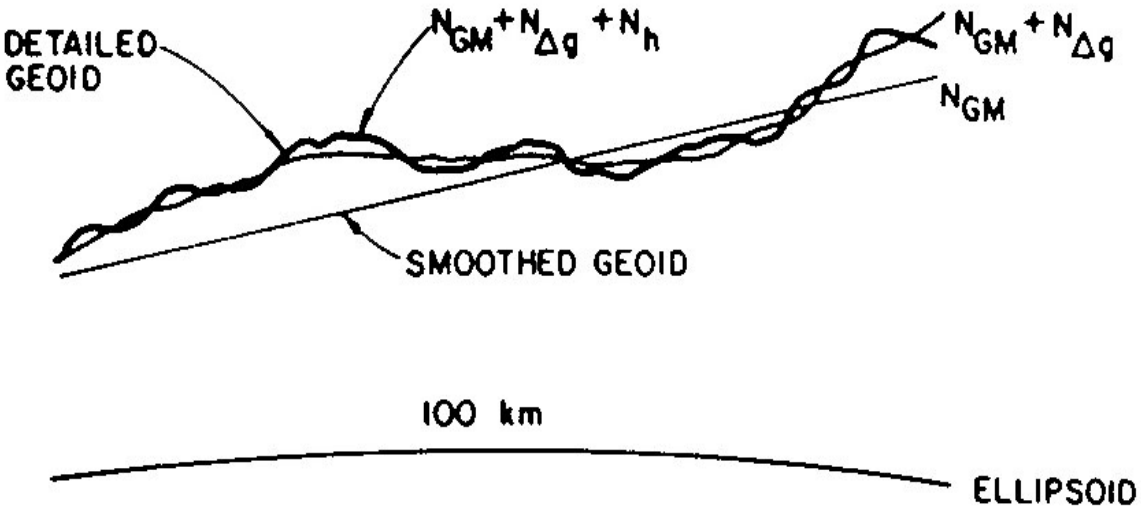

Figure 2.8: Practical computation of the geoid (Schwarz et al. 1987).

The residual gravity anomaly shown as Δg in Figure 2.8 is a determined as:

$$\Delta g = \Delta g^{FA} - \Delta g^{GM} - \Delta g^{H}, \tag{2.41}$$

where Δg^{FA} is the free-air gravity anomaly measured from terrestrial, shipborne, or airborne platforms; Δg^{GM} is the gravity anomaly which represents the long wavelength

component of the gravity signal and is determined from a finite global geopotential model; and lastly, Δg^H is the topography-reduced gravity anomaly.

To summarize, N^{GM} and Δg^{GM} can be evaluated using Eq. (2.36) and (2.37). For small distances, inside a certain area *E*, one may use the planar approximation for Eq. (2.38) where the first term in the $S(\psi)$ is the dominant one (Sansó and Sideris 2013):

$$\frac{1}{\sin\psi/2} = \frac{2}{\psi} = \frac{2R}{l}, \tag{2.42}$$

$$R^2 d\sigma = dxdy, \tag{2.43}$$

and therefore Eq. (2.38) simplifies to:

$$N_P^{\Delta g} = \frac{1}{2\pi\gamma}\iint_E \frac{\Delta g}{l} dxdy, \tag{2.44}$$

where

$$l = \sqrt{(x - x_P)^2 + (y - y_P)^2}. \tag{2.45}$$

The coordinates of the data points are denoted by (x, y) and the coordinates of the computation points are denoted by (x_p, y_P).

It has already been mentioned that Eq. (2.38) only gives the geoid undulation provided that no masses are outside the geoid surface. One way to take care of topographic masses of density ρ is through Helmert's 2nd condensation reduction, which can be approximately applied in three steps (see Figure 2.9; Sansó and Sideris 2013):

1) remove all masses above the geoid,
2) lower the stations from P to P_0 using the free-air reduction F,
3) and restore masses condensed on a layer on the geoid with density $\sigma=\rho H$.

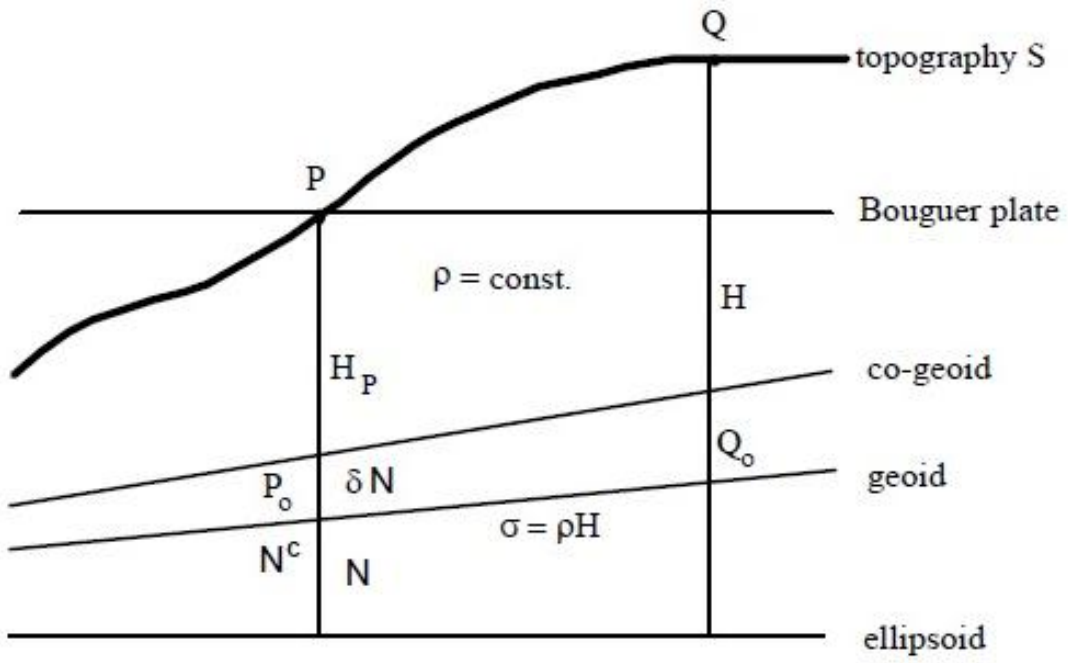

Figure 2.9: Actual and condensed topography in planar approximation (Sideris 1990).

Helmert's 2nd condensation gives Δg on the geoid computed from (Sansó and Sideris 2013):

$$\Delta g = \Delta g_P - A_P + F + A_{P_0}^C, \tag{2.46}$$

where $\Delta g_P + F$ is the free-air gravity anomaly at P, A_P is the attraction of the topography above the geoid at P, and $A_{P_0}^C$ is the attraction of the condensed topography at P_0 (see Figure 2.9). The attraction change is denoted by δA_P (see Eq. (2.49)), which is simply $-A_P + A_{P_0}^C$ in Eq. (2.46). It should be noted that, in this approximation, the attraction of the condensed topography in Eq. (2.46) is computed on the geoid surface in order for the reduced gravity to refer to the geoid (i.e., which is actually the co-geoid in this case) and so that the reduced gravity can be used with Eq. (2.44). For further discussion, one may refer to Wichiencharoen (1982), Wang and Rapp (1990), Sideris (1990), and Sansó and Sideris (2013).

Due to the shifting masses, the potential changes as well by an amount known as the indirect effect on the potential (Sansó and Sideris 2013):

$$\delta T = T_{P_0} - T^C_{P_0,} \tag{2.47}$$

where T_{P_0} is the potential of the topographic masses at P_0 and $T^C_{P_0}$ is the potential of the condensed masses at P_0. Due to this potential change, Eq. (2.38) with Δg from Eq. (2.46) produces a surface that in known as the co-geoid (i.e., a surface different from the geoid). The difference between the geoid and the co-geoid is denoted by δN in Figure 2.9, which is the indirect effect of the shifted topography on the geoid. Ideally, the indirect effect should be small (i.e., the co-geoid should be near the geoid) in order to allow approximations in the geoid modelling computations. Helmert reduced gravity anomalies yields a small indirect effect (e.g., $\partial\ \delta N/\partial H \approx$ 1m/3km; Sansó and Sideris 2013) and is therefore very suitable for geoid determination. Before one can apply Eq. (2.38), the gravity anomalies must be transformed from the geoid to the co-geoid by applying a correction $\delta\Delta g$ known as the indirect effect on gravity (Sansó and Sideris 2013):

$$\delta\Delta g = -\frac{1}{\gamma}\frac{d\gamma}{dh}\delta T. \tag{2.48}$$

The final geoid height is a sum of the co-geoid height and the indirect effect on the geoid. When using the remove-compute-restore technique the terrain effect on Δg and the indirect effect can be respectively approximated in planar approximation as (Sansó and Sideris 2013):

$$\delta A_P = -\Delta g_P^H \approx \frac{1}{2} G\rho \iint_E \frac{H^2 - H_P^2}{l^3} dxdy, \tag{2.49}$$

and

$$\delta N_P = N_P^H \approx -\frac{\pi G\rho}{\gamma} H_P^2 - \frac{G\rho}{6\gamma} \iint_E \frac{H^3 - H_P^3}{l^3} dxdy. \tag{2.50}$$

Thus the remove-compute-restore technique can be applied as follows:

1) Earth surface gravity observations should be reduced on to the geoid.
2) Compute the long wavelength component of the gravity field signal, i.e., Δg^{GM} and N^{GM}, using Eq. (2.36) and Eq. (2.37).
3) Compute the topography-reduced gravity anomaly using Eq. (2.49).
4) Compute the residual gravity anomaly using Eq. (2.41).
5) Evaluate the residual or co-geoid heights by applying Stokes's integral (i.e., Eq. (2.44)).
6) Compute the indirect effect of the topography on the geoid using Eq. (2.50).
7) Restore the effects of the long (i.e., geoid undulations determined from the GGM) and short wavelength components (i.e., indirect effect on the geoid) of the geoid signal to the residual/co-geoid heights (i.e., geoid heights from step (5)).
8) In the case that the reference ellipsoid mass M^e and the normal gravity potential U_0 are different from that of the geoid add the zero-degree term to the geoid undulations (Heisaknen and Mortiz 1967):

$$N_0 = \frac{GM - GM^e}{R^e \gamma} - \frac{W_0 - U_0}{\gamma}, \tag{2.51}$$

where R^e is the mean radius of the reference ellipsoid.

On a final note, the use of Eq. (2.38) is computationally time consuming due to the fact that the integration must take place over the entire surface of the Earth. This can be overcome by reducing the size of the integration area by modifying the Stokes kernel function, as the truncation error that results by limiting the area of integration of the terrestrial gravity anomalies to a spherical cap can be reduced by an appropriate modification of the Stokes kernel (Molodensky et al. 1962; Jekeli 1982; Hsu 1984). Alternatively, increasing the size of the integration area has been shown to improve the results (Schwarz 1984; Sjöberg 1986), though these methods have not proven to be superior to the remove-compute-restore technique (Sansó and Sideris 2013). However, integrals such the one shown in Eq. (2.44) are convolution integrals, and can thus be

evaluated by fast Fourier techniques (FFT) provided that the data is given on regular grids (Sansó and Sideris 2013). Using FFT there is no need for time consuming point-wise numerical summations. Moreover, FFT gives results on the same grid as the data was provided on. Therefore, spectral techniques based on FTT overcome the problem of slow computation speed and provide a homogenous coverage of results, which is beneficial for interpolation and plotting purposes (Sansó and Sideris 2013). Moreover, with FFT there is also no need to modify the Stokes kernel function (Schwarz et al. 1987; Sideris and Forsberg 1990). It is thus recommended that for the computation of large regional and continental geoids, spectral techniques such as FFT should be implemented, especially since gravity and terrain data are readily available on regular grids (Sansó and Sideris 2013).

Gravsoft (developed by C.C. Tscherning, R. Forsberg, P. Knudsen and D. Arabelos at the University of Copenhagen) and *FFTGeoid* (developed by Y.C. Li and M.G. Sideris at the University of Calgary) software products may be used for geoid modelling. It should be noted that *Gravsoft* is not commercially available; however it can be made available by request for the purpose of scientific research.

Lastly, as the focus of this thesis is not geoid modelling but rather the contribution of the GOCE dedicated satellite gravity field mission to the application of vertical datum unification and to the determination of W_0, the treatment of geoid modelling has not been exhaustive herein. For full derivations and more details on any of the material covered in this chapter, Hofmann-Wellenhof and Moritz (2006), Heiskanen and Moritz (1967), Jekeli (2000), and Sansó and Sideris (2013) should be consulted.

CHAPTER 3
EVALUATION OF GOCE GLOBAL GEOPOTENTIAL MODELS

3.1 Introduction

As discussed in the previous chapter, a global geopotential model or a global gravity model is a set of coefficients that model the external gravity field of the Earth and are derived from data collected from dedicated satellite gravity field missions and/or terrestrial data. These coefficients are known as spherical harmonic coefficients and can be used to compute different functionals of the Earth's gravity field. The three dedicated satellite gravity field missions are the Challenging Mini-Satellite Payload (CHAMP), the Gravity Recovery and Climate Experiment (GRACE), and the GOCE mission. The CHAMP satellite was launched July 15, 2000 with the objective to map the Earth's geopotential via the analysis of orbit perturbations (Reigber et al. 2002). The GRACE mission was launched a few years later on March 17, 2002 with the objective to map the global gravity field with a spatial resolution of 400 to 40,000 km every thirty days, and has contributed significantly to the understanding of the time-variable aspect of the Earth's gravity field (Tapley et al. 2004). CHAMP and GRACE have provided static gravity field solutions at the decimetre level of geoid accuracy up to degree and order 60 and 120, respectively (Sneeuw and Schaub 2004). Lastly, GOCE was launched on March 17, 2009 by the European Space Agency in order to measure the Earth's gravity field at an unprecedented accuracy and spatial resolution (Drinkwater et al. 2003). By the end of its mission, the GOCE satellite is expected to determine gravity anomalies with an accuracy of 1 mGal and the geoid with an accuracy of 1-2 cm while achieving a spatial resolution of 100 km. In order to put the GOCE accuracy requirement into context, the estimated cumulative geoid accuracy for the combined model *EGM2008*, which contains terrestrial gravity data, is 7 cm at degree and order 200 while for the GRACE only satellite model *itg-grace2010s* (Mayer-Gürr et al. 2010) it is 20 cm at degree and order 180 (Pail et al. 2011). Since the launch of the GOCE satellite, four generations of GOCE-based GGMs have been released. These GGMs are available for download from the International Centre for Global Earth Models (ICGEM, http://icgem.gfz-

potsdam.de/ICGEM/). Gruber et al. (2011) have shown that with two months of GOCE data, the global geoid accuracy is about 5-6 cm with a 111 km spatial resolution. With the recent release of fourth generation GOCE GGMs that contain approximately 27 months of GOCE observations, the global geoid accuracy is approximately 1.2 cm at a spatial resolution of 100 km, which corresponds to a degree and order of approximately 200 (see Figure 3.9).

The performance of GGMs can be assessed using external datasets such as geoid heights obtained from GNSS and levelling, astro-geodetic deflections, and gravity anomalies, among others (see, e.g., Gruber 2004; Gruber 2009; Hirt et al. 2010; Hirt et al. 2011; Hirt et al. 2012; Huang and Véronneau 2009; Kotsakis and Katsambalos 2009; Ince et al. 2012). External or independent datasets refer to quantities that have not been utilized in the construction of the GGMs. The objective of this chapter is to evaluate the performance of satellite-only GOCE-based GGMs in North America using geoid heights obtained from GNSS and levelling in order to determine the best GOCE-based model in North America for height system unification and W_0 determination. The use of a GOCE satellite-only GGM is preferred for such applications because it provides a globally consistent and unbiased geoid (Gerlach and Rummel 2013). Thus, the aim is to show which GOCE GGM performs best in Canada and the U.S.A.

In the next section of this chapter, the satellite gravity missions CHAMP, GRACE, and GOCE are briefly reviewed. In Section 3.3, the methodology and distribution of the GNSS/levelling benchmarks used for the evaluation of GOCE GGMs in North America are described. Results are presented and discussed in Section 3.4 and a summary is given in Section 3.5.

3.2 Overview of Dedicated Satellite Gravity Field Missions

According to Rummel et al. (2002), when designing dedicated satellite gravity field missions the following four requirements should be considered:

1) uninterrupted satellite tracking in three spatial dimensions,

2) measurement or compensation of the effect of non-gravitational forces,
3) the orbit altitude of the satellite should be as low as possible, and
4) measurement of gravity gradients.

At present, there are three main techniques available for the determination of the Earth's gravity field from dedicated satellite missions: satellite-to-satellite tracking between high and low orbiting satellites (SST-hl), satellite-to-satellite tracking between low Earth orbiting (LEO) satellites (SST-ll), and satellite gravity gradiometry (SGG); see Figures 3.1 to 3.3.

In the SST-hl technique, the orbits of high orbiting satellites such as GNSS are assumed to be known accurately so that an accurate three dimensional position is provided while the velocity and acceleration information of the LEO satellite is determined from satellite-to-satellite tracking between the high and low orbits.

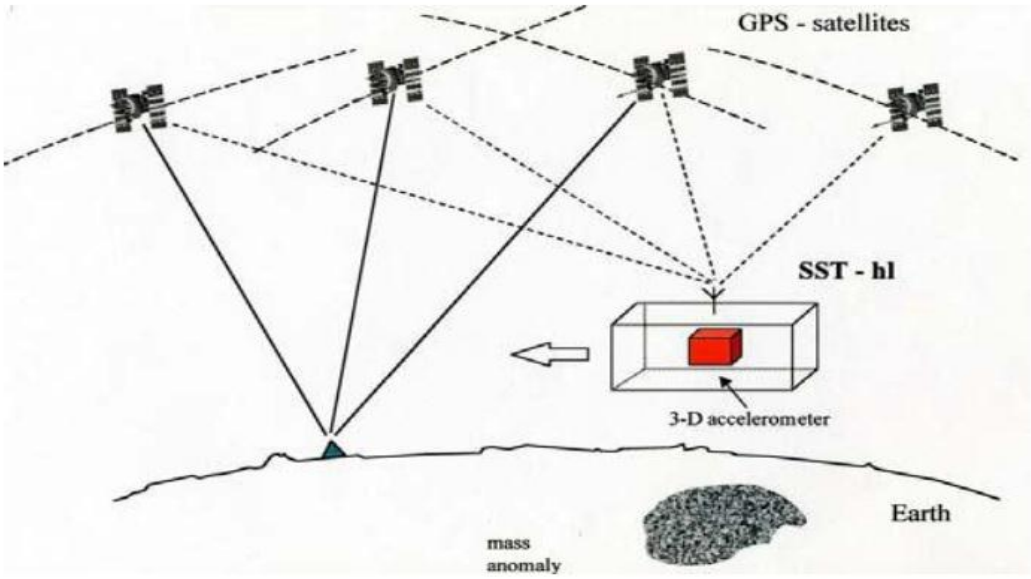

Figure 3.1: Schematic diagram of the concept of satellite-to-satellite tracking in the high-low mode (SST-hl) (Rummel et al. 2002).

The SST-ll principle is based on the line of sight measurement of range and the acceleration difference between two LEO satellites. In the SGG method, gravity acceleration measurements are observed in three dimensions over the short baselines of a

gradiometer. CHAMP utilizes the SST-hl technique, satisfying requirements (1) and (2) as outlined by Rummel et al. (2002). The GRACE satellite mission utilizes the SST-ll technique and satisfies requirements (1), (2), and partially requirement (4). The GOCE mission utilizes the SGG and SST-hl techniques, which satisfy all the requirements posed by Rummel et al. (2002).

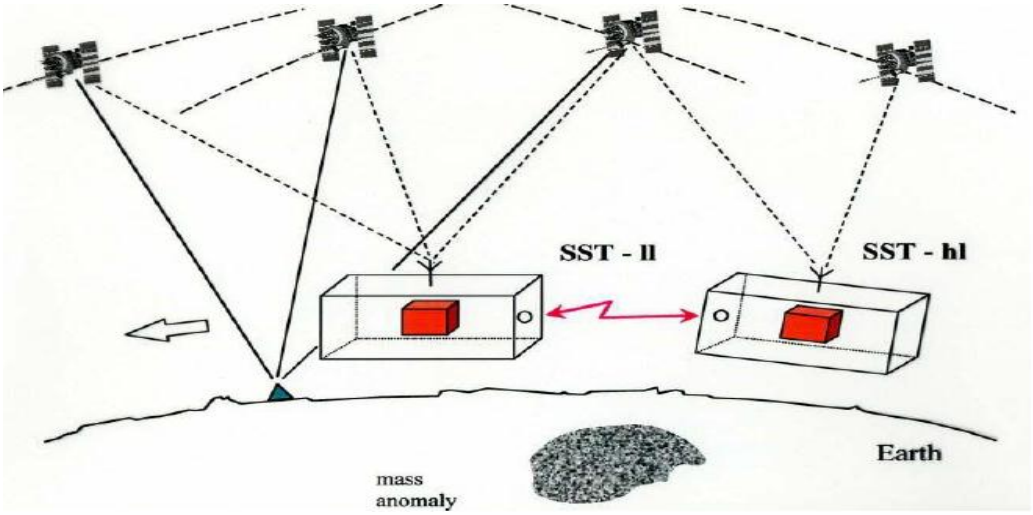

Figure 3.2: Schematic diagram of the concept of satellite-to-satellite tracking in the low-low mode (SST-ll) combined with SST-hl (Rummel et al. 2002).

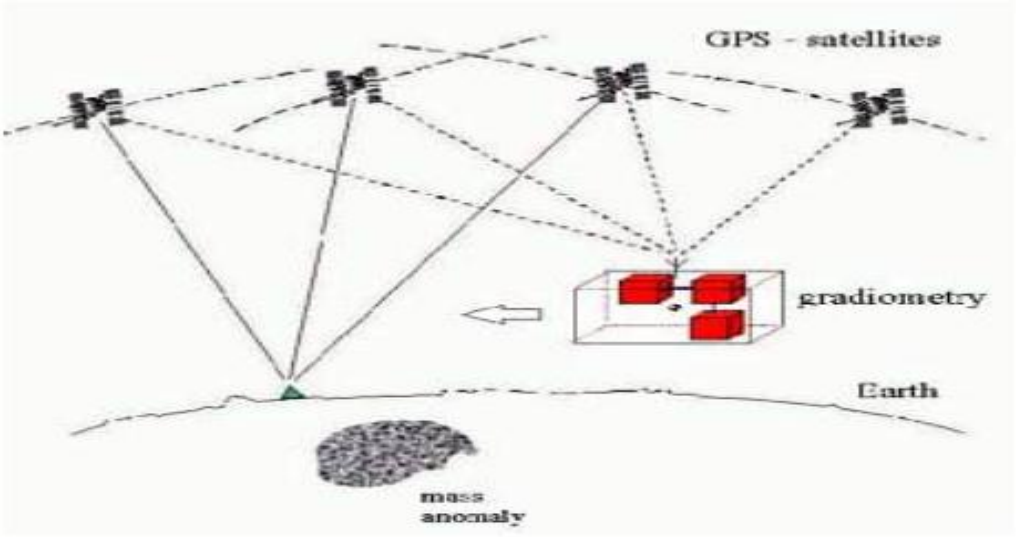

Figure 3.3: Schematic diagram of the concept of satellite gradiometry combined with SST-hl where 2nd order derivatives of the gravitational potential are measured in a LEO satellite by differential accelerometry (Rummel et al. 2002).

The CHAMP mission was put into orbit in order to measure the gravity and magnetic fields of the Earth. It was in operation for over ten years with the mission ending on September 19, 2010. The mission carried a GNSS receiver with continuous 3D tracking capability and a precise accelerometer to measure non-gravitational forces. The orbit of CHAMP was near circular with an 87 degree inclination and an altitude that decayed from approximately 450 km to 300 km by the end of the mission. One of the first developed GGMs using six months of CHAMP data improved the pre-CHAMP era GGM GRIM5-S1 constructed using satellite orbit perturbations (Biancle et al. 2000) by almost one order of magnitude up to degree and order 35 (Reigber et al. 2003; Pail et al. 2011).

The GRACE mission consists of two identical satellites following each other in the same orbit by a separation distance of 200 km. The microwave Ka-band link via an inter-satellite ranging system observes the relative motion of the twin satellites with very high accuracy while the GNSS receivers measure the positions of the satellites, allowing observations between the high and low orbiting satellites. Similarly to CHAMP, the GRACE mission is also equipped with an on-board accelerometer to account for non-gravitational forces. The mission has a near circular orbit with an 89 degree inclination at an orbit altitude of 485 km. According to Pail et al. (2011), the GRACE-based GGMs gained approximately two orders of magnitude in accuracy (i.e., 1 cm geoid error at degree and order 100) as compared with GRIM5-S1.

In contrast to the CHAMP and GRACE missions, the SGG on board the GOCE mission provides medium to short wavelength components of the gravity field as it measures the second derivatives of the gravitational potential while the SST-hl mode is used to determine the orbit and thus provides the long wavelength information of the gravity field. In Chapter 2 it was shown that the gravitational potential can be expressed as a spherical harmonic function (see Eq. (2.2)). Since the second derivate of the gravitational potential is a functional of the potential, it too can be expressed in terms of a spherical harmonic function. Such a function relates the GOCE observations to the spherical harmonic coefficients that make up a GGM. Thus, by solving a large system of equations via least squares the GGM coefficients can be deduced from GOCE observations. A

comprehensive discussion of GOCE data processing can be found in Pail et al. (2011). The GOCE satellite has a sun synchronous orbit with an inclination of 96.7 degrees, and was launched with an initial altitude of 270 km. Due to the inclusion of the gravity gradiometer on board the GOCE mission, as well as the lower orbit altitude, the GOCE-based GGMs are expected to outperform the pre-GOCE era GGMs based only on CHAMP and GRACE data. GOCE observations have allowed for the construction of satellite only GGMs that extend to degree and order 250-260 (see Table 3.1).

The various GGMs that are evaluated in this chapter are listed in Table 3.1. The first generation GOCE models are indicated with *r1* at the end of the model name and have been computed from two months of GOCE observations. The second generation GOCE models are indicated with *r2* at the end of the model name and are constructed from approximately six to eight months of GOCE observations. The third generation GOCE models are indicated with *r3* at the end of the model name and are based on twelve months of GOCE observations while the fourth generation GOCE models are indicated with *r4* at the end of the model name and are based on approximately 27 months of GOCE observations. The DGM-1s model is an exception to this rule, as it contains 10 months of GOCE observations. In addition to the GOCE-based models (which includes GOCE-GRACE combined models), two GRACE-based models are also evaluated as pre-GOCE era models in order to identify any improvements of the new GOCE-based models in North America. Although generally each generation of the GOCE-based models use exactly the same period of GOCE observations, they differ in their computation strategies, the a-priori information used, and their spectral resolutions.

There are four different types of GOCE-based models which are based on how the models are constructed and they include: the time-wise approach indicated by *tim* in the model name, the space-wise approach indicated by *spw* in the model name, the direct approach indicated by *dir* in the model name, and combined models, which have no clear defining feature in their nomenclature.

Table 3.1 Global geopotential models.

Model	**n_{max}**	**Data Source**	**References**
go_cons_gcf_2_dir_r4	260	GOCE direct approach based on 27.5 months of data and go_cons_gcf_2_dir_r3 as a background model	Bruinsma et al. 2010
go_cons_gcf_2_dir_r3	240	GOCE direct approach based on 12 months of data and go_cons_gcf_2_dir_r2 as a background model	Bruinsma et al. 2010
go_cons_gcf_2_dir_r2	240	GOCE direct approach based on 8 months of data and itg-grace2010s as a background model	Bruinsma et al. 2010
go_cons_gcf_2_dir_r1	240	GOCE direct approach based on 2 months of data and eigen-5c as a background model	Bruinsma et al. 2010
go_cons_gcf_2_tim_r4	250	GOCE time-wise approach based on 12 months of data	Pail et al. 2011
go_cons_gcf_2_tim_r3	250	GOCE time-wise approach based on 12 months of data	Pail et al. 2011
go_cons_gcf_2_tim_r2	250	GOCE time-wise approach based on 8 months of data	Pail et al. 2011
go_cons_gcf_2_tim_r1	224	GOCE time-wise approach based on 2 months of GOCE data	Pail et al. 2010a
goco03s	250	GOCE combined model based on 12 month of GOCE data, 7 years of GRACE data, 8 years of CHAMP data and 5 years of SLR	Mayer-Gürr et al. 2012
goco02s	250	GOCE combined model based on 8 months of GOCE data, 7 years of GRACE data, 8 years of CHAMP data and 5 years of SLR	Goiginger et al. 2011
goco01s	224	GOCE combined model based on 2 months of GOCE data and 7 years of GRACE data	Pail et al. 2010b
DGM-1s	250	GOCE combined model based on 10 months of GOCE data and 7 years of GRACE data	Hashemi Farahani et al. 2012
go_cons_gcf_2_spw_r2	240	GOCE space-wise approach based on 8 months of data	Migliaccio et al. 2011

Model	n_{max}	Data Source	References
go_cons_gcf_2_spw_r1	210	GOCE space-wise approach based on 2 months of GOCE data	Migliaccio et al. 2010
itg-grace2010s	180	based on 7 years of GRACE data	Mayer-Gürr et al. 2010
eigen-6s	240	GOCE combined model based on 6.7 months of GOCE data and 6.5 years of GRACE and SLR data	Förste et al. 2011
eigen-5s	150	based on 5 years of GRACE data	Förste et al. 2008
eigen-6c	1420	Satellite/terrestrial combined model based on 6.7 months of GOCE data, 6.5 years of GRACE and SLR data, surface gravimetry, and altimetry	Förste et al. 2011
eigen-5c	360	Satellite/terrestrial combined model based on eigen-5s global geopotential model, surface gravimetry, and altimetry	Förste et al. 2008
EGM2008	2190	Satellite/terrestrial combined model based on itg-grace03s global geopotential model, surface gravimetry, and altimetry	Pavlis et al. 2012

In both the time-wise and direct approaches, a large system of normal equations is solved to estimate the spherical harmonic coefficients of the model. The main difference between these two approaches is that in the direct approach an a-prioi gravity field model is used as a background model and GOCE observations are used to improve this model, whereas the time-wise approach does not include a background model. In the time-wise approach, the GOCE observations are considered as time-series along the orbit. As the time-wise approach is based solely on GOCE data, it can be considered to yield a pure GOCE model. In the space-wise approach, the geopotential spherical harmonic coefficients are recovered from a set of nearly evenly-spaced observations on the mean orbital surface with the main objective of deriving the spherical harmonic coefficients by taking the spatial correlation of the Earth gravity field into account. The combined GOCE-based GGMs utilize observations from several different complementary sources such as CHAMP, GRACE, and SLR. It should be noted that the combined models can be distinguished as satellite-only models (i.e., data observations for satellite sources only)

and satellite/terrestrial models (i.e., gravity observations are derived from surface gravimetry and altimetry). A complete description about different methods used in the development of GOCE-based models can be found in Pail et al. (2011).

3.3 GOCE Model Evaluation using GNSS/Levelling Data

Generally, comparisons with independent gravity field functionals are used to evaluate the performance of the GOCE GGMs (Hirt et al. 2011). In order to estimate the external accuracy (i.e., real geoid or gravity error) of a GGM three basic validation tools are available, which are summarized in Table 3.2 (Gruber 2004). An important drawback of comparisons with independent external datasets is that the results of comparisons are reliable only when the quality of the external data set is high. Gruber (2004) uses comparison with GNSS/levelling data and sea surface topography models to validate GGMs based on CHAMP and GRACE coefficients, asserting that these methods can also be used for the validation of GOCE models.

Gravity observations, such as the first radial derivative of the disturbing potential and the first horizontal derivative of the disturbing potential (i.e., vertical deflections), contain significant spectral power in the medium and higher frequencies (Schwarz 1985; Jekeli 1999), and therefore can be considered a complement to the evaluation of GGMs using GNSS/levelling data (Gruber 2009; Ihde et al. 2010; Gruber et al. 2011; Hirt et al. 2011).

The GNSS/levelling validation method has been used in many studies for the evaluation of a GGM, and has been used specifically to validate the very high-resolution global model *EGM2008* (Förste et al. 2009; Kotsakis and Katsambalos 2009; Jekeli et al. 2009). The *EGM2008* (Pavlis et al. 2012) is complete up to spherical harmonic degree and order 2160, and also provides additional spherical harmonic coefficients up to degree 2190. This corresponds to a spatial resolution of 5 arc minutes, or approximately 9 km. Ince et al. (2012) and Kotsakis and Katsambalos (2009) have used GNSS/levelling to test both the absolute and relative agreement of geopotential models (i.e., GOCE and *EGM2008*, respectively).

Table 3.2: Summary of tools and test datasets for gravity field validation (Gruber 2004).

Tool	Test Data Sets	Range of Test	Quality Parameters	Problems
Precise orbit determination of geodetic and altimeter satellites with a variety of orbit parameters.	Satellite tracking data: Laser, DORIS, GNSS, Altimetry.	Long wavelengths. Degree:0-70 Resolution: 320-20,000 km	Residuals with respect to tracking data in space and frequency domain. Altimeter crossover differences for computed orbits.	Independent tracking data. Quality of altimeter observations. Sensitivity of satellites for gravity field. Non-gravitational disturbances.
Comparison with independent geoid and gravity information.	GNSS/levelling geoid heights. Point and mean gravity anomalies. Astrogeodetic deflections.	Medium to short wavelengths. Degree: 50-250 Resolution: 80-400 km	RMS and mean of geoid height and gravity anomalies differences at the points of comparison and slopes.	Treatment of omission error. Filter model. Impact of long wavelengths.
Analysis of sea surface topography solutions.	Mean sea surfaces from altimetry. Oceanographic sea surface topography solutions.	Long to short wavelengths. Degree: 10-250 Resolution: 80-2000 km	Differences between geodetic and oceanographic solutions. Test for remaining oceanographic signals.	Quality of the mean sea surfaces and oceanographic sea surface topography model. Filtering. Ocean boundaries.

When using GNSS/levelling data, the ellipsoidal heights h^{GNSS} are measured by GNSS technology and the orthometric heights $H^{levelling}$ are derived from levelling data and gravity measurements. The geoid height N is the separation between the geoid and ellipsoid at each station:

$$N^{GNSS/levelling} = h^{GNSS} - H^{levelling}. \quad (3.1)$$

Similarly, the geoid height of each GNSS/levelling station can be computed using the GGMs (i.e., N^{GM}). Thus, the basic idea in using GNSS/levelling data for the evaluation of

GGMs is the comparison of geoid heights obtained using a GGM (i.e., N^{GM}) and geoid height obtained using GNSS/levelling data (i.e., $N^{GNSS/levelling}$).

A problem that occurs when using GNSS/levelling data or any other independent gravity field functional to validate a GGM is the omission error. The GGMs are limited by their maximum degree and order of coefficients, causing an omission error to always be present due to the fact that the high-degree spectral content is missing (Hirt et al. 2011). On the other hand, the terrestrial data to which the GGMs are compared contain the full spectral signal. In order to appropriately compare the two data-sets they need to be comparable in terms of their spectral content, which can be done by low-pass filtering of the terrestrial data to remove high-frequency constituents (Gruber 2004), or by spectral enhancement of the GGM-based functionals in the high and very high frequency range (using a high resolution gravity field model such as *EGM2008* and residual terrain models (RTM)) so that it is more comparable with the full-spectrum terrestrial data (Hirt et al. 2011). It should be noted that the GGM-based functionals can also be enhanced with local gravity and topographic data using a remove-compute-restore scheme as outlined in Chapter 2 in order to model the high frequency spectral content of the gravity field. Low pass filtering using methods such as spectral filters, Gaussian filters, or least-squares collocation (LSC) is a difficult task when the data is irregularly or scarcely distributed, whereas the spectral enhancement method (SEM) can be used for GGM validation as it is independent of the spatial distribution of the terrestrial data (Hirt et al. 2011).

The global magnitude of the omission error can also be estimated by means of a degree variance model. The degree variance method provides an approximation described by the degree variances of the geopotential (scaled to the geoid heights) to the global contribution of the gravity signal (Heiskanen and Moritz 1967; Jekeli et al. 2009):

$$(\sigma_N^2)_n = R^2 \left(\frac{r^b}{r^e}\right)^{2n+2} \sum_{m=0}^{n} (\bar{C}_{nm}^2 + \bar{S}_{nm}^2), \qquad (3.2)$$

where r^e is the radial distance to the ellipsoid and r^b is the radius of the bounding sphere. As the full true gravity spectrum is unknown, in practice, instead of Eq. (3.2), degree variance models fitted to the global gravity data are used or Kaula's rule is applied (Kaula 1966):

$$\sigma_{omission}^{n_{max}} = \sqrt{\sum_{n=n_{max}+1}^{\infty}(\sigma_N^2)_n} = \frac{64}{n_{max}}[m], \tag{3.3}$$

where n_{max} is the maximum degree and order of the geopotential model. It should be noted that the degree variances method does not provide the spatial distribution of the model's omission error but yields only an average global value. There are also other models that can be used for degree variances, such as, e.g., the Tscherning-Rapp model (Tscherning and Rapp 1974).

Another error present that would cause a difference between the geoid undulations derived using the GGM and the geoid undulations derived using GNSS/levelling is the commission error of the GGM, which is the error that is propagated in the model through the errors of the coefficients.

The standard deviation of the difference between the GGM derived geoid undulations and the GNSS/levelling undulations contains the commission and omissions errors of the spherical harmonic model, and also the errors in the GNSS and levelling data while the mean difference accounts for the possible use of different ellipsoids and height datums (Jekeli et al. 2009). The SEM should make the geoid undulations derived from GGMs and the geoid undulations derived from GNSS/levelling as spectrally consistent as possible, but will not entirely eliminate it, as even the SEM omission error estimates are only good up to a finite degree and order.

3.3.1 Methodology

The general comparison methodology used in the evaluation of the GGMs by means of GNSS/levelling undulations is a modification of Gruber's (2009) SEM:

1. Compute the geoid heights from the GGM at the locations of the GNSS/levelling points up to a maximum degree and order n_{max}.

2. Approximate the omission error from the *EGM2008* tide free spherical harmonic model series for degree and order n_{max}+1 to 2190.

3. Add the *EGM2008* omission error estimate to the geoid undulation obtained from the GGM in order to make the GGM geoid undulation and the GNSS/levelling geoid undulations spectrally similar.

4. Geoid height differences are computed between spectrally enhanced model geoid heights and GNSS/levelling geoid heights. The difference is regarded as a quality estimate for the global model used up to the selected n_{max}.

5. For each regional GNSS/levelling dataset a mean value of differences is computed and subtracted in order to take into account inconsistencies in height system definitions.

6. The standard deviation of the "un-biased" geoid height differences is computed.

It should be noted that as the main purpose of this chapter is to inter-compare the GOCE satellite only GGMs, the effect of RTM (see e.g., Hirt et al. 2010) and local/regional gravity measurements have not been utilized. Although the existing spatial tilts found in the levelling networks will affect the quality estimate, it will not affect the relative performance between the models. Thus, within the context of determining the best GOCE

GGM for height system unification and W_0 determination, accounting for the spatial tilts within the levelling networks, though ideally preferable, may be omitted.

The computation of geoid heights from spherical harmonic coefficients has been performed using the *harmonic_synth.f* software (Holmes and Pavlis 2008). The zero-degree term of the geoid height (see Eq. (2.51)) should be added to the computed geoid heights from *harmonic_synth.f*. The GRS80 reference ellipsoid is used and the conventional potential of the global equipotential surface is equal to W_0=62,636,856.00 m^2/s^2 as per the International Earth Rotation and Reference Systems Service (IERS, 2010) convention. Based on the GRS80 ellipsoid parameters and the IERS conventions, the zero-degree term of the geoid height is computed as -43.7 cm.

3.3.2 GNSS/Levelling Benchmarks

GNSS/levelling benchmarks data sets for Canada were provided by the Geodetic Survey Division (GSD) of Natural Resources Canada (NRCan). 1,315 data points with orthometric heights in the Nov07 datum are used for the evaluation of the GOCE global geopotential models in Canada. These data come from adjustments of the levelling network on the Canadian mainland.

The GNSS ellipsoidal heights in this data set come from the 2006 adjustment of the GPS SuperNet network in Canada (Craymer and Lapelle 1997) in ITRF2005 (Altamimi et al. 2007), epoch 2006.0. The ellipsoidal heights were corrected for the effect of the glacial isostatic adjustment of the crust using a GNSS-derived crustal velocity model developed by GSD (i.e., the National Velocity Model 1.0). Figure 3.4 shows the distribution of these 1,315 stations.

The effect of post glacial rebound or glacial isostatic adjustment in North America has an effect on the geoid that ranges between 0.4-1.8 mm/yr, while the maximum vertical crustal displacement may reach up to approximately 12 mm/yr in the Hudson Bay region (Rangelova 2007).

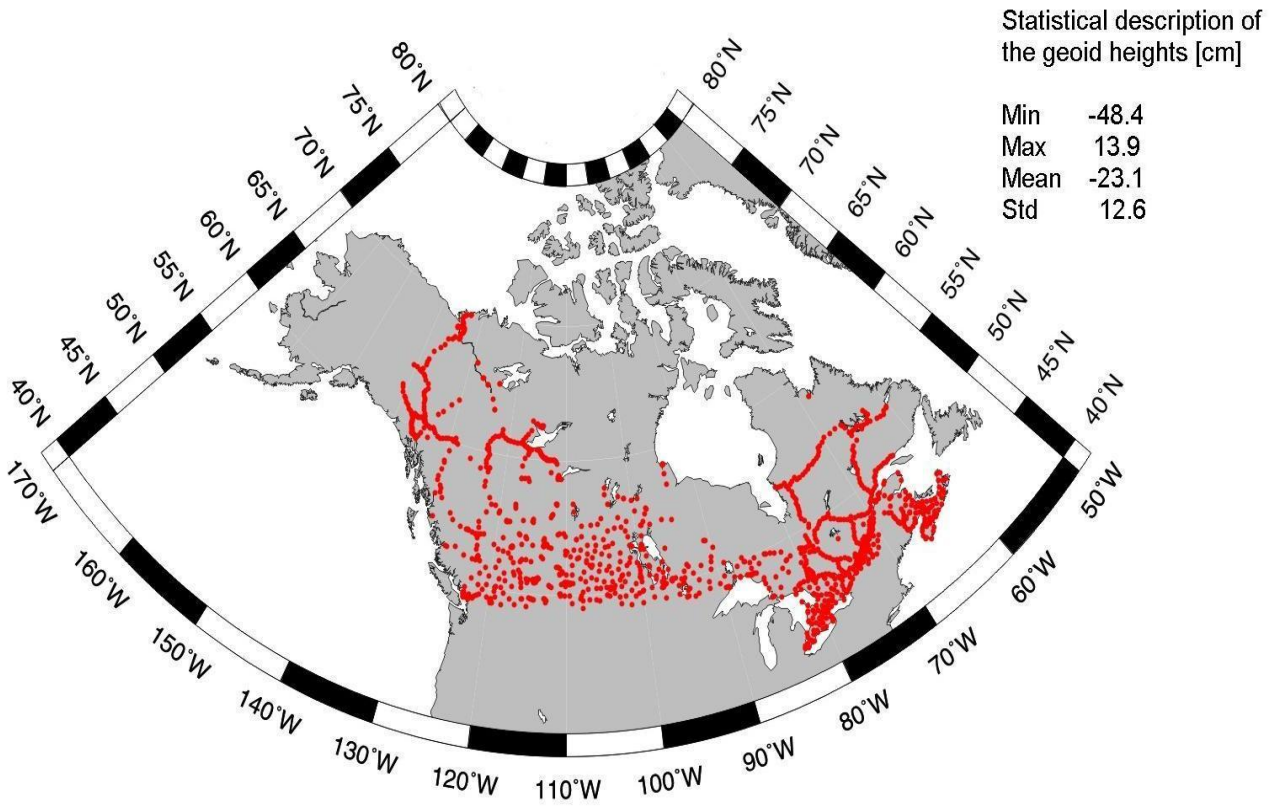

Figure 3.4: Geographical distribution of 1,315 Nov07 GNSS benchmarks in Canada.

The GNSS/levelling data for the U.S.A. was provided by the National Geodetic Survey (NGS) of National Oceanic and Atmospheric Administration (NOAA). This dataset consists of 18,399 points from the continental U.S.A. made available at http://www.ngs.noaa.gov/GEOID/GPSonBM09/.

The GNSS ellipsoidal heights were given in NAD83 (CORS96) 2002.0 and were transformed to ITRF2005 epoch 2006.0 using software developed by NGS (available at http://www.ngs.noaa.gov/TOOLS/Htdp/Htdp.shtml) to make them consistent with the Canadian data points. The orthometric heights are in NAVD88. The geographical distribution of these data points is shown in Figure 3.5.

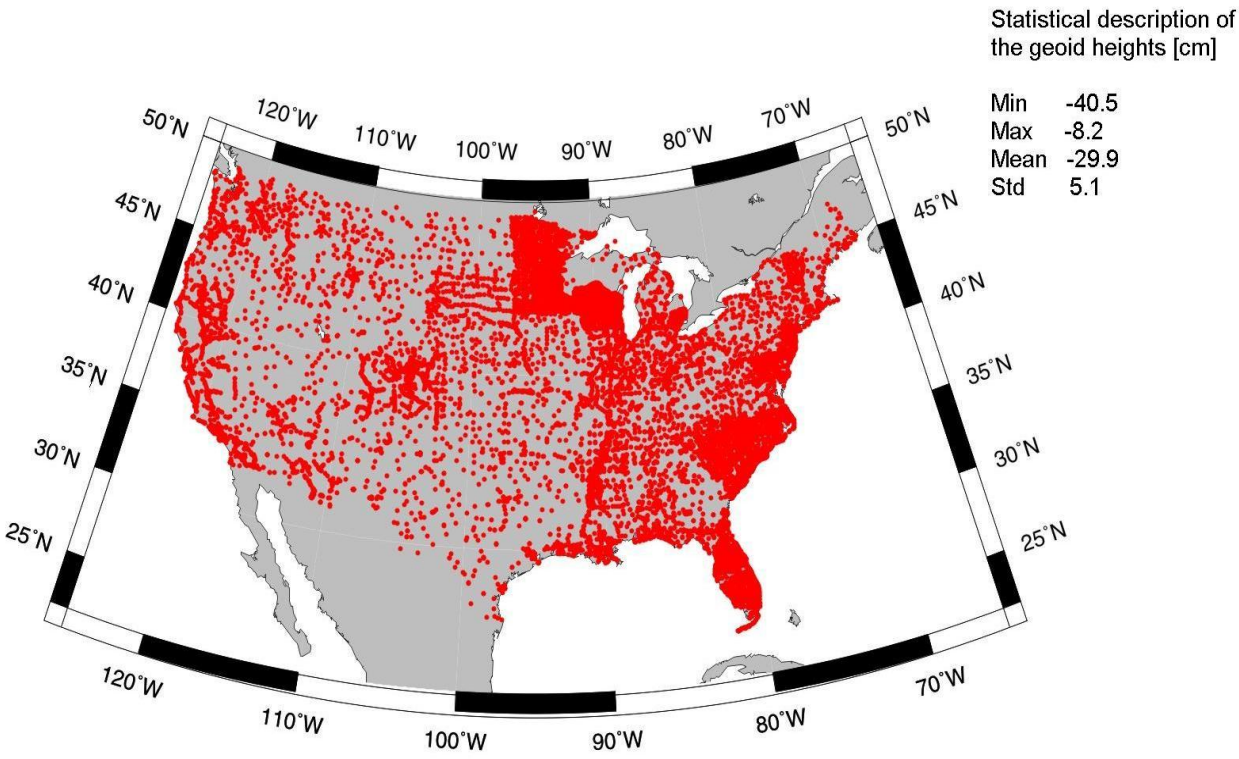

Figure 3.5: Geographical distribution of 18,399 NAVD88 GNSS benchmarks in U.S.A.

Figure 3.6 shows the coverage of the official Canadian gravimetric geoid model *CGG2010* over North America, while Figures 3.7 and 3.8 shows the differences between the *dir_r4+EGM2008* geoid heights and the geoid heights obtained from GNSS/levelling in order to emphasize the existing spatial tilts in the NAVD88 and Nov07 levelling networks.

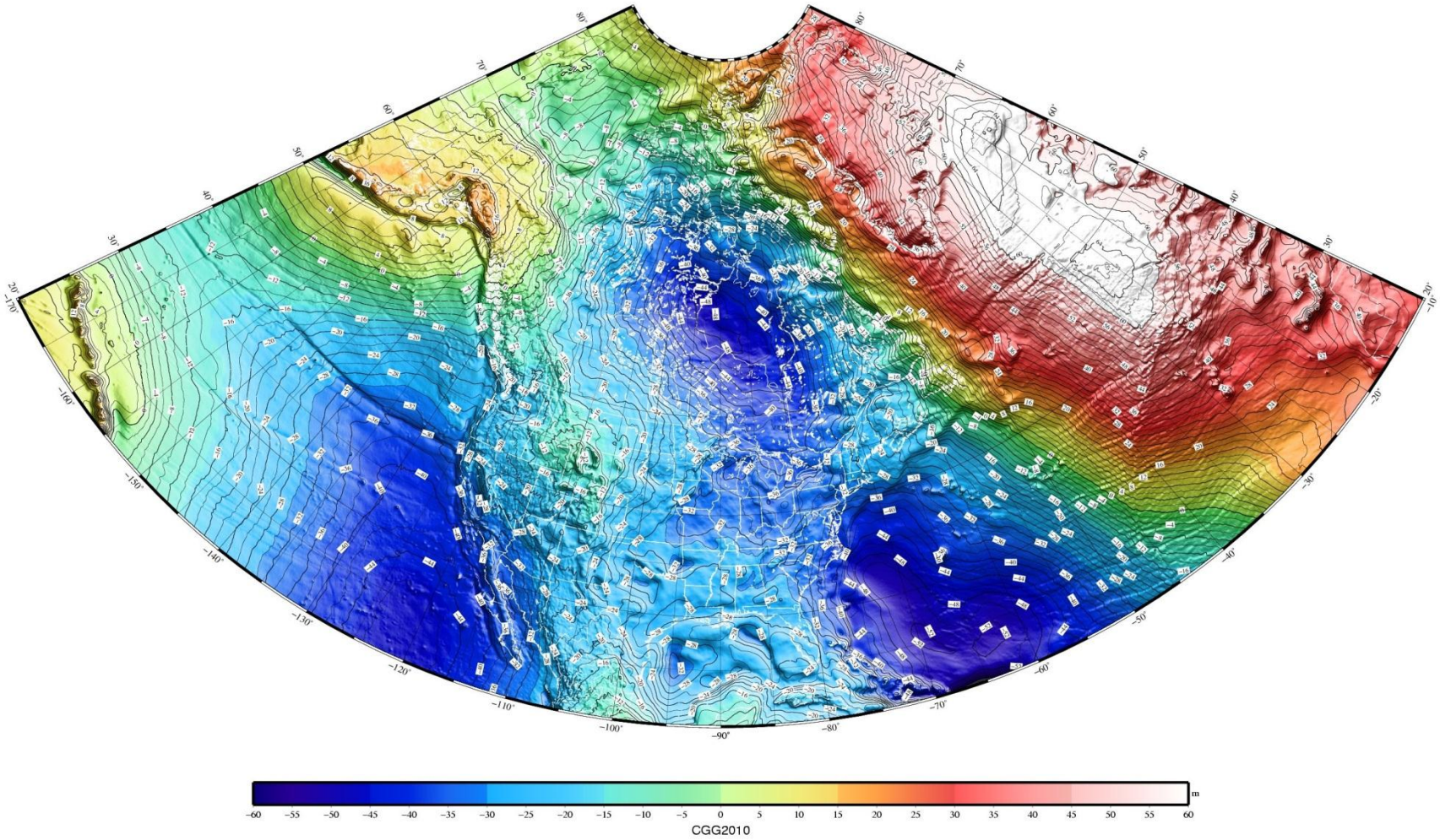

Figure 3.6: *CGG2010* gravimetric geoid model over North America (www.geoid.nrcan.gc.ca/hm/images/cgg2010.jpg).

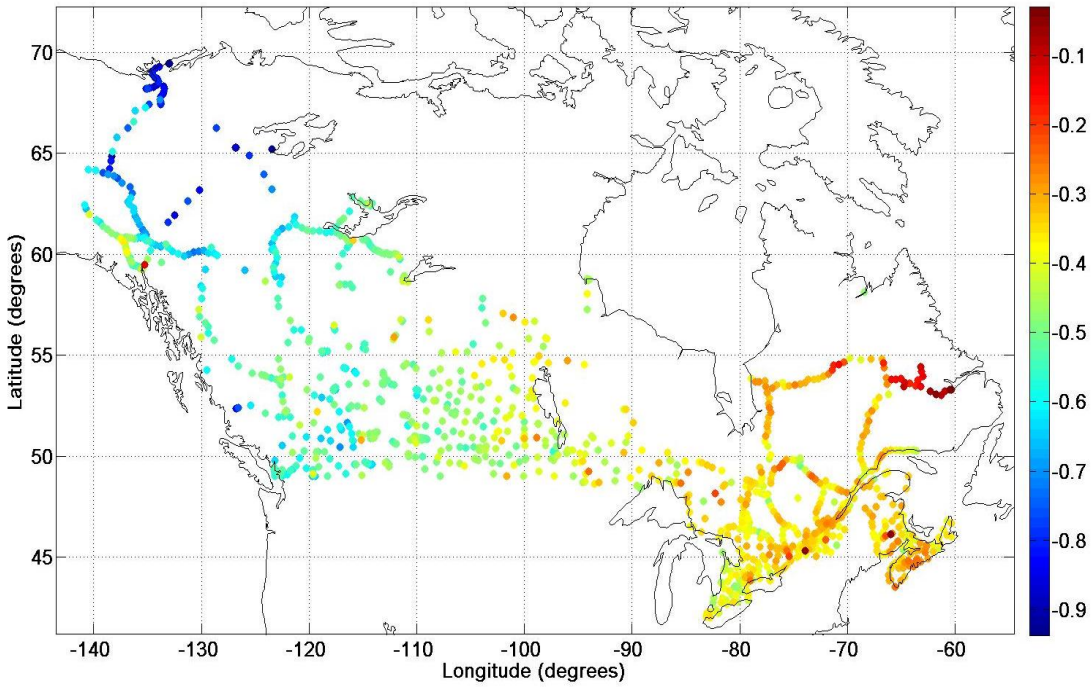

Figure 3.7: Geoid height differences $h\text{-}H\text{-}N^{dir\_r4+EGM2008}$ (in meters) for Canadian Nov07 GNSS/levelling benchmarks.

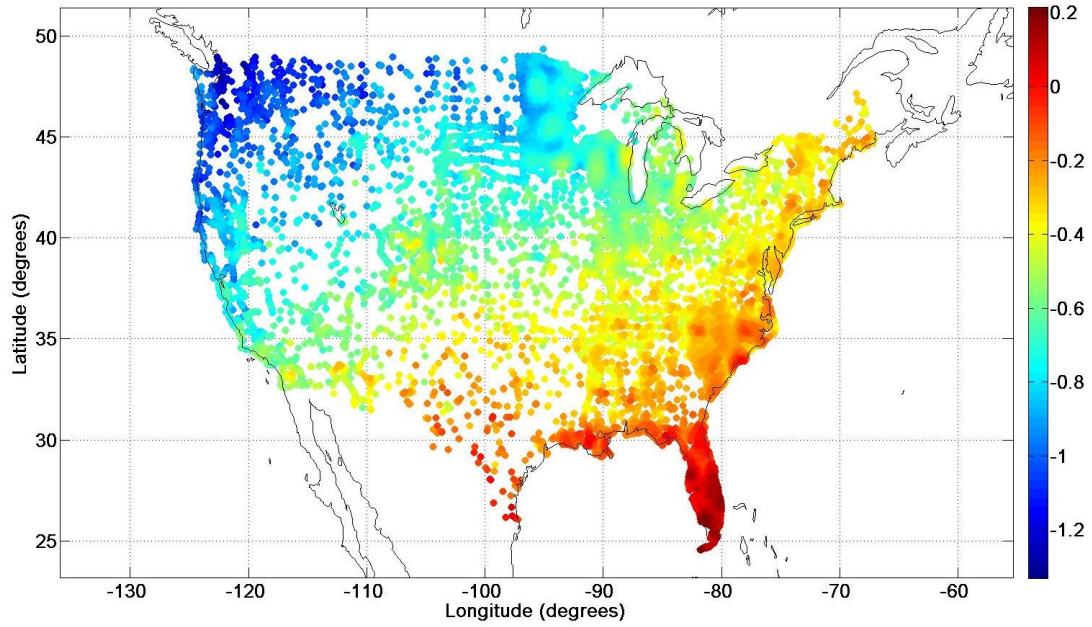

Figure 3.8: Geoid height differences $h\text{-}H\text{-}N^{dir\_r4+EGM2008}$ (in meters) for the U.S.A. NAVD88 GNSS/levelling benchmarks.

It can be seen from Figure 3.7 that in the Nov07 network there is a noticeable east-west tilt and a less significant north-south tilt while Figure 3.8 shows that there is both a

significant east-west tilt and north-south tilt present in the U.S.A. NAVD88 levelling network, which can be attributed to the accumulation of systematic levelling errors and the difference of the mean sea levels between the west and east coasts of North America.

3.4 Results and Discussion

This section describes the evaluation results by means of geoid height comparisons in Canada and the U.S.A. Absolute comparisons are presented and the performance of the GOCE models in different spectral bands is investigated. The omission error of the GGMs is approximated using the high resolution model *EGM2008*.

3.4.1 Global Cumulative Geoid Error from Degree Variances

The cumulative global geoid error can be evaluated from the error degree variances of a GGM. The total cumulative geoid error is the square root of the sum of the error degree variances. Figure 3.9 shows the cumulative geoid errors at different degrees of truncation for the third and fourth generation direct and time-wise GOCE GGMs. As the gravity field model error curves are derived from error estimates as a result of a least squares solution (i.e., utilized in order obtain the spherical harmonic coefficients), they can be regarded as "internal" error estimates. From Figure 3.9, it can be seen that at degree and order 200, which corresponds to a spatial resolution of approximately 100 km, the *dir_r4* model has a cumulative geoid error of approximately 1 cm, while the *tim_r4* model has a cumulative geoid error of approximately 4 cm. This is an improvement over the third generation models, where *dir_r3* has a cumulative geoid error of approximately 3 cm and the *tim_r3* has a cumulative geoid error of approximately 6 cm at degree and order 200.

Thus, with the release of the *dir_r4* model, it appears that the GOCE mission objective of obtaining the geoid with a global accuracy of 1-2 cm at a spatial resolution of 100 km has been achieved. With longer time series of GOCE observations, the time-wise approach may also achieve a global cumulative geoid error of 1-2 cm at truncation degree 200. In

the following sections 3.4.2 and 3.4.3 the "external" error of the GOCE GGMs are estimated by comparison with geoid height derived from GNSS and levelling data.

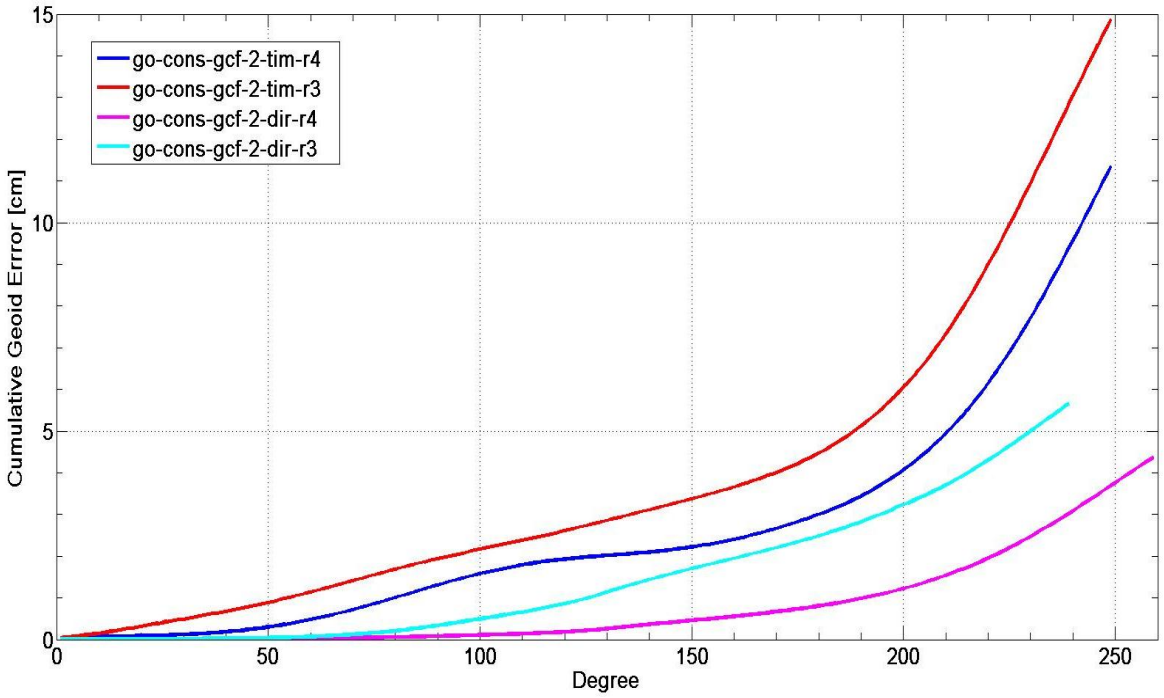

Figure 3.9: Cumulative geoid error (cm) for release-4 and release-3 GOCE GGMs.

3.4.2 Absolute GGM Evaluation using GNSS/Levelling Data

The statistics of geoid height differences after a constant bias fit using 1,315 Canadian GNSS/levelling benchmarks are given in Table 3.3 while the statistics of the geoid height differences extended with *EGM2008* are given in Table 3.4. It is evident based on the results from Table 3.3 that the fourth and third generation GOCE satellite-only models perform better than the second and first generations GOCE satellite-only models. For example, the standard deviation of the geoid height differences for the *tim_r4* model is 29.9 cm, compared to 32.3 cm of *tim_r3*, 33.5 cm of *tim_r2*, and 35.7 cm of *tim_r1*. Similarly, it can be observed from Table 3.3 that the *dir_r4* standard deviation of the geoid height differences is 29.7 cm while for the third generation model *dir_r3* the standard deviation of the geoid height differences is 32.1 cm, and it is 34.7 cm for the second generation model *dir_r2*.

Table 3.3: Statistics of geoid height differences (after a constant bias fit) using 1,315 Canadian GNSS/levelling benchmarks.

Model	n_{max}	Min (cm)	Max (cm)	Std. Dev. (cm)	Mean (cm)
go_cons_gcf_2_dir_r4	260	-108.9	97.7	29.7	-53.5
go_cons_gcf_2_dir_r3	240	-114.4	101.5	32.1	-54.3
go_cons_gcf_2_dir_r2	240	-124.4	110.3	34.7	-55.1
go_cons_gcf_2_dir_r1	240	-117.8	93.7	29.6	-53.2
go_cons_gcf_2_tim_r4	250	-120.0	95.0	29.9	-53.3
go_cons_gcf_2_tim_r3	250	-119.2	104.0	32.3	-54.3
go_cons_gcf_2_tim_r2	250	-124.3	112.5	33.5	-54.9
go_cons_gcf_2_tim_r1	224	-140.4	118.0	35.7	-55.1
go_cons_gcf_2_spw_r2	240	-126.0	121.6	34.1	-56.4
go_cons_gcf_2_spw_r1	210	-166.3	124.7	37.4	-55.3
goco03s	250	-113.9	105.4	31.9	-54.1
goco02s	250	-123.2	113.2	33.2	-54.5
goco01s	224	-140.1	117.3	35.3	-54.7
DGM-1s	250	-113.4	126.3	32.9	-54.2
itg-grace2010s	180	-135.9	135.2	43.6	-59.1
eigen-5s	150	-170.9	215.7	49.3	-64.3
eigen-6s	240	-125.3	106.8	34.8	-55.1
eigen-5c	360	-92.5	66.1	24.2	-50.2
eigen-6c	1420	-50.0	48.5	14.0	-44.4
EGM2008	2190	-55.5	45.7	13.3	-44.1

The first generation model *dir_r1* appears to perform better than the second, third, and fourth generation direct models, this is because the background model for *dir_r1* is *eigen-5c*, which is not a satellite-only model (see Table 3.1). The *eigen-5c* model contains terrestrial gravity data, which means that the higher frequency components of the gravity field are better modelled with *eigen-5c* when compared to GGMs that only contain data from satellite-based platforms. It is shown in Table 3.3 that the GGMs based on the space-wise approach performs on the whole worse than the time-wise and direct approach based GOCE models. For example, *tim_r3* has a standard deviation of 32.3 cm compared to the *spw_r2* which has a standard deviation of 35.7 cm. Of course, the GGMs which include terrestrial gravity data such as *eigen-5c*, *eigen-6c*, and *EGM2008* have the best agreement with the GNSS/levelling data; this is expected as these datasets yield geoid heights that are spectrally more consistent with the geoid heights from GNSS/levelling as compared to geoid heights obtained from GGMs that do not contain terrestrial gravity data.

Table 3.4: Statistics of geoid height differences (after a constant bias fit) with *EGM2008* extended GGMs to degree and order 2,190 using 1,315 Canadian GNSS/levelling benchmarks.

Model	**n_{max}**	**Min (cm)**	**Max (cm)**	**Std. Dev. (cm)**	**Mean (cm)**
go_cons_gcf_2_dir_r4	260	-74.7	45.0	16.6	-45.5
go_cons_gcf_2_dir_r3	240	-69.3	55.4	19.7	-45.3
go_cons_gcf_2_dir_r2	240	-85.0	63.5	23.2	-46.1
go_cons_gcf_2_dir_r1	240	-53.2	47.7	14.4	-44.1
go_cons_gcf_2_tim_r4	250	-66.7	45.3	16.8	-45.3
go_cons_gcf_2_tim_r3	250	-72.1	54.8	20.6	-46.3
go_cons_gcf_2_tim_r2	250	-106.9	58.2	22.4	-46.9
go_cons_gcf_2_tim_r1	224	-63.3	49.7	21.8	-45.4
go_cons_gcf_2_spw_r2	240	-82.9	62.3	21.7	-47.3
go_cons_gcf_2_spw_r1	210	-70.3	66.9	22.4	-44.8
goco03s	250	-74.7	55.7	20.0	-46.1
goco02s	250	-107.8	55.9	22.1	-46.5
goco01s	224	-63.5	52.4	21.2	-45.1
DGM-1s	250	-89.8	52.4	22.8	-46.2
itg-grace2010s	180	-71.4	89.9	23.6	-44.4
eigen-5s	150	-142.2	121.7	32.9	-49.6
eigen-6s	240	-87.3	66.8	23.4	-46.1
eigen-5c	360	-74.5	54.8	18.1	-46.1
eigen-6c	1420	-50.4	48.1	13.7	-44.1
EGM2008	2190	-55.5	45.7	13.3	-44.1

Likewise, results presented in Table 3.4 show more or less the same trends as the results from Table 3.3. The standard deviations and the mean value of the geoid height differences have decreased in general for most of the GOCE-based GGMs, since the models have been extended with *EGM2008,* which incorporates terrestrial gravity data. For example, for *tim_r3* the mean value of the geoid height difference from Table 3.3 is 54.3 cm and it is 46.3 once extended with *EGM2008*. The approximate effect of the GOCE omission error on the mean geoid height difference is thus 8 cm. When comparing the mean geoid height differences between Table 3.3 and 3.4, it can be seen that the effect of the omission error it is greater for GRACE based models, which is at the dm-level. This has do with the fact that GRACE based models are only expanded to a maximum degree and order of 150 to 180 while GOCE based models are usually expanded to a maximum degree and order of 240 to 260. Here it is evident that including the SGG on-board the GOCE mission has helped to resolve higher frequencies of the gravity field when compared with pre-GOCE missions such as GRACE.

The statistics of geoid height differences after a modeling the systematic errors found in the Nov07 GNSS/levelling data with a plane for the 1,315 Canadian GNSS/levelling benchmarks are given in Table 3.5. The same trends observed from the results in Table 3.3 can be observed from the results presented in Table 3.5, despite the fact that the magnitude of the standard deviation of the geoid height differences has decreased on the whole after removing the systematic effects in the levelling network with a planar fit. Again, it is the GGMs with the longest time-series of GOCE observations that have the best agreement with the Nov07 GNSS/levelling data.

Table 3.5: Statistics of geoid height differences (after a planar fit) using 1,315 Canadian GNSS/levelling benchmarks.

Model	**n_{max}**	**Min (cm)**	**Max (cm)**	**Std. Dev. (cm)**	**Mean (cm)**
go_cons_gcf_2_dir_r4	260	-158.9	42.7	25.6	-53.1
go_cons_gcf_2_dir_r3	240	-160.6	40.1	28.6	-53.8
go_cons_gcf_2_dir_r2	240	-171.4	44.3	31.3	-54.6
go_cons_gcf_2_dir_r1	240	-162.9	29.6	26.1	-52.6
go_cons_gcf_2_tim_r4	250	-164.7	31.0	26.5	-52.6
go_cons_gcf_2_tim_r3	250	-164.4	38.8	28.9	-53.8
go_cons_gcf_2_tim_r2	250	-171.1	46.7	30.0	-54.4
go_cons_gcf_2_tim_r1	224	-187.3	61.7	32.5	-54.5
go_cons_gcf_2_spw_r2	240	-174.2.0	55.8	30.6	-55.8
go_cons_gcf_2_spw_r1	210	-213.4	66.2	34.0	-54.7
goco03s	250	-158.8	40.4	28.3	-53.6
goco02s	250	-169.6	47.8	29.5	-53.7
goco01s	224	-186.7	61.0	32.1	-54.2
DGM-1s	250	-159.5	61.2	29.6	-53.7
itg-grace2010s	180	-174.7	93.2	40.6	-58.6
eigen-5s	150	-224.6	140.9	46.2	-63.8
eigen-6s	240	-172.3	40.8	31.4	-54.6
eigen-5c	360	-133.5	5.3	19.3	-49.7
eigen-6c	1420	-78.5	2.2	8.7	-43.9
EGM2008	2190	-79.3	0.8	8.0	-43.6

Table 3.6 shows the statistics of geoid height differences after a constant bias fit for the U.S.A. using 18,399 GNSS/levelling benchmarks, while Table 3.7 shows the same statistics for the geoid height differences with *EGM2008* extended GGMs. The same trends as seen in Canada from Table 3.3 are observed for the U.S.A. from Table 3.6: GOCE satellite-only models that contain longer time-series of GOCE observations

generally have smaller standard deviations of geoid height differences than models with shorter time-series of GOCE observations, with the greatest difference observed between first generation GOCE GGMs and fourth generation GOCE GGMs. Geoid heights obtained from GOCE based GGMs have better agreement with geoid heights from GNSS/levelling when compared with GRACE based GGMs, and lastly, satellite models that also include terrestrial gravity data still has the best performance overall due to their ability to model the higher frequency components of the gravity field signal.

Table 3.6: Statistics of geoid height differences (after a constant bias fit) using 18,399 U.S.A. GNSS/levelling benchmarks.

Model	**n_{max}**	**Min (cm)**	**Max (cm)**	**Std. Dev. (cm)**	**Mean (cm)**
go_cons_gcf_2_dir_r4	260	-184.1	154.9	42.0	-50.1
go_cons_gcf_2_dir_r3	240	-202.5	184.1	44.8	-50.4
go_cons_gcf_2_dir_r2	240	-211.9	188.4	46.1	-50.3
go_cons_gcf_2_dir_r1	240	-167.6	165.6	42.4	-50.9
go_cons_gcf_2_tim_r4	250	-187.5	153.2	42.8	-49.9
go_cons_gcf_2_tim_r3	250	-188.8	170.5	44.3	-50.0
go_cons_gcf_2_tim_r2	250	-195.3	185.7	44.9	-50.6
go_cons_gcf_2_tim_r1	224	-207.1	208.0	46.8	-51.0
go_cons_gcf_2_spw_r2	240	-229.8	225.0	46.8	-50.9
go_cons_gcf_2_spw_r1	210	-242.9	230.2	47.7	-51.3
goco03s	250	-187.7	177.5	44.1	-50.2
goco02s	250	-196.8	187.1	44.6	-50.5
goco01s	224	-209.9	201.1	46.3	-50.7
DGM-1s	250	-201.8	195.6	45.3	-50.7
itg-grace2010s	180	-272.1	249.6	57.2	-50.3
eigen-5s	150	-367.1	365.2	62.8	-48.9
eigen-6s	240	-217.8	186.7	46.4	-49.9
eigen-5c	360	-144.8	136.9	35.3	-50.2
eigen-6c	1420	-86.0	72.7	30.3	-48.0
EGM2008	2190	-81.6	68.7	30.1	-48.0

The most interesting difference between the performance of GOCE GGMs in Canada and the U.S.A. is that the GOCE omission error is not as significant in the U.S.A. For example, the mean value of the geoid height differences for the third generation satellite-only combined model *goco03s* from Table 3.6 is 50.2 cm while the mean value is 47.6 cm for the *goco03s+EGM2008* model from Table 3.7. This difference is less than 3 cm.

Likewise, even for the GRACE based models, the effect of the omission error is approximately 2 cm in the U.S.A.

Table 3.7: Statistics of geoid height differences (after a constant bias fit) with *EGM2008* extended GGMs to degree and order 2,190 using 18,399 U.S.A. GNSS/levelling benchmarks.

Model	**n_{max}**	**Min (cm)**	**Max (cm)**	**Std. Dev. (cm)**	**Mean (cm)**
go_cons_gcf_2_dir_r4	260	-120.2	96.0	33.7	-48.0
go_cons_gcf_2_dir_r3	240	-108.3	90.0	33.3	-47.8
go_cons_gcf_2_dir_r2	240	-143.3	96.3	35.7	-47.6
go_cons_gcf_2_dir_r1	240	-84.6	78.7	30.9	-48.3
go_cons_gcf_2_tim_r4	250	-102.5	82.8	32.6	-47.2
go_cons_gcf_2_tim_r3	250	-112.8	93.0	34.6	-47.7
go_cons_gcf_2_tim_r2	250	-124.7	110.1	35.6	-48.0
go_cons_gcf_2_tim_r1	224	-113.9	94.5	34.2	-48.0
go_cons_gcf_2_spw_r2	240	-127.8	122.9	36.2	-48.3
go_cons_gcf_2_spw_r1	210	-98.1	77.3	33.6	-48.1
goco03s	250	-116.2	92.6	34.3	-47.6
goco02s	250	-123.5	112.0	35.3	-47.9
goco01s	224	-113.5	94.9	33.6	-47.7
DGM-1s	250	-148.1	111.2	35.7	-48.1
itg-grace2010s	180	-97.7	95.7	36.3	-48.7
eigen-5s	150	-169.8	170.6	49.1	-47.2
eigen-6s	240	-147.4	93.2	36.0	-47.2
eigen-5c	360	-119.8	115.5	30.8	-48.6
eigen-6c	1420	-83.7	72.5	30.2	-47.9
EGM2008	2190	-81.6	68.7	30.1	-48.0

The effect of the GOCE GGM omission error is dependent on the topography/terrain, which is the main source of which frequency gravity field signals (Forsberg 1984), as well as the distribution and density of the GNSS/levelling benchmarks. There is a notable difference between the density and distribution of the GNSS/levelling benchmarks in the U.S.A. and Canada. In Canada, the 1,315 benchmarks provide coverage mostly for the southern portion of the country while significant areas in the northern portion of the country remain un-surveyed (see Figure 3.4). Moreover, the mountainous topography found in the western portion of Canada is coarsely surveyed when compared with the GNSS/levelling benchmark distribution in the U.S.A. This effect will be discussed in in the next chapter as well, where GOCE-based GGMs are utilized for the computation of local vertical datum offsets.

Table 3.8: Statistics of geoid height differences (after a planar fit) using 18,399 U.S.A. GNSS/levelling benchmarks.

Model	n_{max}	Min (cm)	Max (cm)	Std. Dev. (cm)	Mean (cm)
go_cons_gcf_2_dir_r4	260	-205.7	148.0	27.4	-46.2
go_cons_gcf_2_dir_r3	240	-196.1	176.9	31.6	-46.4
go_cons_gcf_2_dir_r2	240	-202.3	178.6	33.5	-46.3
go_cons_gcf_2_dir_r1	240	-196.5	158.0	28.3	-46.9
go_cons_gcf_2_tim_r4	250	-215.8	146.6	28.5	-45.9
go_cons_gcf_2_tim_r3	250	-217.2	163.8	30.4	-46.0
go_cons_gcf_2_tim_r2	250	-198.8	178.3	31.7	-46.6
go_cons_gcf_2_tim_r1	224	-208.7	200.3	34.1	-47.0
go_cons_gcf_2_spw_r2	240	-212.1	217.4	34.5	-46.9
go_cons_gcf_2_spw_r1	210	-225.3	222.1	35.6	-47.3
goco03s	250	-211.5	170.6	30.2	-46.2
goco02s	250	-194.4	179.9	31.5	-46.5
goco01s	224	-202.9	202.6	33.6	-46.7
DGM-1s	250	-203.5	188.1	32.7	-46.7
itg-grace2010s	180	-253.4	242.5	47.2	-46.3
eigen-5s	150	-347.0	359.6	53.6	-44.9
eigen-6s	240	-199.8	180.1	33.9	-45.9
eigen-5c	360	-173.6	66.1	19.0	-46.0
eigen-6c	1420	-70.3	-10.3	7.2	-44.0
EGM2008	2190	-67.6	-10.0	6.2	-44.0

Lastly, Table 3.8 shows the statistics of geoid height differences after a planar fit for the U.S.A. using 18,399 GNSS/levelling benchmarks. Again, the same trends observed in Table 3.6 can be observed from the results presented in Table 3.8. As expected, after removing the spatial tilts from the NAVD88 levelling network by fitting a plane to the GNSS/levelling data, the magnitude of the standard deviations in Table 3.8 have decreased overall when compared to the magnitude of the standard deviations presented in Table 3.6.

Thus, for both Canada and the U.S.A. it is recommended to use fourth generation GOCE based GGM for applications such as geoid modelling or unification of height systems.

3.4.3 Performance of the GGMs in Different Spectral Bands

In order to evaluate the GOCE GGM performance in different spectral bands the models are truncated at a selected degree (i.e., from degree and order 10 to the maximum degree and order of the model in intervals of 10 degrees). The spherical harmonic coefficient of each model from the truncation degree to the maximum degree and order of the model is replaced by *EGM2008* coefficients, and the models are additionally extended to degree and order 2190 (i.e., the n_{max} of *EGM2008*). Figure 3.10 shows the performance of the time-wise GOCE GGMs (i.e., the pure GOCE models) and two pre-GOCE era GRACE satellite-only models for Canada while Figure 3.14 shows the same for the U.S.A. Similar trends are observed for both countries. Firstly, an improvement of each successive release of GOCE models due to increasing length of GOCE observations included in each consecutive model generation is observed (i.e., *tim_r4* performs better than *tim_r3* and *tim_r3* performs better than *tim_r2* etc.). Secondly, the GRACE based GGMs lose their signal in lower degrees, while the GOCE models show more signal content in higher spectral bands, which can be attributed to the inclusion of 2 to 27 months of GOCE observations. Thus, it can be concluded that the inclusion of even 2 months of GOCE observations will provide additional information about the gravity field in both Canada and the U.S.A.

In Figure 3.11 the performance of the direct GOCE GGMs are shown along with the background models *eigen-5c* for *dir_r1* and *itg-grace2010s* for *dir_r2* while *dir_r2* is used as the background model for *dir_r3*. Similarly, Figure 3.15 shows the same models for U.S.A. Of course, the same trends as seen in Figures 3.10 and 3.14 with the time-wise GOCE models are also seen with the direct GOCE models. The interesting feature to note is that the *dir_r1* model in Canada shows improvement with respect to *eigen-5c,* which can be attributed to the inclusion of 2 months of GOCE data. However, in the U.S.A this cannot be observed.

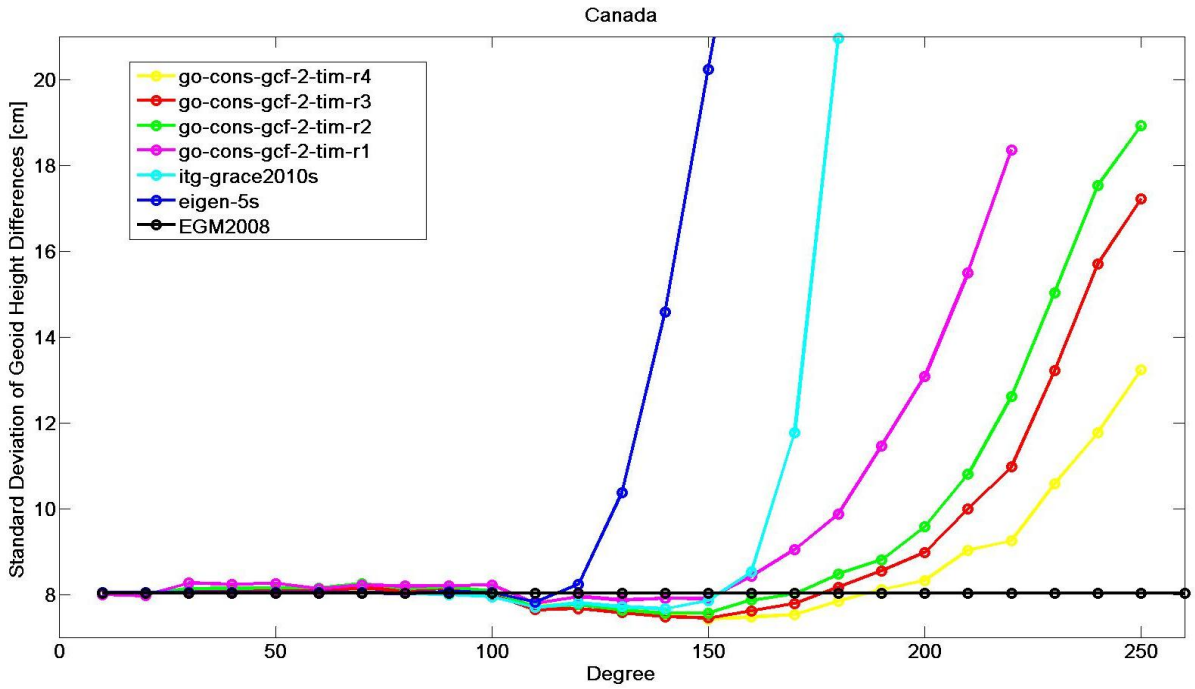

Figure 3.10: Standard deviation of the geoid height differences (after planar fit with omission error estimates from *EGM2008*) for the time-wise approach GOCE-based models and two GRACE-only models.

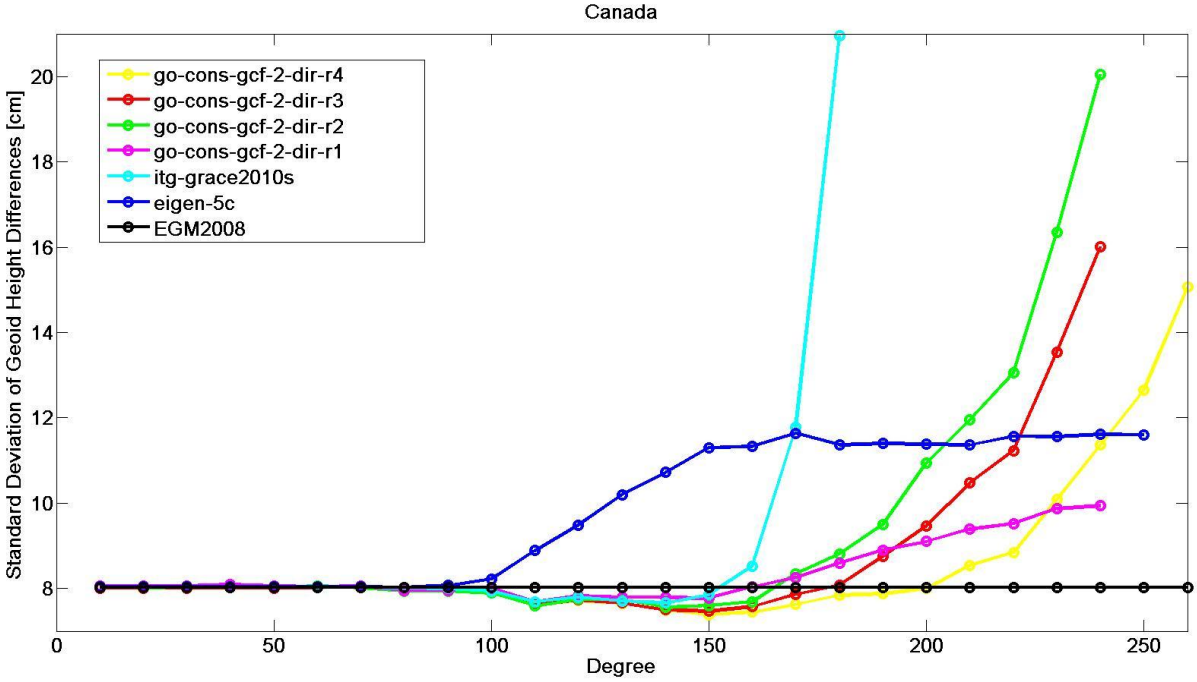

Figure 3.11: Standard deviation of the geoid height differences (after planar fit with omission error estimates from *EGM2008*) for the direct approach GOCE-based model and their background models.

Figure 3.12 shows the performance of the combined GOCE satellite only models for Canada while the same can be seen in Figure 3.16 for the U.S.A. In both Canada and the U.S.A. these models have similar performance up to approximately degree and order 180, while *goco03s* has the best performance in the higher spectral bands due to the fact that it contains the longest time-series of GOCE observations. All of the combined satellite-only models contain approximately seven years of GRACE data, hence the very similar performance in the lower spectral bands of 10 to 100 in terms of spherical harmonic degrees can be seen in Figure 3.12 and Figure 3.16.

It is interesting to note that the fourth generation models (i.e., *dir_r4* and *tim_r4*) that contain more than double the length of GOCE observations when compared with the third generation combined models show little improvement in the medium range spectral band (i.e., between 100 to 200), though the improvement is clear in the higher spectral bands (i.e., above degree 200). The similar performance of the models can be attributed to the use of the same GOCE observations as well as similar data pre-processing (e.g., same de-aliasing models and GNSS orbits are used; Pail et al. 2011). Furthermore, Figures 3.10, 3.11, and 3.12 illustrate that the GOCE GGMs have better performance when compared to *EGM2008* in the medium wavelength range (i.e., from degree and order 100 to 180). Pail et al. (2010b) have shown that GRACE is the most important dataset for the modeling of the long wavelength components for the gravity field (i.e., degree and order 2 to 100) whereas GOCE is a significant contributor from degree and order 100. Due to the improved performance of GOCE GGMs in the medium wavelength range, utilizing a GOCE GGM for local vertical datum offset computations or for W_0 determination is expected to yield a more accurate geoid signal in this particular spectral range (i.e. ~100 to 200) when compared to *EGM2008*.

In Figure 3.13 and Figure 3.17 it can be seen that in both Canada and U.S.A. respectively, the space-wise GOCE models show a significant deviation in performance after degree and order 180 in Canada and 160 in U.S.A. when compared with third and fourth generation GOCE satellite only GGMs.

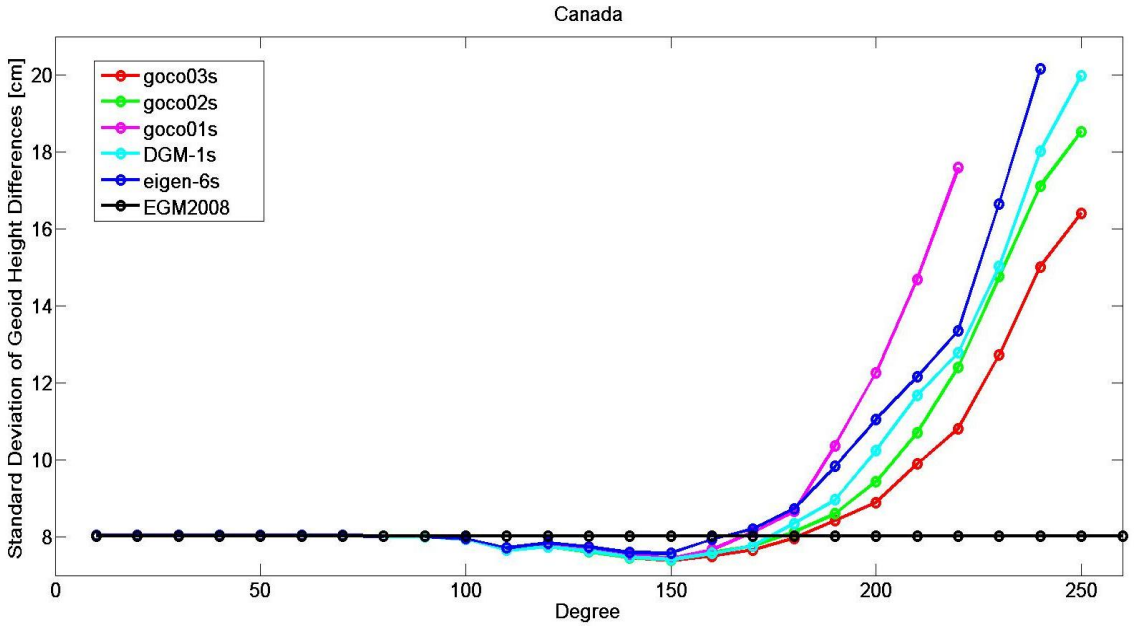

Figure 3.12: Standard deviation of the geoid height differences (after planar fit with omission error estimates from *EGM2008*) for the combined GOCE-based models.

On the whole, it is evident that the GOCE models perform very similarly up to degree and order 180-200, after which all of the models' performances deteriorates. Thus, GOCE satellite-only GGMs should only be used up to degree and order 180 to 200 for applications such as computing local vertical datum offsets. In Canada, *tim_r4* can be used up degree and order 200; *dir_r4* can be used up to degree and order 200-210; and *goco03s* can be used up to degree and order 180-190. In the U.S.A. *tim_r4* can be used up degree and order 190-200; *dir_r4* can be used up to degree and order 190-200; and *goco03s* up to degree and order 180-190.

The results in this section are in agreement with other GOCE model evaluation studies. For example, Ince et al. (2012) have shown that GOCE models generally conform to the accuracy of terrestrial data within the spectral band of degree 90 to 180 in Canada, and tend to deteriorate beyond degree 180. Likewise, Gruber et al. (2011) have shown with the first generation GOCE-based GGMs via the evaluation of geoid slopes differences in Germany that at truncation degrees higher than 180, the pure GOCE models will no longer contain the full gravity field signal due to the attenuation of the gravity signal with

respect to the satellite height. However, with the release of the fourth generation GOCE GGMs, the full gravity signal can be observed up to degree and order 200-210.

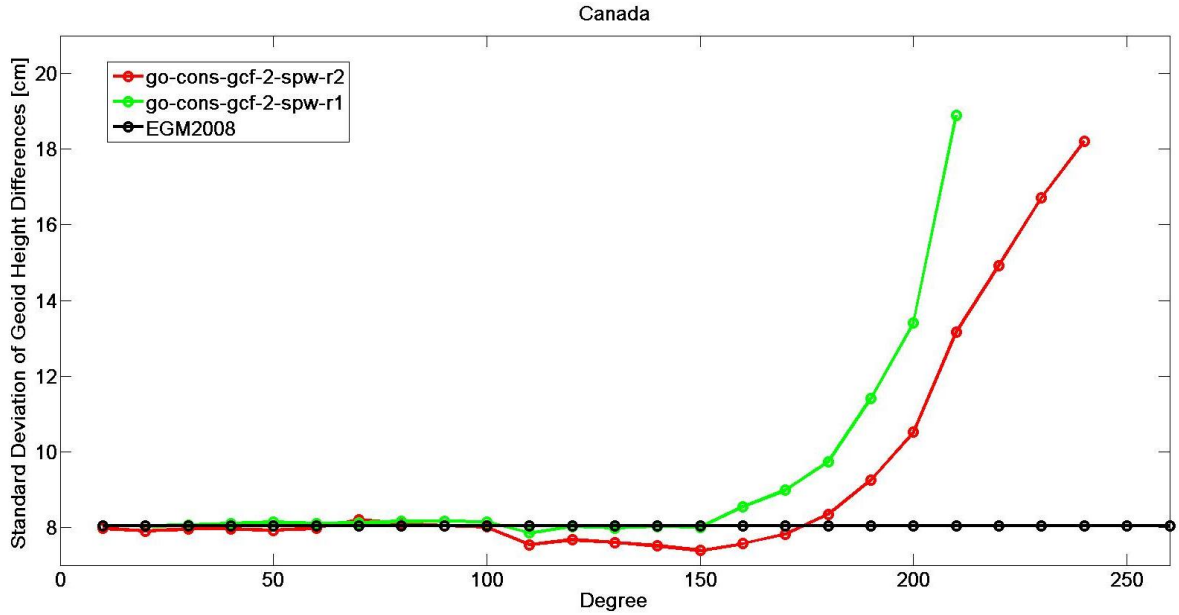

Figure 3.13: Standard deviation of the geoid height differences (after planar fit with omission error estimates from *EGM2008*) for the space-wise GOCE-based models.

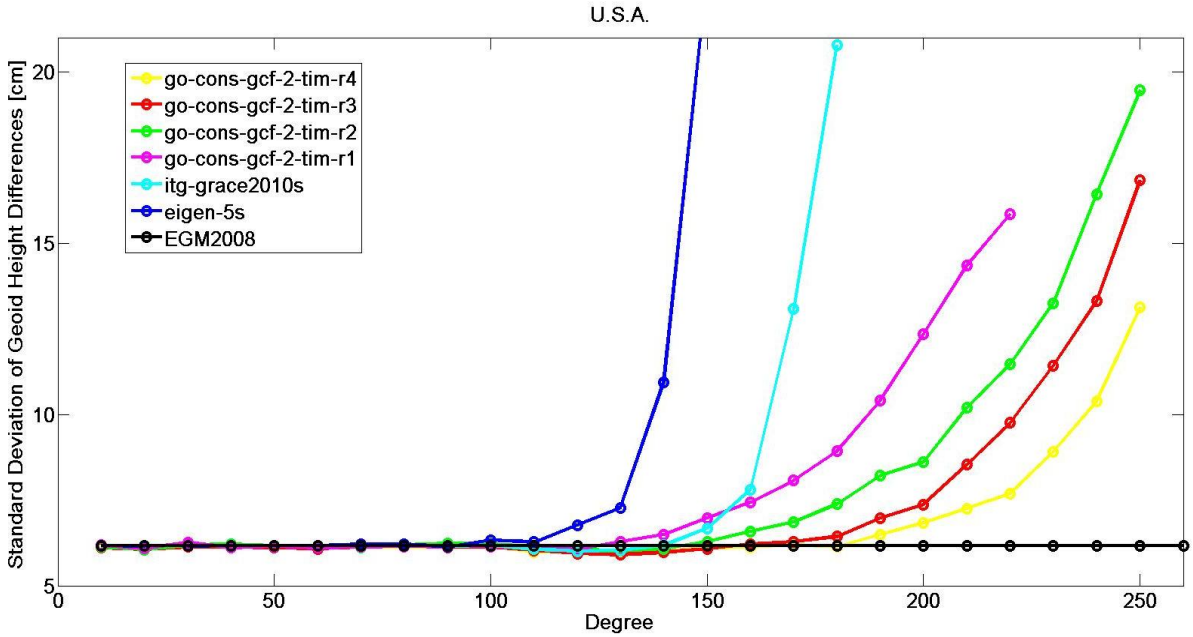

Figure 3.14: Standard deviation of the geoid height differences (after planar fit with omission error estimates from *EGM2008*) for the time-wise approach GOCE-based models and two GRACE-only models.

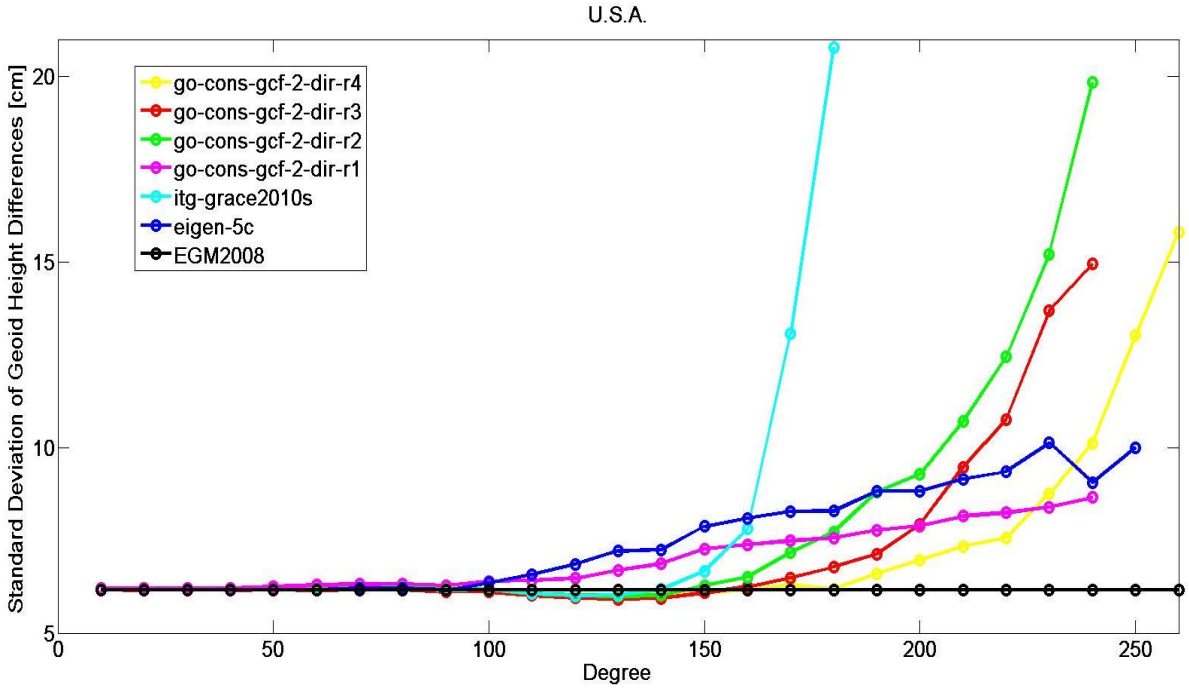

Figure 3.15: Standard deviation of the geoid height differences (after planar fit with omission error estimates from *EGM2008*) for the direct approach GOCE-based model and their background models.

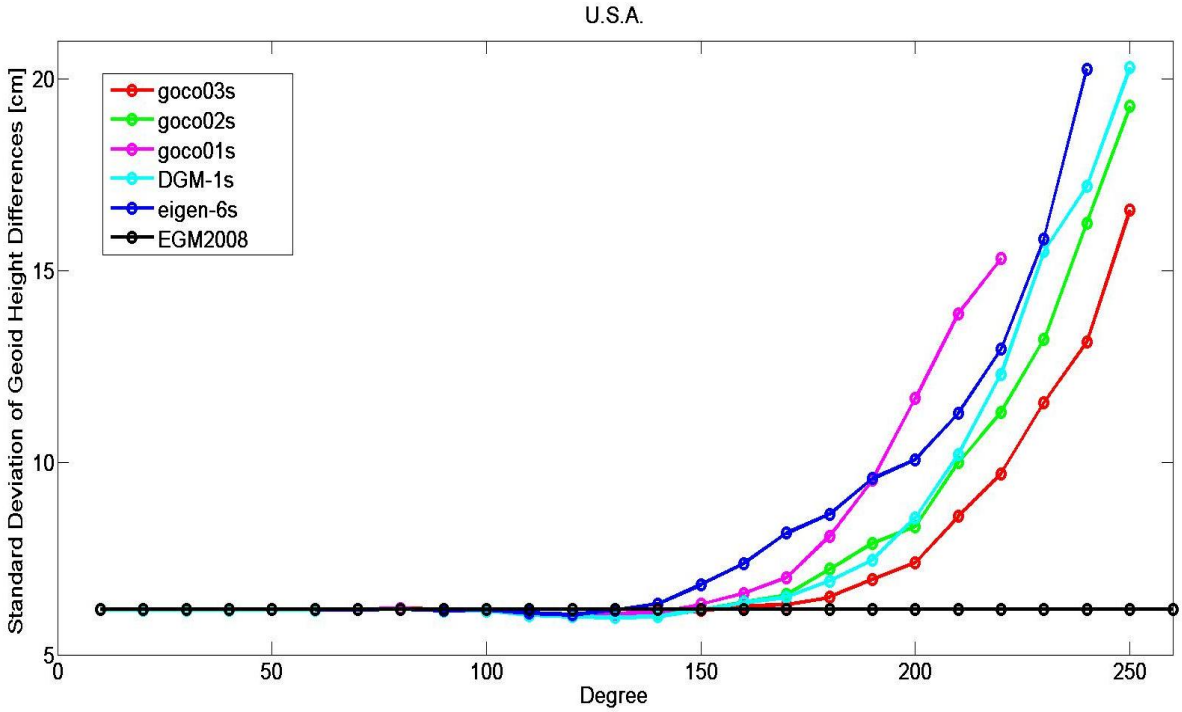

Figure 3.16: Standard deviation of the geoid height differences (after planar fit with omission error estimates from *EGM2008*) for the combined GOCE-based models and their background model.

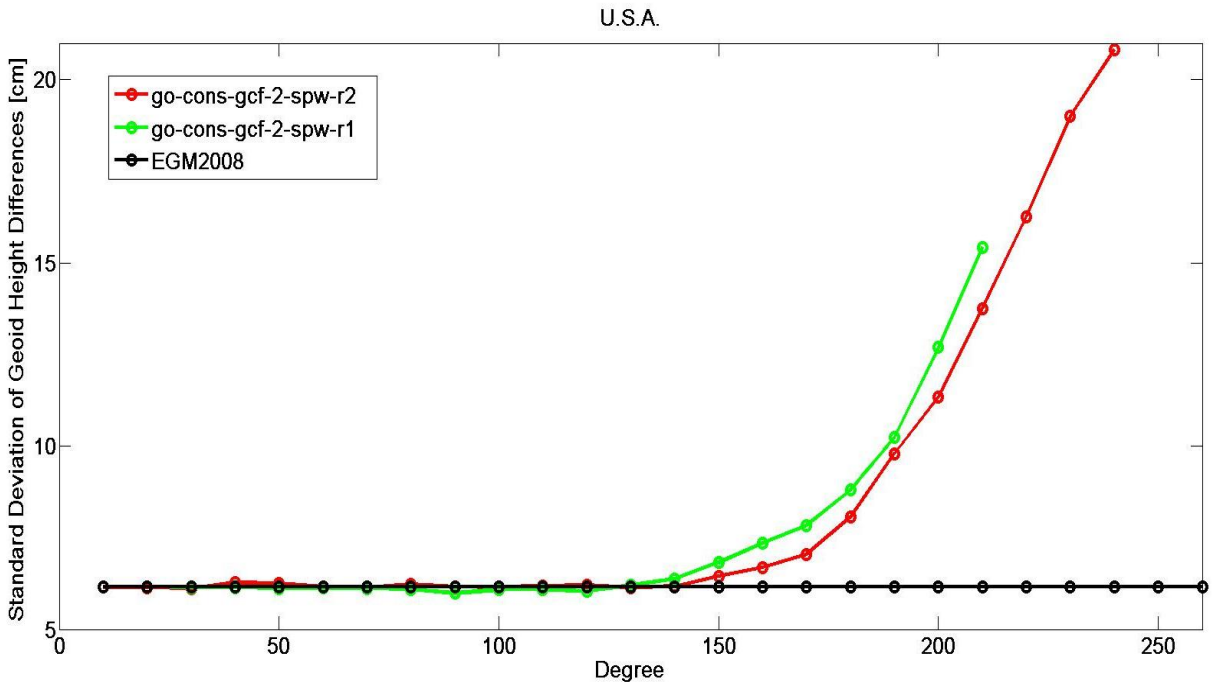

Figure 3.17: Standard deviation of the geoid height differences (after planar fit with omission error estimates from *EGM2008*) for the space-wise GOCE-based models.

3.5 Summary

To conclude, the fourth generation GOCE GGMs have the best performance overall in Canada and U.S.A. when validation is performed with an external dataset such as geoid undulations obtained from GNSS and levelling data. Chapter 4 and Chapter 5 will focus on the use of *goco03s* (expanded to degree and order 180), the *tim_r4* model (expanded to degree and order 200) and the *dir_r4* model (expanded to degree and order 200) for the computation of local vertical datum offsets and for the evaluation W_0. The motivation of utilizing *goco03s* comes from Pail et al. (2010b), where it has been shown that utilizing a combined GRACE and GOCE GGM is expected to yield a more accurate geoid signal in spectral range 100-180 when compared to *EGM2008*. Similarly, the *dir_r4* GGM also contains GRACE data in its background model. The motivation of using *tim_r4* is that it is the only GOCE satellite-only model that does not use any a-priori background model or any complementary data sources in the construction of the model; hence the contributions from GOCE-only observations can be highlighted with the use of *tim_r4*.

From the absolute comparison of geoid height differences the ultra high resolution GGMs *EGM2008* and *eigen_6c* show better performance than the rest of the models for both Canada and U.S.A. This is because both Canada and U.S.A. are gravimetrically well surveyed and thus have a good coverage of terrestrial gravity measurements that can adequately model the higher frequency signals of the gravity field. These terrestrial gravity measurements were used in the development of the ultra-high resolution GGMs and this is the main reason for the superior performance of these models in Canada and U.S.A. The opposite situation is observed in the regions with poor coverage and/or bad quality of terrestrial gravity measurements. For example, the geoid accuracy of *EGM2008* is at the dm-level over large parts of Asia, Africa, South America, and Antarctica due to the lack of high resolution terrestrial data in these regions (Hirt et al. 2012). It is for these regions, where dense terrestrial gravity observations are missing, that GOCE is expected to contribute most significantly.

Lastly, accounting for the effect of RTM can improve the comparison results between the geoid height differences, which can play an important role in the evaluation of GGMs in mountainous regions (Hirt et al. 2011). The contribution higher frequency gravity field content from RTM may be considered for future GGM evaluation studies for North America.

CHAPTER 4
ESTIMATING VERTICAL DATUM OFFSETS IN NORTH AMERICA WITH GOCE GLOBAL GEOPOTENTIAL MODELS

4.1 Introduction

Vertical datum realization and unification has been amongst one of the main topics of research in geodesy, and has been discussed in detail over the last three decades by Colombo (1980), Rummel and Teunissen (1988), Heck and Rummel (1990), Rapp and Balasubramania (1992), Xu (1992), Rummel and Ilk (1995), Jekeli (2000), and Burša et al. (2004), among others. These studies have illustrated that by determining the potential value of a LVD, it is possible to relate different datums around the world, and also to define a world vertical datum.

In theory, the choice of the datum point (or datum origin) and its potential value can be arbitrary, but as heights are in practice given with respect to the MSL, the datum points are usually chosen at or close to tide gauges (tied to the vertical control network), and the adopted potential value at these points are chosen such that the zero level coincides with the MSL. However, due to the fact that the MSL varies both spatially and temporally, the zero level defined from the long term averaging of tide gauge records results in different reference surface between datum zones as illustrated in Figure 4.1, where $O^{(j)}$ and $O^{(k)}$ are the datum origin points that define the reference surfaces in datum zone j and datum k; h_A and h_B are the ellipsoidal heights of point A and point B obtained from GNSS; $H^{(j)}{}_A$ and $H^{(k)}{}_B$ are the orthometric heights obtained from leveling in datum zone j and datum zone k at points A and B, respectively; $N^{(j)}{}_A$ and $N^{(k)}{}_B$ are the geoid undulations obtained from GNSS/levelling in datum zone j and datum zone k at points A and B, respectively; and $\delta N^{(j)}{}_A$ and $\delta N^{(k)}{}_B$ are the local vertical datum offsets with respect to the global conventional geoid $W_{0.}$ It should be noted that the geoid and the ellipsoidal surfaces illustrated in Figure 4.1 are in reality not parallel to each other.

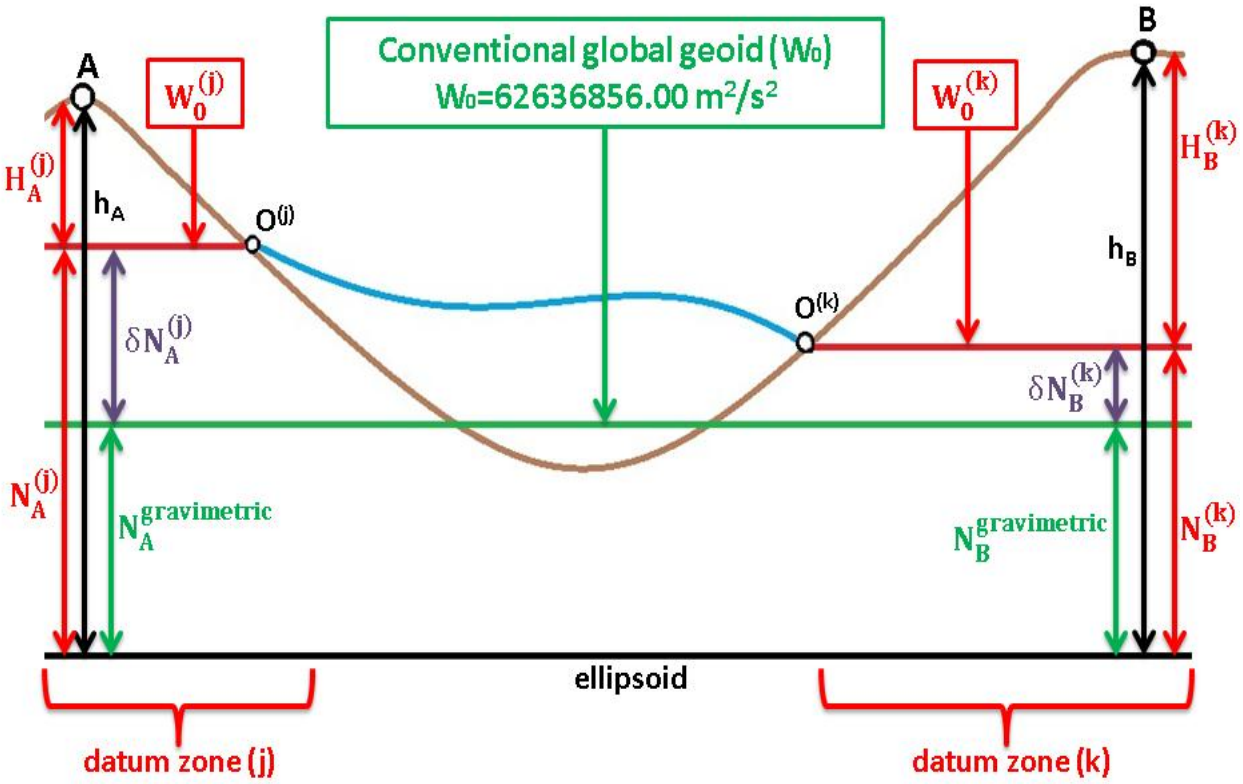

Figure 4.1: Relations between points on different reference surfaces.

The aim of the GOCE mission is to directly provide potential differences between benchmarks in different datum zones (Gerlach and Rummel 2013). The GOCE geoid heights can be combined with ellipsoidal heights derived from space based techniques such as GNSS and physical heights derived from levelling and gravimetry at the benchmarks in order to determine datum offsets between datum zones.

Thus, the potential and the LVD offsets for three vertical datums in North America, (i.e., CGVD28, NAVD88, and Nov07; see Chapter 2 Section 2.5) are computed with respect to a conventional global equipotential surface using GOCE GGMs. In this respect, the following are assessed: the effect of the GOCE model omission errors, the effect of the GOCE model commission error in combination with the errors of the GNSS/levelling data, as well as the effect of the systematic levelling errors on the LVD offsets. The remainder of the chapter is organized as follows: Section 4.2 reviews the methodology and data utilized; results are presented and discussed in Section 4.3; and a summary of the main outcomes are given in Section 4.4.

4.2 Methodology

According to Rummel (2001) there are three basic approaches or methods available for the connection of different datum zones:

1) direct connection by levelling and gravimetry,
2) oceanographic approaches, and
3) indirect connection by solving the geodetic boundary value problem (GBVP).

Option (1) is not suitable for global height unification since it can only be used on continents while option (2) relies on the fact that the mean dynamic topography (MDT; i.e., the height of the sea surface above the geoid) should be precisely known at co-located datum point tide gauges for which the MDT difference between tide gauges from different datum zones would correspond of the datum or height offset between the datum zones (Gerlach and Rummel 2013). The MDT can be obtained from oceanographic models or from altimetry determined mean sea surface (MSS) heights and a precise gravimetric geoid model. However, altimetry determined sea surface heights in coastal regions tend to have poor accuracy due to the fact that the altimetry signal is likely to be contaminated by the land portion of the coastline.

Following the work of Rummel and Teunissen (1988) (i.e., option (3)), one begins with the assumption that there are $J+1$ different LVD zones $\Omega^{(j)}$, $i=\{0, 1,\ldots,J\}$, which refer to different tide gauges and consequently have different reference surfaces. Choosing one of these datums as a reference datum, the height unification method aims to link all the other datum zones to the reference datum Ω^0.

The geopotential difference of datum zone j can be evaluated by

$$\delta W^{(j)} = W_o - W_0^{(j)} \tag{4.1}$$

where W_0 refers to the gravity potential of the selected reference datum and $W_0^{(j)}$ refers to the gravity potential of the LVD in datum zone j.

The offset of the local zero height surface from the reference level surface is:

$$\delta N^{(j)} = \frac{\delta W^{(j)}}{\gamma}. \tag{4.2}$$

The solution to the GBVP for points *P* is given by:

$$T_P = \frac{GM - GM^e}{R} + \frac{R}{4\pi}\iint_{\Omega} S(\psi_{PQ})\left\{\Delta g^{(j)} + \frac{2}{R}\delta W^{(j)}\right\} d\Omega_Q. \tag{4.3}$$

The $\Delta g^{(j)}$ are biased gravity anomalies derived from terrestrial data and the unbiased gravity anomalies are obtained after correcting for the datum offset of datum zone *j*:

$$\Delta g = \Delta g^{(j)} + \frac{2}{R}\delta W^{(j)}. \tag{4.4}$$

The $\Delta g^{(j)}$ represents the gravity anomaly on the topographic surface reduced to the zero height surface in the zone *j* using the orthometric height $H^{(j)}$ using:

$$\Delta g^{(j)} = g_P - \frac{dg}{dh}H_P^{(j)} - \gamma_0, \tag{4.5}$$

where g_P is the measured gravity at the Earth's surface at a point *P* and γ_0 is the normal gravity evaluated at the ellipsoid. It follows that $\Delta g^{(j)}$ is biased since $H^{(j)}$ is biased due to the unknown offset between the height reference surface through datum point O_j and the geoid. The term $\frac{2}{R}\delta W^{(j)}$ is interpreted as the "free-air" reduction which is used to reduce the gravity anomaly $\Delta g^{(j)}$ from the local zero height surface to the level surface defined by the W_0 value. Of course, it is not possible to correct the biased gravity anomalies before one is able to determine $\delta W^{(j)}$. Equation (4.3) is inserted in Bruns's equation (see Chapter 2, Eq. (2.32)):

$$N_P^{(j)} = \frac{T_P - (\Delta W_0) + \delta W^{(j)}}{\gamma}, \tag{4.6}$$

where $\Delta W_0 = W_0 - U_0$.

Thus, the observation equation of the geoid height can be given by:

$$N_P^{(j)} = \left(\frac{GM - GM^e}{R\gamma_0} - \frac{\Delta W_0}{\gamma_0}\right) + \frac{\delta W^j}{\gamma_0} + \frac{R}{4\pi\gamma_0}\iint_\Omega S(\psi_{PQ})\{\Delta g_Q^j\}\, d\Omega_Q + \sum_{i=1}^{J}\frac{1}{2\pi\gamma_0}\delta W_i \iint_{\Omega^i} S(\psi_{PQ})\, d\Omega_Q^i. \quad (4.7)$$

The first bracketed term on the right hand side in Eq. (4.7) is the zero-order term (see Chapter 2, Eq. (2.51)).

The third term in Eq. (4.7) is the solution of the Stokes integral with the local gravity anomalies (i.e., geoid height determined using Stokes integral):

$$N_P = \frac{R}{4\pi\gamma_0}\iint_\Omega S(\psi_{PQ})\Delta g_Q^{(j)}\, d\Omega_Q. \quad (4.8)$$

The fourth term represents the indirect effect of the terrain on the geoid. Using $S_P^i = \frac{1}{2\pi}\iint_{\Omega^i} S(\psi_{PQ}) d\Omega_Q^i$, the fourth term in Eq. (4.7) can be written as:

$$\sum_{i=1}^{J}\frac{1}{2\pi\gamma_0}\delta W_i \iint_{\Omega^i} S(\psi_{PQ})\, d\Omega_Q^i = \sum_{i=1}^{J}\frac{1}{\gamma}S_P^i C_{i0} = \sum_{i=1}^{J} S_P^i\, \delta N^i. \quad (4.9)$$

Substituting Eq. (4.2), Eq. (2.51), Eq. (4.8) and Eq. (4.9), Eq. (4.7) becomes:

$$N_P^{(j)} = N_0 + \delta N^{(j)} + N_P + \sum_{i=1}^{J} S_P^i\, \delta N^i, \quad (4.10)$$

where $\delta N^{(j)}$ is the local datum offset, and $\sum_{i=1}^{J} S_P^i\, \delta N^i$ is the indirect bias term. Thus, the height reference surface of a specific datum zone deviates from the unbiased geoid not only due to its own datum offset (i.e., the direct bias term) but also due to the integration

of biased gravity anomalies (i.e., the indirect bias term). If no satellite based gravity model is used, this error amounts to approximately the same size as the datum offsets, approximately 1 to 2 m globally (Gerlach and Rummel 2013). However, Gerlach and Rummel (2013) have shown that this value decreases using a GOCE GGM with a maximum degree and order of approximately 200; the error does not exceed 1 cm, thus allowing the effect to be neglected in practical height unification. Additionally, investigations in North America have shown that the omission of the indirect bias term for the computation of datum offsets leads to less than 1 cm offset error for a GGM of maximum degree and order 70 (Sideris et al. 2013; Hayden et al. 2012a, see Figure 4.2).

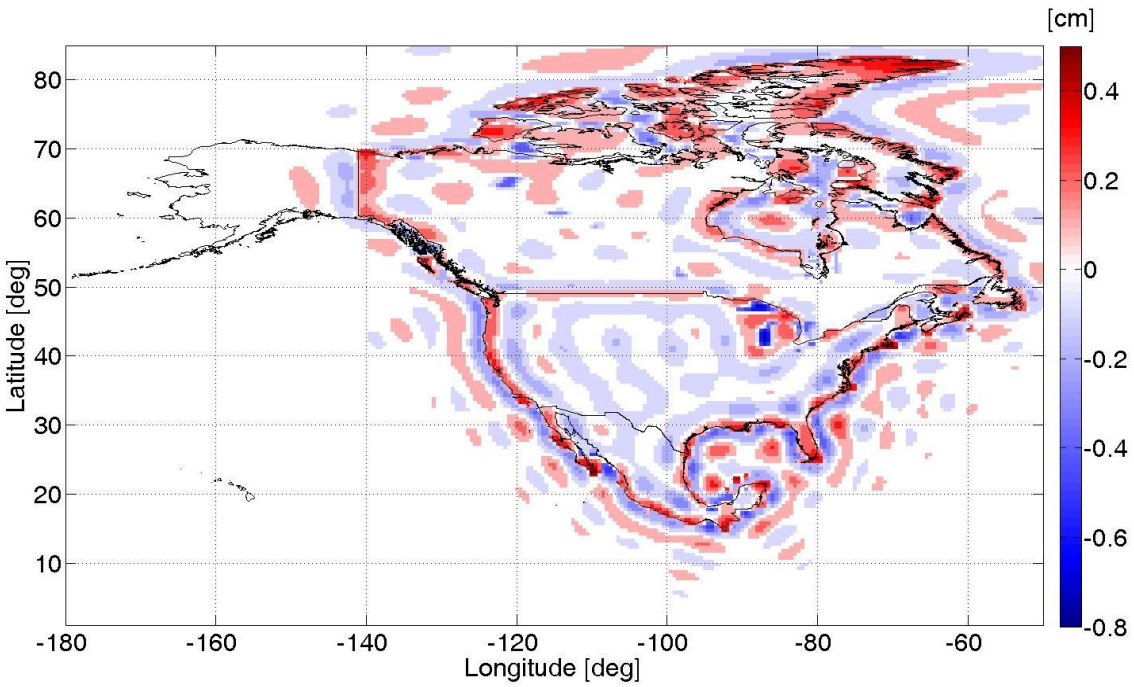

Figure 4.2: Effect of indirect bias term in North America at n_{max} 70 (Sideris et al. 2013).

The geoid height on the left hand side of Eq. (4.10) is computed with the available geodetic and orthometric heights of the point *P* as the difference

$$N_P^{(j)} = h_P - H_P^{(j)}. \tag{4.11}$$

The indirect bias term can be omitted as it has been shown in Figure 4.2 that its effect is less than one centimeter in North America for GGMs used up to at least degree and order 70. Thus, Eq. (4.10) can be re-written as

$$\delta N_P^{(j)} = -N_0 + (h_P - H_P^{(j)} - N_P). \tag{4.12}$$

The geopotential difference can then be computed by multiplying the computed offset by the normal gravity on the ellipsoid:

$$\delta W_P^{(j)} = \gamma_0 \delta N_P^{(j)}. \tag{4.13}$$

Preferably, one would obtain the geoid height N_P in Eq. (4.12) from a high-accuracy satellite-only GGM, such as the GOCE-based models, and evaluate the medium- to short-wavelength geoid signals using local gravity anomalies and topographic information in a remove-restore computational scheme (see Chapter 2, Section 2.6). The Canadian official geoid model *CGG2010* (Huang and Véronneau 2013) and the U.S.A. official geoid model *USGG2012* (www.ngs.noaa.gov/GEOID/USGG2012) are both examples of optimal combinations of a satellite-only GGM, local gravity, and topographic information. The *CGG2010* geoid heights are available on a 2' by 2' grid for a region that covers 20°N to 80°N and -170°W to -10°W while the *USGG2012* geoid heights are available on a 1' by 1' grid for a region that covers 24°N to 58°N and -130°W to -60°W for mainland U.S.A.; in addition coverage for Alaska, Hawaii, Guam and Northern Mariana Islands, Puerto Rico, U.S.A. Virgin Islands, and the American Samoa is also available. Hence, *CGG2010* can be utilized to assess the magnitude of the omission error of the GOCE GGM in a large part of North America (see Chapter 3, Figure 3.6).

One may also use the *EGM2008* (Pavlis et al. 2012) model to approximate the omission error of the GOCE models. However, *EGM2008* is not able to model a gravity field signal with half-wavelengths smaller than 9 km. The global average omission error is approximately 4 cm when the geoid is computed using *EGM2008*, although it can be larger in mountainous terrain (Jekeli 2009). In other words, due to the fact that the

topography of the Earth is the main source of high-frequency gravity field signals (Forsberg 1984), the effect of the omission error in low-lying terrain will tend to be smaller than in mountainous regions (see, e.g., Hirt et al. 2010). Moreover, the residual terrain model (RTM) technique (Forsberg and Tscherning 1981; Forsberg 1984; Forsberg 1985) can be used to model the high-frequency signals not provided by the *EGM2008* model. When using the RTM technique a digital terrain model representing the Earth's topography is referred to a long-wavelength reference surface, which removes the low-frequency components of the digital terrain model already implied by the GGM (Hirt et al. 2010). However, in regions with sufficient terrestrial gravity data coverage, such as Canada or the U.S.A., the remove-compute-restore method allows for a more accurate modelling of the high frequency components of the gravity field. Thus, *CGG2010* and *USGG2012* are better candidates than *EGM2008* to quantify the contribution of the high frequencies of the gravity field that are not modelled by the GOCE GGMs. The gravimetric geoid model developed by Ince et al. (2012), though not an official geoid model of Canada, can be considered an updated gravimetric geoid model with respect to *CGG2010*, as it uses the third generation direct GOCE model for the long wavelength contributions of the gravity field, and can also be used to quantify omission errors.

It should be emphasized that *CGG2010* and *USGG2012* are not completely independent from *EGM2008*. *EGM2008* uses the high-quality Canadian and U.S.A. local gravity information that is used in the computation of *CGG2010* and *USGG2012*. Conversely, *CGG2010* utilizes *goco01s* (Pail et al. 2010) and *EGM2008* from degree 2 to 224 using a weighted averaging based on the coefficient standard deviations and *EGM2008* up to degree and order 2190 (Huang J., Natural Resources Canada, personal communication, November 29, 2012). In *USGG2012*, the *goco02s* model substitutes the GRACE model that went into making *EGM2008* by applying a cosine taper to blend the *goco02s* coefficients with those of *EGM2008*, starting at degree and order 100 and ending at degree and order 200, which produces a modified reference model reflecting GOCE data for the mid-wavelengths of the gravity field signal (Roman D., National Geodetic Survey, personal communication, March 21, 2013). Therefore, one can expect that the effect of

the GOCE omitted signal on the LVD offsets will not differ significantly when it is evaluated by means of *EGM2008, CGG2010,* or *USGG2012*.

4.2.1 Sources of Error affecting LVD Offset Computations

Systematic and random measurement errors, as well as the omission and commission errors from the gravity field models will affect the LVD offsets computed from GNSS/levelling information. According to Kotsakis et al. (2011), a biased LVD offset (i.e., an offset value that differs from the true LVD offset value) may result in the presence of systematic effects and spatially correlated errors in the height data. In such a case, h_P-$H_P^{(j)}$-N_P will not follow the typical trend of a constant offset; rather it may reveal spatial tilts or even a more complex oscillatory pattern over the network of GNSS/levelling benchmarks.

Systematic errors that can contribute to biased LVD offsets comprise of datum inconsistencies between the ellipsoidal heights and the geoid heights, which result from the use of different reference ellipsoids in the geoid model and ellipsoidal heights. Additionally, geometrical distortions in the levelling height data due to over-constraining the LVD to several tide gauge stations (e.g., CGVD28), long and medium wavelength errors in the geoid model, accumulated systematic errors in the levelling network (Entin 1959), improper modelling of temporal height variations, the inconsistent treatment of permanent tide in the geoid, physical and ellipsoidal heights (Ekman 1989; Mäkinen and Ihde 2009), and the uncertainty of the zero-degree term of the Earth's gravity potential, which corresponds to a vertical uncertainty of more than 1 cm for the zero-height surface of a vertical datum (Kotsakis et al. 2011), may also result in a biased LVD offset.

The removal of the systematic effects in the height data can be performed through appropriate corrections and spatial de-trending of the raw geoid height differences or simultaneously with the LVD offset using the extended observation equation:

$$\delta N_P^{(j)} + \boldsymbol{a}_P^T \boldsymbol{x} + v_P = -N_0 + (h_P - H_P^{(j)} - N_P), \tag{4.14}$$

where the term $\boldsymbol{a}_P^T\boldsymbol{x}$ absorbs the systematic errors through a set of parameters $\boldsymbol{x}$ while $\boldsymbol{a_P}$ is a vector of known coefficients dependent on the spatial position of the GNSS/levelling benchmarks, and v_P represents the random error of the geoid height difference at point P. The inseparability between the $\delta N_P^{(j)}$ term and the bias parameter of the corrector model remains an open problem in geodesy for the practical determination of local datum potentials and offsets. A comprehensive discussion regarding examples of parametric models used for the description of systematic effects can be found in Fotopoulos (2003).

Lastly, commission errors of the GGMs for wavelengths that exceed the size of the test area can act as a bias on the LVD offset estimate. This effect cannot be reduced by increasing the sampling distribution of the GNSS/levelling benchmarks and may be especially problematic for small test regions such as the independent levelling networks of Vancouver Island and Newfoundland.

4.2.2 Data

The main datasets include physical heights at benchmarks obtained from levelling and gravimetric measurements, ellipsoidal heights obtained from GNSS on the benchmarks, and geoid heights obtained from GGMs (see Chapter 3, Table 3.1) or gravimetric geoid models (see Table 4.1).

Table 4.1: Gravimetric geoid models.

Model	**Data Source**	**References**
CGG2010	based on terrestrial gravity data and global models goco01s and EGM2008	Huang and Véronneau (2013)
USGG2012	based on terrestrial gravity data and global models goco02s and EGM2008	NGS (2012)
Ince et al. (2012)	Based on terrestrial gravity data and global model go_cons_gcf_2_dir_r3	Ince et al. (2012)

4.2.3 GNSS/Levelling Benchmark Distribution

Two subsets of GNSS/levelling benchmarks are used in Canada while the 18,399 GNSS/levelling benchmarks presented in Chapter 3 for GOCE model evaluation (see Figure 3.5) are utilized for the computation of LVD offsets for the NAVD88 datum in the U.S.A.

The first dataset in Canada refers to 308 benchmarks, where the original ellipsoidal heights and coordinates were given in ITRF2005 (Altamimi et al. 2007) epoch 2006.0 and come from the adjustment of the GPS SuperNet network in Canada (Craymer and Lapelle 1997). These have been updated to ITRF2008 epoch 2008.0 using software developed by the U.S.A. National Geodetic Survey (available at http://www.ngs.noaa.gov/TOOLS/Htdp/Htdp.shtml), taking into account the effect of post-glacial rebound using the velocities from the Argus and Peltier (2010) *GEODVEL1b GPS* solution. This correction was applied using a 2-D linear interpolation and with the assumption that the acceleration of the vertical motion is zero. These benchmarks have physical heights obtained from levelling that refer to CGVD28, NAVD88, and the Nov07 vertical datums (see Figure 4.3).

The next dataset refers to levelling data given with respect to the Nov07 vertical datum. There are three main regions: Canadian Mainland (CML), Newfoundland (NFD), and Vancouver Island (VAN).

For the Canadian mainland (see Figure 4.4), the relief of the terrain ranges from mean sea level to 500 m for eastern and most of central Canada while the topography becomes quite rugged for the western portion of the country where the elevation ranges from 500 m to 3000 m, reaching a maximum of 5000 m or more in a few selected areas (Natural Resources Canada 2007).

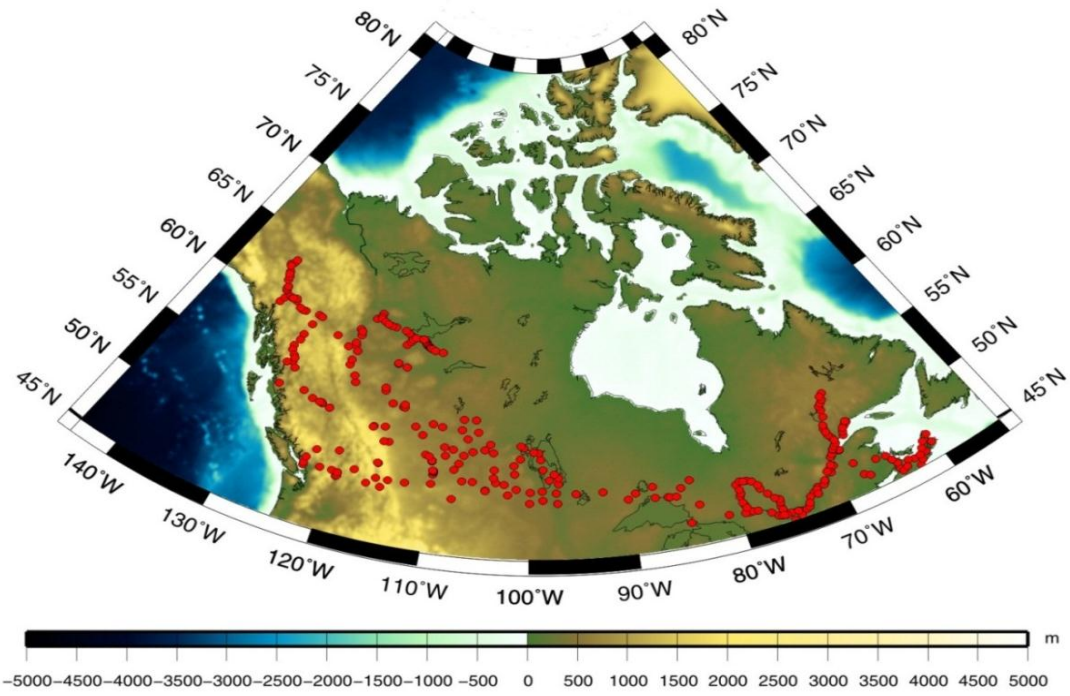

Figure 4.3: Distribution of 308 GNSS/levelling benchmarks common in Nov07, CGVD28, and NAVD88 vertical datums.

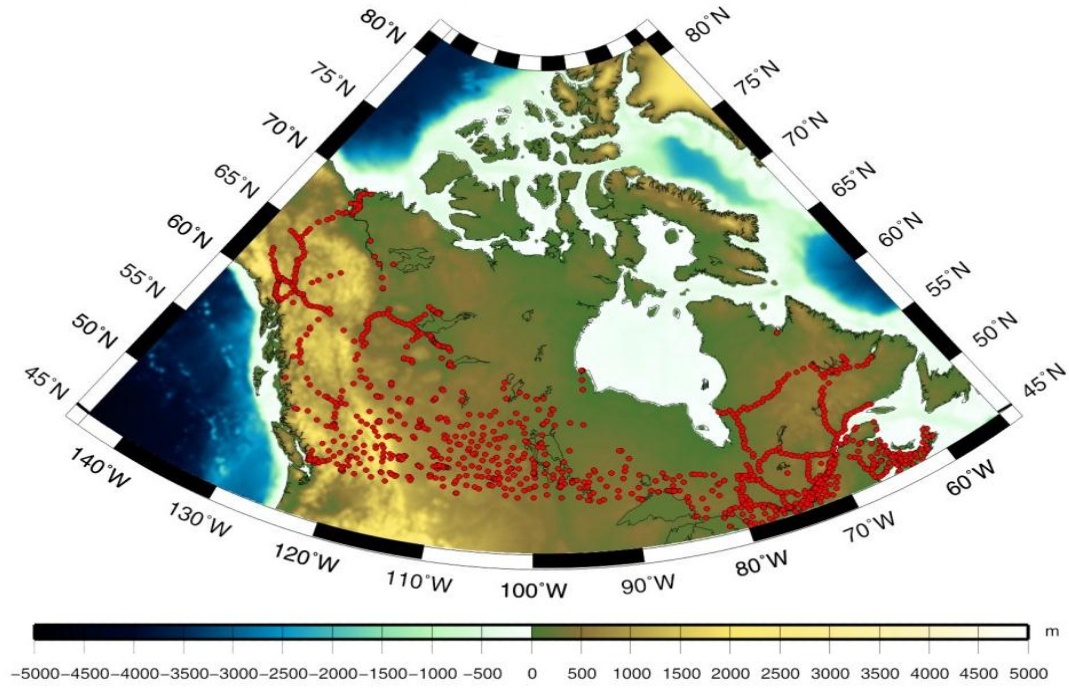

Figure 4.4: Distribution of 1,315 GNSS/levelling benchmarks in the Nov07 vertical datum for the Canadian mainland (CML).

The topography of Vancouver Island as shown in Figure 4.5 can be considered medium rugged terrain, where coastal elevations range from 100 to 500 m while the average elevation of the interior of the island ranges from 500 to 1500 m, reaching a maximum of 2000 m (Natural Resources Canada 2007).

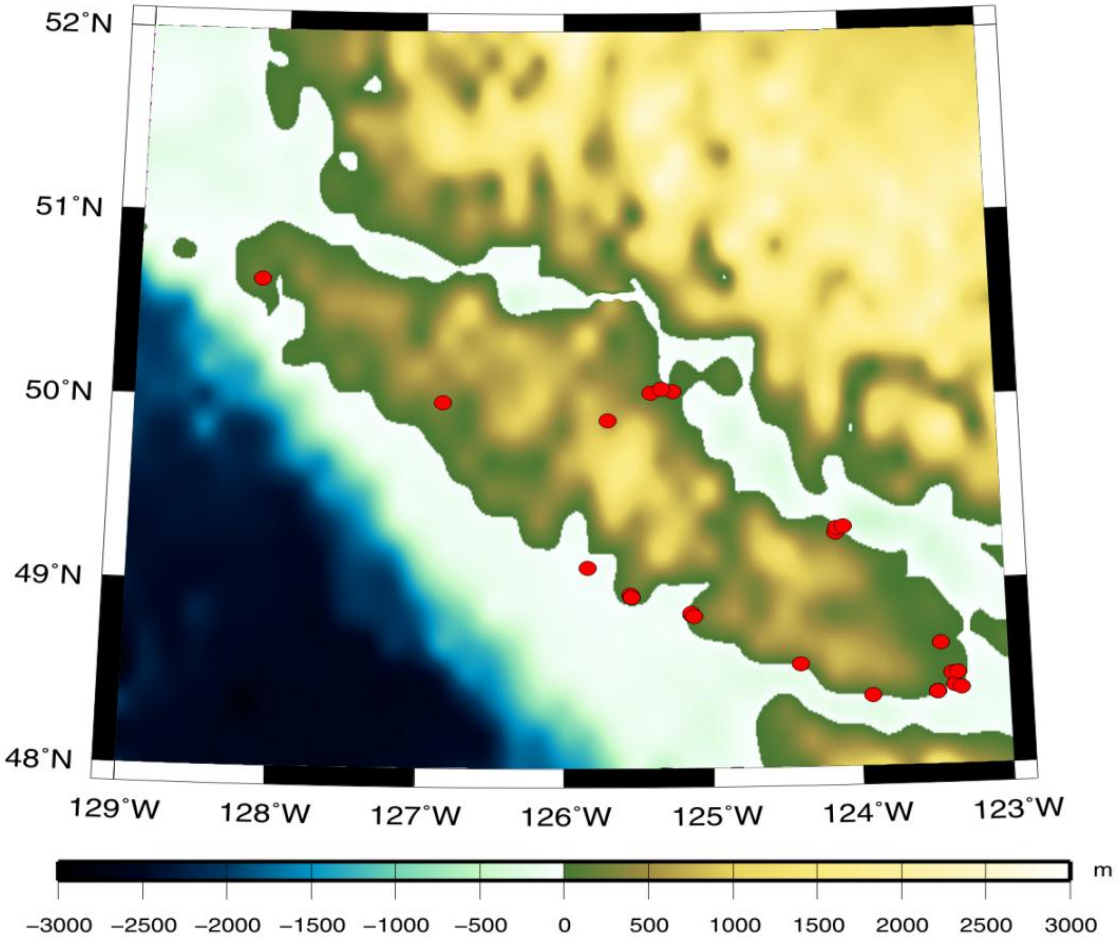

Figure 4.5: Distribution of 26 GNSS/levelling benchmarks in Nov07 vertical datum for Vancouver Island (VAN).

In contrast to Vancouver Island, the terrain of Newfoundland as shown in Figure 4.6 is much more flat, ranging in elevation from mostly 100 to 500 m, reaching a maximum of 700 m in a few areas (Natural Resources Canada 2007).

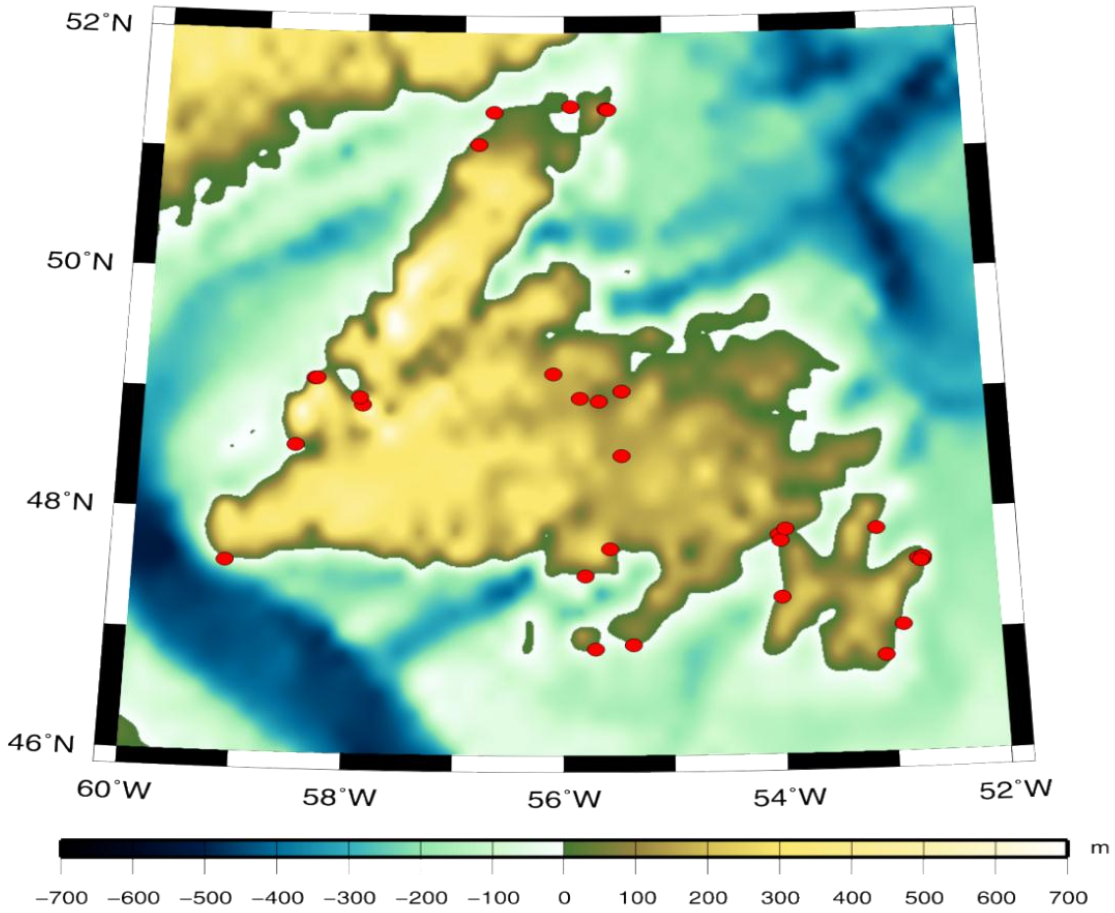

Figure 4.6: Distribution of 34 GNSS/levelling benchmarks in Nov07 vertical datum for Newfoundland (NFD).

4.3 Results and Discussion

In order to assess the performance of the GOCE-based models for the computation of LVD offsets, the results are compared with those obtained with gravimetric geoid models in Table 4.1. As shown in Chapter 3, the *goco03s* model performs well up to degree and order 180 in both Canada and U.S.A., while the *tim_r4* performs well up to degree and order 200. In Canada the *dir_r4* has good performance up to degree and order 210, and it has good performance up to degree and order 200 in the U.S.A. Thus, the GOCE models are extended from degree and order 181 to 2190, 201 to 2190, and 211 to 2190 using *EGM2008* in order to evaluate the effect of the omission error on the computed LVD offsets. All computations have been implemented with the GRS80 ellipsoid parameters. The 2010 International Earth Rotation and Reference System Service's (IERS)

conventional value of 62636856.00 m^2/s^2 (Petit and Luzum 2010) was used for W_0 defining the global equipotential surface. The height data are all in a tide-free system.

4.3.1 Estimating CGVD28, NAVD88, and Nov07 LVD Offsets in Canada using 308 GNSS/Levelling Benchmarks

Table 4.2 presents the LVD offsets of Nov07, NAVD88, and CGVD28 for the data set of 308 GNSS/levelling benchmarks distributed mainly along the southern region of Canada (see Figure 4.3). The results are shown in terms of the potential difference between the reference conventional surface and the local datum (i.e., $\delta W^{(j)}$) and the offset of the LVD (i.e., $\delta N^{(j)}$). For the least-squares evaluation of Eq. (4.12), a unit weight matrix has been used, assuming a constant and uncorrelated noise in the known heights at all data points; the error estimates shown in the tables indicate a formal statistical accuracy only. The main objective of this section is to estimate the effect of the GOCE model omission error on LVD offset estimations, and as such the effects of systematic errors have not been taken into account for the numerical computations presented herein.

The effect of the GOCE omission error is quite significant in Canada when computing LVD offsets. For example, from Table 4.2 , the Nov07 offset computed with *goco03s+EGM2008* is -44.8 cm and the offset computed with *tim_r4+EGM2008* is -44.9 cm while the GOCE only models yield -58.2 cm and -53.3 cm, respectively. Thus, the effect of the GOCE GGM omission error on the LVD offsets can be quantified as 13 cm for the third generation GOCE GGM truncated at degree and order 180, and 8 cm for the fourth generation GOCE GGMs truncated at degree and order 200 and 210. Based on the results from Table 4.2, it can be seen that both *dir_r4* and *tim_r4* perform very similarly when the models are truncated at degree and order 200 and 210, respectively; the difference between the evaluated LVD offsets is less than 1 cm. The similar performance is expected as both models use the same 27 months of GOCE observations and similar data pre-processing (Pail et al., 2011). Likewise, the *itg-grace2010s* omission error affects the computed LVD offsets by 13 cm.

It is expected that the results obtained with *CGG2010*, *EGM2008*, GRACE+*EGM2008*, and the GOCE+*EGM2008* models will be similar as the same high quality gravity data are utilized by all three models. For example, the Nov07 offset evaluated with *EGM2008* is -44.8 cm and with *CGG2010* it is -45.2 cm. It can be seen that *CGG2010* yields a 13 cm difference between the offsets computed with *goco03s*, *a*nd an 8 cm difference between the offset computed with *tim_r4*, which is similar to the omission error approximated by *EGM2008*. However, a 15 cm effect is observed when *itg-grace2010s* is used. Based on the smaller offset difference, it can be concluded that *tim_r4* or *dir_r4* should be preferred to *itg-grace2010s* for the LVD offset computations.

It can also be observed from Table 4.2 that the formal standard deviations of the estimated LVD offsets decrease when using models that incorporate the higher frequency information of the gravity field. For example, the standard deviation of the Nov07 offset using *goco03s* is 2.1 cm while it reduces to 0.7 cm in the *goco03s+EGM2008* case. This is because the geoid heights computed with the GOCE+*EGM2008* models are more spectrally consistent with the GNSS-levelling geoid heights than the geoid heights computed with the truncated GOCE models of degree 180. In general, it can also be observed that the standard deviations of the estimated NAVD88 (e.g., 2.2 cm) and CGVD28 (e.g., 1.7 cm) offsets are larger than the standard deviation of the Nov07 offset (e.g., 0.7 cm), which can be explained by the differences in the existing systematic errors and local datum distortions in NAVD88 and CGVD28 described in Chapter 2 Section 2.5.

4.3.2 Estimating Nov07 LVD Offsets for CML, VAN, and NFD Networks

Table 4.3 shows the Nov07 offset computed with the *CGG2010,* Ince et al. (2012), *goco03s+EGM2008,* and *tim_r4+EGM2008* models, as well as the *goco03s* and *tim_r4* models. The LVD offsets for VAN and NFD are evaluated for a local level surface that is different from that of the Nov07 CML network.

Table 4.2: Potential and vertical datum offsets for Nov07, NAVD88, and CGVD28 vertical datum evaluated with 308 GNSS/levelling benchmarks.

Vertical Datum	$\delta W^{(j)}$ (m^2/s^2)	$\delta N^{(j)}$ (cm)	$\delta W^{(j)}$ (m^2/s^2)	$\delta N^{(j)}$ (cm)
	goco03s n_{max}:180		**goco03s + EGM2008 n_{max}:180 + 181 to 2190**	
Nov07	-5.71± 0.20	-58.2 ± 2.1	-4.40 ± 0.06	-44.8 ± 0.7
NAVD88	-9.23 ± 0.30	-94.0 ± 3.1	-7.91 ± 0.22	-80.6 ± 2.2
CGVD28	-2.77 ± 0.20	-28.3 ± 2.0	-1.46 ± 0.16	-14.9 ± 1.7
	tim_r4 n_{max}: 200		**tim_r4 + EGM2008 n_{max}:200 + 201 to 2190**	
Nov07	-5.23 ± 0.17	-53.3 ± 1.8	-4.41 ± 0.07	-44.9 ± 0.7
NAVD88	-8.74 ± 0.27	-89.1 ± 2.7	-7.92 ± 0.22	-80.7 ± 2.2
CGVD28	-2.29 ± 0.20	-23.3 ± 2.0	-1.47 ± 0.16	-15.0 ± 1.7
	dir_r4 n_{max}: 210		**dir_r4 + EGM2008 n_{max}:210 + 211 to 2190**	
Nov07	-5.23 ± 0.17	-53.3 ± 1.8	-4.39 ± 0.07	-44.7 ± 0.7
NAVD88	-8.75 ± 0.27	-89.1 ± 2.8	-7.90 ± 0.22	-80.5 ± 2.2
CGVD28	-2.30 ± 0.20	-23.4 ± 2.0	-1.45 ± 0.16	-14.8 ± 1.7
	itg-grace2010s n_{max}: 180		**itg-grace2010s + EGM2008 n_{max}: 180 + 181 to 2190**	
Nov07	-5.88 ± 0.23	-59.9 ± 2.3	-4.57 ± 0.12	-46.5 ± 1.3
NAVD88	-9.39 ± 0.32	-95.7 ± 3.3	-8.08 ± 0.24	-82.3 ± 2.5
CGVD28	-2.94 ± 0.22	-30.0 ± 2.3	-1.63 ± 0.19	-16.6 ± 1.9
			CGG2010	
Nov07	--	--	-4.42 ± 0.06	-45.2 ± 0.6
NAVD88	--	--	-7.92 ± 0.21	-81.0 ± 2.1
CGVD28	--	--	-1.49 ± 0.17	-15.3 ± 1.7
			EGM2008 n_{max}:2190	
Nov07	--	--	-4.39 ± 0.06	-44.8 ± 0.6
NAVD88	--	--	-7.91 ± 0.21	-80.6 ± 2.2
CGVD28	--	--	-1.45 ± 0.16	-14.8 ± 1.7

Table 4.3: Potential and vertical datum offsets for Nov07 vertical datum evaluated with GNSS/levelling benchmarks from CML, NFD, and VAN regions of Canada.

Regions	$\delta W^{(j)}$ (m^2/s^2)	$\delta N^{(j)}$ (cm)
CGG2010		
CML (1315)	-4.40 ± 0.03	-45.0 ± 0.3
NFD (34)	-4.31 ± 0.19	-44.1 ± 1.9
VAN (26)	-3.81 ± 0.13	-38.9 ± 1.3
Ince et al. (2012)		
CML (1315)	-4.44 ± 0.03	-45.3 ± 0.3
NFD (34)	-3.71 ± 0.11	-37.8 ± 1.1
VAN (26)	-4.00 ± 0.10	-40.8 ± 0.9
goco03s n_{max}: 180		
CML (1315)	-5.81 ± 0.11	-59.2 ± 1.1
NFD (34)	-4.29 ± 0.49	-43.7 ± 5.0
VAN (26)	-1.02 ± 1.45	-10.4 ± 14.8
goco03s + EGM2008 n_{max}: 180 + 181 to 2190		
CML (1315)	-4.36 ± 0.04	-44.5 ± 0.4
NFD (34)	-3.28 ± 0.10	-33.5 ± 1.1
VAN (26)	-4.05 ± 0.11	-41.3 ± 1.1
tim_r4 n_{max}: 200		
CML (1315)	-5.45 ± 0.09	-55.5 ± 1.0
NFD (34)	-3.98 ± 0.48	-40.6 ± 4.8
VAN (26)	-2.40 ± 1.11	-24.4 ± 11.3
tim_r4 + EGM2008 n_{max}: 200 + 201 to 2190		
CML (1315)	-4.34 ± 0.04	-44.3 ± 0.4
NFD (34)	-3.14 ± 0.11	-32.0 ± 1.1
VAN (26)	-3.97 ± 0.13	-40.5 ± 1.3
dir_r4 n_{max}: 210		
CML (1315)	-5.36 ± 0.09	-54.7 ± 0.9
NFD (34)	-4.07 ± 0.37	-41.5 ± 3.8
VAN (26)	-2.97 ± 0.97	-30.3 ± 9.9
dir_r4 + EGM2008 n_{max}: 210 + 211 to 2190		
CML (1315)	-4.33 ± 0.04	-44.2 ± 0.4
NFD (34)	-3.36 ± 0.10	-34.2 ± 1.1
VAN (26)	-3.95 ± 0.16	-40.3 ± 1.6
tim_r4 n_{max}: 250		
NFD (34)	-3.45 ± 0.37	-35.2 ± 3.8
VAN (26)	-3.78 ± 0.77	-38.5 ± 7.9

The results shown in Table 4.3 for the CML test network reflect the same trends presented for the results in Table 4.2. Once again, the LVD offsets presented in Table 4.3 demonstrate that the addition of the higher frequencies of the gravity field signal to the

GOCE GGMs is an important factor for the accurate determination of the LVD offsets in Canada. Therefore, it is recommended that a rigorously combined GOCE GGM and local gravity and terrain data should be used when using GOCE-based GGMs for the evaluation of LVD offsets in Canada.

The results from Table 4.3 emphasize the fact that simply increasing the number of GNSS/levelling benchmarks will not necessarily reduce the effect of the GOCE omission error on the LVD offsets. For example, the offset for the CML network computed with 1,315 benchmarks and the *tim_r4* model is -55.5 cm while it was -53.3 cm when evaluated with 308 benchmarks. In this case, increasing the number of benchmarks has actually increased the effect of the GOCE omission error by 2 cm. This increase in the effect of the GOCE omission error can be explained by the fact that a portion of the newly added points are located in the rugged terrain of western Canada; as well the distribution of the benchmarks in the CML network is not necessarily improved with respect to the 308 benchmark case of the previous section (see Figures 4.3 and 4.4). Thus, another factor that will affect the LVD offset estimate, in addition to the density of the benchmarks, is the configuration of the GNSS-levelling network.

For the offsets estimated on the two islands (i.e., VAN and NFD) the effects of the limited geographical coverage and sparse and irregular distribution of the GNSS/levelling benchmarks can be observed from the results in Table 4.3. For example, the offset evaluated for VAN using *goco03s* only is -10.4 ± 14.8 cm when compared to -38.9 ± 1.3 cm with *CGG2010* and -40.8 ± 0.9 cm with the Ince et al. (2012) model. Using the 3-sigma test, it can be seen that the offset computed with *goco03s* (as well as the *tim_r4* model) yields a statistically insignificant LVD offset for Vancouver Island as the estimated LVD offset is smaller than three times its formal error. This insignificant result can be further explained by the effect of the GOCE omission error on the LVD offset of Vancouver Island, which is expected to be quite significant due to its rugged terrain (see Figure 4.5). In other words, neither the *goco03s* nor the *tim_r4* model truncated at degree and order 180 and 200, respectively, sufficiently models the geoid signal on Vancouver Island. On the other hand, it can be seen from Table 4.3 that when the offset is evaluated

with *tim_r4* expanded to degree and order 250 the value is -38.5 ± 7.9 cm, which is in much better agreement to the offset values evaluated with *CGG2010* and the Ince et al. (2012) gravimetric geoid models.

As expected, in the case for Newfoundland, the effect of the GOCE omission error on the LVD offset appears to be less significant when compared with Vancouver Island, the effect on the LVD offset reaches a maximum of 10 cm when comparing results obtained using *goco03s* to *goco03s+EGM2008*. As well, when evaluating the LVD offset for NFD with *tim_r4* expanded degree and order 250, the contribution of the higher degree spherical harmonic coefficients is not as stark as in the case of VAN. The difference between the LVD offset estimated with *tim_r4* expanded to degree and order 200 and the LVD offset estimated with *tim_r4* to degree and order 250 is approximately 5 cm for the NFD test network and approximately 14 cm for the VAN test network.

Table 4.4: LVD offset for Nov07 datum for CML, NFD, and VAN regions using error information for the ellipsoidal, orthometric, and geoid heights.

Region	$\delta N^{(j)}$ **(cm) without error information**	$\delta N^{(j)}$ **(cm) with error information**	**Difference (cm)**
goco03s n_{max}:180			
CML (1315)	-59.2 ± 1.1	-63.2 ± 1.0	4.0
NFD (34)	-43.7 ± 5.0	-56.9 ± 2.5	13.2
VAN (26)	-10.4 ± 14.8	77.3 ± 8.9	87.7
CGG2010			
CML (1315)	-45.0 ± 0.3	-41.6 ± 0.3	3.4
NFD (34)	-44.1 ± 2.0	-40.6 ± 1.7	3.4
VAN (26)	-39.9 ± 1.3	-37.5 ± 1.3	2.4

Table 4.4 shows the LVD offsets computed with the inclusion of the ellipsoidal height, orthometric height, and geoid height error using *goco03s* and *CGG2010* in order to

evaluate the effect of including accuracy information on the LVD offset estimations. The variances of the spherical harmonic coefficients were used when propagating the commission errors from the GOCE model to the geoid heights. The average error for the geoid heights obtained from *goco03s* is 3.4 cm. The error estimates for the ellipsoidal heights, orthometric heights, and geoid heights obtained from the *CGG2010* model were provided by GSD. For the VAN test network the mean ellipsoidal height error is approximately 1 cm, the mean orthometric height error is approximately 2 cm, and the average error for the geoid heights obtained from the *CGG2010* model is 5 cm. For the NFD test network, the average ellipsoidal and orthometric height errors are the same as for the VAN test network while the average geoid height error from the *CGG2010* model is 2 cm. Lastly, for the CML test network the mean ellipsoidal height error is 1 cm, the mean orthometric height error is 6 cm, and the mean geoid height error obtained from the *CGG2010* model is 3 cm.

Based on the results presented in Table 4.4, a 4 cm difference can be observed in the LVD offset computed using GOCE commission error information up to degree and order 180, in combination with the error estimates for the ellipsoidal and levelling heights, when compared to the LVD offset estimated without any error information for the CML region. This effect is more pronounced for Newfoundland, where the difference is 13 cm. One of the reasons contributing to this difference can be explained by the fact that the geographical coverage of the NFD network is much smaller when compared to the geographic coverage of the CML network, and therefore it is more likely to be affected by the commission errors of the GGM wavelengths that exceed the size of the test area. The large difference of almost 88 cm for Vancouver Island may be due to the uncertain reliability of the control data and their errors on Vancouver Island, in addition to the fact that utilizing only the *goco03s* model extended to degree and order 180 for the VAN test network yields statistically insignificant results. Moreover, using only the variances of the spherical harmonic coefficients may also have an effect as the inclusion of a full variance co-variance matrix may yield different results. Thus, for each of the islands, the computed potential and offset for the Nov07 datum demonstrate that the GGM

inaccuracies and the measurement errors cannot average out over the limited geographic coverage and number of GNSS/levelling benchmarks found in each region.

With the goal of unifying height datums with 1 cm accuracy (CVRS Conventions 2007), it can be observed from Table 4.4 that the inclusion of accuracy information for even high resolution models may be necessary. Utilizing the accuracy information provided with the *CGG2010* model yields in combination with the errors of the ellipsoidal and levelling heights results in a 2 to 3 cm difference in the LVD offsets for CML, NFD, and VAN test networks when compared to LVD offsets computed without accuracy information.

4.3.3 The Effect of Systematic Errors on LVD Offsets

In this section, the systematic effects in the height data and their effect on the estimated LVD offset are examined. For the evaluation of the LVD offset, Eq. (4.14) is used with the following options for the bias corrector term (Kotsakis et al. 2011):

Null model: $\boldsymbol{a_P^T x} = 0,$ (4.15)

1-Parameter Model: $\boldsymbol{a_P^T x} = \delta s H_P^j,$ (4.16)

2-Parameter Model: $\boldsymbol{a_P^T x} = x_1(\varphi_P - \varphi_0) + x_2(\lambda_P - \lambda_0)\cos\varphi_P,$ (4.17)

and

Combined Model: $\boldsymbol{a_P^T x} = x_1(\varphi_P - \varphi_0) + x_2(\lambda_P - \lambda_0)\cos\varphi_P + \delta s H_P^j.$ (4.18)

No systematic errors or other biases are modeled within the height data when using Eq. (4.15). The scale parameter δs in Eq. (4.16) may be viewed as an apparent scale difference between LVD orthometric heights and the GNSS/geoid based orthometric heights as the raw residuals/geoid height differences $h_P - H_P^{(j)} - N_P$ are often

topographically correlated. The application of the systematic model shown in Eq. (4.16) will only be successful in a test network that has a significant height variability so that the offset parameter $\delta N_P^{(j)}$ and the scale parameter δs can be sufficiently separated through the least-squares estimation (Kotsakis et al. 2011) of Eq. (4.14). In general, if one expects to obtain realistic estimates of the LVD offset, the vertical offset term should not be strongly correlated with the adopted bias corrector term model. Thus the bias corrector term model should not contain any components that remain constant or almost constant over the test network. As discussed in the previous section, it should be noted that for test networks with limited geographic coverage, the long-wavelength geoid errors will contaminate the least-squares estimate of the LVD offset, thus for such networks it is necessary to include the GGM commission errors for spatial wavelengths the exceed the size of the test area when utilizing bias corrector term models to estimate the effect of systematic errors on LVD offsets. For the model in Eq. (4.17), φ_P is the latitude of the GNSS/levelling benchmark and λ_P is the longitude; the overall tilt consists of a N-S component x_1, and a W-E component x_2 with respect to the centroid of the test network (φ_0, λ_0). The combined model shown by Eq. (4.18) consists of a combination of the 1-parameter and the 2-parameter model.

The geoid height differences are plotted in Figures 4.7 to 4.10 in order to show the spatial tilts present in the respective GNSS/levelling networks while the distribution of the orthometric heights of the Canadian Nov07, NAVD88, CGVD28, and the U.S.A. NAVDD88 test networks are shown in Figures 4.11 to 4.14, respectively. Figures 4.7 to 4.9 show that for the Canadian Nov07, NAVD88, and CGVD28 test networks there exists a significant east-west tilt, and a less significant north-south tilt while for the U.S.A. NAVD88 test network, shown in Figure 4.10, there is both a significant east-west and north-south tilt.

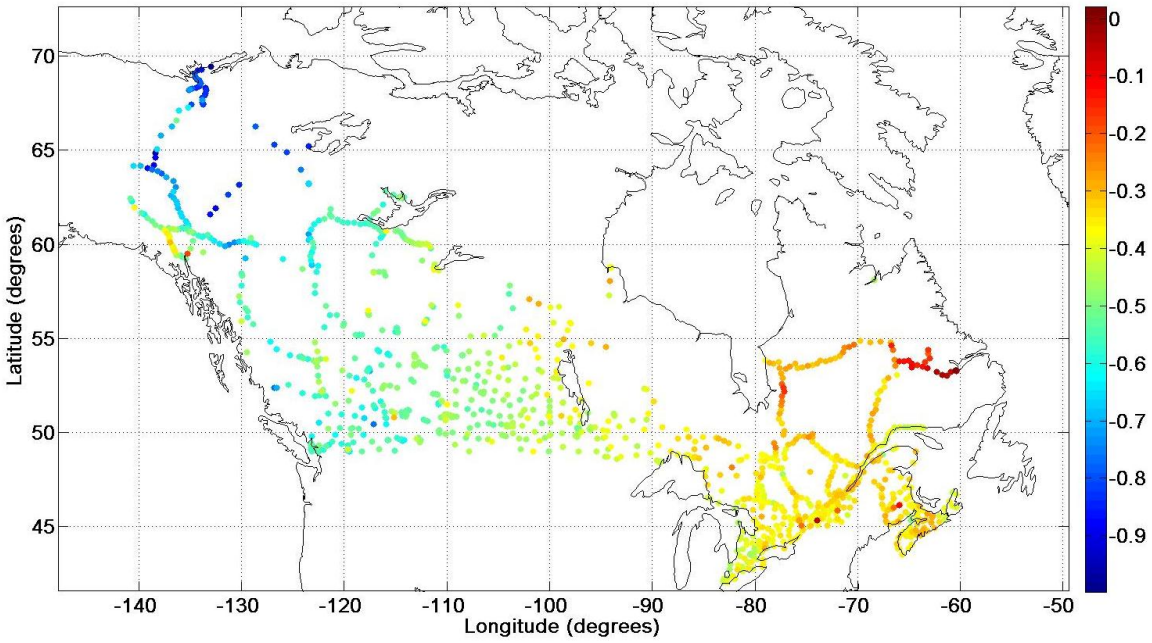

Figure 4.7: Geoid height differences $h\text{-}H\text{-}N^{EGM2008}$ (in meters) for the CML Nov07 GNSS/levelling benchmarks.

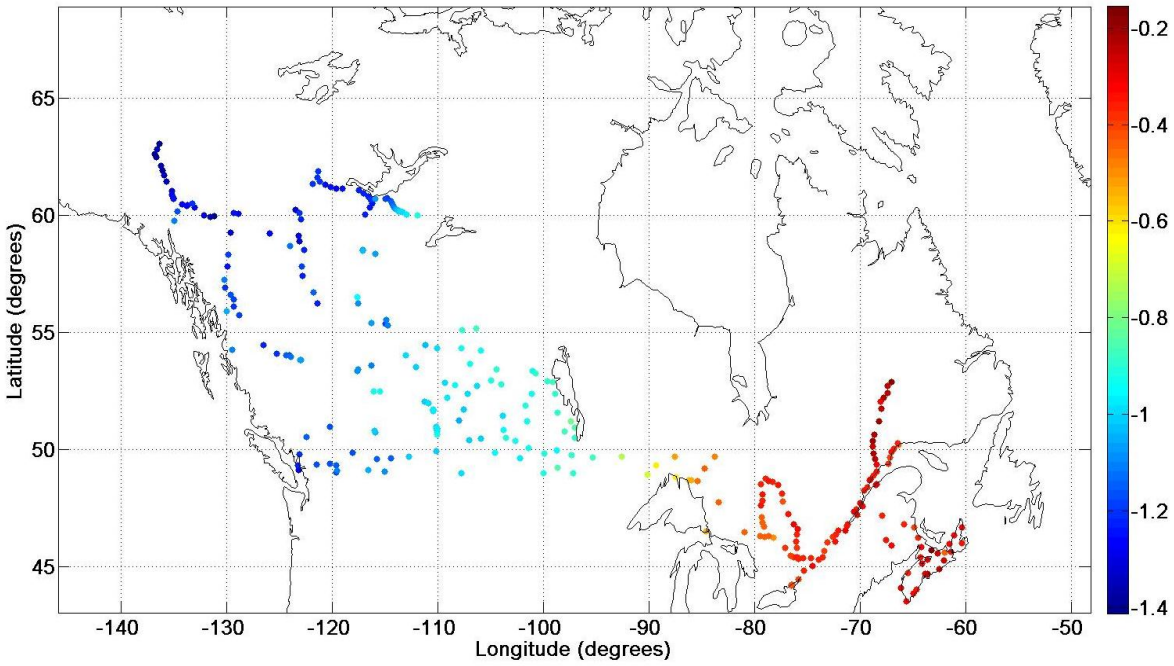

Figure 4.8: Geoid height differences $h\text{-}H\text{-}N^{EGM2008}$ (in meters) for the NAVD88 GNSS/levelling benchmarks.

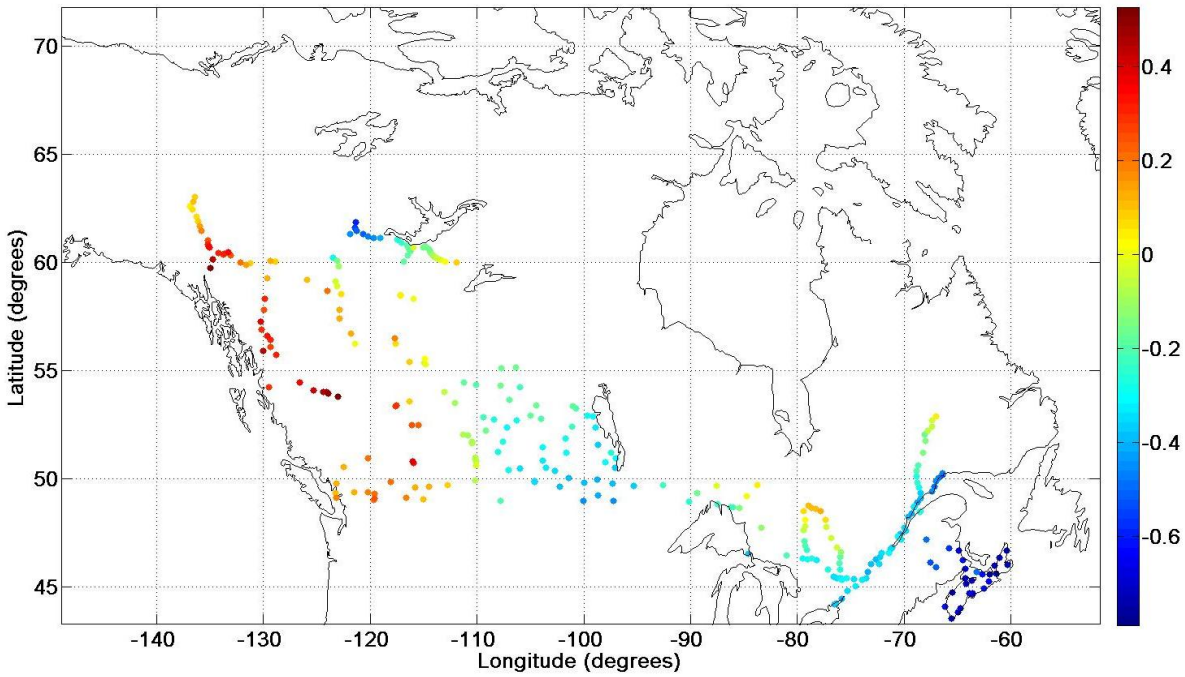

Figure 4.9: Geoid height differences $h\text{-}H\text{-}N^{EGM2008}$ (in meters) for the CGVD28 GNSS/levelling benchmarks.

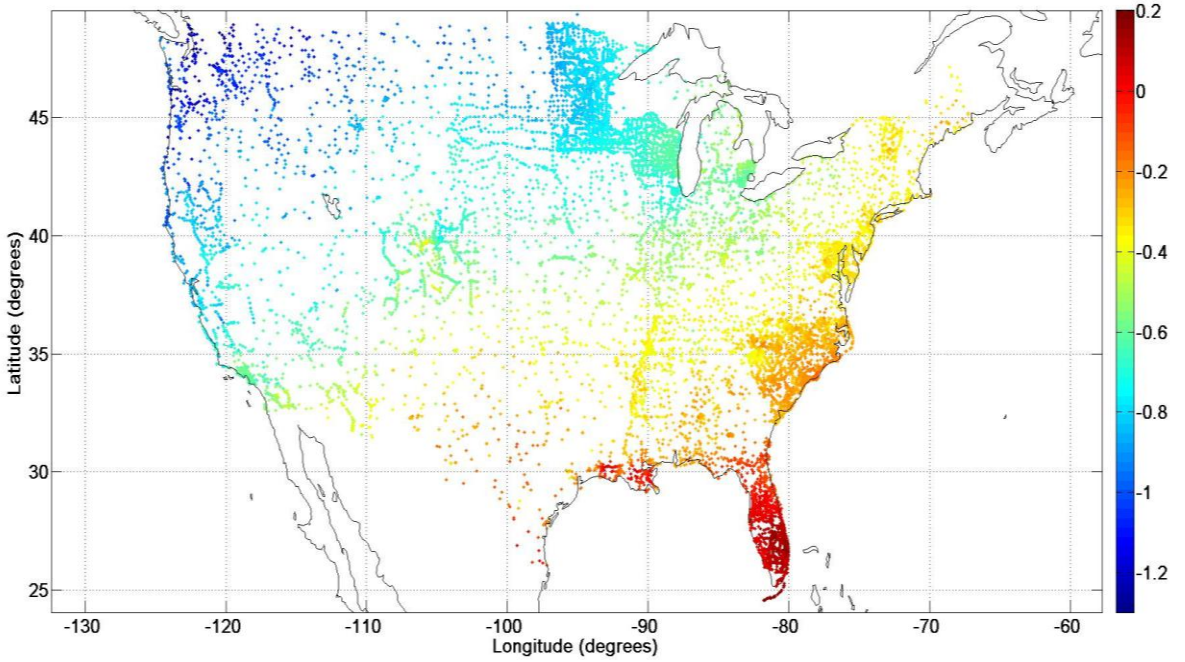

Figure 4.10: Geoid height differences $h\text{-}H\text{-}N^{EGM2008}$ (in meters) for the U.S.A. NAVD88 GNSS/levelling benchmarks.

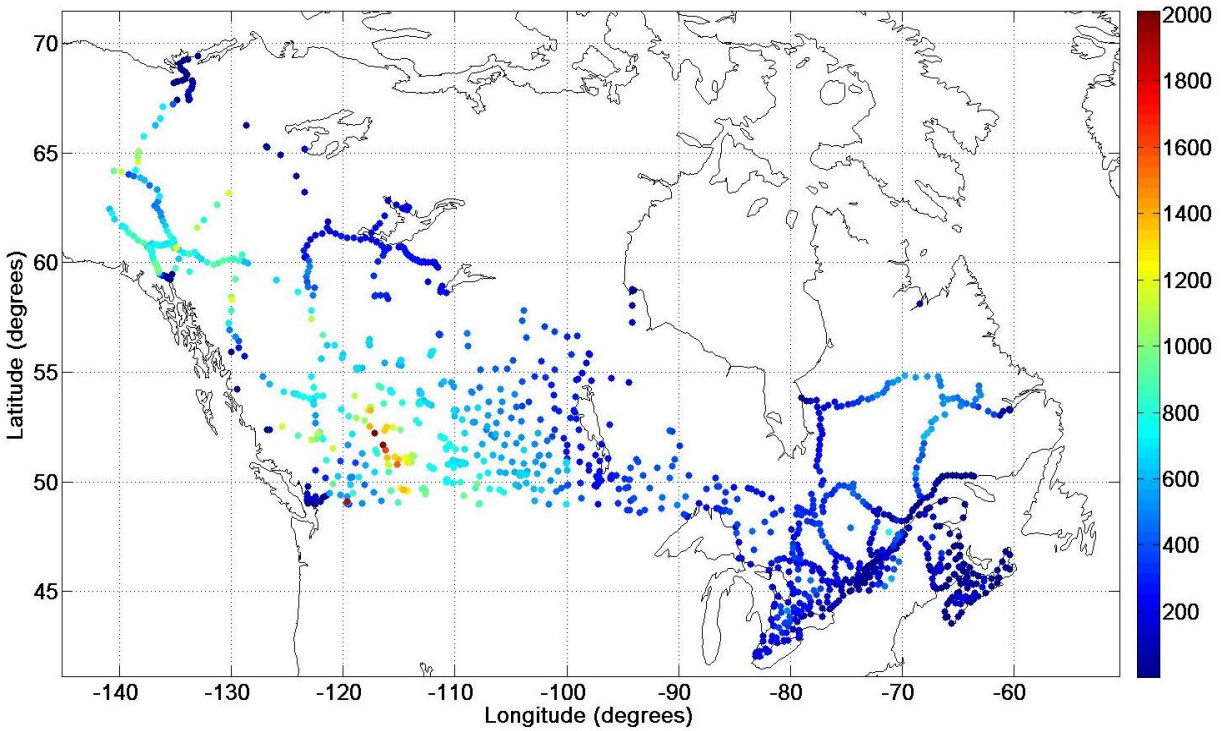

Figure 4.11: Distribution of *H* (m) in Nov07 GNSS/levelling network (1,315 benchmarks).

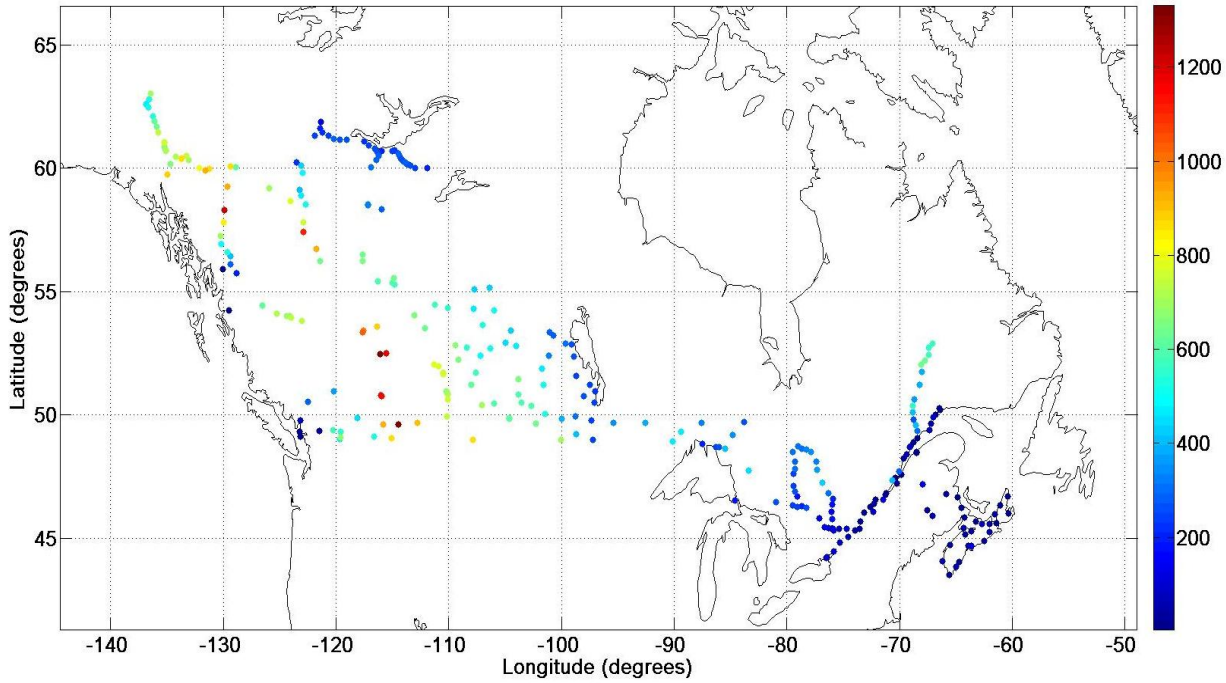

Figure 4.12: Distribution of *H* (m) in NAVD88 GNSS/levelling network (308 benchmarks).

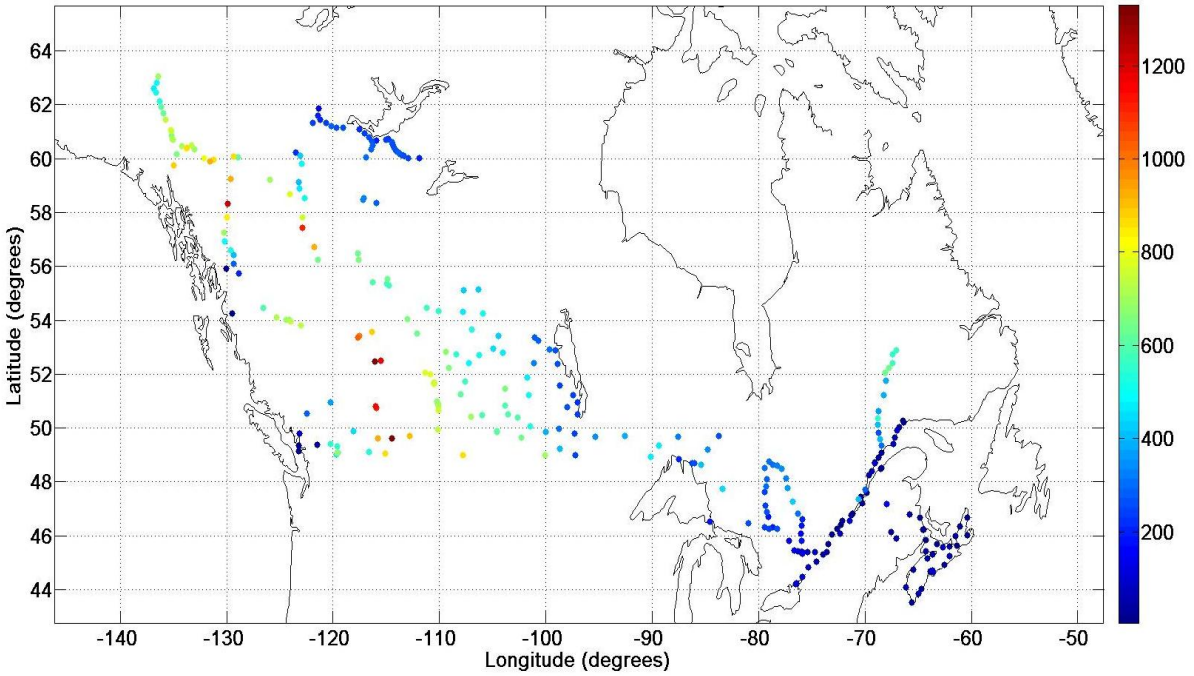

Figure 4.13: Distribution of *H* (m) in CGVD28 GNSS/levelling network (308 benchmarks).

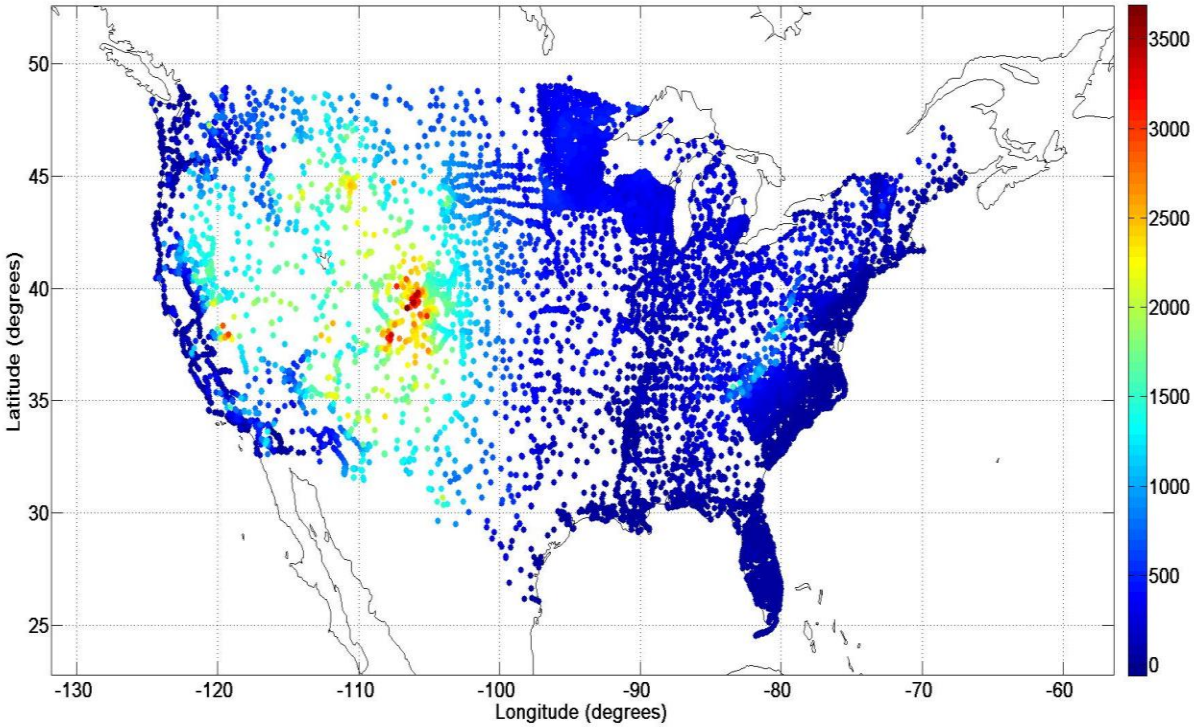

Figure 4.14: Distribution of *H* (m) in U.S.A. NAVD88 GNSS/levelling network.

The LVD offsets and the root-mean-square (RMS) error values, which are estimated from the $\hat{v}_P$ term in Eq. (4.14) using the adjusted geoid height residuals in order to show the consistency among the ellipsoidal, orthometric, and geoid heights, are presented in Tables 4.5 to 4.12 using the four corrector term models.

Table 4.5: LVD offsets for Canada using null model.

Model	**$\delta N^{(j)}$ (cm)**	**$\delta W^{(j)}$ (m^2/s^2)**	**RMS (cm)**
NAVD88 (308 Benchmarks)			
CGG2010	-80.99 ± 2.10	-7.95 ± 0.21	36.84
EGM2008	-80.56 ± 2.18	-7.91 ± 0.21	38.33
goco03s	-94.04 ± 3.07	-9.23 ± 0.30	53.82
goco03s+EGM2008	-80.64 ± 2.20	-7.91 ± 0.22	38.52
CGVD28 (308 Benchmarks)			
CGG2010	-15.25 ± 1.73	-1.50 ± 0.17	30.44
EGM2008	-14.82 ± 1.66	-1.45 ± 0.16	29.04
goco03s	-28.30 ± 2.04	-2.78 ± 0.20	35.87
goco03s+EGM2008	-14.90 ± 1.65	-1.46 ± 0.16	28.99
Nov07 (1,315 Benchmarks)			
CGG2010	-45.01 ± 0.34	-4.42 ± 0.03	12.24
EGM2008	-44.16 ± 0.37	-4.33 ± 0.04	13.41
goco03s	-59.19 ± 1.08	-5.81 ± 0.11	39.09
goco03s+EGM2008	-44.45 ± 0.37	-4.36 ± 0.04	13.57

When utilizing the 1-parameter bias corrector term model (see Table 4.6), the reduction in the RMS value ranges from approximately 8 cm for the CGVD28 and NAVD88 networks to approximately 1 cm for the Nov07 network in Canada when compared with the null model (see Table 4.5). Figure 4.11 shows that there is not significant height variability throughout the test network for Nov07, in particular for the eastern and central portions of Canada; therefore, one does not expect to see a significant improvement in the consistency among the ellipsoidal, orthometric, and geoid heights when using the 1-parameter model. In other words, the scale parameter in the 1-parameter model remains nearly constant for a significant portion of the test network. The test networks of NAVD88 and CGVD28 in Canada contain slightly more height variability in the western portion of the networks when compared with Nov07 as can be seen from Figure 4.12 and Figure 4.13. The NAVD88 and CGVD28 LVD offsets differ quite significantly between the null model and 1-parameter model case; the offset difference is approximately 30 cm

and 27 cm for the NAVDD88 and CGVD28 test networks, respectively (see Table 4.5 and 4.6). For the Nov07 network this difference is only 5 cm.

Table 4.6: LVD offsets for Canada using 1-parameter model.

Model	**$\delta N^{(j)}$ (cm)**	**$\delta W^{(j)}$ (m^2/s^2)**	**δs**	**RMS (cm)**
NAVD88 (308 Benchmarks)				
CGG2010	-51.43 ± 2.78	-5.05 ± 0.27	$-7.85 * 10^{-4}$	29.30
EGM2008	-49.78 ± 2.89	-4.88 ± 0.28	$-7.90 * 10^{-4}$	30.46
goco03s	-58.73 ± 4.43	-5.76 ± 0.43	$-9.06 * 10^{-4}$	46.74
goco03s+EGM2008	-49.77 ± 2.91	-4.88 ± 0.29	$-7.92 * 10^{-4}$	30.66
tim_r4+EGM2008	-49.71 ± 2.93	-4.88 ± 0.29	$-7.95 * 10^{-4}$	30.91
dir_r4+EGM2008	-49.75 ± 2.93	-4.88 ± 0.29	$-7.90 * 10^{-4}$	30.86
CGVD28 (308 Benchmarks)				
CGG2010	-42.40 ± 2.13	-4.16 ± 0.21	$6.97 * 10^{-4}$	22.49
EGM2008	-40.74 ± 2.03	-4.00 ± 0.20	$6.66 * 10^{-4}$	21.44
goco03s	-49.72 ± 3.03	-4.88 ± 0.30	$5.50 * 10^{-4}$	32.01
goco03s+EGM2008	-40.74 ± 2.03	-4.00 ± 0.15	$6.64 * 10^{-4}$	21.42
tim_r4+EGM2008	-40.67 ± 2.04	-3.99 ± 0.20	$6.61 * 10^{-4}$	21.54
dir_r4+EGM2008	-40.71 ± 2.05	-4.00 ± 0.20	$6.66 * 10^{-4}$	21.61
Nov07 (1,315 Benchmarks)				
CGG2010	-41.11 ± 0.50	-4.03 ± 0.05	$-1.05 * 10^{-4}$	11.77
EGM2008	-39.14 ± 0.53	-3.84 ± 0.05	$-1.35 * 10^{-4}$	12.67
goco03s	-54.82 ± 1.64	-5.38 ± 0.16	$-1.18 * 10^{-4}$	38.90
goco03s+EGM2008	-39.41 ± 0.54	-3.87 ± 0.05	$-1.36 * 10^{-4}$	12.84
tim_r4+EGM2008	-39.18 ± 0.56	-3.84 ± 0.05	$-1.37 * 10^{-4}$	13.24
dir_r4+EGM2008	-39.10 ± 0.57	-3.84 ± 0.06	$-1.36 * 10^{-4}$	13.38

From the results in Table 4.7, it can be observed that when utilizing the 2-parameter model, the reduction in the RMS value is significant for all three test networks when compared with the null model. For the NAVD88 network this reduction can be quantified as approximately 30 cm, while for CGVD28 the reduction in RMS is approximately 10 cm, and for Nov07 the reduction is approximately 5 cm. Thus, when comparing with the use of the 1-parameter bias corrector term model, the 2-parameter model performs better overall for all three test networks When utilizing the 2-parameter model, the LVD offset estimates presented in Table 4.7 do not change from that of the null model case presented in Table 4.5, because the adjusted spatial tilt is taken with respect to the centroid of the test network, and therefore will not interfere with the mean offset of the LVD with respect to the global equipotential surface.

Table 4.7: LVD offsets for Canada using 2-parameter model.

Model	δN^j (cm)	δW^j (m^2/s^2)	NS (m/deg)	WE (m/deg)	RMS (cm)
NAVD88 (308 Benchmarks)					
CGG2010	-80.99 ± 2.10	-7.95 ± 0.21	-0.004	0.023	8.15
EGM2008	-80.56 ± 2.18	-7.91 ± 0.21	-0.003	0.025	8.12
goco03s	-94.04 ± 3.07	-9.23 ± 0.30	0.025	0.038	30.01
goco03s+EGM2008	-80.64 ± 2.20	-7.91 ± 0.22	-0.002	0.025	8.29
tim_r4+EGM2008	-80.70 ± 0.48	-7.92 ± 0.05	-0.003	0.025	8.42
dir_r4+EGM2008	-80.53 ± 0.49	-7.90 ± 0.05	-0.003	0.025	8.56
CGVD28 (308 Benchmarks)					
CGG2010	-15.25 ± 1.13	-1.50 ± 0.11	-0.014	-0.020	19.80
EGM2008	-14.82 ± 1.11	-1.45 ± 0.11	-0.012	-0.018	19.50
goco03s	-28.30 ± 1.87	-2.78 ± 0.18	0.015	-0.005	32.41
goco03s+EGM2008	-14.90 ± 1.12	-1.46 ± 0.11	-0.012	-0.018	19.63
tim_r4+EGM2008	-14.96 ± 1.14	-1.47 ± 0.11	-0.013	-0.018	19.87
dir_r4+EGM2008	-14.79 ± 1.14	-1.45 ± 0.11	-0.012	-0.018	19.93
Nov07 (1,315 Benchmarks)					
CGG2010	-45.01 ± 0.23	-4.42 ± 0.02	-0.003	0.005	8.30
EGM2008	-44.16 ± 0.23	-4.33 ± 0.02	-0.002	0.007	8.19
goco03s	-59.19 ± 0.96	-5.81 ± 0.09	0.010	0.015	34.73
goco03s+EGM2008	-44.45 ± 0.22	-4.36 ± 0.02	-0.001	0.007	8.11
tim_r4+EGM2008	-44.27 ± 0.23	-4.34 ± 0.02	-0.002	0.007	8.46
dir_r4+EGM2008	-44.17 ± 0.24	-4.33 ± 0.02	-0.002	0.007	8.67

There is not a significant decrease in the RMS values when utilizing the combined model with respect to the 2-parameter model. From Table 4.8 it can be seen that the reduction is less than 1 cm for NAVD88 and Nov07, while an approximate 1-2 cm reduction is observed for CGVD28. As the addition of the scale parameter in the combined model shows no significant improvement over the 2-parameter model, it can therefore be concluded that the 2-parameter model is sufficient for modelling the spatial tilts found in the Canadian test networks, in particular, the NAVD88 and Nov07 networks.

For the combined model case (see Table 4.8), the difference in the LVD offset estimation with respect to the null model is approximately 2-3 cm for the NAVD88 and Nov07 test networks while the difference is approximately 12 cm for the CGVD28 test network (see Table 4.5 and 4.8). As the numerical differences of the LVD offsets estimated using the different bias corrector term models are caused by the different correlations between the offset term and the nuisance parameters of each bias-corrector term model, in conjunction

with the existing systematic effects in the height data of each test network, the overall greater RMS values obtained for the CGVD28 network shows that CGVD28 contains more complex local distortions when compared to NAVD88 and Nov07 due to the various issues outlined in Chapter 2 Section 2.5.

Table 4.8: LVD offsets for Canada using combined model.

Model	**δN (cm)**	**δW (m^2/s^2)**	**δs**	**NS (m/deg)**	**WE (m/deg)**	**RMS (cm)**
NAVD88 (308 Benchmarks)						
CGG2010	-83.62 ± 0.94	-8.21 ± 0.09	$6.74 * 10^{-5}$	-0.003	0.025	8.01
EGM2008	-83.57 ± 0.94	-8.20 ± 0.09	$7.72 * 10^{-5}$	-0.001	0.026	7.94
goco03s	-102.43 ± 3.50	-10.05 ± 0.34	$2.15 * 10^{-4}$	0.028	0.041	29.64
goco03s+EGM2008	-83.84 ± 0.95	-8.23 ± 0.09	$8.21 * 10^{-5}$	-0.001	0.027	8.10
tim_r4+EGM2008	-83.93 ± 0.97	-8.23 ± 0.10	$8.27 * 10^{-5}$	-0.002	0.027	8.22
dir_r4_EGM2008	-83.90 ± 0.98	-8.23 ± 0.10	$8.63 * 10^{-5}$	-0.001	0.027	8.36
CGVD28 (308 Benchmarks)						
CGG2010	-27.23 ± 2.19	-2.67 ± 0.21	$6.74 * 10^{-5}$	-0.009	-0.014	18.63
EGM2008	-27.19 ± 2.14	-2.67 ± 0.21	$7.72 * 10^{-5}$	-0.008	-0.013	18.23
goco03s	-46.04 ± 3.63	-4.52 ± 0.36	$2.15 * 10^{-4}$	0.022	0.003	30.86
goco03s+EGM2008	-27.45 ± 2.16	-2.69 ± 0.21	$8.21 * 10^{-5}$	-0.007	-0.012	18.34
tim_r4+EGM2008	-27.54 ± 2.19	-2.70 ± 0.21	$3.23 * 10^{-4}$	-0.008	-0.012	18.58
dir_r4_EGM2008	-27.51 ± 2.19	-2.70 ± 0.22	$3.26 * 10^{-4}$	-0.008	-0.012	18.62
Nov07 (1,315 Benchmarks)						
CGG2010	-47.54 ± 0.39	-4.66 ± 0.04	$6.81 * 10^{-5}$	-0.001	0.007	8.11
EGM2008	-46.75 ± 0.39	-4.59 ± 0.04	$6.98 * 10^{-5}$	-0.000	0.008	7.99
goco03s	-71.61 ± 1.63	-7.03 ± 0.16	$3.35 * 10^{-4}$	0.016	0.021	33.64
goco03s+EGM2008	-47.32 ± 0.38	-4.67 ± 0.04	$7.72 * 10^{-5}$	-0.000	0.008	7.86
tim_r4+EGM2008	-47.22 ± 0.40	-4.63 ± 0.04	$7.93 * 10^{-5}$	-0.000	0.008	8.21
dir_r4+EGM2008	-47.17 ± 0.41	-4.63 ± 0.04	$8.07 * 10^{-5}$	-0.000	0.008	8.41

Lastly, it can be seen from LVD offset values from Tables 4.5-4.8 that using a GOCE only model is not sufficient for modelling the spatial tilts found within the levelling networks. In general, the RMS value when using the GOCE satellite only model versus the terrestrial/satellite combined models is significantly greater. For example, the RMS value for the offset estimated using *goco03s* and the combined bias corrector term model is 33.64 cm while the *goco03s+EGM2008* model yields an RMS value of 7.86 cm for the Nov07 network (see Table 4.8)

Lastly, Tables 4.9-4.12 show the LVD offsets and the RMS error values computed using the four bias corrector term models for the U.S.A. NAVD88 test network. Overall the same trends are observed for the U.S.A. NAVD88 network as was discussed for the NAVD88 and Nov07 test networks in Canada. Additionally, it can be observed from Table 4.9 that the effect of the GOCE omission error on the LVD offset is approximately 2-3 cm, which can be ascribed to the density and configuration of the GNSS/levelling benchmarks of the U.S.A. NAVD88 network.

Table 4.9: U.S.A. NAVD88 LVD offsets using null model.

Model	**δN^j (cm)**	**δW^j (m^2/s^2)**	**RMS (cm)**
CGG2010	-48.08 ± 0.22	-4.71 ± 0.02	29.94
USGG2012	-51.13 ± 0.22	-5.01 ± 0.02	29.93
EGM2008	-48.35 ± 0.22	-4.74 ± 0.02	30.05
goco03s	-50.04 ± 0.39	-4.90 ± 0.04	52.60
goco03s+EGM2008	-48.38 ± 0.22	-4.74 ± 0.02	30.02
tim_r4	-50.77 ± 0.35	-4.98 ± 0.03	47.77
tim_r4+EGM2008	-48.06 ± 0.22	-4.71 ± 0.02	29.85
dir_r4	-51.00 ± 0.35	-5.00 ± 0.04	47.93
dir_r4+EGM2008	-48.29 ± 0.22	-4.73 ± 0.02	29.86

Table 4.10: U.S.A. NAVD88 LVD offsets using 1-parameter model.

Model	**δN^j (cm)**	**δW^j (m^2/s^2)**	**δs**	**RMS (cm)**
CGG2010	-39.48 ± 0.25	-3.87 ± 0.03	$-2.65 * 10^{-4}$	27.50
USGG2012	-42.66 ± 0.25	-4.18 ± 0.03	$-2.61 * 10^{-4}$	27.57
EGM2008	-39.64 ± 0.25	-3.88 ± 0.03	$-2.68 * 10^{-4}$	27.55
goco03s	-40.06 ± 0.46	-3.93 ± 0.05	$-3.07 * 10^{-4}$	50.77
goco03s+EGM2008	-39.74 ± 0.25	-3.89 ± 0.03	$-2.66 * 10^{-4}$	27.56
tim_r4+EGM2008	-39.46 ± 0.25	-3.87 ± 0.02	$-2.65 * 10^{-4}$	27.41
dir_r4+EGM2008	-39.71 ± 0.25	-3.89 ± 0.03	$-2.64 * 10^{-4}$	27.43

Table 4.11: U.S.A. NAVD88 LVD offsets using 2-parameter model.

Model	**δN^j (cm)**	**δW^j (m^2/s^2)**	**NS (m/deg)**	**WE (m/deg)**	**RMS (cm)**
CGG2010	-48.08 ± 0.05	-4.71 ± 0.02	-0.036	0.013	5.88
USGG2012	-51.13 ± 0.05	-5.01 ± 0.01	-0.036	0.013	6.10
EGM2008	-48.35 ± 0.05	-4.74 ± 0.02	-0.036	0.013	6.16
goco03s	-50.04 ± 0.39	-4.90 ± 0.04	-0.031	0.021	41.46
goco03s+EGM2008	-48.38 ± 0.05	-4.74 ± 0.02	-0.035	0.013	6.50
tim_r4+EGM2008	-48.06 ± 0.05	-4.71 ± 0.01	-0.035	0.013	6.82
dir_r4+EGM2008	-48.29 ± 0.05	-4.73 ± 0.01	-0.035	0.013	6.97

Table 4.12: U.S.A. NAVD88 LVD offsets using combined model.

Model	**δN^j (cm)**	**δW^j (m^2/s^2)**	**δs**	**NS (m/deg)**	**WE (m/deg)**	**RMS (cm)**
CGG2010	-49.59 ± 0.06	-4.86 ± 0.01	$4.64 * 10^{-5}$	-0.036	0.014	5.63
USGG2012	-52.67 ± 0.06	-5.16 ± 0.01	$4.73 * 10^{-5}$	-0.036	0.014	5.84
EGM2008	-49.72 ± 0.06	-4.87 ± 0.01	$4.23 * 10^{-5}$	-0.036	0.014	5.96
goco03s	-52.90 ± 0.41	-5.19 ± 0.04	$8.82 * 10^{-5}$	-0.032	0.023	41.33
goco03s+EGM2008	-49.86 ± 0.06	-4.89 ± 0.01	$4.56 * 10^{-5}$	-0.036	0.014	6.27
tim_r4+EGM2008	-49.55 ± 0.07	-4.86 ± 0.01	$4.58 * 10^{-5}$	-0.035	0.014	6.61
dir_r4+EGM2008	-49.79 ± 0.07	-4.88 ± 0.01	$4.64 * 10^{-5}$	-0.035	0.014	6.75

Table 4.13: CML LVD offsets computed by removing systematic effects from raw geoid height residuals before the estimation of the offset using various parametric models.

Model	**δN^j (cm)**	**δW^j (m^2/s^2)**	**RMS (cm)**
CML 1-Parameter Model			
dir_r4+EGM2008	-16.88 ± 0.65	-1.65 ± 0.06	23.51
tim_r4+EGM2008	-16.97 ± 0.65	-1.67 ± 0.06	23.41
CGG2010	-17.71 ± 0.65	-1.72 ± 0.01	23.50
CML 2-Parameter Model			
dir_r4+EGM2008	-45.19 ± 0.25	-4.43 ± 0.02	9.41
tim_r4+EGM2008	-45.29 ± 0.25	-4.44 ± 0.02	8.96
CGG2010	-46.03 ± 0.25	-4.52 ± 0.02	8.94
CML 3-Parameter Model			
dir_r4+EGM2008	-43.04 ± 0.47	-4.22 ± 0.05	17.18
tim_r4+EGM2008	-43.14 ± 0.47	-4.23 ± 0.04	17.07
CGG2010	-43.88 ± 0.42	-4.31 ± 0.04	15.22

The final numerical analysis of this section, examines the effect of removing the systematic errors before the computation of the LVD offsets. The results for the CML test

network are shown in Table 4.13 while the results for the U.S.A. NAVD88 network are shown in Table 4.14.

It can be observed from Table 4.13 and 4.14 that the 2-parameter model still yields the overall best RMS estimates when compared to the use of the 1-parameter or combined model. In fact, the 1-parameter model should not be utilized if the systematic errors are to be removed before the estimation of the LVD offset as it yields RMS estimates that are worse than when using the null model. Moreover, the LVD offset estimates differ by almost 20 cm for the U.S.A. NAVD88 network and almost 29 cm for the CML network when comparing the use of the 1-parameter model with the null case.

Table 4.14: U.S.A. NAVD88 LVD offsets computed by removing systematic effects from raw geoid height residuals before the estimation of the offset using various parametric models.

Model	δN^j (cm)	δW^j (m^2/s^2)	RMS (cm)
U.S.A. NAVD88 1-Parameter Model			
dir_r4+EGM2008	-25.98 ± 0.25	-2.55 ± 0.06	33.01
tim_r4+EGM2008	-25.75 ± 0.25	-2.52 ± 0.02	33.35
USGG2012	-28.83 ± 0.25	-2.83 ± 0.02	33.50
U.S.A. NAVD88 2-Parameter Model			
dir_r4+EGM2008	-48.66 ± 0.05	-4.77 ± 0.01	7.10
tim_r4+EGM2008	-48.44 ± 0.05	-4.75 ± 0.01	6.98
USGG2012	-51.51 ± 0.05	-5.05 ± 0.01	6.31
U.S.A. NAVD88 3-Parameter Model			
dir_r4+EGM2008	-48.24 ± 0.13	-4.73 ± 0.01	16.97
tim_r4+EGM2008	-48.01 ± 0.13	-7.71 ± 0.01	16.93
USGG2012	-51.08 ± 0.12	-5.01 ± 0.01	16.47

When using the 2-parameter model to model the spatial tilts found within the levelling networks it does not matter is the offset is estimated simultaneously with the spatial tilts or if the spatial tilts are removed before the estimation of the offset term, as the differences in the LVD offset estimates are approximately 1 cm or less.

4.3.4 Estimating LVD Offsets using Tide Gauges

The spatial tilts of the Canadian CGVD28 network and the U.S.A. NAVD 88 network can be observed when computing the LVD offsets with tide gauges. Figures 4.15 and 4.16 show the distribution of the tide gauges used to compute the CGVD28 and NAVD88 offsets in Canada and the U.S.A., respectively. The tide gauge data sets were provided by the National Oceanography Centre at the University of Southampton.

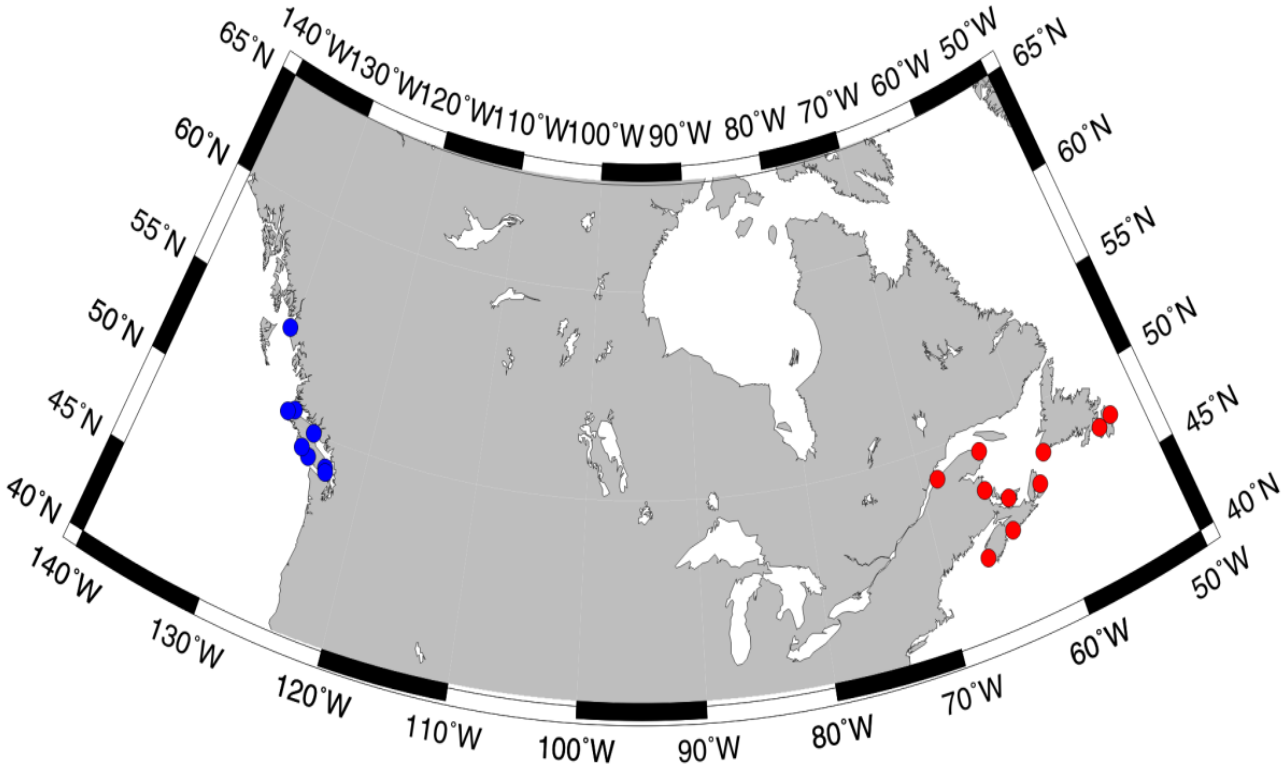

Figure 4.15: Tide gauge stations with MSL referenced to CGVD28 vertical datum; 10 stations on the Atlantic Coast and 6 stations on the Pacific Coast.

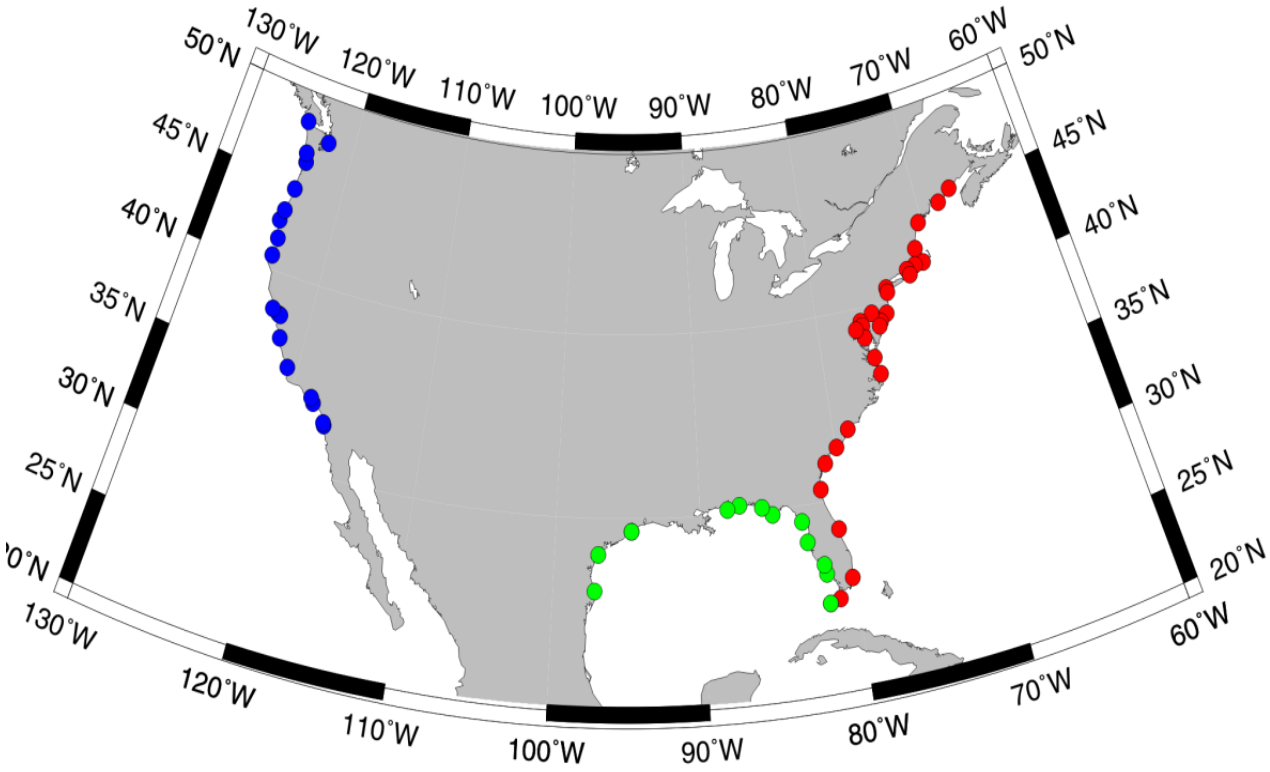

Figure 4.16: Tide gauge stations with MSL referenced to NAVD88 vertical datum; 28 stations on the Atlantic Coast, 18 stations on the Pacific Coast, and 13 stations on the Gulf Coast.

The distribution of the geoid height differences are shown in Figures 4.17 and 4.18 for the Canadian and U.S.A. tide gauges, respectively. From figure 4.17 it can be seen that the geoid height differences for tide gauges tied to the CGVD28 network range from approximately -0.1 m to 0.3 m on the Pacific coast, while the geoid height differences of the Atlantic coast range from approximately -0.2 m to –0.7 m. For the U.S.A. tide gauges tied to the NAVD88 network, the geoid height differences for the Pacific coast range from -0.4 m to -1.2 m while the geoid height differences range from -0.3 m to 0.1 m for the Atlantic coast and from -0.3 to 0.3 m for the Gulf coast. These geoid height difference distributions shown in Figures 4.17 and 4.18 correspond with Figures 4.9 and 4.10 (along the coasts), respectively.

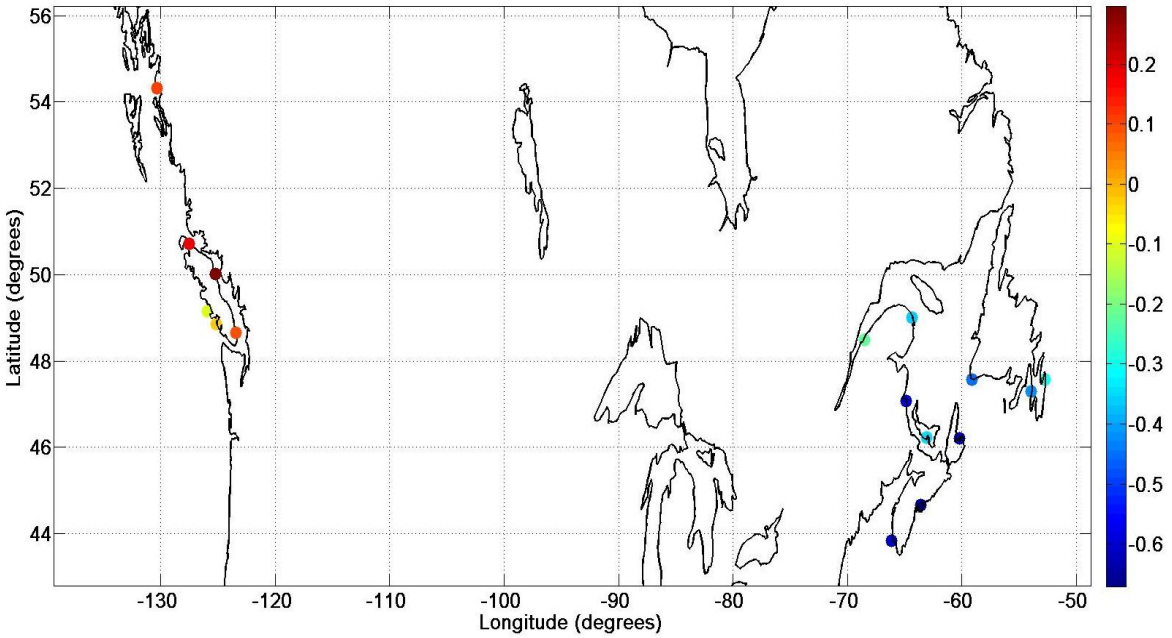

Figure 4.17: Geoid height differences $h\text{-}H\text{-}N^{EGM2008}$ (in meters) for the CGVD28 referenced tide gauges.

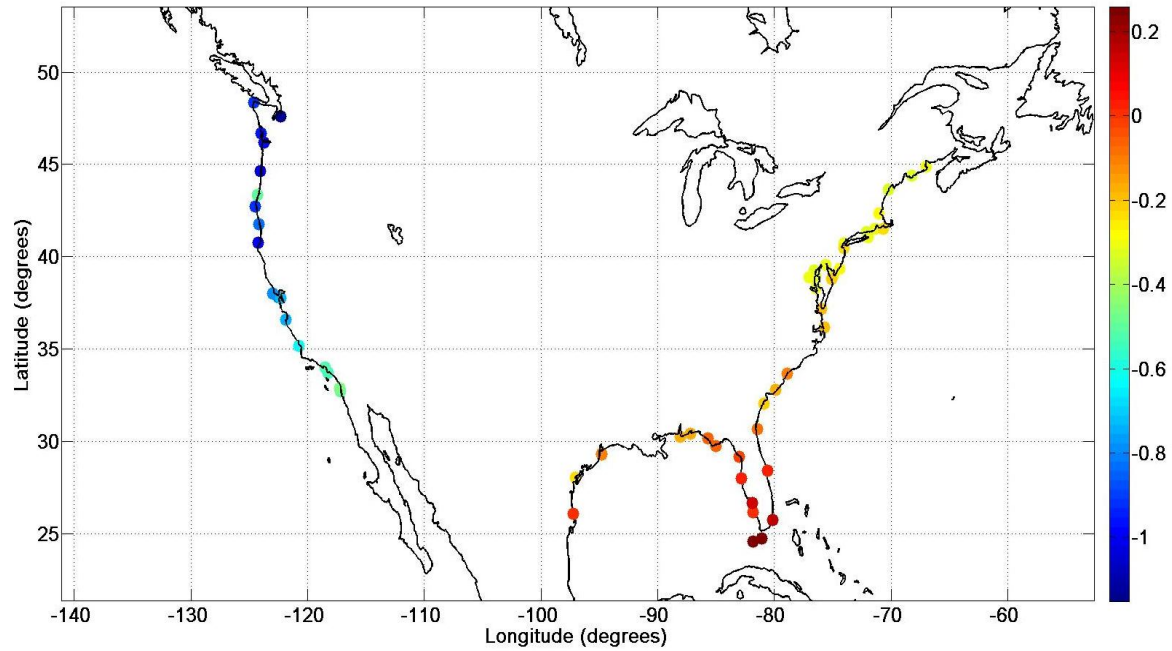

Figure 4.18: Geoid height differences $h\text{-}H\text{-}N^{EGM2008}$ (in meters) for the NAVD88 referenced tide gauges.

First the LVD offsets for the Canadian tide gauges tied to the CGVD28 network will be examined. In Table 4.15 the CGVD28 offset is estimated with all of the available 16 tide

gauges, where it appears that the effect of the GOCE omission error is no longer between 8-13 cm. For example, the difference between the *tim_r4* model and *tim_r4+EGM2008* model is 1-2 cm. The effect of the GOCE model omission error on the LVD offsets is not evident in this case because the negative and positive geoid heights differences between the Pacific and Atlantic coasts average out, hence masking the effect of the GOCE model omission error. The effect of the GOCE model omission errors are more evident when estimating the offset at individual tide gauges, which are shown visually in Figures 4.19 and 4.20. It is also interesting to note that offsets estimated with the gravimetric geoid models (i.e., *CGG2010* and *USGG2012*) and *tim_r4+EGM2008* are close, but differences as large as 10 cm exist for CGVD28 for offsets evaluated at individual Canadian tide gauges and 8 cm for NAVD88 offsets evaluated at individual U.S.A. tide gauges (see, e.g., the circled points in Figures 4.19 and 4.20).

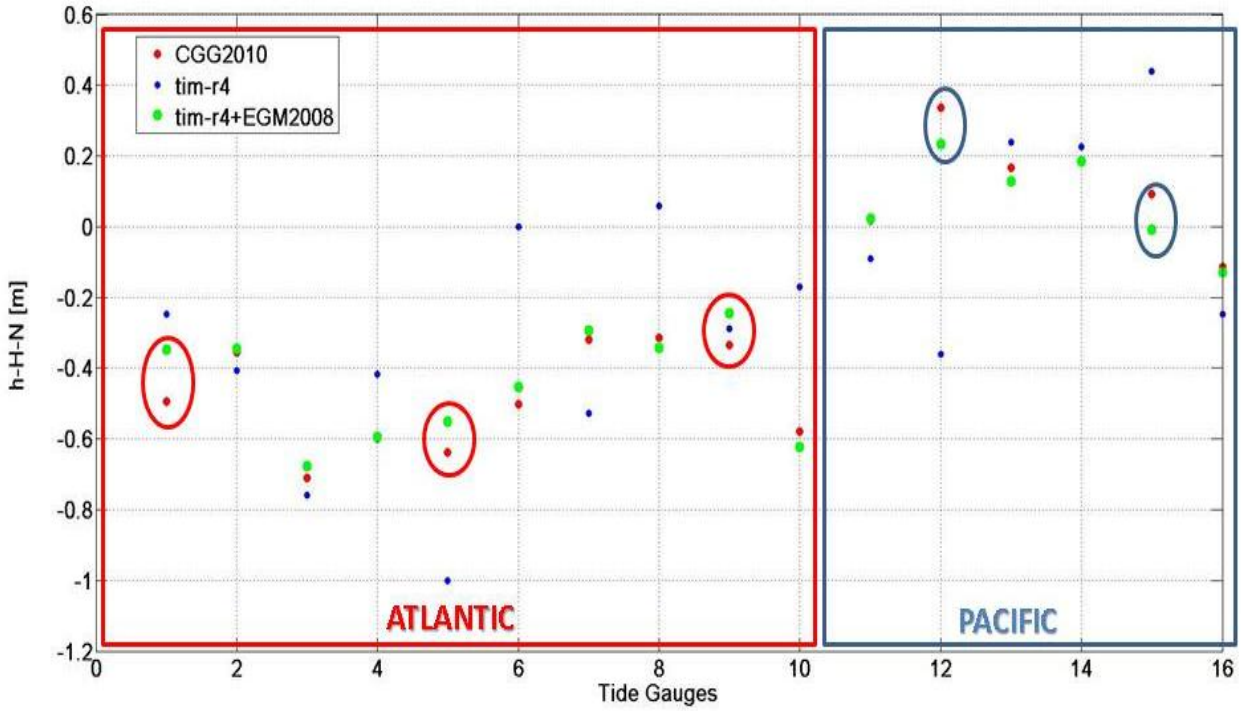

Figure 4.19: CGVD28 offsets at Canadian tide gauges.

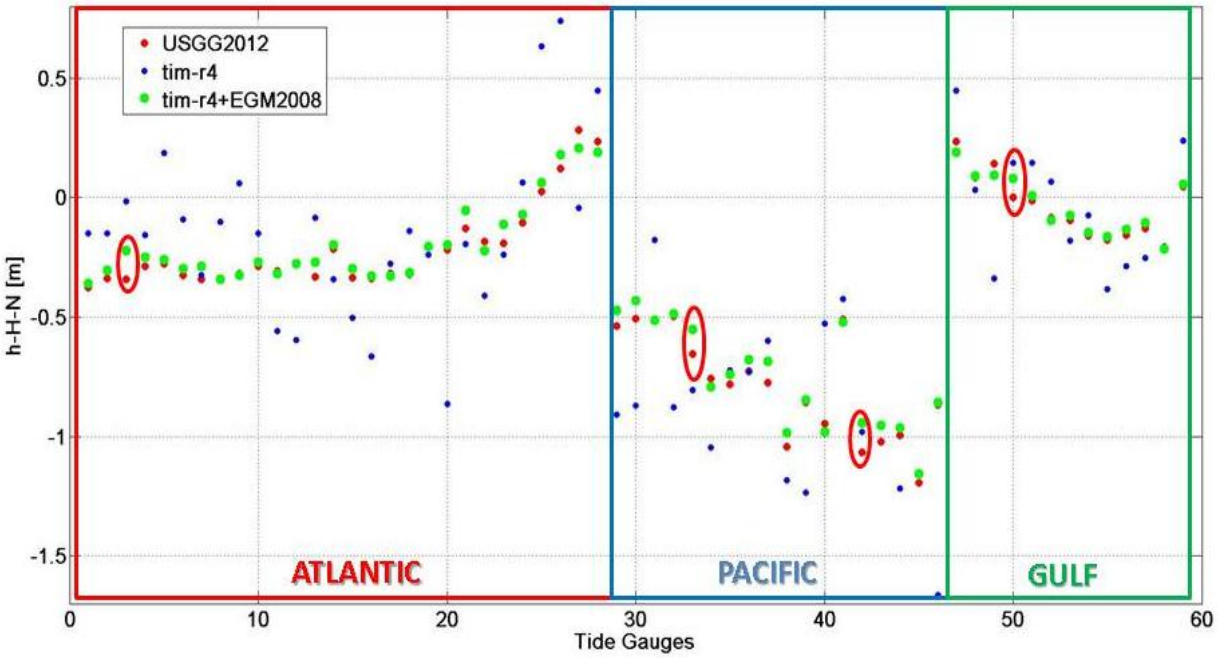

Figure 4.20: NAVD88 offsets at U.S.A. tide gauges.

Table 4.15: CGVD28 offset with 16 Canadian tide gauges.

GGM	δN^j (cm)	δW^j (m^2/s^2)	W_0^j (m^2/s^2)
tim_r4	-24.13 ± 10.69	-2.73 ± 1.05	62636858.37
tim_r4+EGM2008	-25.24 ± 7.41	-2.48 ± 0.73	62636858.48
EGM2008	-25.28 ± 7.75	-2.48 ± 0.76	62636858.48
CGG2010	-25.99 ± 8.31	-2.55 ± 0.82	62636858.55
Ince et al.	-26.68 ± 8.42	-2.63 ± 0.83	62636858.62

Table 4.16: CGVD28 offset with 12 Canadian tide gauges.

GGM	δN^j (cm)	δW^j (m^2/s^2)	W_0^j (m^2/s^2)
tim_r4	-27.81 ± 13.39	-2.73 ± 1.31	62636858.73
tim_r4+EGM2008	-24.70 ± 9.63	-2.43 ± 0.94	62636858.43
CGG2010	-24.35 ± 10.35	-2.39 ± 1.02	62636858.39
Ince et al.	-25.51 ± 10.69	-2.50 ± 1.05	62636858.50
USGG2012	-26.08 ± 10.28	-2.56 ± 1.01	62636858.56

In Table 4.16, the offset is evaluated with 12 tide gauges in order to assess the CGVD28 offset estimated with the U.S.A. official gravimetric geoid model *USGG2012* as 4 out of the 16 Canadian tide gauges fall outside of the extent of the *USGG2012* geoid grid. Again, the same trends observed from the results in Table 4.15 are seen in Table 4.16. The LVD offset estimated with *USGG2012* differs by less than 1 cm when compared

with the gravimetric geoid model developed by Ince et al. (2012) while it differs by approximately 2 cm when compared with *CGG2010*.

Tables 4.17 and 4.18 show LVD offsets estimated using 2 high quality tide gauges from the Atlantic and 5 high quality tide gauges from the Pacific that are in common with the tide gauge data set utilized for W_0 evaluation in Chapter 5. In this case, "high quality" refers to a tide gauge that has long term daily water level records without significant data gaps for the accurate evaluation of MSL. Specifically, the tide gauge stations utilized for the computation of LVD offsets in the Atlantic are stations 365 and 2330 while for the Pacific the tide gauges correspond to stations 8408, 9354, 8074, 8615, and 8545 (see Chapter 5, Table 5.1).

Table 4.17: CGVD28 offset with 2 Canadian tide gauges (Atlantic).

GGM	**δN^j (cm)**	**δW^j (m^2/s^2)**	**W_0^j (m^2/s^2)**
goco03s	-7.11 ± 9.38	-0.70 ± 0.92	62636856.70
goco3s+EGM2008	-49.55 ± 4.01	-4.86 ± 0.40	62636860.86
tim_r4	-5.01 ± 9.87	-0.49 ± 0.97	62636856.49
tim_r4+EGM2008	-47.45 ± 4.50	-4.66 ± 0.44	62636860.66
EGM2008	-49.12 ± 5.25	-4.82 ± 0.52	62636860.82
CGG2010	-44.66 ± 5.37	-4.38 ± 0.53	62636860.38
Ince et al.	-48.53 ± 3.97	-4.76 ± 0.39	62636860.76

Table 4.18: CGVD28 offset with 5 Canadian tide gauges (Pacific).

GGM	**δN^j (cm)**	**δW^j (m^2/s^2)**	**W_0^j (m^2/s^2)**
goco03s	-2.82 ± 12.44	-0.28 ± 1.22	62636856.28
goco3s+EGM2008	6.26 ± 5.38	-0.61 ± 0.53	62636855.39
tim_r4	-1.76 ± 12.40	-0.17 ± 1.21	62636856.17
tim_r4+EGM2008	7.34 ± 5.32	0.72 ± 0.52	62636855.28
EGM2008	9.02 ± 5.85	0.88 ± 0.57	62636855.12
CGG2010	10.46 ± 6.22	1.02 ± 0.61	62636854.97
Ince et al.	10.62 ± 5.93	1.04 ± 0.58	62636854.96

From the results presented in Tables 4.17 and 4.18 it is evident that utilizing only *goco03s* or the *tim_r4* model only is not sufficient for estimating LVD offset; the offsets computed with *goco03s* or *tim_r4* yields a statistically insignificant LVD offsets as the estimated LVD offsets are smaller than three times their formal errors. For example, the CGVD28 offset for the Atlantic is -5.01 ± 9.87 cm and for the Pacific it is -1.76 ± 12.40

cm when utilizing *tim_r4* only. These results are similar to those obtained by the VAN test network for the Nov07 datum (see Table 4.3). In general, the formal errors presented in Tables 4.17 and 4.18 are greater than when using GNSS/levelling benchmarks to compute LVD offsets (see Table 4.5). The standard deviation of the geoid heights differences accounts for the GNSS/levelling measurement errors, the global gravity model commission and omission errors, and may also include the effects of systematic errors, such as tilts of the LVD or the long wavelength errors in the geoid models. However, the long wavelength geoid errors will begin to average out as the number of GNSS/levelling benchmarks increase over a larger geographical region. Thus, the increased magnitude of the formal errors for the LVD offsets evaluated with tide gauges can be attributed to the fact that the geoid model and measurement errors will not average out over such a small number of sparsely distributed tide gauge stations within a limited geographic region.

The mean geoid height difference evaluated with the Ince et al. (2012) gravimetric geoid model using 2 Atlantic tide gauges is -0.49 m while the mean geoid height difference for Pacific with 5 tide gauges is 0.11 m. This represents a difference of approximately 60 cm between the Atlantic and Pacific coasts. This predominant east-west tilt in CGVD28 is due to the fact that the datum has been constrained to the MSL on both the Pacific and Atlantic coasts in Canada (see Chapter 2, Section 2.5). According to Woodworth et al. (2012) the tilt of the CGVD28 datum accounts for the 40-50 cm geoid height difference from Rimouski to the Pacific coasts and 10-20 cm from Rimouski to the Atlantic Coast, while Hayden et al. (2013) have shown that the MSL for the Pacific coast is approximately 60 cm above the MSL of the Atlantic coast in Canada. This separation was also reported by Sturges (1967) who showed that the MSL values at the tide gauges on the Pacific coast were systematically 60-70 cm higher than those of similar latitude on the Atlantic coast.

Next the NAVD88 LVD offset is evaluated with U.S.A. tide gauges. Table 4.19 shows LVD offsets computed using all 59 available U.S.A. tide gauges. The NAVD88 LVD offsets in Table 4.19 are the result of the average of the geoid height differences for

Atlantic, Pacific, and Gulf coasts while Tables 4.20, 4.21, and 4.22 show the LVD offsets evaluated with tide gauges on the Atlantic, Pacific, and Gulf coasts, respectively. The mean geoid height difference for the U.S.A. Atlantic coast when using *EGM2008* is -0.26 m while it is -0.85 m for the Pacific coast, and it is -0.11 m for the Gulf coast. This can also be seen visually from Figure 4.18, which highlights the east-west and north-south spatial tilts found within the U.S.A. NAVD88 network.

Table 4.19: NAVD88 offset with 59 U.S.A. tide gauges.

GGM	δN^j (cm)	δW^j (m^2/s^2)	W_0^j (m^2/s^2)
goco03s	-43.73 ± 8.04	-4.28 ± 0.79	62636860.28
goco3s+EGM2008	-39.48 ± 4.49	-3.86 ± 0.44	62636859.86
tim_r3	-43.59 ± 8.07	-4.26 ± 0.79	62636860.26
tim_r3+EGM2008	-39.33 ± 4.51	-3.85 ± 0.44	62636859.85
tim_r4	-43.72 ± 8.10	-4.28 ± 0.79	62636860.28
tim_r4+EGM2008	-39.47 ± 4.51	-3.87 ± 0.44	62636859.87
EGM2008	-40.64 ± 4.52	-3.97 ± 0.44	62636859.97
CGG2010	-40.22 ± 4.98	-3.93 ± 0.49	62636859.93
USGG2012	-42.00 ± 4.58	-4.11 ± 0.45	62636860.11

Table 4.20: NAVD88 offset with 28 U.S.A. tide gauges (Atlantic).

GGM	δN^j (cm)	δW^j (m^2/s^2)	W_0^j (m^2/s^2)
tim_r4	-22.32 ± 8.70	-2.19 ± 0.85	62636858.19
tim_r4+EGM2008	-25.71 ± 3.18	-2.52 ± 0.31	62636858.52
EGM2008	-26.20 ± 3.21	-2.57 ± 0.31	62636858.57
CGG2010	-23.30 ± 3.61	-2.28 ± 0.35	62636858.28
USGG2012	-28.27 ± 3.34	-2.77 ± 0.33	62636858.77

Table 4.21: NAVD88 offset with 18 U.S.A. tide gauges (Pacific).

GGM	δN^j (cm)	δW^j (m^2/s^2)	W_0^j (m^2/s^2)
tim_r4	-100.30 ± 15.00	-9.83 ± 1.48	62636865.83
tim_r4+EGM2008	-83.27 ± 5.07	-8.16 ± 0.50	62636864.16
EGM2008	-84.66 ± 5.03	-8.30 ± 0.49	62636864.30
CGG2010	-89.25 ± 5.09	-8.75 ± 0.50	62636864.75
USGG2012	-85.89 ± 5.22	-8.41 ± 0.51	62636864.42

Table 4.22: NAVD88 offset with 13 U.S.A. tide gauges (Gulf).

GGM	δN^j (cm)	δW^j (m^2/s^2)	W_0^j (m^2/s^2)
tim_r4	-11.50 ± 9.55	-1.13 ± 0.94	62636857.13
tim_r4+EGM2008	-8.45 ± 3.41	-0.83 ± 0.33	62636856.83
EGM2008	-10.77 ± 3.61	-1.06 ± 0.35	62636857.06

GGM	δN^j (cm)	δW^j (m^2/s^2)	W_0^j (m^2/s^2)
CGG2010	-8.77 ± 4.31	-0.86 ± 0.42	62636856.86
USGG2012	-10.78 ± 3.80	-1.06 ± 0.37	62636857.06

4.4 Summary

The objective of this chapter was to study the performance of the most recent GOCE-based GGMs for the purpose of computing the potential and height datum offset of the CGVD28, NAVD88, and Nov07 levelling-based vertical datums. In order to accomplish this, the potential and geoid height differences were evaluated with a GOCE only satellite model (i.e., *tim_r4*), GOCE-GRACE satellite models (i.e., *goco03s* and *dir_r4*), a GRACE only model (i.e., *itg-grace2010s*), the high resolution gravity field model *EGM2008*, and the regional gravimetric geoid models *CGG2010*, *USGG2012*, and Ince et al. (2012).

With the goal to unify vertical datums with 1 cm accuracy it can be concluded that the effect of the truncation degree of the GOCE model is an important factor. In Canada, the effect of the GOCE omission error ranges between 8 and 13 cm for LVD offset computations. This can be attributed to the irregular and spare distribution of the GNSS/levelling benchmarks found in the Canadian test networks, in particular, for regions such as western Canada where the topography is quite rugged. The effect of the GOCE omission error on LVD offset estimation indicates that the contributions of the higher frequencies of the gravity field is very important when evaluating the potential and the height offsets of the Nov07, NAVD88, and CGVD28 datums using Canadian GNSS/levelling benchmark information and GOCE GGMs. In contrast, the effect of the GOCE omission error on LVD offsets is less significant in the U.S.A. when using GNSS/levelling information; the effect is only 2-3 cm and can be explained by the fact that the U.S.A. test network contains a dense and homogenous distribution of GNSS/levelling benchmarks that covers an appreciably large geographical area. However, as the objective is to unify vertical datums with 1 cm accuracy, the effect of the GOCE omission error on the LVD offsets for the U.S.A. NAVD88 network should therefore also be taken into account.

Additionally, the effect of the ellipsoidal, levelling, and geoid height errors contribute up to 4 cm to LVD offsets computed over the Canadian mainland, and can have a dm-level impact for island regions. Therefore, in addition to including the accuracy information of the GNSS/levelling data and GGM coefficients, the residual geoid heights should ideally be evaluated with Stokes integration using local gravity data. The high frequency contribution of the topography should also be taken into account using a remove-compute-restore scheme where a GOCE-GRACE combination model can contribute to the long to medium wavelength components of the gravity field signal. The inclusion of these factors is necessary when using the GNSS/levelling data over the Canadian mainland to compute the LVD offsets, and are especially important for regions with very few benchmarks, limited geographical coverage, and/or rugged terrain, such as independent levelling networks on islands, where the geoid model errors and the measurement errors of the GNSS/levelling heights are not likely to average out. Hence, the inclusion of these factors should be considered for future investigations.

Using tide gauges with MSL referenced to CGVD28 in Canada and NAVD88 in U.S.A. to compute LVD offsets emphasizes the spatial tilts found within each network. For both networks the mean geoid height differences differ by approximately 60 cm between the Atlantic and Pacific coasts. For the CGVD28 network that is constrained by multiple tide gauges on the Atlantic and Pacific coasts this difference coincides with the difference in MSL between the two coasts whereas the U.S.A. NAVD88 network is only constrained to the height of the primary tidal benchmark at Rimouski, Quebec (Zilkoski et al. 1992), meaning that the geoid height differences and the potentials evaluated for either coast does not necessarily coincide with the potential of the MSL (which will be examined in Chapter 5).

Due to the existence of the spatial tilts in levelling networks, the removal of systematic effects from the height data is an important step for the computation of LVD offsets. For the Canadian mainland GNSS/levelling networks both a small north-south spatial tilt and a relatively larger west-east spatial tilt exist in the Nov07 and NAVD88 datums, which

can be modelled with a 2-parameter bias corrector term model as it yields the smallest RMS value for the adjusted geoid height residuals. Likewise, in the U.S.A. both a north-south and west-east spatial tilt is present within the NAVD88 network, which can also be modelled using the 2-parameter bias corrector term model. When using the 2-parameter model, the spatial tilts may be estimated either before or simultaneously along with the offset term as the difference between these methods on the LVD offset estimate reaches a maximum of 1 cm depending on the geoid model utilized.

For the CGVD28 network, it is recommended that further investigations into the local distortions and systematic effects are likely necessary, as the LVD offset values differed quite significantly between the use of the different bias corrector term models. Moreover, the RMS value remained close to 20 cm when computing LVD offsets using all three different bias corrector term models, which is approximately 10 cm greater than the RMS values for the Canadian NAVD88 and Nov07 networks for the 2-parameter and combined model cases. Including a larger number of GNSS/levelling benchmarks into the analysis could also be a factor in modeling the systematic effects in the CGVD28 network, if indeed the systematic effects follow a more complex pattern than simple spatial tilts.

CHAPTER 5
EVALUATION OF W_0 USING CANADIAN TIDE GAUGES AND GOCE GLOBAL GEOPOTENTIAL MODELS

5.1 Introduction

One of the key factors in the implementation of the geoid-based vertical datum in Canada is to have a common datum with the U.S.A., and by extension a common geoid model for North America. Therefore, one of the primary concerns in choosing a common geoid model is to jointly agree upon which W_0 value should be chosen as the zero height surface. In order to satisfy the definition that the geoid is the level surface of constant gravity potential that best represents the MSL at rest, the W_0 value can be evaluated by averaging the potentials of points on the mean water surface, which can be computed from the mean sea surface topography that is referenced to an equipotential surface with a known potential.

There are three basic options for obtaining the sea surface topography:

1) the combination of tide gauge records and a geoid model,
2) the combination of satellite altimetry sea surface heights and a geoid model,
3) and oceanic sea surface topography models.

Sea surface topography models are generally estimated from satellite altimetry and geodetic measurements, but may also include measurements such as seawater temperature, salinity data, tide gauge observations, and ocean surface drifter velocities (e.g., Rapp and Wang 1994; Ekman and Mäkinen 1996; Rio et al. 2004; Bingham and Haines 2006; Thompson and Demirov 2006; Foreman et al. 2008; Anderson and Knudsen 2009; Maximenko et al. 2009; Thompson et al. 2009, among others). For the most part, W_0 has been computed globally using satellite altimetry observations (e.g., Burša et al. 1998; Sánchez 2009; Dayoub et al. 2012; Yonghai and Jiancheng 2012), and to a lesser extent, the geopotential at tide gauges has also been used to determine regional

W_0 (e.g. Grafarend and Ardalan 1997; Ardalan et al. 2002; Bolkas et al. 2012; Hayden et al. 2012b; Hayden et al. 2013).

In order to avoid inconsistencies included in terrestrial gravity data due to the use of different height datums when estimating W_0, the use of a satellite only global geopotential model (GGM) is preferred. The focus of this chapter is the determination of the W_0 for the new Canadian vertical datum utilizing recently released satellite-only GOCE GGMs in combination with tide gauge records. As previously discussed in Chapter 3 and Chapter 4, the effect of the omission errors of the GOCE satellite only models may be significant at the tide gauge locations along the Canadian coasts and may bias the mean potential of the local mean sea level. In order to quantify the approximate omission errors resulting from GOCE-only global geopotential models, W_0 is also computed with the use of high resolution geoid models (e.g., *CGG2010* (Huang and Véronneau 2013) and *EGM2008* (Pavlis et al. 2012)). Specifically, contributions of Canadian tide gauges for the determination of W_0 are examined by averaging the potential of points on the mean water surface evaluated from the geometrical mean sea surface topography using tide gauge records that have been averaged over 19 years (in order to eliminate the variations due to the tides) with the effects of sea level rise and vertical land motion accounted for. Furthermore, regional SST models are utilized as an independent approach for validating W_0 results obtained from tide gauges and gravity field models. Additionally, a wide range of global SST models are also used to validate the W_0 results obtained from the tide gauge records.

5.2 Methodology

The basic procedure for computing W_0 value through tide gauge averaging can be outlined as follows:

1) Selection of tide gauges which have been surveyed with GNSS;
2) Selection of a geoid model;
3) Computation of the gravity potential W of the local mean sea level height at each respective tide gauge; and

4) Computation of W_0 as the mean W value from all the tide gauges.

5.2.1 Distribution of Tide Gauge Stations and Water Level Data

The determination of MSL requires the removal of all periodic constituents existing in the tide gauge record, where the longest constituent is the lunar nodal tidal constituent of 18.6 years. Therefore, a near uniform distribution of tide gauge stations with up to date long-term time series, preferably up to one lunar nodal cycle (i.e., approximately19 years) or multiples of this cycle, is ideal in order to obtain a W value that best represents the MSL around the Canadian coastline. Furthermore, the 19-year data span will also average out effects of sea levels due to weather such as wind stress, changes in atmospheric pressure, and storm events (Pugh 1987).

Tide gauges along the Canadian Pacific, Atlantic, and Arctic coasts were selected for the determination of the mean W_0 value based on the following criteria:

1) The tide gauge has a corresponding benchmark which has been surveyed with GNSS;
2) The tide gauge benchmark should be in good condition according to the Canadian Hydrographic Service (CHS); and
3) The tide gauge has water level data for 19 years from 1992 to 2011 without significant data gaps (i.e., no more than 2-3 years of missing data).

Only a small portion of tide gauges available in Canada meet the above criteria for the determination of W_0. Specifically, there are 12 tide gauges in the Pacific, 10 tide gauges in the Atlantic, and 1 tide gauge in the Arctic that contain 19 years of water level data. In order to extend the analysis the Arctic, tide gauges with at least 12 months of data after 1990 were also included, and the local MSL was computed from monthly water level data obtained from the CHS, thus there are 38 tide gauges in total. The final list of stations used is given in Table 5.1 and the geographic distribution of the tide gauges is shown in Figure 5.1.

The daily water level records for Canadian tide gauges are available from http://www.meds-sdmm.dfo-mpo.gc.ca/isdm-gdsi/twl-mne/index-eng.htm. The MSL for tide gauges with 19 years of data was evaluated by first averaging daily water levels to monthly time series, and then from monthly to annual time series, and lastly the 19-year average was computed. For time series with less than 24 days in a month, the monthly averages were interpolated from neighbouring values using the nearest neighbour value if only one monthly sea level value was available or the average of the two nearest neighbour values if two monthly sea level values were available. If the time series contained 24 or more days of water level records, the monthly averaged value was computed with the number of daily records available. The monthly time series with five or more months of missing data for annual averages were also interpolated from neighbouring values where possible with the same treatment as the daily water level time series.

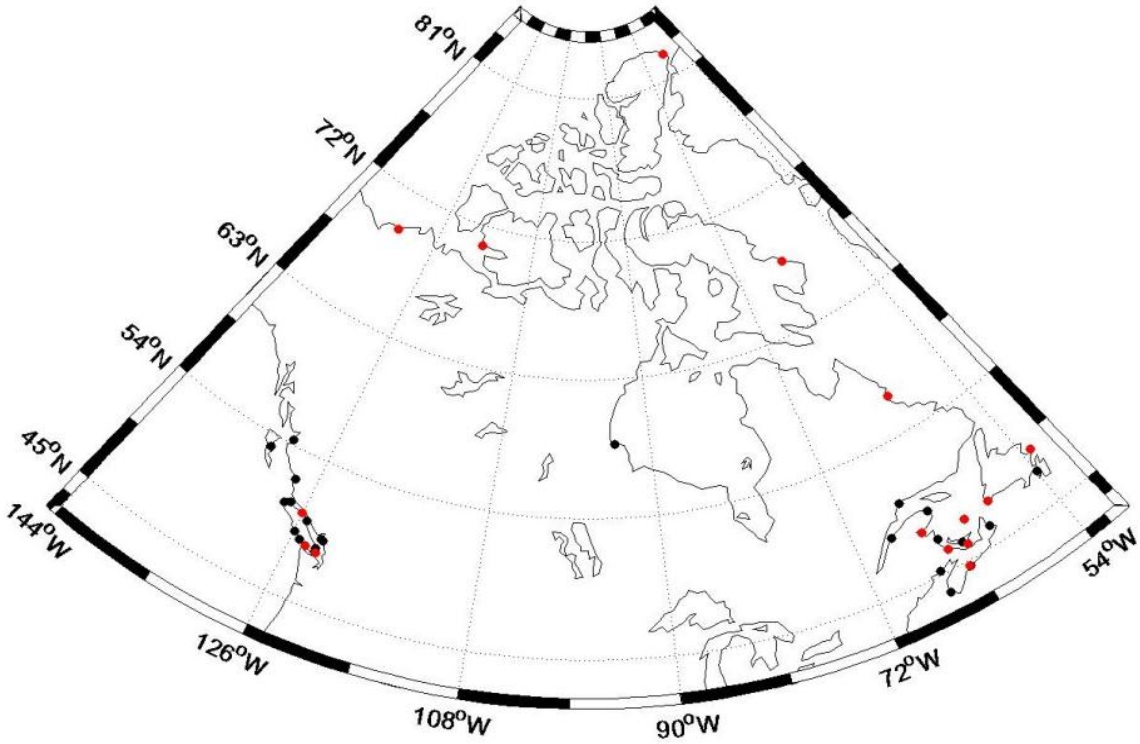

Figure 5.1: Geographical distribution of tide gauges in Canada used for W_0 computation (**Red:** Tide gauge stations with data gaps **Black:** Tide gauge stations without data gaps).

Table 5.1: Canadian tide gauge stations and local mean sea levels at epoch 2008.0.

Tide Gauge Station	Latitude (˚)	Longitude (˚)	MSL (m)
PACIFIC REGION WITH 19 FULL YEARS OF WATER LEVEL DATA			
7120	48.4240	-123.3710	1.9201
7277	48.6536	-123.4515	2.3137
7795	49.3370	-123.2530	3.1190
8074	50.0420	-125.2470	2.8931
PACIFIC REGION WITH 19 FULL YEARS OF WATER LEVEL DATA			
8408	50.7220	-127.4890	2.9059
8615	49.1540	-125.9130	2.0909
8735	50.5130	-128.0290	2.2238
9850	53.2520	-132.0720	3.9944
7735	49.2870	-123.1100	3.0982
PACIFIC REGION WITH 19 FULL YEARS OF WATER LEVEL DATA			
8545	48.8360	-125.1360	2.0464
8976	52.1630	-128.1430	2.8757
9354	54.3170	-130.3240	3.9098
PACIFIC REGION WITH DATA GAPS			
7130	48.4237	-123.3027	2.0277
8215	50.3980	-125.9610	2.9197
8525	48.5550	-124.4210	2.0477
ATLANTIC REGION WITH 19 FULL YEARS OF WATER LEVEL DATA			
612	46.2167	-60.2500	0.8276
835	47.3000	-53.9833	1.3773
1700	46.2333	-63.1167	1.7657
2000	47.0833	-64.8833	0.8164
2330	48.9970	-64.3805	1.0384
2780	50.1948	-66.3768	1.5838
2985	48.4783	-68.5137	2.2687
365	43.8333	-66.1167	2.5976
490	44.6667	-63.5833	1.0551
65	45.2510	-66.0630	4.4707
ATLANTIC REGION WITH DATA GAPS			
491	44.6833	-63.6167	1.0728
665	47.5667	-59.1333	1.1971
990	48.6510	-53.1150	0.6083
1430	56.5500	-61.6833	1.4182
1680	45.9500	-62.7500	1.4391
1805	46.2270	-64.5460	1.2319
1970	47.3789	-61.8573	0.9209
2145	47.9000	-65.8500	1.3714
ARCTIC REGION WITH 19 FULL YEARS OF WATER LEVEL DATA			
5010	58.7667	-94.1833	2.5972
ARCTIC REGION WITH DATA GAPS			

Tide Gauge Station	Latitude (˚)	Longitude (˚)	MSL (m)
3765	82.4919	-62.3173	0.4558
3980	67.5167	-64.0667	0.7834
ARCTIC REGION WITH DATA GAPS			
6380	70.7363	-117.7612	0.3886
6485	69.4382	-132.9944	0.4467

5.2.2 Global Geopotential Models

In order to obtain the gravity potential at the tide gauge sites, global geopotential models or regional gravimetric geoid models are required. Ideally, a satellite-only model that is globally consistent is preferred as it avoids inconsistencies included in the terrestrial gravity anomalies due to the use of different height datums. However, in practice the omission error of the satellite-only gravity field models will affect the determination of the potential at each tide gauge. Due to the limited number of tide gauges available and since the W_0 is based on the averaging of these potential values, the effect of the GGM omission error on W_0 is an important factor to be investigated. For that reason, regional geoid models based on terrestrial gravity and terrain data are also included in the analysis. The same models utilized in Chapter 4 for local vertical datum offset computations are used in this chapter for W_0 determination (see Tables 3.1 and 4.1).

5.2.3 Sea Surface Topography Models

In order to validate the W_0 results obtained from tide gauge averaging, three regional sea surface topography models have been utilized. The first model covers the North-East region of the Pacific Ocean (Foreman et al. 2008) and was developed by M.G.G. Foreman at the Department of Fisheries and Oceans Canada (DFO). The other two models are for the northern Atlantic Ocean and were developed by D.G. Wright from DFO and K. R. Thompson and E. Demirov from Dalhousie University (Thompson and Demirov 2006). The Foreman model is a variable density model, with the SST nodes being quite dense along the coast and sparse for the deep ocean. The grid spacing for the Wright model is approximately 15 arc minutes while the grid spacing for the Thompson & Demirov model is approximately 20 arc minutes. Additionally, ten global SST models

have been obtained from the National Oceanography Centre at the University of Southampton: Maximenko (Maximenko et al. 2009), CLS (Rio et al. 2011), ECCO2-JPL (Menemenlis et al. 2005), OCCAM12 (Webb et al. 1997), GECCO (Köhl and Stammer 2008), ECCO-godae (Köhl et al. 2007), Liverpool Fine (Marshall et al. 1997a), Liverpool Coarse (Marshall et al. 1997b), GOCE-1 (Woodworth et al. 2012), and GOCE-2 (Woodworth et al. 2012). These SST models provide an independent approach for validating the W_0 results obtained from the tide gauges and gravity field models. All models are given in the mean-tide system and their coverage for North America is shown in Figures 5.2-5.12.

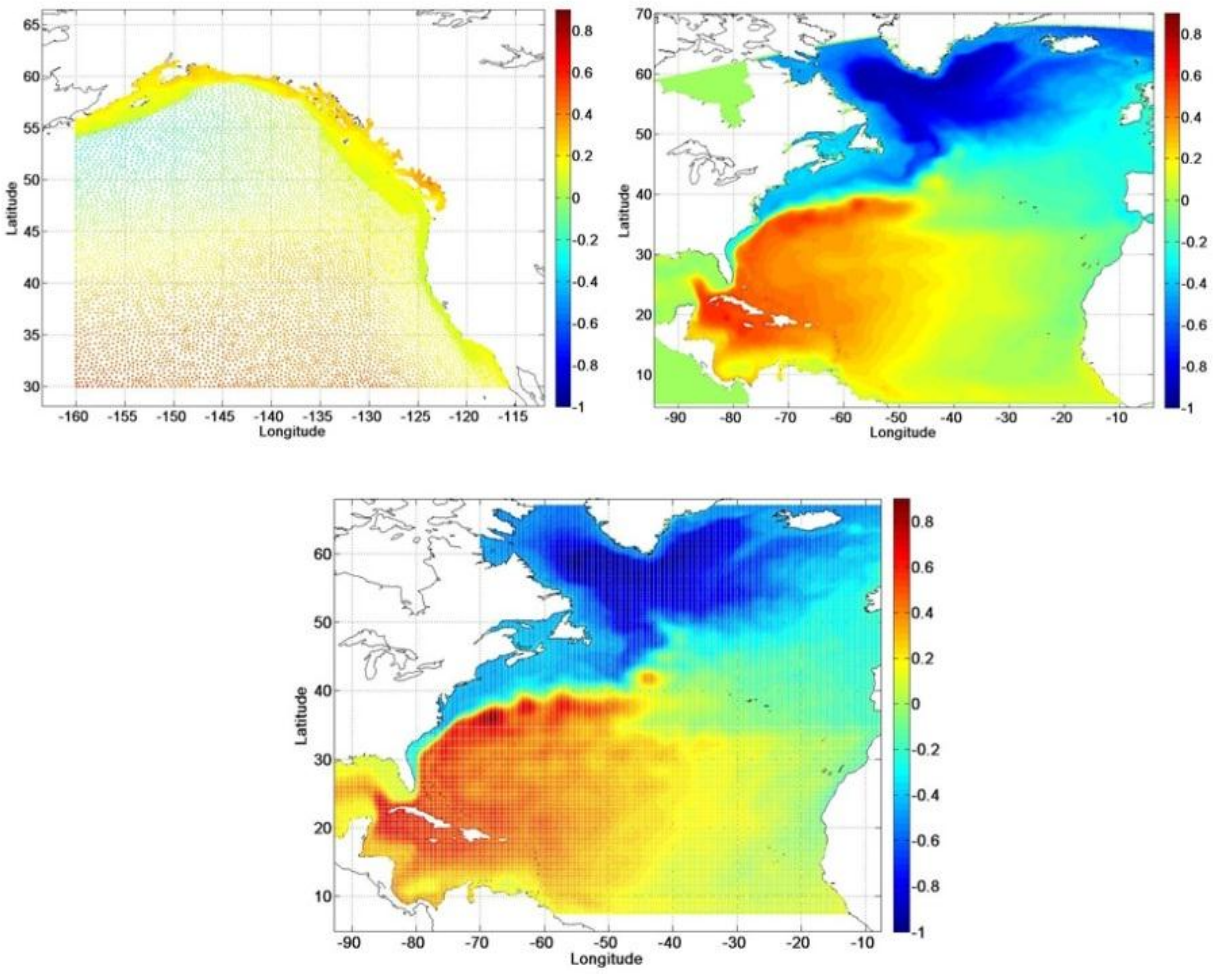

Figure 5.2: Regional oceanic models with SST values in meters (**Top Left:** Foreman **Top Right:** Wright **Bottom:** Thompson & Demirov).

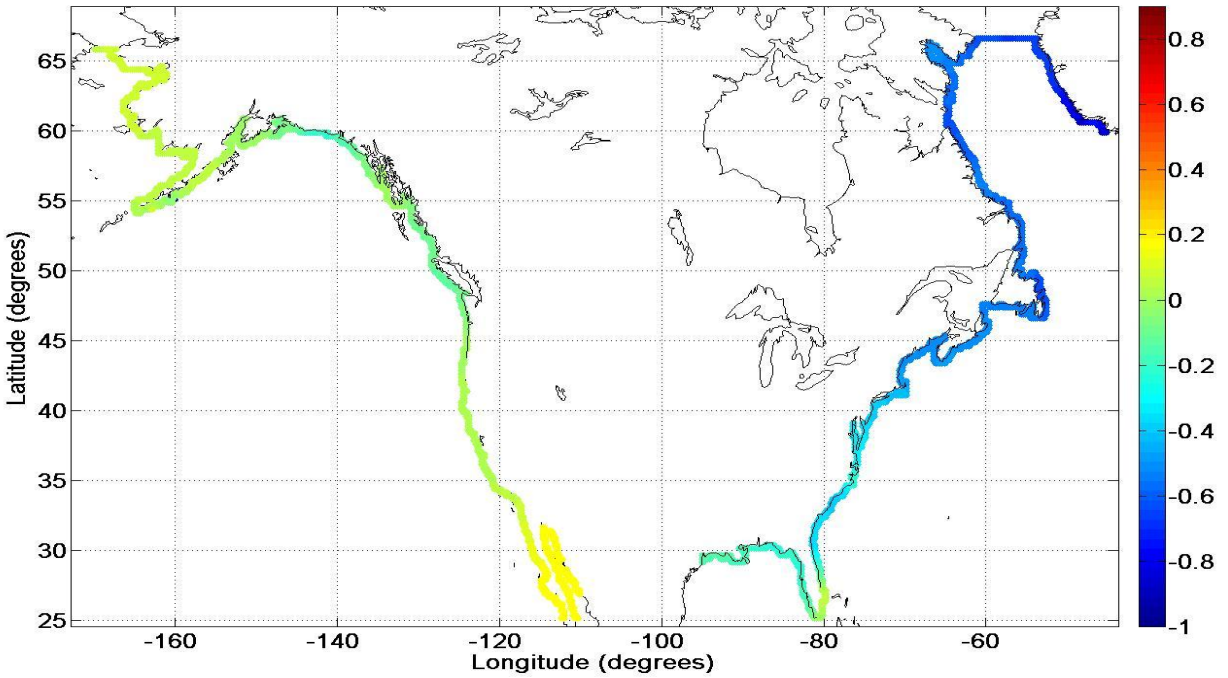

Figure 5.3: Maximenko with SST values in meters (Geodetic: GRACE, drifter velocity, altimetry).

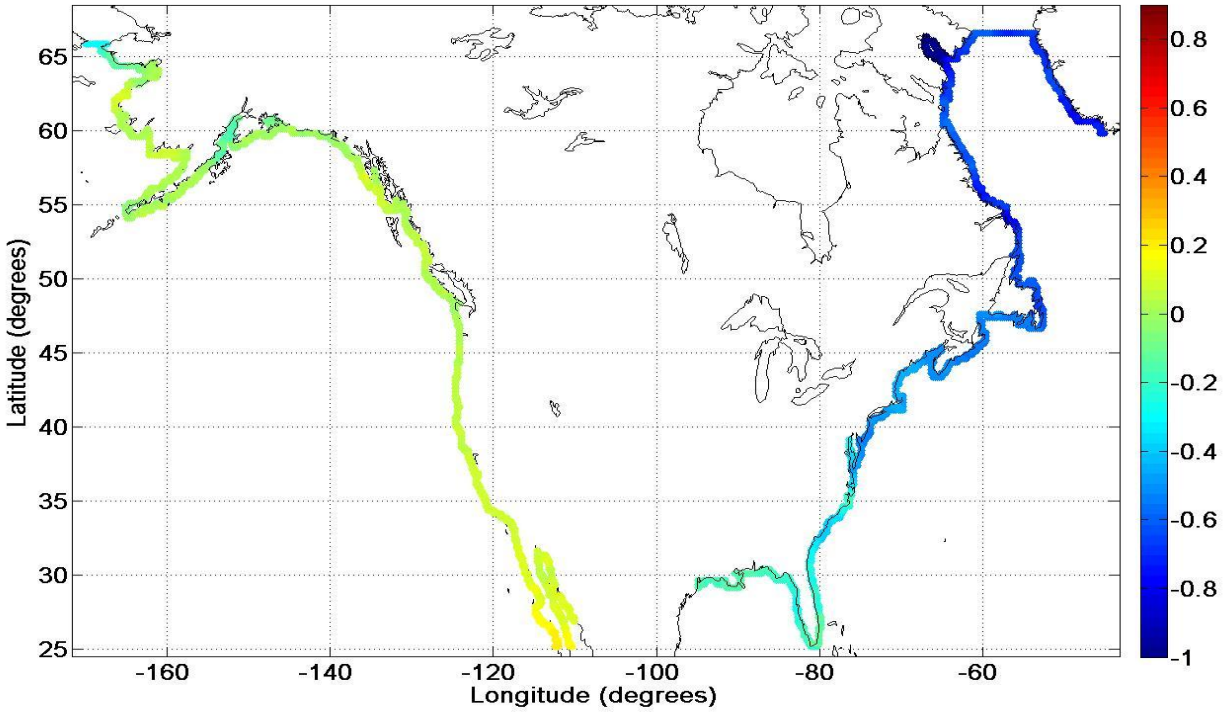

Figure 5.4: CLS with SST values in meters (Geodetic: GRACE, drifter velocity, altimetry, hydrography).

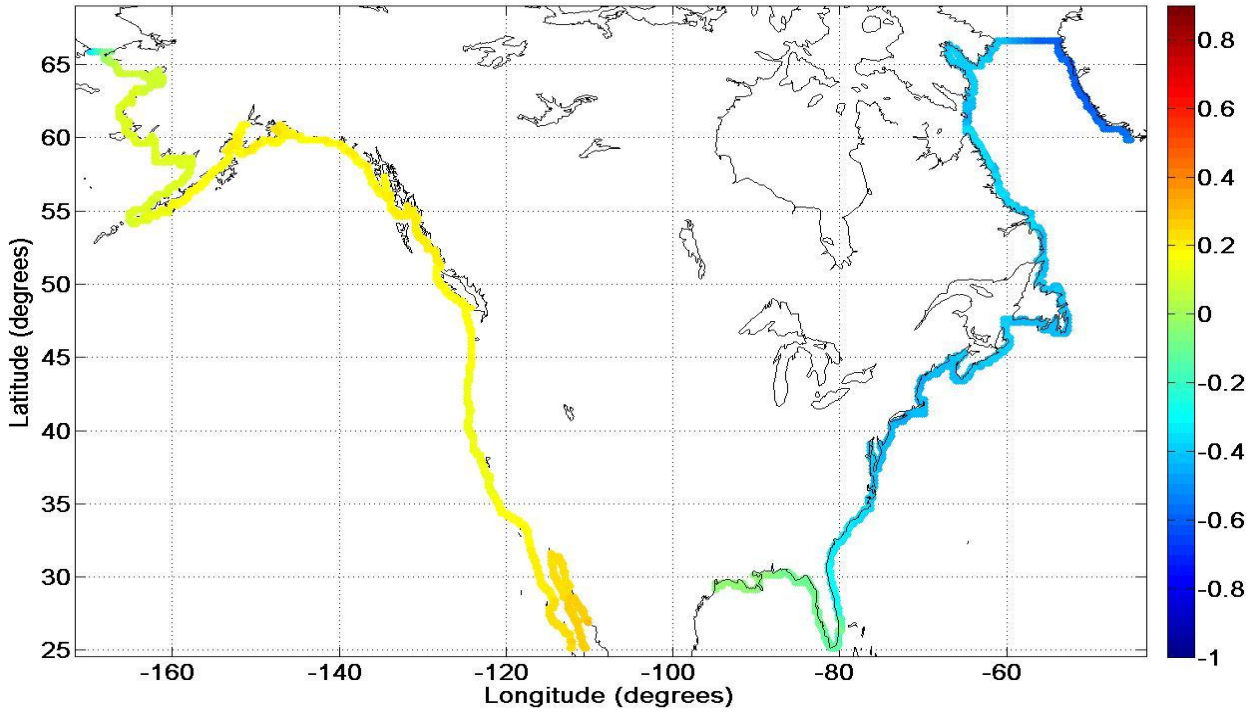

Figure 5.5: ECCO2-JPL with SST values in meters (Oceanographic: data assimilation of many variables including geodetic).

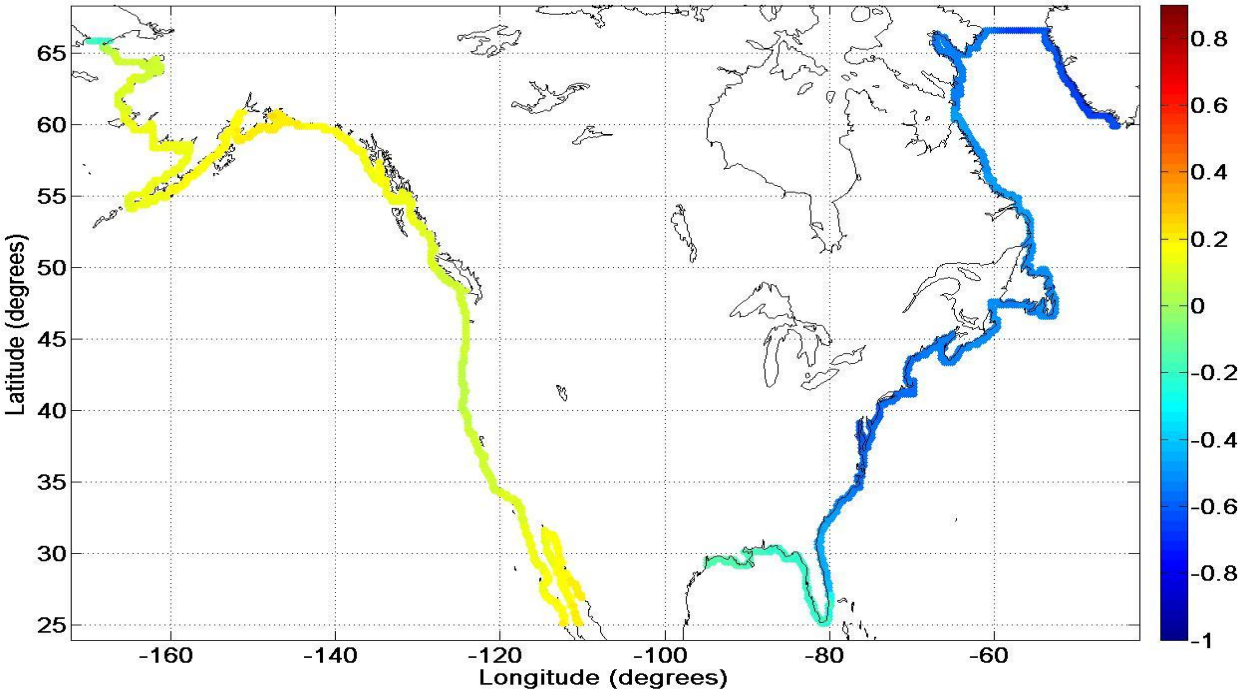

Figure 5.6: OCCAM12 with SST values in meters (Oceanographic: no data assimilation).

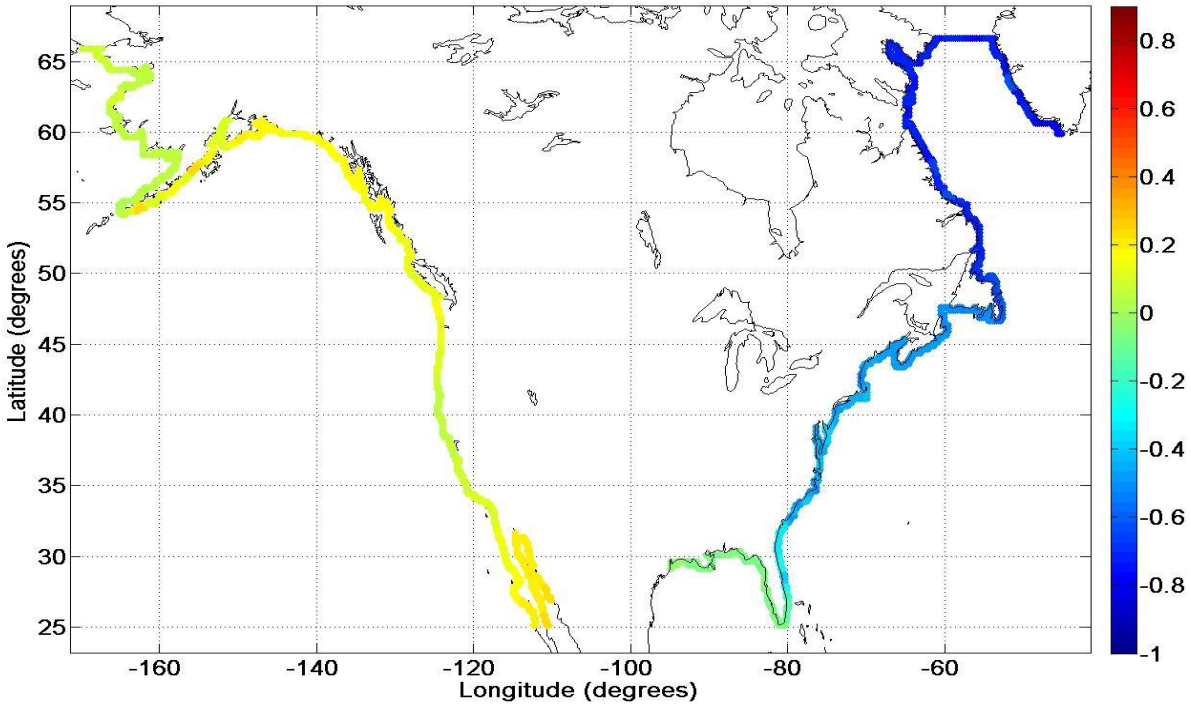

Figure 5.7: GECCO with SST values in meters (Oceanographic: data assimilation of many variables including geodetic).

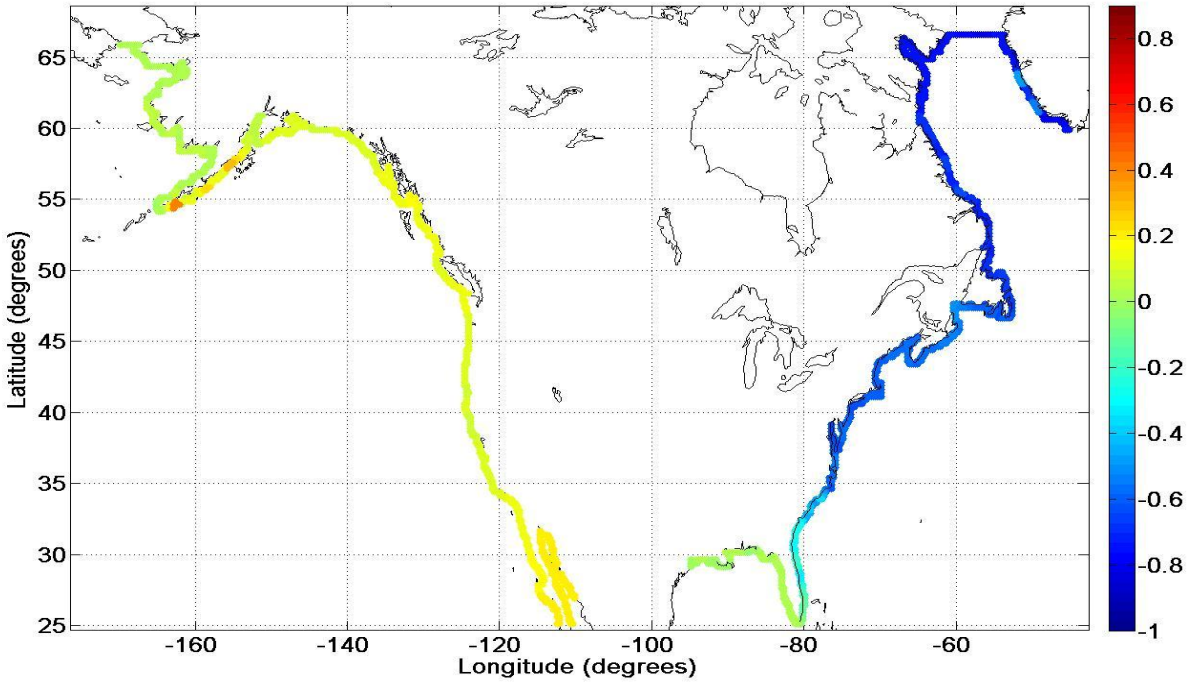

Figure 5.8: ECCO-godae with SST values in meters (Oceanographic: data assimilation of many variables including geodetic).

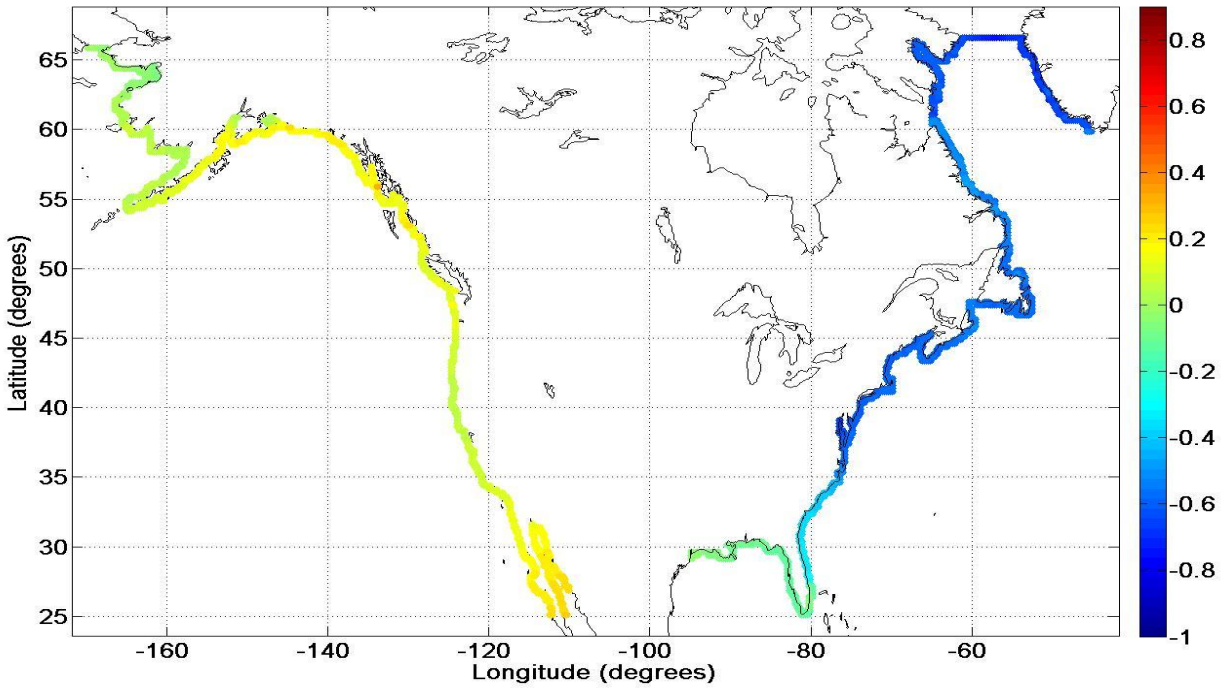

Figure 5.9: Liverpool Fine with SST values in meters (Oceanographic: data assimilation of hydrography).

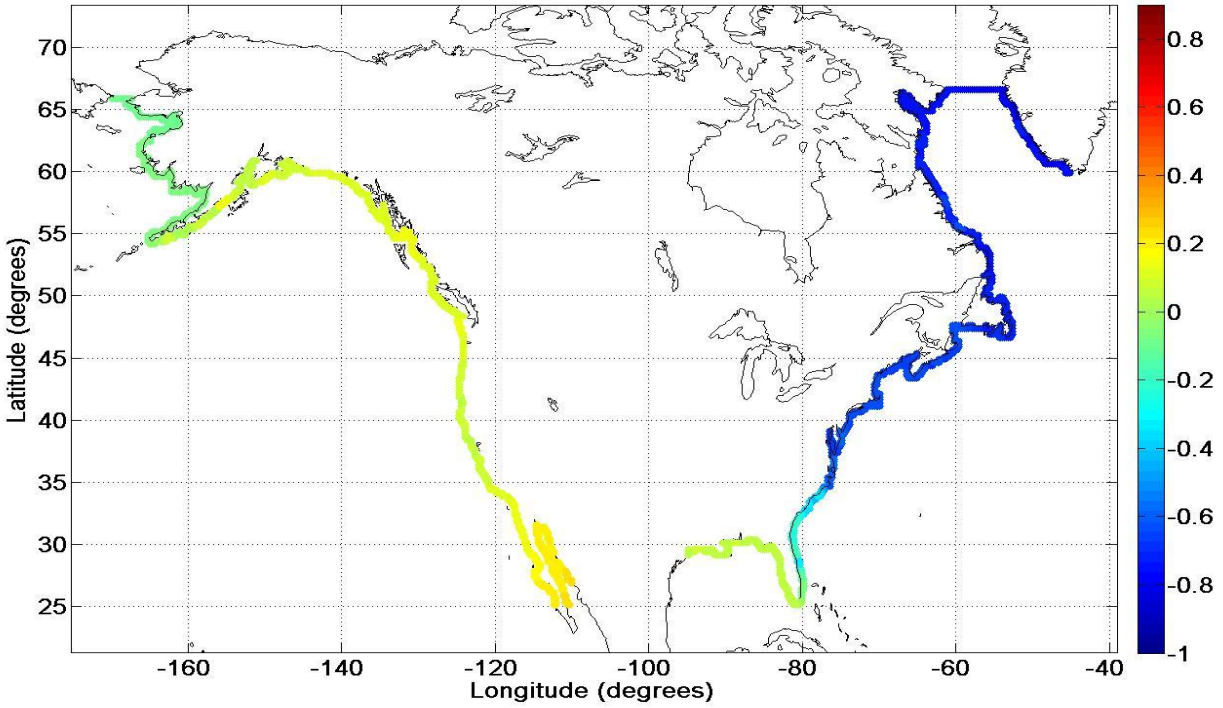

Figure 5.10: Liverpool Coarse with SST values in meters (Oceanographic: data assimilation of hydrography).

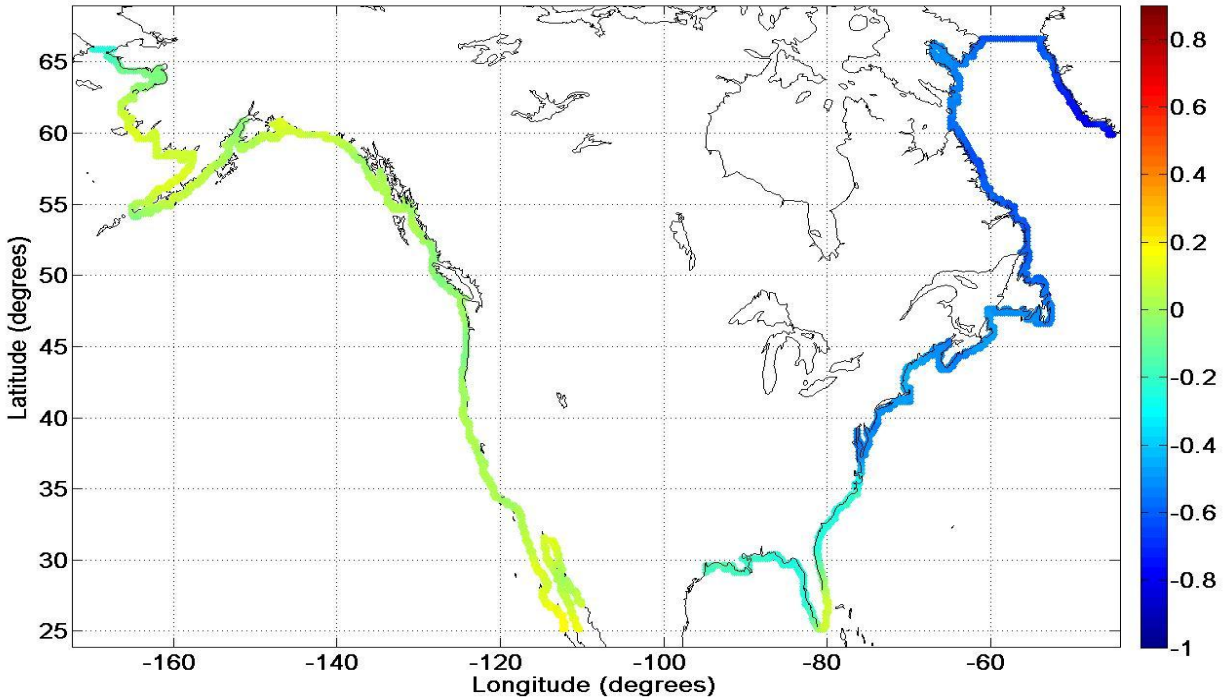

Figure 5.11: GOCE-1 with SST values in meters (CLS 01 mean sea surface (MSS) (Bingham et al. 2008; aviso.oceanobs.com) – go_cons_gcf_dir_r2).

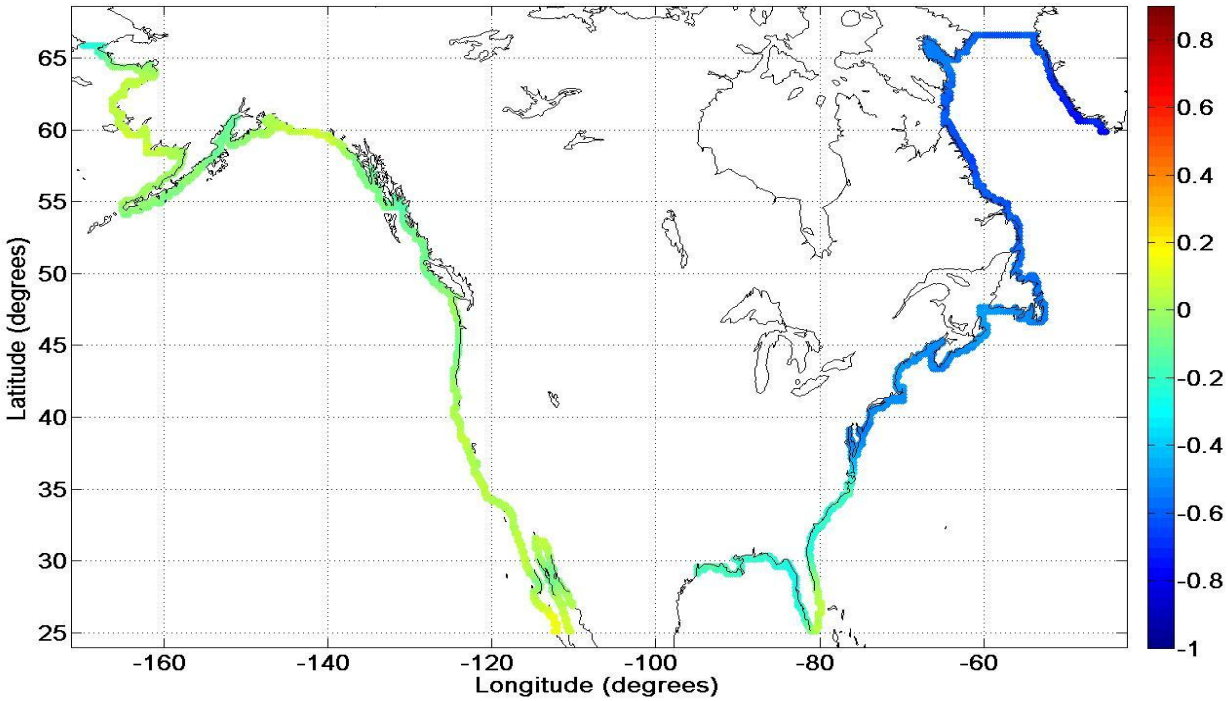

Figure 5.12: GOCE-2 with SST values in meters (CLS 11 MSS (Bingham et al. 2008; aviso.oceanobs.com) – go_cons_gcf_dir_r3).

The SST models presented in Figures 5.2-5.12 have been generated by the two general approaches for the determination of SST at the coast: the geodetic approach and the oceanic approach. In the geodetic approach, the ellipsoidal heights of the MSL at the tide gauge stations are compared to the heights of the geoid above the ellipsoid from a geoid model, or alternatively, the ellipsoidal heights of the sea level obtained from satellite radar altimetry are compared with geoid model heights (Woodworth et al. 2012). The advantage of using tide gauges is that the SST can be obtained directly at the coast while using altimetry observations means that the evaluation of the SST is performed some tens of km offshore (Woodworth et al. 2012). The oceanic approach consists of utilizing oceanographic and meteorological measurements such as coastal sea level, ocean currents, temperatures, salinities, air pressures, and winds (Woodworth et al. 2012). It can be observed from Figures 5.2-5.12 that although the SST models are constructed using different approaches and different data sets, they produce on the whole, similar SST values on both the Atlantic and Pacific Coasts in North America.

Since the mean sea surface topography represents the separation between the mean sea surface and an equipotential surface (Foreman et al. 2008), it is essential that the potential of the equipotential surface that was used in the generation of the SST models be known in order to estimate the potential of the mean water surface. The potential value of the equipotential surface used for the construction of the SST models can be estimated by:

1) Utilizing the methodology presented in the next section (see Eq. (5.4)) by subtracting the SST obtained from the SST models from the mean water level computed from the tide gauge records with the use of a geoid model with a known reference potential;
2) Comparing the SST values from the SST models with those obtained from satellite altimetry and a geoid model with known reference potential; and by
3) Utilizing a modified version of the methodology presented in Chapter 4 to compute local vertical datum offsets (e.g., Burša et al. 2004; Kotsakis et al. 2011) where ellipsoidal heights are replaced with sea surface heights (SSH) and orthometric heights are replaced with SST values obtained from the SST models.

For the purposes of this study, option 1 and 3 were utilized in order to determine the potential value of the equipotential surface to which the SST values are referenced.

The geometrically derived SST (see Eq. (5.3)) at the tide gauges is used as a criterion for external validation of the SST models. Table 5.2 compares the SST determined from GNSS at the tide gauges with the SST values obtained from the SST models with the difference computed using (Ekman 1989; Mäkinen and Ihde 2009):

$$\delta SST = SST_{TG,TF} - \left[SST_{Model,MT} + 0.68\left(\left(9.9 - (29.6sin^2\varphi)\right)0.01\right)\right], \qquad (5.1)$$

where $SST_{TG,TF}$ is the SST value obtained using tide gauge records and a geoid model in the tide free system, $SST_{Model,MT}$ is the sea surface topography obtained from a SST model given in the mean-tide system, and φ is the latitude of the SST node from the model. Based on the results from Table 5.2, the regional SST models and the global ECCO2-JPL model have the best agreement with the geometrically determined SST at tide gauges, with a mean difference that is less than 3 cm.

Table 5.2: Comparison of geometrically determined SST at tide gauge with *CGG2010* and SST interpolated to tide gauge station locations from various SST models.

SST Model	Mean Difference (cm)	Standard Deviation (cm)	Number of Tide Gauges
Foreman+Wright	2.80	7.65	22
Foreman+Thompson & Demirov	1.30	6.86	22
Maximenko	23.07	8.50	22
CLS	17.47	6.42	22
ECCO2-JPL	2.57	5.64	22
OCCAM12	12.33	7.08	22
GECCO	9.33	7.22	22
ECCO-godae	13.33	9.37	22
Liverpool Fine	12.33	8.89	22
Liverpool Coarse	17.69	12.30	22
GOCE1	19.24	7.09	22
GOCE2	21.55	8.44	22

In the following figures (i.e., Figures 5.13-5.18), the SST determined at tide gauges using the models *goco03s*, *goco03s+EGM2008*, and *CGG2010* are visually compared to the SST values interpolated from the regional oceanic SST models.

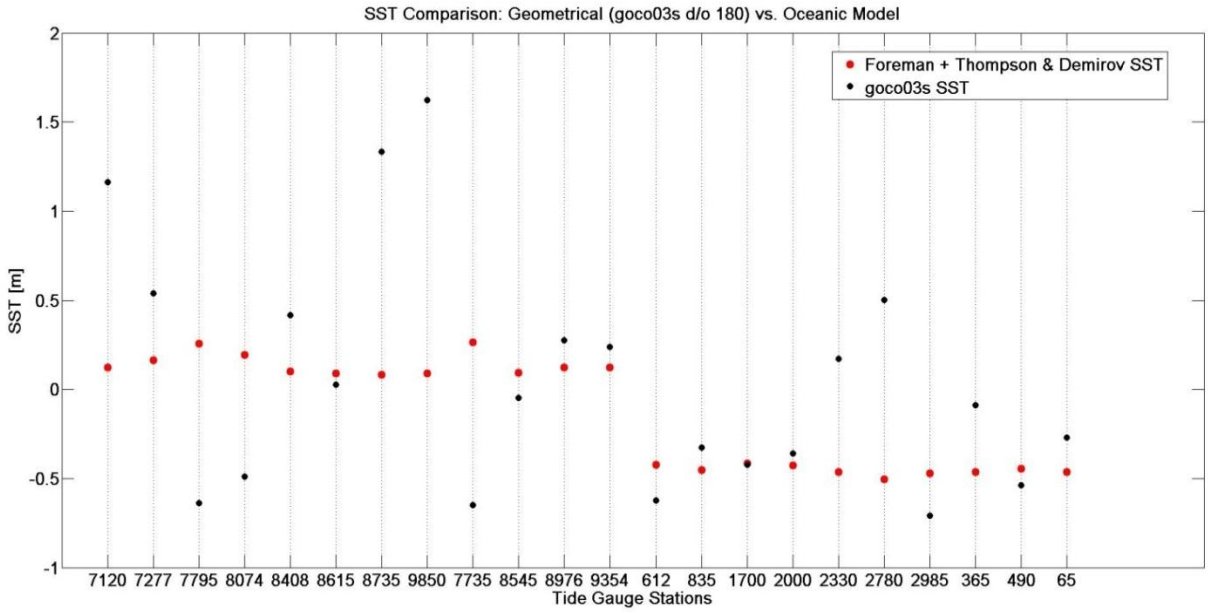

Figure 5.13: Comparison between SST determined using tide gauge records and *goco03s* and SST from Foreman & Thompson oceanic SST model.

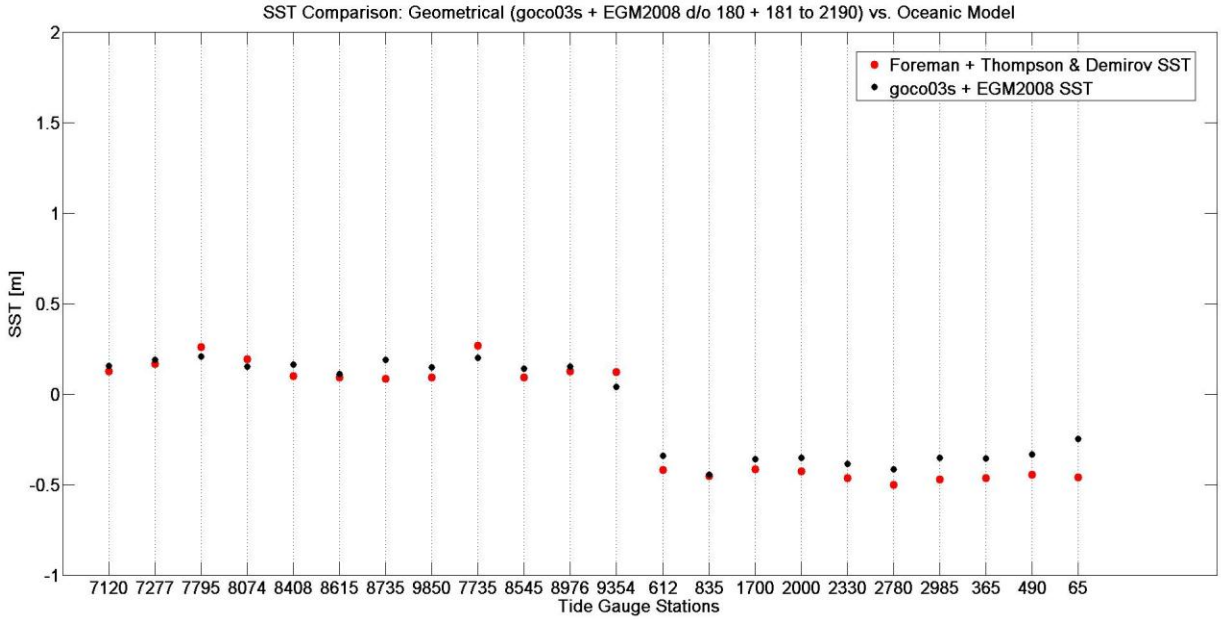

Figure 5.14: Comparison between SST determined using tide gauge records and *goco03s+EGM2008* and SST from Foreman & Thompson oceanic SST model.

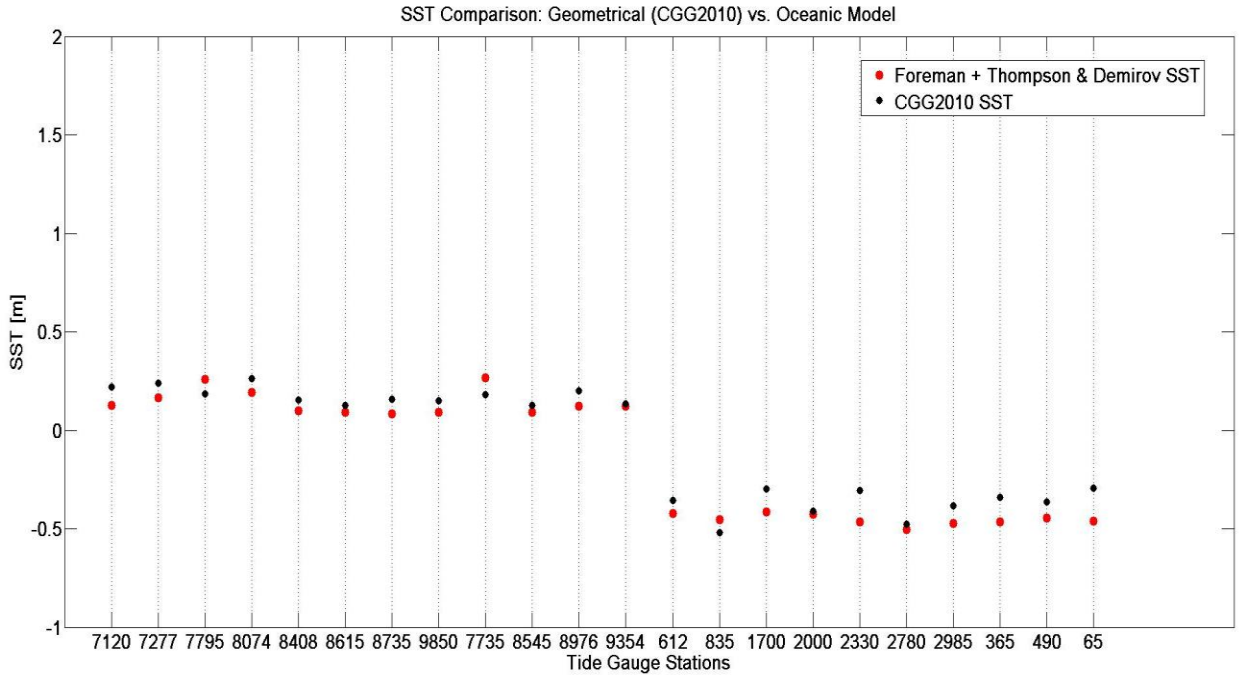

Figure 5.15: Comparison between SST determined using tide gauge records and *CGG2010* and SST from Foreman & Thompson oceanic SST model.

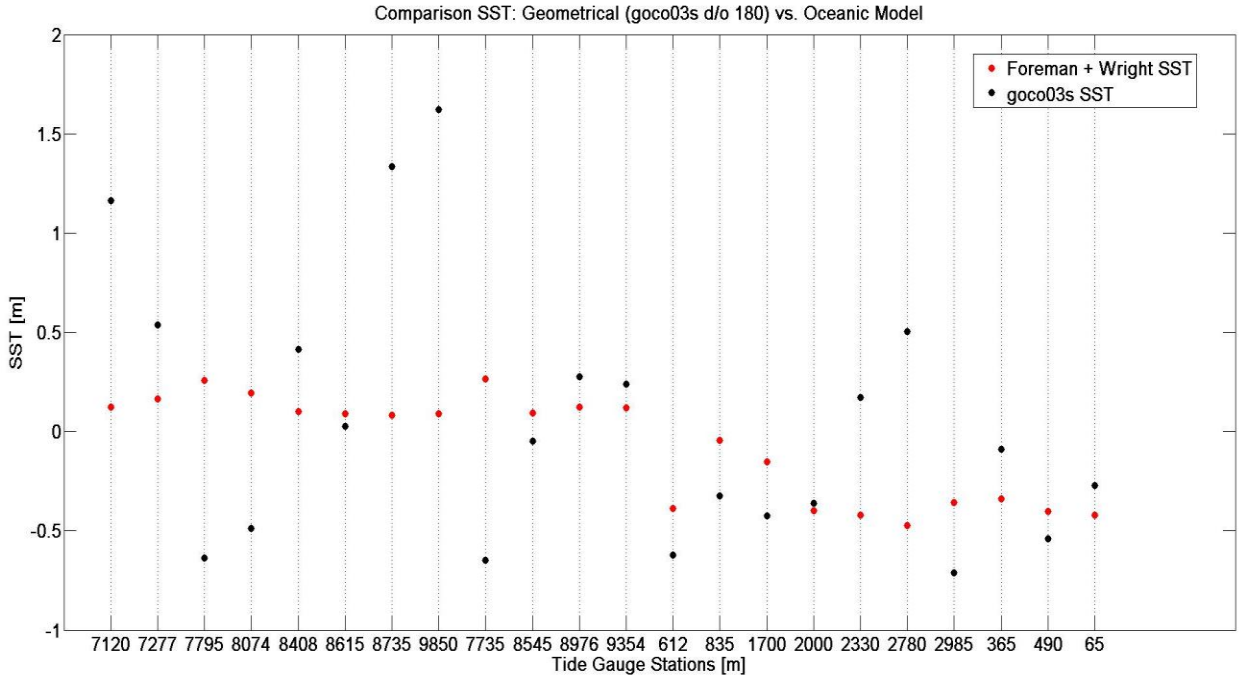

Figure 5.16: Comparison between SST determined using tide gauge records and *goco03s* and SST from Foreman & Wright oceanic SST model.

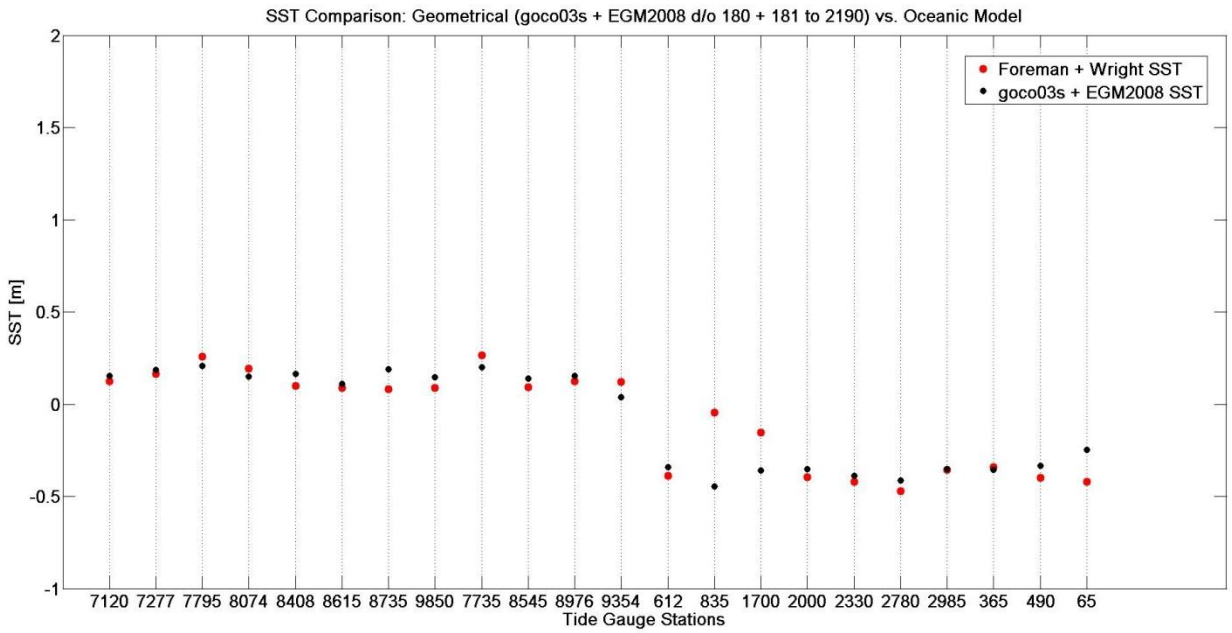

Figure 5.17: Comparison between SST determined using tide gauge records and *goco03s+EGM2008* and SST from Foreman & Wright oceanic SST model.

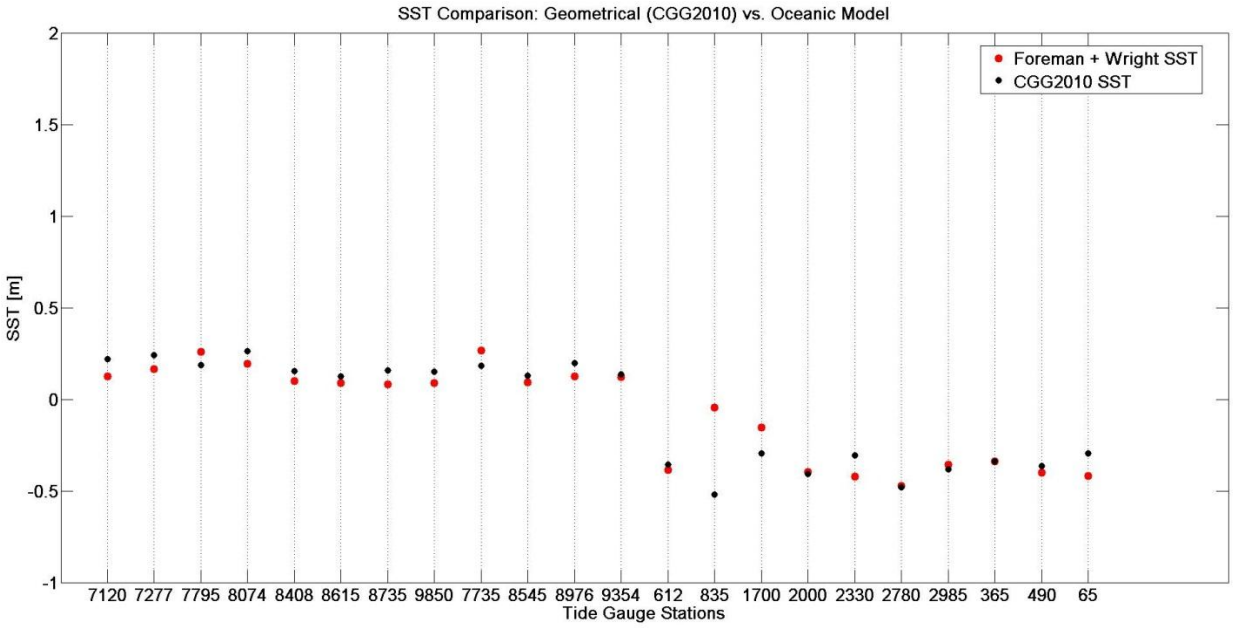

Figure 5.18: Comparison between SST determined using tide gauge records and *CGG20120* and SST from Foreman & Wright oceanic SST model.

The choice of the geoid model is crucial for the accurate determination of SST. For example, Figure 5.13 and Figure 5.16 show that using the *goco03s* model truncated at degree and order 180 may result in a discrepancy in the SST estimated by the regional oceanic models that can reach up to 1 m at select tide gauges. In contrast, when using the

high resolution models *CGG2010* and *goco03s+EGM2008* for the estimation of SST, a good agreement can be observed with the SST estimates obtained from the regional SST models, which can be seen from Figure 5.14 and Figure 5.15, as well as from Figure 5.17 and Figure 5.18. In such a case, a maximum deviation of approximately 0.5 m is observed for the Foreman and Wright combination of SST models for tide gauge station 835 when compared with the SST obtained using tide gauge records and a geoid model.

5.2.4 Methodology for Estimating W_0 using Tide Gauge Information and SST Models

The potential of a point (W_P) on the mean water surface can be estimated from the mean SST, which is based on a time-averaged sea surface where the periodic effects of the tides are averaged out. The mean SST is referenced to an equipotential surface with a known potential W_N. As the SST is the separation between the MSL and the geoid, it can be approximated by the following (Sánchez 2009):

$$SST_P = \frac{W_N - W_P}{\gamma_P}, \tag{5.2}$$

where W_N is the potential of the geoid (the equipotential surface) and γ_P is the normal gravity computed at the geoid using the latitude of the computational point.

Figure 5.19 shows the various observation quantities needed for the geometrical evaluation of the SST using tide gauge data; the SST at a tide gauge can therefore be expressed as:

$$SST = h - N - CD + Z_0, \tag{5.3}$$

where h is the ellipsoidal height of the tidal benchmark, N is the geoid height, CD is the height of the tidal benchmark above the chart datum, and Z_0 is the height of the local MSL above the chart datum.

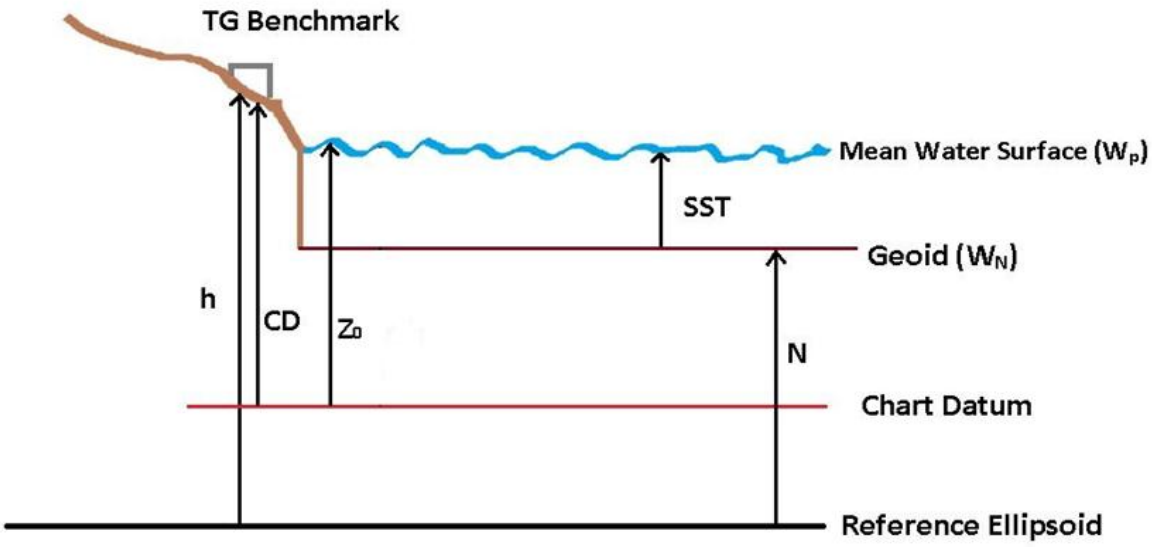

Figure 5.19: Geometrical evaluation of sea surface topography at tide gauges (Hayden et al. 2013).

A tide-free system, a mean-tide system, or a zero-tide system can be used for the evaluation of Eq. (5.3). According to the IERS 2010 handbook (Petit and Luzum 2010), a tide-free quantity will have the total tidal effects removed, though in practice such a quantity is not fully realizable. The IERS 2010 convention recommends using a zero-tide system for geopotential quantities in order to eliminate the external component of the permanent tide, and a mean-tide system that eliminates the periodic variations of the tidal effects for quantities relating to station positions (Petit and Luzum 2010). Within this chapter the tide-free system has been adopted for the sake of convenience as *h* and *N* were given in a tide-free system. The difference between using a mean-tide and a tide-free system is 0.5 m^2/s^2 or approximately 5 cm in terms of an averaged W_0 value (Hayden et al. 2012b), and as this difference is smaller than three times the formal error, it does not result in statistically different W_0 values.

The SST in Eq. (5.3) can be converted to a potential difference, which is then subtracted from the potential of the equipotential surface W_N. Thus, based on Eq. (5.2) and Eq. (5.3) the potential at point *P* can be computed from:

$$W_P = W_N - [(h - N - CD + Z_0)\gamma_P]. \quad (5.4)$$

The W_0 value or the mean potential of the water surface is computed by means of the least-squares solution of the system of observation equations evaluated by Eq. (5.4), which for equally-weighted observations is simply the average of all the W_P computed at each tide gauge. It should be noted that Eq. (5.4) is used when evaluating the SST from tide gauge data.

If one wants to evaluate W_P using a SST model, then the following equation should be used:

$$W_P = W_N - (SST_P \gamma_P). \tag{5.5}$$

For the sake of consistency, the SST models should be converted from a mean-tide system to a tide-free system for the adequate comparison of the W_0 values obtained from tide gauges and those obtained using sea surface topography models. The tide-free value SST_{TF} can be obtained using the conversion given in Eq. (5.6) below (Ekman 1989; Mäkinen and Ihde 2009):

$$SST_{TF} = SST_{MT} + 0.68\left(\left(9.9 - (29.6 sin^2 \varphi)\right)0.01\right), \tag{5.6}$$

where SST_{MT} is the sea surface topography given in the mean-tide system, and φ is the latitude of the SST node from the model.

The mean potential is obtained by a weighted average when W_0 is evaluated from SST models using:

$$W_0 = \frac{\sum(W_{P_i} cos\varphi_i)}{\sum(cos\varphi_i)}, \tag{5.7}$$

or

$$W_0 = \frac{\sum(W_{P_i}\frac{1}{\gamma_i})}{\sum\frac{1}{\gamma_i}}, \quad (5.8)$$

where W_{Pi} is the potential of the water surface estimated from a SST node in the model, and φ_i is the latitude of the SST node from the model. It should be noted that Eq. (5.7) can only be considered an approximation as it does not comply with the Gauss-Listing definition of the geoid (Gauss 1828; Bessel 1837; Listing 1873). The $cos\varphi_i$ term in Eq. (5.7) assigns less weight to higher latitude terms, which reflects the fact that SST accuracy decreases with latitude as many SST models assimilate altimetry data. On the other hand, Eq. (5.8) does comply with the Gauss-Listing definition (see Chapter 2, Section 2.2). Then again, the use of either Eq. (5.7) or Eq. (5.8) yields essentially the same W_0 results; the difference is on the order of 0.01 m^2/s^2, which equates to a 1 mm error in SST (Hayden et al. 2012b).

It should also be noted that the tide gauges on the Atlantic coast located near the St. Lawrence River may be affected by river discharge (Bourgault and Koutitonsky 1999). In order to mitigate such effects, one may adjust the local MSL (i.e., Z_0) for deep ocean SST. The SST shown in Figure 5.19 is obtained from a SST model, and the difference between the geometrical SST computed using geodetic data at the tide gauge and the SST from a model results in the correction to be applied to Z_0. In order to avoid SST values near the coast, which are more likely to be erroneous due to the localized effects of the coastline, an averaged oceanic SST at 50 km from the tide gauge location is used when evaluating the correction to be applied to Z_0. This is especially the case if the SST model incorporates altimetry data such as the geodetic-based SST models presented in Section 5.2.3, since the altimetry signal is likely to be contaminated by the land portion of the coastline. In this study the regional SST models are utilized for this correction as they have better coverage when compared to the global models of ocean regions near the coast. Additionally, the Foreman model is very dense in the coastal region when compared with the global models, and is therefore less likely to be subject to interpolation errors. The difference in W_0 is at most 0.10 m^2/s^2 or 1 cm when using a

correction from the regional SST models interpolated 50 km away from the tide gauges or one that is interpolated to the tide gauge locations.

The values for *h*, *CD*, and Z_0 were all brought to the same epoch of 2008.0. The motivation for this comes from the fact that this study is part of the ESA STSE – GOCE+ "Height System Unification with GOCE" project, and in order to have consistency among the various computations from the different research teams involved, the common reference epoch of 2008.0 was chosen.

The ellipsoidal height *h* was originally given in ITRF 2005 epoch 2006.0 which was then converted to ITRF 2008 epoch 2008.0 using software developed by NGS available at http://www.ngs.noaa.gov/GEOID/GPSonBM09/. Corrections for vertical land motion were also applied. The acceleration of the vertical motion is assumed to be zero and that there is only a constant velocity difference:

$$h = h_{2008.0} + ((2008.0 - 2006.0) * VLM), \quad (5.9)$$

where $h_{2008.0}$ is the ellipsoidal height in ITRF 2008 epoch 2008.0 and *VLM* is the vertical land motion velocity estimate. For the Pacific region, the vertical land motion rates are mainly due to seismic variations, and these values were obtained from the GNSS-based rates evaluated by Mazzotti et al. (2008). For the Atlantic and Arctic region, the vertical land motion rates are primarily due to post-glacial rebound, and these values were interpolated at the tide gauge locations from the Argus and Peltier (2010) *GEODVEL1b GPS* solution

Similarly, *CD* and Z_0 are adjusted by determining their epochs. The Z_0 has an epoch of 2001.5, which is the average of the time series that ranges from 1992 to 2011. The *CD* values have variable epochs which have been provided by the Canadian Hydrographic Service. For the Pacific region, the CHS did not have epoch information for the chart datum, so the *CD* values were left as originally given in the data files obtained by NRCan. Furthermore, the CHS did not have complete epoch information for the chart

datum in the Atlantic region, thus the epoch information of the nearest available tide gauge was utilized if this information was missing for a particular station. In order to bring the epoch of all the *CD* and Z_0 values to 2008.0, both sea level rise and vertical land motion had to be taken into account.

The vertical land motion rate was applied with the following manner to Z_0:

$$Z_{0_{VLM}} = \frac{\sum Z_{0_{Annual}}}{19} + \frac{19 * VLM}{19}, \tag{5.10}$$

and the sea level rise as

$$Z_{0_{2008.0}} = Z_{0_{VLM}} + (v_{sea\ level\ rise}(2008.0 - 2001.5)), \tag{5.11}$$

where $Z_{0_{Annual}}$ is the yearly is averaged water level time series and $v_{sea\ level\ rise}$ is the rate of the sea level rise. The absolute sea level rate used was the 20th century average for North America: 1.8 mm/yr ±0.2 mm/yr (Church et al. 2004; Snay et al. 2007; Mazzotti et al. 2008).

Similarly for the *CD* values the following equation was used in order to bring the values to epoch 2008.0:

$$CD_{2008.0} = CD + \left(VLM(2008.0 - epoch_{CD})\right) + \left(v_{sea\ level\ rise}(2008.0 - epoch_{CD})\right), \tag{5.12}$$

where $epoch_{CD}$ is the epoch of the chart datum.

On a final note, it should be mentioned that corrections given in Eq. (5.9) to Eq. (5.12) do not have a significant effect on W_0, since the velocity corrections are of the order of mm/year and thus they add only a few millimetres to *h*, *CD*, and Z_0 (Rangelova et al. 2012).

5.3 Results and Discussion

5.3.1 W_0 Evaluation with Tide Gauges and GOCE GGMs

In the ideal case, considering that the W_0 is a single averaged value mainly dependent on low-frequency spectral content, the effect of the GOCE omission error is not expected to be significant. However, as previously shown in Section 5.2.3, the effect of the GOCE omission error can be significant at selected tide gauges, and will not average out over the limited number of gauges available for Canada. In Table 5.3, W_0 results for the Pacific and Atlantic regions with full 19 years of water level data are presented in order to compare the results with those computed using the various SST models. As the regional SST models are of variable density, in particular the Foreman model, they may cause the W_0 values to be biased as there are more SST nodes in Pacific than for the regional models in the Atlantic, thus the W_0 of the Pacific and Atlantic are examined separately using *goco03s* in Table 5.3. The standard deviations are estimated by the a-posteriori variance factor of the adjustment of Eq. (5.4) using a unit weight matrix; thus the error estimates shown in the tables indicate a formal statistical accuracy.

Table 5.3: W_0 values for Pacific and Atlantic tide gauges with 19 years of water level data with GGMs expanded to degree and order 180 and 2,190 (add 62,636,800.00 m^2/s^2 to values in table).

GGM Model	Pacific	Atlantic
goco03s n_{max}:180	52.59 ± 2.13	58.30 ± 1.16
goco03s+EGM2008 n_{max}:180+181 to 2190	54.18 ± 0.13	59.21 ± 0.16

It can be observed from Table 5.3 that for the result with the extended *goco03s+EGM2008* model, the mean W_0 is close to 62636854.00 m^2/s^2 for the Pacific and 62636859.00 m^2/s^2 for the Atlantic. The potential decreases in the Pacific since the SST for this region is mostly positive, which is also verified by the SST models for this region as shown in Section 5.2.3. For the Atlantic region, the SST is for the most part negative, thus it is reasonable for the potential to increase with respect to the W_N surface

used in Eq. (5.4). For the Pacific region, the effect of the omission error on the W_0 value averages to 1.59 m^2/s^2 or approximately a 16 cm difference when the satellite only model is compared with the spectrally enhanced model. For the Atlantic region the effect of the omission error averages to 0.92 m^2/s^2 (or 9 cm).

Table 5.4: W_0 values evaluated using Pacific and Atlantic tide gauges with 19 years of water level data and different gravity field models (add 62,636,800.00 m^2/s^2 to values in the table).

Gravity Field Model Expanded to Degree and Order n_{max}	**W_0 using Z_0 without Correction (m^2/s^2)**	**W_0 using Foreman and Wright Corrected Z_0 (m^2/s^2)**	**W_0 using Foreman and Thompson & Demirov Corrected Z_0 (m^2/s^2)**
goco03s n_{max}: 180	55.50 ± 1.39	55.52 ± 1.38	56.03 ± 1.43
goco03s+EGM2008 n_{max}: 180+181 to 2190	56.78 ± 0.56	56.81 ± 0.56	57.31 ± 0.65
go_cons_gcf_2_tim_r4 n_{max}: 200	55.23 ± 1.14	55.25 ± 1.14	55.76 ± 1.20
go_cons_gcf_2_tim_r4+EGM2008 n_{max}: 200+201 to 2190	56.64 ± 0.55	56.66 ± 0.56	57.17 ± 0.64
go_cons_gcf_2_tim_r4 n_{max}: 250	56.43 ± 0.97	56.45 ± 0.95	56.96 ±1.01
go_cons_gcf_2_tim_r4 n_{max}: 250 (with error info)	56.55 ± 0.95	56.57 ±0.94	57.09 ± 1.00
go_cons_gcf_2_tim_r4+EGM2008 n_{max}: 250+251 to 2190	56.60 ± 0.62	56.63 ± 0.65	57.14 ± 0.71
go_cons_gcf_2_dir_r4 n_{max}: 210	55.46 ± 1.11	55.49 ± 1.11	55.99 ± 1.16
go_cons_gcf_2_dir_r4+EGM2008 n_{max}: 210+2111 to 2190	56.68 ± 0.57	56.70 ± 0.57	57.21 ± 0.65
CGG2010	56.71 ± 0.60	56.74 ± 0.59	57.24 ± 0.69

Table 5.4 shows W_0 values obtained using Z_0 that has been corrected for deep ocean SST using the regional SST models. Again, the effect of the GOCE model omission error on the W_0 value reaches approximately 1.30 m^2/s^2 (or 13 cm) when using a combination of Pacific and Atlantic tide gauges.

The effect of the omission error on W_0 when using *tim_r4* expanded to the maximum available degree and order of 250 is approximately 2 cm when no error information is utilized and less than 1 cm when error information is utilized. The error estimates utilized may yield an overly positive estimate of the actual effect as no readily available error information was available for the *h*, *CD*, and Z_0 values, thus constant error values were assumed (i.e., 2 cm, 5 cm, and 1 cm, respectively), and only the variances of the *tim_r4* model was utilized for the propagation of the errors to the geoid height. In actuality, the errors of the *h*, *CD*, and Z_0 values could be larger.

Correcting Z_0 for the SST of the deep ocean has an effect that is less than 1 cm when utilizing the Wright SST model. On the other hand, the contribution of this correction is approximately 5 cm when utilizing the Thompson & Demirov SST model. Thus, the variability between SST models can be an appreciable factor in W_0 estimation when only a small number of tide gauges are available.

5.3.2 W_0 Evaluation with Tide Gauges and Gravimetric Geoid Models

In this section, results for W_0 evaluated with Eq. (5.4) using geoid undulations obtained from regional gravimetric geoid models are presented. As both the *CGG2010* and Ince et al. (2012) gravimetric geoid models use the same terrestrial data to model the high frequency contributions of the gravity field, it is expected that they will perform similarly when evaluating W_0. Likewise, gravimetric geoid models are also expected to perform consistently with the spectrally enhanced GOCE+*EGM2008* models presented in the previous section. Hence, the gravimetric geoid models in this section provide another measure of the difference in performance of the GOCE only models and that of the high resolution gravity models when evaluating W_0 from tide gauge averaging.

The results from Table 5.5 are consistent with those results utilizing the spectrally enhanced GOCE models with *EGM2008* shown in Table 5.4. This is expected as the *EGM2008* model also utilizes the same terrestrial data used to construct the *CGG2010* and Ince et al. (2012) gravimetric geoid models in order to account for medium to short wavelength contributions of the gravity field (Pavlis et al. 2012). The results computed using the gravimetric geoid models help to further highlight the fact that simply utilizing the GOCE models truncated at degree and order 180, 200, or 210 is not sufficient for determining W_0 from tide gauge averaging as the omission error affecting the SST and in turn the potential at each tide gauge could be large, which will affect the W_0 determination due to sparsely distributed and limited number of available tide gauges.

Table 5.5: W_0 values for three Canadian regions computed with regional gravimetric geoid models (add 62,636,800.00 m^2/s^2 to all values).

Geoid Model	**CGG2010**	**Ince et al. (2012)**
Pacific tide gauges with 19 years of water level data		
Mean W_0 (m^2/s^2)	54.25 ± 0.13	54.17 ± 0.11
Atlantic tide gauges with 19 years of water level data		
Mean W_0 (m^2/s^2)	59.67 ± 0.23	59.60 ± 0.19
All Arctic tide gauge stations (5 Stations)		
Mean W_0 (m^2/s^2)	60.15 ± 0.17	60.19 ± 0.28
Pacific and Atlantic tide gauges with 19 years of water level data		
Mean W_0 (m^2/s^2)	56.71 ± 0.60	56.64 ± 0.60
Pacific and Atlantic tide gauges with 19 years of water level data + All Arctic tide gauges		
Mean W_0 (m^2/s^2)	57.35 ± 0.56	57.30 ± 0.56
All tide gauges (38 Stations)		
Mean W_0 (m^2/s^2)	57.44 ± 0.47	57.38 ± 0.46

The W_0 values estimated using *CGG2010* and Ince's model can be considered statistically similar as the differences in the W_0 values range from 0.04 m^2/s^2 to 0.08 m^2/s^2, which is well within the range of three times their formal errors that vary from 0.3 m^2/s^2 to 0.8 m^2/s^2. For example, the W_0 value computed using *CGG2010* for the Pacific region is 62636854.25 m^2/s^2 while for the Atlantic region it is 62636859.67 m^2/s^2, and for the Arctic region the W_0 value averages to 62636860.15 m^2/s^2. When utilizing the model developed by Ince et al. (2012) the W_0 value for the Pacific is 62636854.17 m^2/s^2, for the

Atlantic it is 62636859.60 m^2/s^2, and it is 62636860.19 m^2/s^2 for the Arctic. It is also interesting to note, that the SST in the Arctic is most likely negative, as the W_0 values obtained are similar to those obtained using Atlantic tide gauges, where the difference is at most 0.48 m^2/s^2 (or approximately 5 cm).

5.3.3 W_0 Evaluation with SST Models

In order to validate the results obtained from tide gauge averaging, the W_0 value is computed using various SST models with SST values interpolated to tide gauge locations using 2-D linear interpolation. The results are presented in Table 5.6. When using SST models for the evaluation of W_0, the standard deviations in Table 5.6 and Table 5.7 are computed as the standard deviation of the sample using equation (5.7).

Table 5.6: W_0 values evaluated with SST interpolated from models at tide gauges.

SST Models	W_0 (m^2/s^2)
Local: Foreman and Wright	62636856.75 ± 2.73
Local: Foreman and Thompson & Demirov	62636857.15 ± 3.15
Maximenko	62636857.29 ± 2.15
CLS	62636856.74 ± 2.70
ECCO2-JPL	62636857.28 ± 2.89
OCCAM12	62636857.23 ± 3.11
GECCO	62636856.94 ± 3.26
ECCO-godae	62636857.33 ± 3.54
Liverpool Fine	62636857.23 ± 3.46
Liverpool Coarse	62636856.76 ± 3.87
GOCE1	62636856.91 ± 2.41
GOCE2	62636857.14 ± 2.18

Overall, the W_0 results in Table 5.6 are in good agreement with results obtained using tide gauges and high resolution gravity field models (i.e., GOCE+*EGM2008*) and the gravimetric geoid models. When compared to the result obtained with *CGG2010* without using a SST corrected Z_0 in Table 5.4, the maximum difference is observed with the application of the ECCO-godae model, where the difference is 0.62 m^2/s^2 or approximately 6 cm. The best agreement with the *CGG2010* and the Ince et al. (2012) W_0

results from Table 5.5 occurs for the regional models Foreman and Wright and the SST model Liverpool Coarse where the difference is at most 0.12 m^2/s^2 or approximately 1 cm. When comparing the model obtained W_0 values to the W_0 value obtained using *CGG20120* with a SST corrected Z_0 from Table 5.4, there is excellent agreement with the Maximenko, ECCO2-JPL, OCCAM12, ECCO-godae, Liverpool Fine, and GOCE2 global SST models, with a maximum difference of 0.1 m^2/s^2 or 1 cm.

Lastly, W_0 values are computed using the SST models in order to estimate the average potential for North American Pacific and Atlantic, which are presented in Table 5.7. It should be noted that the ten global models are limited to the coastal region while the regional models include the deep oceans, extending from 130ºW to 115ºW for the Pacific and 80ºW to 50ºW for the Atlantic.

Table 5.7: W_0 values evaluated for the Pacific and Atlantic oceans using SST models.

SST Models	**Pacific W_0 (m^2/s^2) Latitude: 30˚N to 60˚N Longitude: 150˚ W to 115˚W**	**Atlantic W_0 (m^2/s^2) Latitude: 30˚N to 60˚N Longitude: 80˚ W to 50˚W**
Tide Gauges with CGG2010	*62636854.17 ± 0.19*	*62636860.70 ± 0.18*
Local: Foreman	62636854.25 ± 0.63	--
Local: Wright	--	62636857.28 ± 4.50
Local: Thompson & Demirov	--	62636857.11 ± 5.04
Maximenko	62636854.69 ± 1.03	62636859.61 ± 6.86
CLS	62636854.04 ± 0.65	62636859.99 ± 6.87
ECCO2-JPL	62636854.69 ± 0.29	62636860.84 ± 6.84
OCCAM12	62636854.24 ± 0.29	62636861.09 ± 6.75
GECCO	62636854.11 ± 0.24	62636861.08 ± 6.85
ECCO-godae	62636854.23 ± 0.37	62636861.77 ± 6.74
Liverpool Fine	62636854.15 ± 0.31	62636861.33 ± 6.75
Liverpool Coarse	62636853.32 ± 0.35	62636861.23 ± 6.72
GOCE1	62636854.33 ± 0.45	62636859.79 ± 6.85
GOCE2	62636854.75 ± 0.82	62636859.73 ± 6.86

Based on the results in Table 5.7, it can be inferred that the SST is highly variable for the Atlantic while the opposite is true of the SST found in the Pacific as the standard

deviations for the Atlantic range from 4.50 m^2/s^2 to 6.86 m^2/s^2 while the standard deviation for the Pacific ranges from 0.24 m^2/s^2 to 1.03 m^2/s^2 with the use of the different SST models. The MSL of the Pacific is approximately 20 cm above the global conventional W_0 value 62636856.00 m^2/s^2 adopted by the IERS 2010 (Petit and Luzum 2010) while the MSL of the Atlantic is approximately 40 cm below this surface. From Table 5.7 it can be observed that the Thompson & Demirov and Wright SST models yield a lower potential for the Atlantic when compared with the 10 other global SST models because these two models include the deep ocean part of the South Atlantic where warmer waters from the Gulf Stream create a positive SST (see Figure 5.2). For example, the W_0 value for the Atlantic using the Thompson & Demirov and Wright SST models is 62636857.11 m^2/s^2 and 62636857.28 m^2/s^2, respectively. In contrast, for the global model ECCO2-JPL the W_0 value for the Atlantic is 62636860.84 m^2/s^2, which represents a maximum difference of 3.73 m^2/s^2 (or 38 cm) when compared to the use of the regional models.

Thus, when utilizing the regional SST models in the evaluation of W_0 as an average over North America, one expects a decrease in potential when compared to the Canadian case as the SST values off the Canadian Atlantic coast are mostly negative. For example, when using the Foreman + Wright SST model combination yields a W_0 value of 62636855.77 m^2/s^2 and the Foreman + Thompson & Demirov combination yields a W_0 value of 62636855.68 m^2/s^2 for North America.

5.4 Summary

The objectives of this chapter include the evaluation of W_0 from tide gauge records and geoid models within the context of realizing a new geoid-based and GNSS-accessible vertical datum for Canada in order to replace the outdated CGVD28, and to validate the results of tide gauge averaging utilizing SST models. One of the main goals was to assess the performance of the GOCE-based GGMs for the purpose of estimating W_0 in Canada using tide gauges. This was done by evaluating the SST at tide gauges utilizing the *goco03s*, *tim_r4*, and *dir_r4* GOCE satellite-only models. Based on plots comparing the

SST values obtained from regional SST models with those obtained using *goco03s* and tide gauge records, it was expected that the omission error of the GOCE-only models would have a significant effect on the computed W_0 value due to the small number of tide gauges available on the Atlantic and Pacific coasts. In order to test this, the GOCE models were spectrally extended with the high resolution gravity model *EGM2008*. Furthermore, the performance of the GOCE only models for the estimation of W_0 was compared with that of two gravimetric geoid models.

It was shown that the effect of the GOCE omission error on W_0 averages to 16 cm in the Pacific and 9 cm in the Atlantic, and averages to 13 cm when both Pacific and Atlantic tide gauges are utilized. Thus, it can be concluded that the truncation degree of the GOCE models is important for W_0 determination; in particular, the truncation degrees of 180-210 are not adequate when evaluating W_0 from scattered tide gauge points in Canada as the higher frequency contributions of the gravity field are not properly modeled. On the other hand, it has been shown that when the GOCE *tim_r4* model is expanded to its maximum degree 250, the effect of the GOCE omission error on the estimation of W_0 is between 1 to 2 cm. However, further investigation is needed in order to accurately quantify the effects of the GOCE model commission errors and the measurement errors on the W_0 value.

Thus, based on the results from Chapter 4 and this chapter, the effect of the GOCE omission error on the averaged W_0 is expected to be negligible for well distributed stations, which also indicates that the use of a satellite-only GGM may be sufficient for the computation of W_0 in regions with very good coverage and distribution of tide gauge or GNSS levelling benchmarks. Based on the results in this study, it is recommended that a high resolution geoid model such as *CGG2010* or *EGM2008* should be used when computing W_0 by the tide gauge averaging method in order to adequately model the high frequency components of the gravity field, in particular for regions with poor coverage and distribution of tide gauges. On the other hand, it is recommended to use regional SST models for the determination of W_0 in North America, as they have the best agreement with the geometrically determined SSTs and adequately reflect the positive SST of the

South Atlantic when compared with the global models. By extension of this reasoning, the ECCO2-JPL global SST model can also be utilized.

It is expected that data gaps in the water level time series, missing epoch information for the chart datums on both the Pacific and Atlantic coasts, interpolation errors for epoch information for the chart datums, interpolation errors for determining post-glacial rebound velocities at tide gauges, and utilizing MSL values that are based on time series shorter than 19 years will affect the quality of the tide gauge data. However, in this study, the effect of these limitations on the final MSL obtained from tide gauge data were not investigated, and therefore may be considered for future investigations. The main factor to consider is the interpolation error of the SSTs at the tide gauges locations when validating the tide gauge averaging results with the use of SST models. Depending on the assimilation of different data types in the SST model, such as the incorporation of altimetry data, the quality of the SST values near the coast acquired from a model needs to be carefully considered.

One needs to utilize a 19-year water level time series for the estimation of W_0 of the local MSL in order to average out the effects of the tides and the weather. Such a requirement limits the number and the distribution of tide gauges available for determining W_0 at the Canadian coasts. Data gaps in the water level time series have been avoided by interpolating values from neighbouring ones. At any rate, it is not expected that this will significantly affect the W_0 results since the MSL values have been averaged from daily to monthly to annual, and finally to 19-year averages.

Furthermore, the height of the tidal benchmark *CD* will not be significantly affected due to missing epoch information or interpolation errors, since when updating the epoch of the chart datum to 2008.0, it is only a matter of a few millimetres to one centimetre difference, and as such it will not have a significant effect on the final W_0 value. This is because the geoid is a smooth surface and W_0 is obtained by averaging. Likewise, this applies for interpolation errors of the post-glacial rebound rates where the annual

velocities are of the order of millimetre. Thus, the effect in the final W_0 computation was not significant.

The potentials obtained from tide gauge averaging in this chapter cannot be considered an average for all of North America since U.S.A. tide gauges were not included in the study. This limitation can be overcome by utilizing SST models to compute W_0 instead of tide gauges as a good agreement has been discerned between the SST estimated from tide gauge data and the SST values obtained from models. The main factor for the consistency between the SST values from models and those obtained using tide gauge information is the use of an accurate and high resolution geoid model.

Moreover, the Arctic region lacks sufficient water level data and SST model coverage. Therefore, SST values from this region cannot be included when estimating a continental average for W_0. Consequently, the W_0 results presented within this chapter using tide gauge averaging are primarily biased to the Pacific and Atlantic coasts in the southern region of Canada.

Without the inclusion of Arctic SST values for the estimation of a North American W_0 value, it can be discerned that the W_0 values presented within this chapter are coincidentally close to the standard IERS (2010) global value of 62636856.00 m^2/s^2. In other words, the W_0 values presented within this chapter cannot be considered statistically different from the IERS 2010 conventional value as the difference between these W_0 values is less than three times their formal errors. The W_0 values are visually summarized in Figures 5.21 and 5.22. The main consequence of adopting the IERS 2010 W_0 value for the geoid-based and GNSS-accessible vertical datum that will replace CGVD28 in Canada is that it represents an average over the entire North American continent; subsequently it will not reflect the potential of the local MSL along the coasts in Canada as illustrated in Figure 5.20. For example, in the Pacific, it may appear that some heights are below the observable local mean sea level in that region.

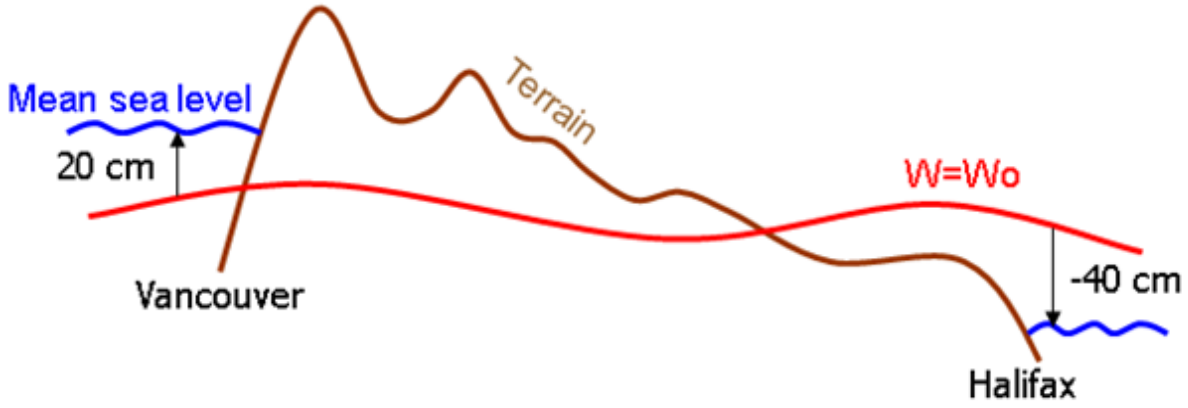

Figure 5.20: Differences in local MSL between west and east coast of Canada with respect to IERS (2010) W_0 62636856.00 m^2/s^2.

Lastly, it should be noted that climate-related changes will affect the MSL, due to factors such as the addition of melt water from Greenland, Alaska glaciers, and Canadian ice caps, and the possible expansion of the ocean due to warming of the ocean surface. Consequently, these effects will influence the W_0 value over a decade and longer. However, since the adopted W_0 value for North America is a conventional value, it does not necessarily represent the exact value of the coastal mean sea level for North America.

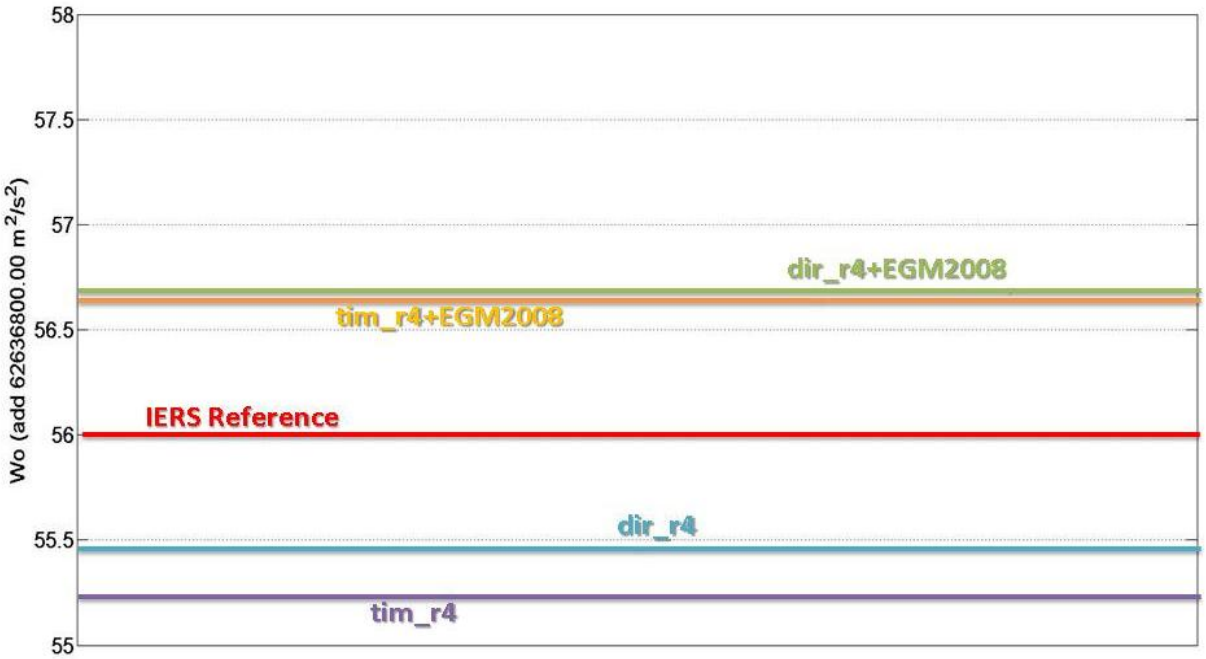

Figure 5.21: Summary of W_0 estimates using GOCE GGMs and tide gauge information.

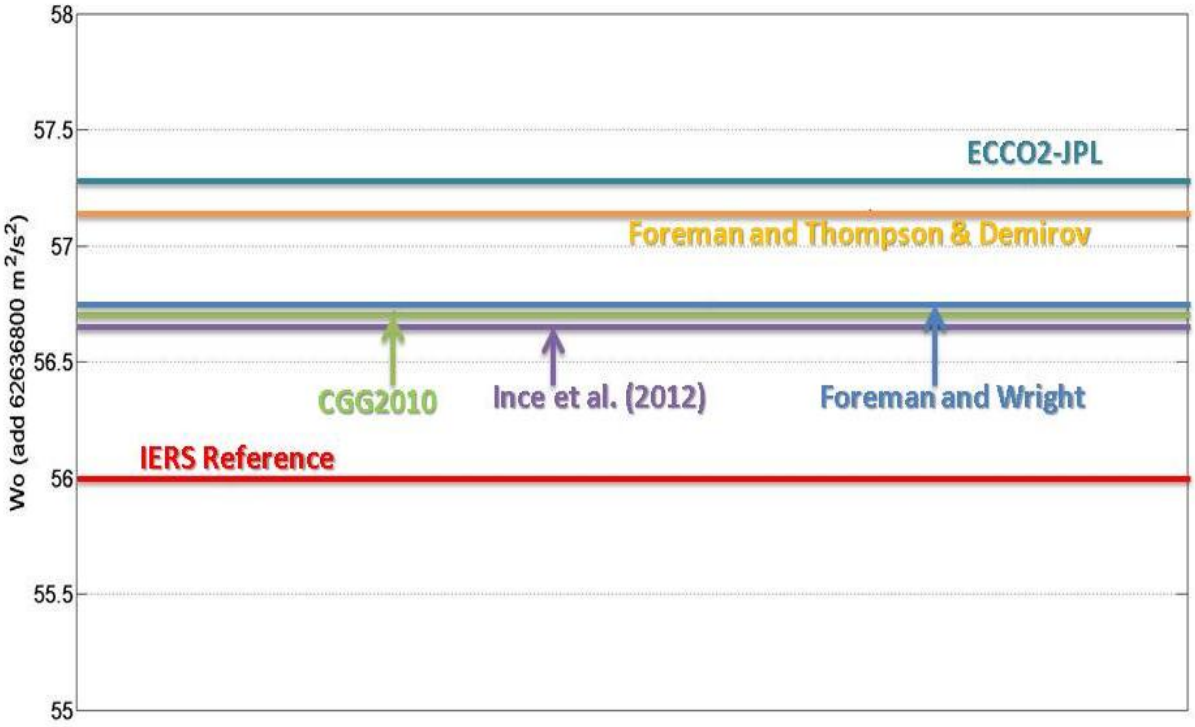

Figure 5.22: Summary of W_0 estimates using gravimetric geoid models and tide gauge information, and SST models.

CHAPTER 6
CONCLUSIONS

6.1 Thesis Statement

The main motivation of this thesis was to assess whether a GGM or a geoid model constructed from satellite only observations is sufficient for geodetic applications such as datum unification or the determination a conventional W_0 value for a regional geoid-based vertical datum, as these applications depend on a highly accurate and globally consistent geoid or gravity field model. The use of a satellite only geopotential model avoids the biases present in terrestrial data that is needed for gravimetric geoid modelling, which has been essential for establishing accurate geoid models, since gravity and topography data is needed to sufficiently model the high frequency contributions of the gravity field. By the end of its lifespan, it is expected that the GOCE mission will achieve a 1-2 cm geoid accuracy at a spatial resolution of approximately 100 km. In essence it would then provide the long awaited satellite only geopotential models that will simplify tasks such as datum unification and the establishment of a global height system. In order to answer the question of whether a satellite-only gravity field model is sufficient for datum unification and regional W_0 determination in North America, the following topics were investigated:

- Evaluation of recently released satellite only global geopotential models with a focus on GOCE-based models.
- Estimation of local vertical datum offsets for classical levelling-based vertical datums in North America for the purpose of datum unification using GOCE satellite only models.
- Estimation of W_0 for the implementation of a geoid-based GNSS-accessible vertical datum that will replace the outdated CGVD28 in Canada using regional tide gauges and GOCE satellite only models, in addition to EGM2008 extended GOCE models and gravimetric geoid models in order study the effect of the GOCE model omission error on W_0.

6.2 Conclusions

The following conclusions can be made from the GGM model evaluations:

- GOCE satellite-only models have overall better agreement with independent terrestrial data sets when compared to pre-GOCE era satellite (GRACE and CHAMP) models
- The agreement of GOCE models when compared with independent terrestrial datasets improve as the time series of GOCE observations increases. The fourth generation *tim_r4* and *dir_r4* have the best overall performance in North America, which is expected due to the fact that these models contain a time series of GOCE observations that is at least double the length of the previously released models.
- GOCE satellite-only GGMs have good agreement with the independent GNSS/levelling data up to the spectral band of harmonic degree 210 in North America.
- The fourth generation GOCE models *tim_r4* and *dir_r4* show improvement in the higher spectral bands when compared with the third generation GOCE satellite-only models.
- Due to the increasing effect of the GOCE commission error above the spectral band of harmonic degree 200-210, the GOCE only models are truncated at degree and order 200-210 for the use in applications of estimating local vertical datum offsets and W_0.
- The *dir_r4* model, which contains a GRACE-based background model, has achieved a 1.2 cm global geoid accuracy at degree and order 200, which satisfies the GOCE mission objective of achieving 1-2 cm geoid accuracy at a spatial resolution of approximately 100 km. With a longer time series of GOCE observations, (i.e., fifth generation GOCE models) it is expected that the pure GOCE model based on the time-wise approach may also achieve the GOCE mission goals.

The following conclusions can be made from the estimation of local vertical datum offsets for North American vertical datums using GOCE GGMs:

- The effect of the GOCE model omission error on LVD offsets when using Canadian GNSS/levelling benchmarks and fourth generation GOCE models is 8 cm. The effect of the GOCE model omission error on the LVD offset estimate is 2-3 cm when using the U.S.A. GNSS/levelling data. This difference is attributed to the respective configuration and density of the GNSS/levelling benchmarks available in each respective country.
- The effect of the GOCE omission error on the estimation of the local vertical datum offset is amplified for regions with rough topography, sparse/irregular GNSS/levelling benchmark configuration, and limited number of benchmarks/tide gauges, especially in relation to the total size of the test network. Due to this, a GOCE-based model should be used in a remove-compute-restore scheme with gravity and terrain data in order to rigorously model the higher frequency contributions of the gravity field.
- GOCE commission error and the measurement errors of the GNSS and levelling data need to be taken into account, in particular for regions with limited geographic coverage, when estimating local vertical datum offsets as the effect on the LVD offset estimate can reach the dm-level.
- The spatial tilts found in the Canadian Nov07 and NAVD88 networks, and the U.S.A. NAVD88 network can be modelled with a 2-parameter corrector term model. The model parameters may be estimated simultaneously with the LVD offset estimates or the spatial tilts may be removed before the least-squares estimation of the LVD offset, as the effect on the LVD offset estimate is at most 1 cm.

The following conclusions regarding the estimation of W_0 using GOCE GGMs and tide gauge information can be made:

- GOCE satellite only models truncated at degree and order 180 are not sufficient for estimating accurate SST values using geodetic information at tide gauges. Differences between SST values obtained from regional SST models and those obtained using GOCE satellite only models truncated at degree and order 180 can reach up to 1 m.

- GOCE satellite only models truncated at degree and order 180, 200, and 210 are not sufficient for W_0 estimation when a limited number of tide gauges are available; the effect of the GOCE omission error on the W_0 value is at the dm-level when compared with W_0 estimates obtained with gravimetric geoid models and the ultra-high resolution GGM *EGM2008*.
- SST models validate the W_0 results obtained using tide gauge records and gravimetric geoid and high resolution gravity field models.
- In addition to tide gauge averaging, the regional SST models can be used to estimate W_0 for North America.

In conclusion, a satellite only geopotential model that can accurately model the geoid signal in regions where less than ideal conditions and datasets are the reality is not currently available. Thus, it is recommended that GOCE GGMs be rigorously combined with gravity and topography data, if such data sets are available.

6.3 Recommendations

In order to accurately compute LVD offsets the following are recommended:

- Removal of spatial tilts preferably before the estimation of the LVD offset in order to avoid the inseparability between the LVD offset term and the bias parameters of the corrector term model. If one wants to estimate the spatial tilts and the LVD offsets simultaneously in the least-squares adjustment, the choice of the parametric model needs to be carefully considered (see, e.g., Kotsakis et al. 2011). Moreover, the testing of various parametric models may be necessary to determine which corrector term model will most effectively remove the systematic errors found within the levelling network (see, e.g., Fotopoulos 2003).
- Inclusion of error information for the ellipsoidal, orthometric, and geoid heights if this data is available. This is especially important for test networks with a limited geographic coverage as the commission error of the GGM for wavelengths that exceed the size of the test area may act as a bias on the LVD offset estimate.

- The use of a high resolution geoid model that incorporates local gravity and terrain data is recommended in order to adequately model the effect of the GGM omission error. In such a case, the GOCE-based *dir_r4* model may be used in a remove-compute-restore scheme for geoid modelling as outlined in Chapter 2 Section 2.6 as it will contribute to the long to medium wavelengths of the gravity field signal.
- The methodology presented in Chapter 4 Section 4.2 may be utilized for LVD offset computations.

The estimation of W_0 can be achieved using tide gauge data or using SST models. If using tide gauge averaging method to compute W_0 the following are recommended:

- Evaluate the 19-year average MSL at tide gauges using tide gauges that have long term water level records without significant data gaps (i.e., no more than 2-3 years of missing water level data).
- Bring *h*, *CD*, and Z_0 in Eq. (5.4) to the same epoch by accounting for vertical land motion and sea level rise using Eq. (5.9), Eq. (5.11), and Eq. (5.12).
- Correct Z_0 using deep ocean SST using SST models in order to mitigate effects of river discharge at tide gauges. For North America, the use of regional SST models (i.e., Foreman, Wright, and Thompson & Demirov) is recommended.
- Use of a high resolution geoid model (e.g., GOCE+*EGM2008*, *EGM2008*, *USGG2012*, *CGG2010*, or Ince et al. (2012)) in order to accurately estimate the SST of the mean water level at a tide gauge. Ideally, a gravimetric geoid model that utilizes the fourth generation GOCE GGMs is preferable.
- Estimate W_0 by the means of the least-square solution of the system of observation equations evaluated by Eq. (5.4). If accuracy information for *h*, *CD*, Z_0, and *N* are available then they can be included.

If using SST models for W_0 determination in North America the following are recommended:

- Use of regional SST models (i.e., Foreman, Wright, and Thompson & Demirov) and ECCO2-JPL global model due to best agreement with geometrical SST

evaluated at tide gauges. Regional models have good coastal and deep ocean coverage.

- Use of Eq. (5.8) to estimate W_0 as it complies with the Gauss-Listing definition of the geoid.

6.4 Future Investigations

There are other investigations that can be conducted in order to further study the limitations and benefits of the GOCE satellite-only GGMs for a variety of geodetic applications:

- GOCE models can be evaluated with other types of independent terrestrial datasets, such as, e.g., astro-geodetic deflections and SST, other than GNSS/levelling benchmarks. Again, comparisons are only valid if the reliability of the terrestrial datasets is good. Also, one may also include the effect of the residual terrain signal and parameterize systematic effects that might be present in the terrestrial data when conducting a GGM evaluation.
- For applications such as estimating local vertical datum offsets, one should ideally propagate the GOCE commission errors using a fully populated variance-covariance matrix. This is not a trivial task as it requires the inversion of computationally demanding matrices; studies such as Gerlach and Fecher (2012) have investigated how to make this task more feasible. As well, the errors of gravity/topographic data, and that of the control data (i.e., ellipsoidal and orthometric heights from GNSS and levelling) should be included.
- One may also investigate the temporal effects such as rising sea level due to climate change on the determination of SST and in turn W_0 determination.
- GOCE models can be utilized in gravimetric geoid modelling, for applications such as the implementation of a regional geoid-based vertical datum, in order to see if there is improvement with respect to past gravimetric geoid models that have not utilized recently released GOCE models for long to medium wavelength contributions of the gravity field.

And, lastly, further investigations into the systematic errors of the CGVD28 network may be necessary, as the parametric models used within this study may not be adequate to model the more complex systematic errors and distortions present within the CGVD28 network.

REFERENCES

Altamimi Z., Sillard P. and Boucher C., 2007, ITRF2005 A new release of the International Terrestrial Reference Frame, J. Geophys. Res., 112, doi: 10.1029/2007JB004949.

Anderson O.B. and Knudsen P., 2009, DNSC08 mean sea surface and mean dynamics topography models, J Geophys. Res., 114, C11001, DOI: 10.1029/2008JC005179.

Ardalan A., Grafarend E. and Kakkuri J., 2002, National height datum, the Gauss-Listing geoid level value w_0 and its time variation $\dot{w}_0$ (Baltic Sea Level Project: epochs 1990.8, 1993.8, 1997.4), J Geod., 76, 1-28.

Argus D.E. and Peltier W.R., 2010, Constraining models of postglacial rebound using space geodesy: a detailed assessment of model ICE-5G (VM2) and its relatives, Geophys. J. Int., 181, 697-723.

Balasubramania N., 1994, Definition and realization of the global vertical datum, OSU Report No. 427, The Ohio State University, Columbus, U.S.A.

Bessel F.W., 1837, Über den Einfluss der Unregelmässigkeiten der Figur der Erde auf geodätische Arbeiten und ihre Vergleichung mit den Astronomischen Bestimmungen, Astronomische Nachrichten, 14, 269.

Biancale R., Balmino G., Lemoine J-M.,.Marty J-C., Moynot B., Barlier F., Exertier P., Laurain O., Gegout P., Schwintzer P., Reigber C., Bode A., Gruber T., König R.,Massmann F-H., Raimondo J.C., Schmidt R. and Zhu S.Y., 2000, A new global Earth's gravity field model from satellite orbit perturbations: GRIM5-S1, Geophys. Res. Lett., 27, 22, 3611–3614.

Bingham R. and Haines K., 2006, Mean dynamic topography: Intercomparisons and errors, Philos. Trans. R. Soc., Ser. A., 264, 903-916.

Bingham R.J., Haines K. and Hughes C.W., 2008, Calculating the ocean's mean dynamic topography from a Mean Sea Surface and a Geoid, J Atmos. Ocean. Tech., 25, 1808-1822.

Bolkas D., Fotopoulos G. and Sideris M.G., 2012, Referencing regional geoid-based vertical datums to national tide gauge networks, J Geod. Sci., 2, 4, 363-369.

Bourgault D. and Koutitonsky V.G., 1999, Real-time monitoring of the freshwater discharge at the head of the St. Lawrence Estuary, Atmosphere-Ocean 37, 2, 203-220.

Burša M., Kouba J., Raděj K., True S.A., Vatrt V. and Vojtíšková M., 1998, Mean Earth's Equipotential Surface from TOPEX/POSEIDON Altimetry, Studia Geoph. et Geod., 42, 459-466.

Burša M., Kenyon S., Kouba J., Šima Z., Vatrt V. and Vojitišková M., 2004, A global vertical reference frame based on four regional vertical datums, Stud. Geophys. Geod., 48, 493-502.

Bruinsma S.L., Marty J.C., Balmino G., Biancale R., Foerste C., Abrikosov O. and Neumayer H., 2010, GOCE Gravity Field Recovery by Means of the Direct Numerical Method, Proceeding at the ESA Living Planet Symposium, 27th June - 2nd July 2010, Bergen, Norway; See also: earth.esa.int/GOCE.

Church J.A., White N.J., Coleman R., Lambeck K. and Mitrovica J., 2004, Estimates of the regional distribution of sea level rise over the 1950-2000 period, J Clim., 17, 2609-2625.

Colombo O.L., 1980, A world vertical network, OSU Report No. 296, The Ohio State University, Columbus, U.S.A.

Craymer M.R. and Lapelle E., 1997, The GPS Supernet: An Integration of GPS Projects Across Canada, Internal Report, Geodetic Survey Division, Natural Resources Canada, Ottawa, Canada.

CVRS Conventions, 2007, Conventions for the Definition and Realization of a Conventional Vertical Reference System (CVRS), IAG Inter-Commission Project, ICP 1.2 Vertical Reference Frames.

Dayoub N., Edwards S.J. and Moore P., 2012, The Gauss-Listing geopotential value W_0 and its rate from altimetric mean sea level and GRACE, J Geod., 86, 9, 681-694.

Drinkwater M.R., Floberghagen R., Haagmans R., Muzi D. and Popescu A., 2003, VII: Closing Session: GOCE: ESA's First Earth Explorer Core Mission, Space Sci. Rev., 108, 1-2, 419-432.

Ekman M., 1989, Impacts of geodynamic phenomena on systems for height and gravity, Bull. Geod., 63, 281-296.

Ekman M. and Mäkinen J., 1996, Mean sea surface topography in the Baltic Sea and its transition area to the North Sea: a geodetic solution and comparison with oceanographic models, J Geophys. Res., 101, C5, 11993-11.

Entin I.I., 1959, Main Systematic Errors in Precise Levelling, Bull. Geoid., 52, 1, 37-45.

Foreman M.G.G., Crawford W.R., Cherniawsky J.Y. and Galbraith J., 2008, Dynamic ocean topography for the northeast Pacific and its continental margins, Geophys. Res. Letters, 35, L22606, DOI: 10.1029/2008GL035152.

Forsberg R., and Tscherning C., 1981, The use of height data in gravity field approximations by collocation, J. Geophys. Res., 86, B9, 7843-7854.

Forsberg R., 1984, A study of terrain reductions, density anomalies and geophysical inversion methods in gravity field modelling, OSU Report No. 355, Department of Geodetic Science and Surveying, Ohio State University, Columbus, U.S.A.

Forsberg R., 1985, Gravity field terrain effect computations by FFT, Bull. Geod., 59, 4, 342-360, doi: 10.1007/BF02521068.

Förste C.H., Flechtner F., Schmidt R., Stubenvoll R., Rothacher M., Kusche J., Neumayer H., Biancale R., Lemoine J.M. , Barthelmes F., Bruinsma S., König R. and Meyer U.L., 2008, EIGEN-GL05C - A new global combined high-resolution GRACE-based gravity field model of the GFZ-GRGS cooperation, Geophysical Research Abstracts, Vol. 10, EGU2008-A-03426, 2008, EGU General Assembly 2008.

Förste C., Stubenvoll R., König R., Raimondo J., Flechtner F., Barthelmes F., Kusche J., Dahle C., Neumayer H., Biancale R., Lemoine J. and Bruinsma S., 2009, Evaluation of EGM2008 by comparision with other recent global gravity field models, Newton's Bull., 4, 26-37.

Förste C.H., Bruinsma S., Shako R., Marty J.C., Flechtner F., Abrikosov O., Dahle C.H., Lemoine J.M., Neumayer H., Biancale R., Barthelmes F., König R. and Georges Balmino G., 2011, EIGEN-6 - A new combined global gravity field model including GOCE data from the collaboration of GFZ-Potsdam and GRGS-Toulouse, Geophysical Research Abstracts, Vol. 13, EGU2011-3242-2, 2011, EGU General Assembly 2011.

Fotopoulos G., 2003, An analysis on the optimal combination of geoid, orthometric and ellipsoidal height data, PhD Thesis, UCGE Report No. 20185, Department of Geomatics Engineering, University of Calgary, Calgary, Canada.

Gauss C.F., 1828, Bestimmung des Breitenunterschiedes zwischen den Sternwarten von Göttingen und Altona, Vandenhoek und Ruprech, Göttingen.

Gerlach C. and Fecher T., 2012, Approximations of the GOCE error variance-covariance matrix for least-squares estimation of height datum offsets, J. Geod. Sci., 2, 4, 247-256.

Gerlach C. and Rummel R., 2013, Global height system unification with GOCE: a simulation study on the indirect bias term in the GBVP approach, J. Geod.,87, 1, 57-67.

Goiginger H., Hoeck E., Rieser D., Mayer-Gurr T., Maier A., Krauss S., Pail R., Fecher T., Gruber T., Brockmann J.M., Krasbutter I., Schuh W.D., Jaeggi A., Prange L., Hausleitner W., Baur O. and Kusche J., 2011, The combined satellite-only global gravity field model GOCO02S, Proceeding at the 2011 General Assembly of the European Geosciences Union, Vienna, Austria, April 4-8, 2011.

Grafarend E.W. and Ardalan A.A., 1997, W_0: an estimate in the Finnish Height Datum N60, epoch 1993.4, from twenty-five GPS points of the Baltic Sea Level Project, J Geod., 71, 673-679.

Gruber T., 2004, Validation concepts for gravity field models from satellite missions, In: Lacoste H (ed), Proceedings of the 2nd international GOCE user workshop "GOCE, The Geoid and Oceanography", ESA SP-569, ESA. ISBN (Print):92-9092-880- 8, ISSN:1609-042X.

Gruber T., 2009, Evaluation of the EGM2008 gravity field by means of GPS-levelling and sea surface topography solutions: External quality evaluation reports of EGM2008, Newton's Bull., 4, 3-17.

Gruber T., Visser P.N.A.M., Ackermann C. and Hosse H., 2011, Validation of GOCE gravity field models by means of orbit residuals and geoid comparisions, J. Geod., 85, 11, 845-860.

Hashemi Farahani H., Ditmar P., Klees R., Liu X., Zhao Q. and Guo J., 2012, The Earth's static gravity field model DGM-1S from an optimal combination of GRACE and GOCE data: computation and validation aspects, J Geod, in review.

Hayden T., Amjadiparvar B., Rangelova R. and Sideris M.G., 2012a, Estimating Canadian vertical datum offsets using GNSS/levelling benchmark information and GOCE global geopotential models, J Geod. Sci., 2, 4, 257-269.

Hayden T., Rangelova E., Sideris M.G. and Véronneau M., 2012b, Evaluation of W_0 in Canada using tide gauges and GOCE gravity field models, J Geod. Sci., 2, 4, 290-301.

Hayden T., Rangelova E., Sideris M.G. and Véronneau M., 2013, Contribution of Tide Gauges for the Determination of W_0 in Canada, IAG Symp., 141, Springer-Verlag, Accepted March 14, 2013.

Heck B. and Rummel R., 1990, Strategies for solving the vertical datum problem using terrestrial and satellite geodetic data, IAG Symposium Series, 104, 116-128, Springer, Berlin.

Heiskanen W. and Mortiz H., 1967, Physical geodesy, WH Freeman, San Francisco, U.S.A.

Hirt C., Featherstone W.E. and Marti U., 2010, Combining EGM2008 and SRTM/DTM2006.0 residual terrain model data to improve quasigeoid computations in mountainous areas devoid of gravity data, J. Geod., 84, 557-567.

Hirt C., Gruber T. and Featherstone W.E., 2011, Evaluation of the first GOCE static gravity field models using terrestrial gravity, vertical deflections, and EGM2008 quasi-geoid heights, J. Geod., 85, 10, 723-740.

Hirt C., Kuhn M., Featherstone W.E. and Göttl F., 2012, Topographic/isostatic evaluation for new-generation GOCE gravity field models, J. Geophys. Res., 117, B05407, doi: 10.1029/2011JB00878.

Hoffman-Wellenhof B. and Helmut M., 2006, Physical Geodesy, 2nd Ed., SpringerWein, New York.

Holmes S.A. and Pavlis N.K., 2008, Spherical harmonic synthesis software harmonic_synth, http://earth-info.nga.mil/GandG/wgs84/gravitymod/new_egm/new_egm.html.

Hsu H.P., 1984, Applied Fourier analysis, Harcourt Brace Jovanovich, San Diego, IEEE, 1967, Special issue of the fast Fourier transform and its applications to digital filtering and spectral analysis, IEEE Transactions on Audio and Electroacoustics,AU-15, 2, 43-117.

Huang J. and Véronneau M., 2009, Evaluation of the GRACE-Based Global Gravity Models in Canada, Newton's Bull., 4, 66-72.

Huang J. and Véronneau M., 2013, Canadian Gravimetric Geoid Model, J. Geod., Accepted.

Ihde J. and Sánchez L., 2005, A unified global height reference system as a basis for IGGOS, J. Geodyn., 40, 400-413.

Ihde J., 2007, IAG ICP 1.2 Final Report, IAG Inter-Commission Project, ICP 1.2 Vertical Reference Frames.

Ihde J, Wilmes H., Muller J., Denker H., Voigt C. and Hosse M., 2010, Validation of Satellite Gravity Field Models by Regional Terrestrial Data Sets, In: System Earth via

Geodetic-Geophysical Space Techniques Advanced Technologies in Earth Sciences, Part 3, 227-296.

Ince E.S., Sideris M.G., Huang J. and Véronneau M, (2012), Assessment of the GOCE Global Gravity Models in Canada, Geomatica, 66, 2, 125-145.

Jekeli C., 1982, Optimizing kernels of truncated integral formulas in physical geodesy, Proceeding of the IAG General Meeting, Tokyo, Japan, May 7-15.

Jekeli C., 1999, An analysis of vertical deflections derived from high degree spherical harmonic models, J. Geod., 73, 1, 10-22.

Jekeli C., 2000, Heights, the Geopotential, and Vertical Datums, OSU Report No. 459, Ohio State University, Columbus, U.S.A.

Jekeli C., Yanh H.J. and Kwon J.H., 2009, Evaluation of EGM2008—globally and locally in South Korea, Newt. Bull., 4, 38-49.

Kaula W.M., 1966, Theory of Satellite Geodesy, Blaisdell Publ. Co., Waltham Mass., U.S.A.

Kearsley A.H.W., Sideris M.G., Krynski J., Forsberg R. and Schwarz K.P., 1985, White Sands revisited - A comparison of techniques to predict deflections of the vertical, UCSE Report No. 30007, The University of Calgary, Calgary, Canada.

Köhl A., Stammer D. and Cornuelle B., 2007, Interannual to decadal changes in the ECCO global synthesis, J Phys. Oceanogr., 37, 313-337.

Köhl A. and Stammer D., 2008, Variability of the Meridional Overturning in the North Atlantic from the 50 years GECCO State Estimation, J Phys. Oceanogr., 38, 1913-1930.

Kotsakis K. and Sideris M.G., 1999, On the adjustment of combined GPS/Levelling/geoid networks, J. Geod., 73, 8, 412-421.

Kotsakis C. and Katsambalos K., 2009, Evaluation of EGM08 based on GPS and orthometric heights over the Hellenic mainland. Newton's Bull., 4, 144-163.

Kotsakis C., Katsambalos K. and Ampatzidis D., 2011, Estimation of the zero-height geopotential level W_0^{LVD} in a local vertical datum from inversion of co-located GPS, leveling and geoid heights: a case study in the Hellenic islands, J. Geod., doi: 10.1007/s00190-011-0530-7.

Listing J.B., 1873, Über unsere jetzige Kenntnis der Gestalt und Größe der Erde, Dietrichsche Verlagsbuchhandlung, Göttingen.

Mäkinen J. and Ihde J., 2009, The permanent tide in height systems, IAG Symp. Series, 133, 81-87, Springer, Berlin.

Marshall J., Hill C., Perelman L. and Adcroft A., 1997a, Hydrostatic, quasi-hydrostatic, and non-hydrostatic ocean modelling, J Geophys. Res., 102, C3, 5733-5752.

Marshall J., Adcroft A., Hill C., Perelman L. and Heisey C., 1997b, A finite-volume, incompressible Navier-Stokes model for studies ocean on parallel computers, J Geophys. Res., 102, 5753-5766.

Maximenko N., Niiler P., Centurioni L., Rio M.H., Melnickenko O., Chambers D. et al., 2009, Mean Dynamic Topography of the Ocean derived from Satellite and Drifting Buoy Data using Three Different Techniques, J Atmos. and Ocean. Tech., 26, 2, 1910-1919.

Mayer-Gürr T., Eicker A. and Ilk K.H., 2007, available at http://www.igg.unibonn.de/apmg/index.php?id=itg-grace03.

Mayer-Gürr T., Kurtenbach E. and Eicker A., 2010, http://www.igg.unibonn.de/apmg/index.php?id=itg-grace2010.

Mayer-Gürr T. et al., 2012, The new combined satellite only model goco03s, abstract submitted to GGHS2012, http://www.goco.eu/.

Mazzotti S., Jones C. and Thomson R.E., 2008, Relative and absolute sea level rise in western Canada and northwestern United States from a combined tide gauge-GPS analysis, J Geophys. Res., 113, C11019, DOI: 10.1029/2008JC004835.

Menemenlis D., Fukumori I. and Lee T., 2005, Using Green's functions to calibrate an ocean general circulation model, Mon. Weather Rev., 133, 5, 1224-1240.

Migliaccio F., Reguzzoni M., Sanso F., Tscherning C.C. and Veicherts M., 2010, GOCE data analysis: the space-wise approach and the first space-wise gravity field model, Proceedings of the ESA Living Planet Symposium, 28 June - 2 July 2010, Bergen, Norway. See also: earth.esa.int/GOCE.

Migliaccio F., Reguzzoni M., Gatti A., Sanso F. and Herceg M., 2011, A GOCE-only global gravity field model by the space-wise approach, Proceedings of the 4th International GOCE User Workshop, 31 March - 1 April 2011, Munich.

Molodensky M.S., Eremeev V.F. and Yurkina M.I., 1962, Methods for study of the external gravitational field and figure of the Earth, Israel Program for Scientific Translations,IV-62, Jerusalem.

Mortiz H., 1966, Linear solutions to the geodetic boundary value problems, OSU Report No. 79, Ohio State University, Columbus, U.S.A.

National Geodetic Survey, NGS, 2012, USGG2012, available at www.ngs.noaa.gov/GEOID/USGG2012.

Natural Resources Canada, 2007, The Atlas of Canada, available at http://atlas.nrcan.gc.ca/auth/english/maps/reference/national/reliefinteractive.

Pail R., Goiginger H., Mayrhofer R., Schuh W.D., Brockmann J.M., Krasbutter I., Hoeck E. and Fecher T., 2010a, GOCE gravity field model derived from orbit and gradiometry data applying the time-wise method, Proceedings of the ESA Living Planet Symposium, 28 June - 2 July 2010, Bergen, Norway, See also: earth.esa.int/GOCE.

Pail R., Goiginger H., Schuh W.D., Höck E., Brockmann J.M., Fecher T. et al., 2010b, Combined satellite gravity field model GOCO01S derived from GOCE and GRACE, Geophys. Res. Lett., 37, L20314, doi:10.1029/2010GL044906.

Pail R., Bruinsma S., Migliaccio F., Foerste C., Goiginger H., Schuh W.D. et al., 2011, First GOCE gravity field models derived by three different approaches, J. Geod., 85, 11, 819-843.

Pan M. and Sjöberg L.E., 1998, Unification of vertical datums by GPS and gravimetric geoid models with applications in Fennoscandia, J. Geod. , 72, 64-70.

Pavlis N.K., Holmes S.A., Kenyon S.C. and Factor J.K., 2012, The development and evaluation of the Earth Gravitational Model 2008 (EGM2008), J. Geophys. Res., 117, B04406, doi: 10.1029/2011JB008916.

Petit G. and Luzum B., eds., 2010, IERS Convention 2010, IERS Technical Note 36, Verlag den Bundesamtes für Kartographie und Geodäsie, Frankfurt.

Pugh D.T., 1987, Tides, Surges, and Mean Sea Level, John Wiley & Sons Ltd., Chichester.

Rangelova E.V., 2007, A Dynamic Geoid Model for Canada, Ph.D Thesis, University of Calgary, Calgary, Canada.

Rangelova E., van der Wal W.and Sideris M.G., 2012, How Significant is the Dynamic Component of the North American Vertical Datum?, J Geod. Sci., 2, 4, 281-289.

Rapp R.H. and Rummel R., 1975, Methods for the computations of detailed geoids and their accuracy, OSU Report No. 233, Ohio State University, Columbus, U.S.A.

Rapp R.H. and Balasubramania N., 1992, A conceptual formulation of a world height system, OSU Report No. 421, The Ohio State University, Columbus, U.S.A.

Rapp R.H. and Wang Y.M., 1994, Dynamic topography estimates using Geosat data and a gravimetric geoid in the Gulf Stream region, Geophys. J Int., 117, 2, 511-528.

Reigber C., Lühr H. and Schwintzer P., 2002, CHAMP mission status, Adv. Space Res., 30, 129-134.

Reigber C., Jochmann H., Wünsch J., Neumayer K.H. and Schwintzer P., 2003, First insight into temporal gravity variability from CHAMP, In: Reigber C, Lühr H, Schwintzer P (eds), First CHAMP mission results for gravity, magnetic and atmospheric studies, Springer, New York, 128–133.

Rio M.H. and Hernandez F., 2004, A mean dynamic topography computed over the world oceans from altimetry, in situ measurements, and a geoid model, J Geophys. Res., 109, C12032, DOI: 10.1029/2003JC002226.

Rio M.H., Guinehut S. and Larnicol G., 2011, New CNES-CLS09 global mean dynamic topography computed from the combination of GRACE data, altimetry and in situ measurements, J Geophys. Res., 116, C07018.

Rummel R. and Teunissen P., 1988, Height datum definition, height datum connection and the role of the geodetic boundary value problem, Bull. Géod., 62, 477-498.

Rummel R. and Ilk K.H., 1995, Height datum connection - the ocean part, Allgemeine Vermessungsnachrichten, 8-9, 321–330.

Rummel R., 2001, Global unification of height systems and GOCE, In: Sideris M.G. (ed.), Gravity, geoid and geodynamics 2000, Springer, Berlin, 13-20.

Rummel R., Balmino G., Johannessen J., Visser P. and Woodworth P., 2002, Dedicated gravity field missions-principles and aims, J. Geodyn., 33, 3-20.

Sánchez L., 2009, Strategy to Establish a Global Vertical Reference System, H. Drewes (ed.), *Geodetic Reference Frames*, IAG Symp., 134, 273-278.

Sansó F. and Sideris M.G., 2013, Geoid Determination Theory and Methods, Springer, Berlin.

Schwarz K.P., 1984, Data types and their spectral properties, Proceeding of the International Summer School on Local Gravity Field Approximation, Beijing, China, Aug. 21-Sept. 4.

Schwarz K.P., 1985, Data types and their spectral properties, UCSE Report No. 60003, Division of Surveying Engineering, University of Calgary, Calgary, Alberta, Canada.

Schwarz K.P., Sideris M.G. and Forsberg R., 1987, Orthometric heights without leveling. Journal of Surveying Engineering, 113, 1, 28-40.

Shum C.K., Woodworth P.L., Andersen O.B., Egbert E., Francis O., King C., Klosko S., Le Provost C., Li X., Molines J.M., Parke M., Ray R., Schlax M., Stammer D., Thierney

C., Vincent P. and Wunsch C., 1997, Accuracy assessment of recent ocean tide models, J. Geophys. Res., 102, C11, 173-194.

Sideris M.G., 1990, Rigorous gravimetric terrain modelling using Molodensky's operator, Manuscripta Geodaetica, 15, 97-106.

Sideris M.G. and Forsberg R., 1990, Review of geoid prediction methods in mountainous Regions, Proceeding of the 1st International Geoid Commission Symposium, June 11-13, Milan, Italy.

Sideris M.G., Rangelova E. and Amjadiparvar B., 2013, First Results on Height System Unification in North America using GOCE, IAG Symp., 138, Springer-Verlag, Accepted.

Sjöberg L.E., 1986, Comparison of some methods of modifying Stokes' formula, Proceeding of the International Symposium on the Definition of the Geoid, Florence, Italy, May 26-30.

Snay R., Cline M., Dillinger W., Foote R., Hilla S., Kass W. et al., 2007, Using global positioning-system derived crustal velocities to estimate rates of absolute sea level change from North America tide gauge records, J Geophys. Res., 112, B04409, DOI: 10.1029/2006JB004606.

Sneeuw N. and Schaub H., 2005, Satellite clusters for future gravity field missions, IAG Symp., 129, 12-17, Springer.

Strange W.E., 1982, An evaluation of orthometric height accuracy using borehole gravimetry, Bull Geod., 56, 300-311.

Sturges W., 1967, Slope of sea level along the Pacific Coast of the United States, J. Geophys. Res., 72, 14, 3627-3637.

Sturges W., 1974, Sea level slope along continental boundaries, J. Geophys. Res., 79, 6, 825-830.

Tapley B.D., Bettadpur S., Watkins M. and Reigber C., 2004, The gravity recovery and climate experiment: Mission overview and early results, Geophys. Res. Lett., 31, L09607, DOI: 10.1029/2004GL019920.

Thompson K.R. and Demirov E., 2006, Skewness of sea level variability of the world's oceans, J Geophys. Res., 111, C05005, DOI: 10.1029/2004JC002839.

Thompson K.R., Huang J., Véronneau M., Wright D.G. and Lu Y., 2009, The mean sea surface topography of the northwest Atlantic: Comparison of estimates based on satellite, terrestrial gravity, and oceanographic observations, J Geophys. Res., 114, C07015, DOI: 10.1029/2008JC004859.

Torge W., 1980, Geodesy, Walter de Gruyter, Berlin, New York.

Torge W., 2001, Geodesy, Walter de Gruyter, Berlin New York, 3rd edition.

Tscherning C. and Rapp R.H., 1974, Closed covariance expressions for gravity anomalies, geoid undulations, and deflections of the vertical implied by anomaly degree variance models, OSU Report No. 208, Ohio State University, Columbus, U.S.A.

Vaníček P., 1991, Vertical Datum and NAVD88, Surv. and Land Info. Sys., 51, 2, 83-86.

Véronneau M., 2006, Demystifying the vertical datum in Canada: A case study in the Mackenzie Delta, Technical Report, Natural Resources Canada, Ottawa, Ontario, Canada, available at http://www.geod.nrcan.gc.ca/hm/pdf/verticaldatumsdeltav10_e.pdf.

Véronneau M. and Héroux P., 2006, Canadian Height Reference System Modernization: Rational Status and Plans, Technical Report, Natural Resources of Canada, Ottawa, Ontario, Canada, available at http://www.geod.nrcan.gc.ca/hm/pdf/geocongres_e.pdf.

Véronneau M., Duval R. and Huang J., 2006, A gravimetric geoid model as a vertical datum for Canada, Geomatica, 60, 2, 165-172.

Véronneau M., 2012, Adjustment of Levelling Data in Canada: Nov07, Technical Report, Natural Resources Canada, Ottawa, Ontario, Canada.

Vincent S. and Marsh J., 1974, Gravimetric global geoid, Proceeding of the International Symposium on the use of Artificial Satellites for Geodesy and Geodynamics, National Technical University, Athens, Greece.

Wang Y.M. and Rapp R.H., 1990, Terrain effects on geoid undulation computations, Manuscripta Geodaetica, 15, 23-29.

Webb D.J., Coward A.C., de Cuevas B.A. and Gwilliam C.S., 1997, A multiprocessor ocean general circulation model using message passing, J Atmos. Ocean. Tech., 14, 175-182.

Wichiencharoen C., 1982, The indirect effects on the computation of geoid undulations, OSU Report No. 336, The Ohio State University, Columbus, U.S.A.

Woodworth P.L., Hughes C.W., Bingham R.J. and Gruber T., 2012, Towards worldwide height system unification using ocean information, Journal of Geodetic Science, 2, 4, 302-318.

Xu P., 1992, A quality investigation of vertical datum connection, Geophys. J. Int., 110. 361-370.

Yonghai C. and Jiancheng L., 2012, Determination of mean sea level geopotential from global gravity field model and global sea surface height model, J Geod. and Geodyn., 32, 5, 58-62.

Zilkoski D.B., Richards J.H. and Young G.M., 1992, Results of the General Adjustment of the North American Vertical Datum of 1988, Surveying and Land Information Systems, 52, 3, 133-149.